GENE REGULATORY MECHANISMS DRIVING TEMPORAL DYNAMICS OF LINEAGE SPECIFIC DIFFERENTIATION IN THE CRANIAL NEURAL CREST

by

Maria Rose Replogle

A Dissertation Submitted in

Partial Fulfillment of the

Requirements for the Degree of

Doctor of Philosophy

in Biological Sciences

at

The University of Wisconsin-Milwaukee

May 2020

ABSTRACT

GENE REGULATORY MECHANISMS DRIVING TEMPORAL DYNAMICS OF LINEAGE SPECIFIC DIFFERENTIATION IN THE CRANIAL NEURAL CREST

by

Maria Rose Replogle

The University of Wisconsin-Milwaukee, 2020
Under the Supervision of Ava J. Udvadia, PhD

Genetic and environmental perturbations impacting neural crest (NC) development can result in pleiotropic structural and functional birth defects, many of which are associated with pediatric syndromes. As developmental precursors, the NC has the unique capacity to give rise to a diverse array of ectodermal and mesoectodermal cell types, from neurons and glia of the peripheral nervous system to the cartilage and bone of the face. In order to transition from a multipotent progenitor to a specific cell type, NC cells must undergo a series of dynamic morphological and behavioral transformations that gradually unfold over time. However, the NC is rare and transient cell population, and the genetic programming that governs the transition through the intermediate stages of differentiation toward a specific cell fate remain poorly understood. In order to investigate the temporal regulation of this process we established a robust *in vitro* model system of mammalian cranial and trunk NC cell differentiation. Systematic characterization of directed differentiation along the neural and chondrogenic lineages revealed reproducible, temporal benchmarks indicative of the intermediate stages underlying the progression, many of which mimic those described *in vivo*. Using this culture system, we

explicitly interrogated cranial NC cells to uncover the dynamic gene expression changes that occur as the multipotent progenitors transition over time to become peripheral neurons or cartilage matrix-producing chondrocytes. Our analysis revealed that cranial NC cell diversification toward either cell type is mediated through gradual coordination of both common and lineage-specific programming, as well as concurrent suppression of competing cell fates. We further identified distinct transcriptional signatures corresponding to the intermediate state, as well as putative regulators that govern the overall progression in a stage-specific and time-sensitive manner. These data serve as a powerful tool for discovering previously unappreciated mechanisms contributing to cell fate acquisition in the NC, and novel molecular targets of genetic and environmental factors that contribute to NC-related birth defects and disorders.

For Daddy

I can still hear you tell me that you are proud of me

I miss you with all my heart

and I love you always

TABLE OF CONTENTS

Page

LIST OF FIGURES

Page

LIST OF TABLES

Page

LIST OF ABBREVIATIONS

a-MEM	alpha minimal essential medium
ADAM	disintegrin and metalloprotease
Alx3	aristaless-like homeobox 3
AMP	adenosine monophosphate
AMPK	adenosine monophosphate-activated protein kinase
ANOVA	analysis of variance
Arntl (Bmal1)	aryl hydrocarbon receptor nuclear translocator-like
Ascl1	achaete-scute family bHLH transcription factor 1
αSMA	alpha smooth muscle actin
ATAC	assay for transposase-accessible chromatin
Atf5	activating transcription factor 5
ATP	adenosine triphosphate
Bapx1 (Nkx3-2)	bagpipe homeobox protein homolog 1 (NK3 homeobox 2)
BDNF	brain-derived neurotrophic factor
bHLH	basic helix-loop-helix
BLAST	basic local alignment search tool
BMP	bone morphogenic protein
bp	base pair
Brn3a (Pou4f1)	brain-specific homeobox/POU domain protein 3A
bZIP	basic leucine zipper
C2H2	cys2-his2 zinc finger

C3	complement component 3
C3aR	complement component 3a receptor
Cabin1	calcineurin binding protein 1
CBP/p300	histone acetyltransferase creb-binding protein
Cbx2	chromobox 2
cDNA	complementary DNA
ChIP	chromatin immunoprecipitation
CIL	contact inhibition of locomotion
Clock	circadian locomotor output cycles kaput
CNS	central nervous system
Col2a1	collagen, type II, alpha 1
Col9a2	collagen, type IX, alpha 2
Col10a1	collagen, type X, alpha 1
Col11a2	collagen, type XI, alpha 2
Cry1	cryptochrome 1 (photolyase-like)
CXCR4	chemokine (C-X-C motif) receptor 4
Dach1	dachshund family transcription factor 1
DAPI	4',6-diamidino-2-phenylindole
DBD	DNA-binding domain
Dbp	D site albumin promoter binding protein
Dct	dopachrome tautomerase
DE	differentially expressed
Dlx5	distal-less homeobox 5

Dlx6	distal-less homeobox 6
DMEM	Dulbecco's Modified Eagle Medium
DNMT1	DNA methyltransferase (cytosine-5) 1
E-cadherin	epithelial cadherin
E#	embryonic day (mouse)
ECL	enhanced chemiluminescence
ECM	extracellular matrix
EDTA	ethylenediaminetetraacetic acid
Egr1	early growth response 1
EMT	epithelial-to-mesenchymal transition
Epas1 (Hif2a)	endothelial PAS domain protein 1
Eph	Eph receptor
ErbB3	erb-b2 receptor tyrosine kinase 3
ET3	endothelin 3
Ets1	E26 avian leukemia oncogene 1, 5' domain
EYFP	enhanced yellow fluorescent protein
F-actin	filamentous actin
FACS	fluorescence activated cell sorting
FDR	false discovery rate
FGF	fibroblast growth factor
FISH	fluorescent in situ hybridization
Fos	Fos proto-oncogene, AP-1 Transcription Factor Subunit
FoxD3	forkhead box D3

Foxi1	forkhead box I1
Foxi3	forkhead box I3
Foxj1	forkhead box J1
Foxm1	forkhead box M1
Foxs1	forkhead box S1
GABA	gamma aminobutyric acid
gapdh	glyceraldehyde-3-phosphate dehydrogenase
Gata	GATA binding protein
Gbx2	gastrulation brain homeobox 2
GFAP	glial fibrillary acidic protein
Glis3	GLIS family zinc finger 3
GO	gene ontology
GRN	gene regulatory network
GuHCl	guanidine hydrochloric acid
H3K9	histone H3, lysine 9
Hand2	heart and neural crest derivatives expressed 2
Hes1	hes family bHLH transcription factor 1
Hes5	hes family bHLH transcription factor 5
hESC	human embryonic stem cells
Hey1	hairy/enhancer-of-split related with YRPW motif 1
HI-FCS	heat inactivated fetal calf serum
HIF	hypoxia-inducible factor
Hif3a	hypoxia inducible factor 3, alpha subunit

Hivep3	human immunodeficiency virus type I enhancer binding protein 3
HMG	high mobility group-box
HuC/D	ELAV-like RNA binding proteins
IACUC	institutional animal care and use committee
Id	inhibitor of DNA binding 1, HLH protein
IGF	Insulin-like growth factor
Insm1	insulinoma-associated 1
IRES	internal ribosome entry site
ITS	Insulin-Transferrin-Selenium
Jun	Jun proto-oncogene, AP-1 Transcription Factor Subunit
kDa	kilo Dalton
Klf9	Kruppel-like factor 9
L-DOPA	3,4-Dihydroxy-L-phenylalanine
LMNA	lamin A
Lmo4	LIM domain only 4
MBP	myelin basic protein
MEF2	myocyte enhancer factor 2
Meox2	mesenchyme homeobox 2
MFI	mean fluorescence intensity
MGI	Mouse Genome Informatics
MITF	melanogenesis associated transcription factor
MMP	metalloprotease
MSC	mesenchymal stem cell

Msx1	msh homeobox 1
Mxd3	Max dimerization protein 3
Mxi1	Max interactor 1, dimerization protein
Mybl2	myeloblastosis oncogene-like 2
Myc	myelocytomatosis oncogene
N-cadherin	neural cadherin
NC	neural crest
NCSC	neural crest stem cell
NeuroD	neurogenic differentiation factor
NGF	nerve growth factor
Ngn	neurogenin
NMII	non-muscle myosin II
NPB	neural plate border
NT-3	neurotrophin 3
NTRK1 (TrkA)	neurotrophic tyrosine kinase, receptor, type 1
NTRK2 (TRkB)	neurotrophic tyrosine kinase, receptor, type 2
NTRK3 (TrkC)	neurotrophic tyrosine kinase, receptor, type 3
Oct6 (Pou3f1)	Octamer-binding transcription factor/POU domain class 3
P#	passage number
Pa2g4 (EBP1)	proliferation-associated 2G4 (ErbB3 receptor-binding protein)
Pax3	paired box 3
PBS	phosphate buffered saline
PBST	phosphate buffered saline with Tween20

PCP	planar cell polarity
PDGF	platelet-derived growth factor
Per	period circadian clock 1
PFA	paraformaldehyde
Phox2a	paired-like homeobox 2a
PNS	peripheral nervous system
Pura	purine rich element binding protein A (Puratrophin-1-like)
PVDF	polyvinylidene difluoride
qRT-PCR	quantitative reverse transcription polymerase chain reaction
r#	rhombomere number
R26R	ROSA26 reporter construct
Rac1	Rac family small GTPase 1
Ret	ret proto-oncogene
Rfx	regulatory factor X
Rho	ras family homolog family member
RIN	RNA integrity number
ROCK	Rho-associated protein kinase
RT-PCR	reverse transcriptase-polymerase chain reaction
Runx	runt related transcription factor
RxrG	retinoid X receptor gamma
SABER	signal amplification by exchange reaction
SCN	suprachiasmatic nucleus
Sdf1 (Cxcl12)	stromal cell-derived factor 1 (chemokine (C-X-C motif) ligand 12)

SDS-PAGE	sodium dodecyl sulfate polyacrylamide gel electrophoresis
SEM	standard error of the mean
Six4	sine oculis-related homeobox 4
SMAD	mothers against decapentaplegic homolog
Snail1	snail family zinc finger 1
Snail2 (Slug)	snail family zinc finger 2
Sox5	SRY (sex determining region Y)-box 5
Sox6	SRY (sex determining region Y)-box 6
Sox9	SRY (sex determining region Y)-box 9
Sox10	SRY (sex determining region Y)-box 10
Stat5a	signal transducer and activator of transcription 5A
SUV39H1	suppressor of variegation 3-9 homolog 1
T (brachyury)	T-box transcription factor T
TBS	tris buffered saline
TBST	tris buffered saline with Tween20
Tbx6	T-box 6
Tead2	TEA domain family member 2
TFAP2 (AP2)	transcription factor AP-2
TGFβ	transforming growth factor beta
TH	tyrosine hydroxylase
TIMP	tissue inhibitor of metalloprotease
TPM	transcripts per million
TUJI	neuron-specific class III β-tubulin

Twist	twist basic helix-loop-helix transcription factor
Tyr	tyrosinase
UTR	untranslated region
UWBC	University of Wisconsin Biotechnology Center
Vdr	vitamin D (1,25-dihydroxyvitamin D3) receptor
VEGF	vascular endothelial growth factor
Wnt	wingless-type MMTV integration site family
Zbtb16	zinc finger and BTB domain containing 16
Zbtb20	zinc finger and BTB domain containing 20
Zic1	zinc finger protein of the cerebellum 1

ACKNOWLEDGEMENTS

This work would not have been possible without the help and support of many wonderful people for which I am eternally grateful.

First and foremost, I am especially thankful to my mentor, Dr. Ava Udvadia. Her guidance, expertise, unwavering encouragement and support throughout my studies has been integral to my development as a scientist, and to my own personal growth. Thank you for showing me that I really did have it in me all along.

I would like to thank the members of my committee: Drs. Jennifer Gutzman, Julie Oliver, Doug Steeber, Kurt Svoboda, and Murray Blackmore. The advice and resources they have provided over the years has been invaluable to the completion of this work, and to my professional development. I am most appreciative to Dr. Julie Oliver for sharing her expertise on tissue culture, and to both her and Dr. Doug Steeber for making me feel like I was part of their labs. Similarly, I am grateful to Dr. Jennifer Gutzman for her constant support, and for sharing her expertise on matters both big and small. Special thanks to Dr. Kurt Svoboda for his guidance on all things microscopy in pursuit of capturing the most beautiful images. Many thanks to Dr. Murray Blackmore for providing essential reagents when they were needed, and for his helpful comments in discussion of this work.

I would also like to acknowledge others that have significantly contributed to completion of the research presented in this dissertation. I am especially grateful to Dr. Michael Laiosa, and previous members of his lab, for their assistance in isolating primary neural crest cells via FACS, and for providing a space to culture them. Special thanks to Dr. Vivian Lee, who generously provided the mouse strains for this project, and valuable

insight into the world of neural crest. I would like to thank Dr. Paul Auer for his expertise and assistance in processing and analyzing the transcriptomic data. I would also like to acknowledge the endowments made to the Biological Sciences department and the UWM Graduate School that have provided funding for resources and travel associated with this work.

Over the course of my studies I have had the privilege to teach alongside some amazing people. I have learned a great deal from Drs. Sergei Kuchin, Claire de la Cova, Steven Forst and Peter Wejksnora in the art of teaching a course, and those lessons have helped to shape my own teaching philosophy. I am also thankful to my fellow TAs, especially Kristin Ciezki, Ashwariya Shevade, Libby Falat, Kerry Brown and Sarah Sarich for their teamwork and camaraderie, which made teaching all that more fun.

I would not have been able to make it through the daily ins and outs of graduate school had it not been for my amazing labmates. To all the Udvadilinis - both past and present, and including an army of undergraduates - the time that we have spent together in the pursuit of science has been some of the most memorable for me. I am so grateful to you all. I would like to extend a special thanks to Dena Hammond-Weinberger, Jen Forecki, Ishwariya Venkatesh, and Angie Schmoldt for guiding my initial journey, and for all their encouragement along the way. For making the lab what it is today, I would especially like to thank Sumona Dhara, Sarah Sarich, Heather Leskinen, and Jason Bacon. Your unending support, and enthusiasm for science made for an inspiring, creative and super fun lab environment. I could not have wished for better brothers- and sisters-in-science. Working alongside you all has been such a pleasure. I would also like to extend a heartfelt thank you to Vidya Sambukumar, who has been with me at every

step of this journey. Thank you for always being there to share in my successes and my hardships, and for your valuable suggestions and insight into my project. Our combined forces are equivalent to 20 postdocs; let us always be twins in everything.

Importantly, none of this would have been possible without the love and support of my family. I am especially thankful to my husband, Andrew Replogle, who has always been there for me no matter what. Your unconditional love, understanding, and encouragement has been a rock in challenging times. Thank-you for supporting me in pursuit of my dreams. I love you very much. I am grateful to my children, Kahlan and Ethan, for being the spark in my life that brings me such joy and happiness. I am so proud of you both, and Momma loves you always. I would like to especially acknowledge my Mother, Jane, my Grandmother, Rose, and my Aunts, Aunt Chicken and Joyce. Thank-you all for your unending support and encouragement, and for always being there when I needed you the most. I love you all, always and always. To my brother, Larry - you might be my younger brother, but I have always looked up to you. You have a beautiful family, and I am so proud of all you have accomplished. And last but not least, I would like to acknowledge my husband's family – Teri, Mike, Katie, Heather and Melissa. I am honored to be part of the Murphy clan, thank you all for your love and support throughout the years.

Have patience with all things,

but first with yourself.

~ Saint Frances de Sales

CHAPTER I

General Introduction

The neural crest (NC) comprises a transient, multipotent progenitor population that uniquely contributes to a wide variety of tissues and structures in vertebrate animals. NC cells were originally described by Wilhem His in 1868 as a band of cells derived from the ectodermal germ layer in a distinct region arising at the interface between the neural plate and the presumptive epidermis. During gastrulation, inductive cues subsequently activate a cascade of transcriptional events leading to NC specification, and subsequent delamination from the neuroepithelial border territory. Underlying this event is the epithelial-to-mesenchymal transition (EMT), which endows NC cells with their extensive migratory properties. Depending on where they originate from along the anterior-posterior axis of the embryo, migratory NC cells are directed along established pathways defined by environmental cues to their final site of arrest. A defining feature of the NC is the potential to generate a diverse array of cell types, including ectodermal derivatives, such as the neurons and glia of the peripheral nervous system (PNS), to mesoectodermal derivatives, such as the cartilage, bone, and connective tissues of the face and throat (Le Douarin, 1982). Given its broad developmental potential, the NC is often referred to as the “fourth germ layer” (Hall, 2000), and it is regarded as a significant evolutionary driver underlying the formation of articulated jaws, and cephalic sensory organs in the vertebrate head (Gans and Northcutt, 1883).

Over the past century, the NC has been the subject of extensive study, and debate, especially upon discovering that mesenchymal tissues and structures could be produced from the ectoderm (eg. Landacre, 1921; Platt, 1883, 1887). Advances in experimental techniques, such as ablation and cell-tracking using vital dyes, performed across a multiple model organisms helped to confirm early discoveries regarding the contribution of the NC during development (eg. Dushane, 1938; Hörstadius and Sellman, 1941; Twitty and Bodenstein, 1941). In particular, pioneering transplantation experiments using quail-chick chimeras enabled tracing of avian NC cells as they migrated throughout the embryo, and identification of distinct cell fates along the anterior-posterior axis (Le Douarin, 1982). Concurrently, our understanding of NC development in mammalian embryos was greatly facilitated by the advent of the Cre-LoxP reporter system (Sauer and Henderson, 1988), in which expression of a fluorescent or LacZ reporter containing loxP-flanked stop cassettes is driven by tissue-specific expression of Cre recombinase. Transgenic mouse lines harboring Cre-LoxP reporter alleles driven by NC-specific promoters (Wnt1-cre, Danielian et al., 1998; P0-cre, Yamauchi et al., 1999; Sox9-cre, Akiyama et al., 2005; Sox10-cre, Matsuoka et al., 2005) provided *in vivo* lineage-tracing and visualization of migratory pathways, as well as the ability to genetically manipulate and purify NC cells. Furthermore, methods for isolating, expanding and differentiating avian (Baroffio et al., 1991; Calloni et al., 2009; Cohen and Konigsberg, 1975; Etchevers, 2011; Kerosuo et al., 2015; Sieber- Blum and Cohen, 1980; Trentin et al., 2004) and rodent (Bixby et al., 2002; Etchevers, 2011; Ishii et al., 2012; Maurer et al., 2007; Pfaltzgraff et al., 2012; Stemple and Anderson, 1992) NC cells *in vitro* provided a platform for dissecting mechanisms contributing to multipotency and differentiation potential.

To date, the NC continues to be one of the most studied progenitor population in the developing vertebrate embryo as it is an attractive model for uncovering the mechanisms driving multipotency and self-renewal, EMT, migration and guidance, and cell fate acquisition. In addition, understanding the molecular mechanisms mediating the progressive stages of NC cell development is extremely valuable, particularly for therapeutic purposes. For instance, genetic or environmental factors impacting proper NC development can result in pleiotropic structural and functional anomalies (Bolande, 1997), which can manifest as pediatric syndromes or disorders characterized by variable phenotypes and severities (Noack Watt and Trainor, 2014). Studies of NC growth and differentiation expand upon our knowledge of the etiology underlying many NC-related malformations, and enable development of novel diagnostic tools, treatments and therapies. Additionally, disruption of NC cell development can even lead to a predisposition to highly aggressive cancers, such as neuroblastoma, glioblastoma, and melanoma. During metastasis, cancerous cells will undergo EMT upon leaving the primary tumor, thus acquiring migratory abilities that allow them to travel long distances in the body. It is thought that cancerous cells utilize similar mechanisms employed by the NC cells during development (Keruso and Bronner-Fraser, 2012; Theveneau and Mayor, 2012), and therefore the NC acts as a good model for studying cancer progression (Hanahan and Weinberg, 2011).

Underlying the remarkable properties of the NC is a temporal cascade of extrinsic and intrinsic influences that together regulate NC development from induction to specification to migration and, finally, lineage diversification. Recent information inferred from genome-wide analyses and gene perturbation studies have led to the identification

of transcriptional and epigenetic inputs that contribute to the different steps (Meulemans and Bronner-Fraser, 2004; Sauka-Spengler and Bronner-Fraser, 2008; Simões-Costa et al., 2014). Culmination of this information has led to the assembly of a gene regulatory network (GRN) orchestrating the progression of NC cell development (Fig. 1; reviewed in Martik and Bronner, 2017). Each step in the GRN is characterized by a gene expression module comprised of positive and repressive gene regulatory interactions that noedt only drive the associated process, but activate the expression downstream gene batteries encoding regulators that initiate the next step. In this way the GRN acts as a feed-forward loop, which when coupled with the combined action of several signaling pathways, is capable of executing precise morphological, behavioral and physiological outputs (Davidson, 2010).

Currently, most of the regulatory information compiled focuses on NC cell induction, specification and migration. While modules for various NC derivatives have been formulated, the information is restricted to genetic control of the terminally differentiated state. However, differentiation is a dynamic, multistep process where multipotent NC progenitors gradually acquire morphological and behavioral characteristics necessary for cell type-specific function. Thus, we are currently lacking modules that represent the initiation of lineage-specific programming and the subsequent progression through the intermediate stages of differentiation toward a particular cell type. This absence of information precludes our ability to determine how genetic or environmental insult might accelerate or delay the differentiation process, resulting in NC-related defects and disorders.

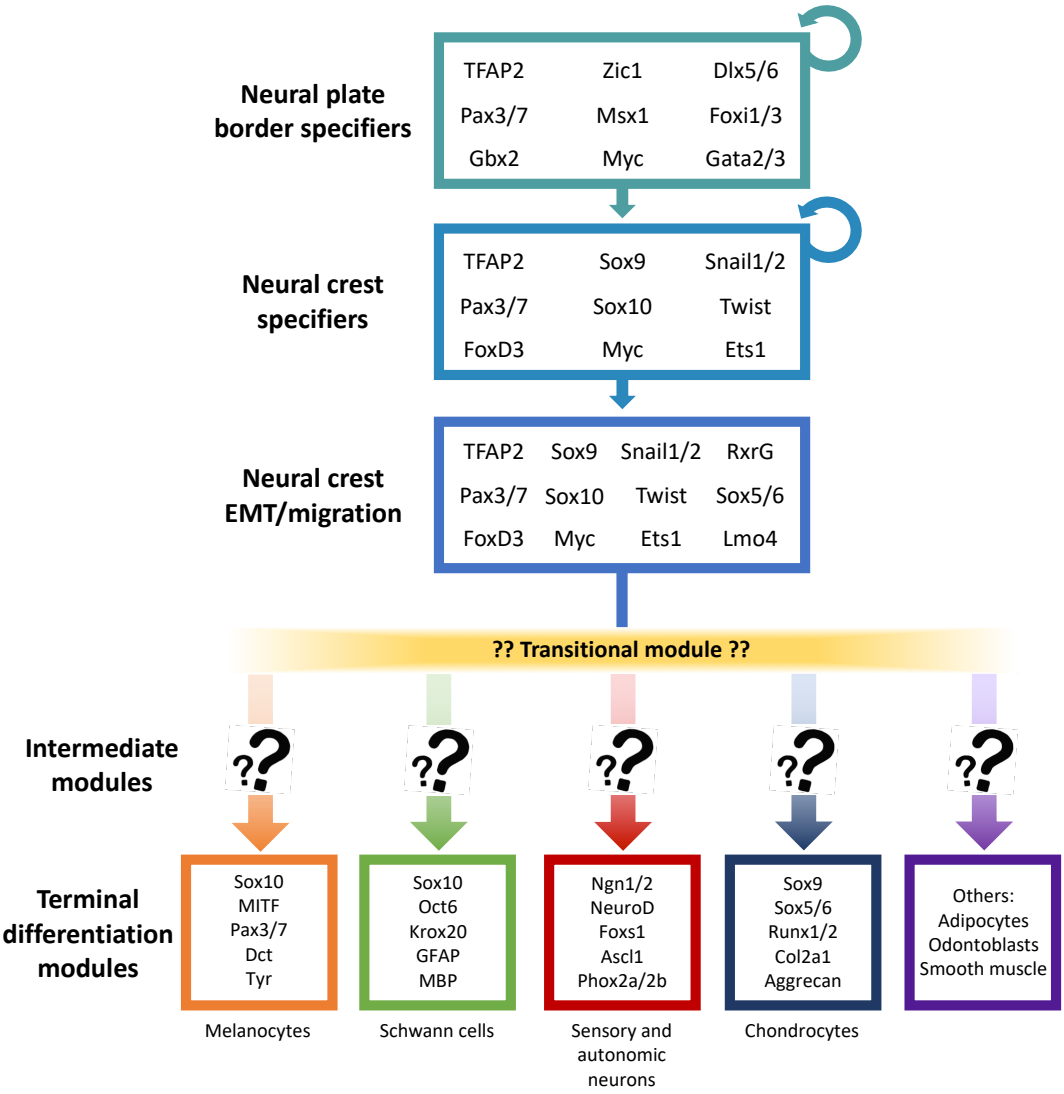

Figure 1: Overview of the current gene regulatory network (GRN) governing neural crest cell development. Cumulative information gathered from genome-wide analyses and gene perturbation studies across various vertebrate models has led to the assembly of a putative GRN for the different phases of NC cell development (reviewed Martik and Bronner, 2017). Each module comprises transcription factors that participate in cross-regulatory and auto-regulatory interactions to govern gene expression associated with a particular phase, but also drive initiation of the next phase. Reciprocal signaling interactions in the ectoderm lead to the activation of neural plate border specifiers, which define the neural plate border domain, and control downstream expression of NC specifiers (Groves and LaBonne, 2014; Meulemans and Bronner-Fraser, 2004; Prasad et al., 2012). NC specifiers endow cells within the neural plate border with an identity indicative of premigratory NC precursors (Aybar et al., 2003; Dottori et al., 2001; Khudyakov and Bronner-Fraser, 2009). Stabilization of the NC specification module results in the activation of the EMT effector program, which enables premigratory NC cells to delaminate from the neural plate border territory and become motile (Barriga et al., 2013; Cano et al., 2000; Cheung et al., 2005; Simões-Costa et al., 2014). Migratory NC cells undergo differentiation in to various NC cell derivatives. While differentiation modules for various cell types have been formulated (Akiyama et al., 2002; Kim et al., 1998; Lee et al., 2000; Marmigère and Ernfors, 2007; Morikawa et al., 2009; Murisier et al., 2007; Stolt and Wegner, 2016), the information is limited to the genes involved in maintaining the terminally differentiated state. Consequently, the transcriptional programming governing the initial transition towards a specific cell type, and the regulatory factors driving the subsequent progression through the intermediate stages of differentiation into that cell type are not well understood.

The overall purpose of the research presented in this dissertation was to expand our understanding of the intrinsic programming governing the temporal progression of NC cell differentiation. To achieve this, our goal was to first establish a robust culture system modelling the intermediate stages of mammalian differentiation along ectodermal and mesoectodermal lineages. With this tool in hand, we next sought to identify mechanisms that regulate the timing of NC cell differentiation in order to begin filling in the missing modules in the current GRN regarding the intermediate stages of this process, and increase our overall understanding of the genetic regulation of NC cell diversification. In this chapter, we present a brief overview of NC development, with a particular focus on our current understanding of the programming controlling terminal differentiation.

Overview of NC cell development

Formation of the NC: Induction and Specification

During gastrulation NC cells are induced in the ectodermal germ layer in a region that lies at the edge of what will become the central nervous system (CNS) and epidermis, called the neural plate border (NPB). Establishment of the NPB occurs in a series of steps mediated by reciprocal signaling interactions between the neural and non-neural ectoderm, as well as the underlying paraxial mesoderm (Groves and LaBonne, 2014; Prasad et al., 2012). The first step involves the dynamic interplay between three major signaling pathways: WNT, BMP and FGF, although Notch and retinoic acid activity also contribute to defining the NPB domain. While the sources of these signals and contribution to NPB induction might vary between species, the consensus model indicates that intermediate WNT and BMP levels, combined with FGF signals secreted from the

paraxial mesoderm, are necessary to define the NPB domain from which the NC cells are formed.

Stabilization of morphogen gradients activate a transcriptional circuit in the NPB that leads to the expression of NPB specifiers: TFAP2, Msx1, Zic1, Pax3/7, Dlx5/6, and others (Meulemans and Bronner-Fraser, 2004). Coordination of gene activation depends on differential enhancer activity in response to WNT, BMP and FGF activity (Garnett et al., 2012). At first, the expression of these genes across the domain is not uniform, and NPB cells are capable of contributing to neural, NC and placodal cell fates (Roellig et al., 2017). However, initiation of positive feedback loops within the module, and continued cross-regulatory interactions between the NPB and neighboring territories, serve to sharpen the boundaries of each distinct domain, thus separating the future NC from other cell fates (Matsuo-Takasaki et al., 2005; Nikitina et al., 2008; McLarren et al., 2003). Refinement of the NPB region also potentiates expression of key regulators which drive NC specification, such as Msx1, Pax3/7 and TFAP2.

Initiation of NC specification occurs at the late gastrula stage with the expression of Ets1, FoxD3, Snail1, and Snail2 (also known as Slug) (Khudyakov and Bronner-Fraser, 2009), all of which are direct transcriptional targets of NPB specifiers. These transcriptional regulators are responsible for activating a suite of NC specifier genes that together solidify NC cell fate. In this regulatory program, FoxD3 activates Sox10 expression in mouse NC (Dottori et al., 2001), while Snail1 and Snail2 promote expression of Twist1 and Sox9 in frog NC (Aybar et al., 2003). In addition, NC specifiers interact with one another in cross-regulatory and auto-regulatory loops in order to promote robust maintenance of the transcriptional circuitry. The period of NC specification is

relatively short, concluding when the neural folds begin to elevate as the neural tube closes during the process of neurulation. At this stage of development, premigratory NC precursors exhibit a distinct regulatory state characterized by expression of a full complement of NC specifier genes: cMyc, Ets1, FoxD3, Id, Pax3/7, Snail1/2, SoxE factors (Sox 8/9/10), TFAP2a, and Twist.

Stabilization of the specification program serves as a catalyst for activation of the EMT effector program, which enables NC cells to delaminate from the NPB and become invasive. As such, NC specifiers are known to play direct role in regulating cell-cell interactions and cytoskeletal changes required for EMT. In addition, many continue to be expressed in migratory NC, and are required for downstream lineage diversification. For instance, Sox10 expression persists in cells that contribute to peripheral neurons and glia, as well as melanoblasts (Aoki et al., 2003; Kim et al., 2003), whereas Sox9 regulates differentiation of cartilage-matrix producing chondrocytes in the head (Lefebrvre et al.,1997). Moreover, SoxE factors have been shown to be crucial for maintaining multipotent potential and survival of the NC (Haldin and LaBonne, 2010). Similarly, other specifiers are also known to be involved in regulating stem cell characteristics and differentiation potential. Clonal analysis of NC stem cells (NCSCs) isolated from FoxD3 mutant mice display a severe reduction in self-renewal, and the ability to give rise to neurons, glia and melanocytes (Mundell and Labosky, 2011), indicating a role for FoxD3 in maintaining stem cell-like characteristics, and modulating cell fate choice by preserving neural potential. Additionally, cMyc has been shown to regulate the timing of differentiation through repression of its downstream target, Id3 (Light et al., 2005), thus preventing premature cell fate decisions. Persistent expression of Id3 in NC cells causes

ectopic Sox10 expression, thus promoting a neural phenotype in cells that would have normally adopted a chondrocyte cell fate. These studies demonstrate an essential role for NC specifiers in establishing a progenitor state during the early stages of NC development through maintenance of stem cell-like properties, such as self-renewal and multipotent potential, but also in the timely activation of downstream programming associated with migration and differentiation.

Mechanisms of NC migration

Delamination and epithelial-to-mesenchymal transition

Once specified, NC cells undergo a series of cellular changes in order to physically separate from the neuroectoderm, and become motile. This multistep process is mediated by an EMT effector program which coordinates signaling and transcriptional inputs to regulate dramatic changes in cell-cell adhesion, cell-extracellular matrix (ECM) interactions, and cytoskeletal architecture, allowing the NC cells to become less adhesive and more motile. While all NC cells undergo EMT, the timing of delamination is different depending on species. For instance, delamination occurs before the neural tube has closed completely in mouse and *Xenopus (*Hörstadius, 1950), but after neural tube closure in chick (Duband and Thiery, 1982). The axial origin along the length of the embryo also contributes to subtle variations in how this process unfolds. Cephalic NC cells tend to emerge as a collective, and delamination is not coupled with cell cycle (Theveneau et al., 2007). In contrast, posterior trunk NC cells emerge progressively over time, and delamination is linked with G1/S phase transitions in the cell cycle (Kalcheim and Burstyn-Cohen, 2005; Thiery et al., 1982). One explanation for these variations

include spatiotemporal differences in the upstream regulators responsible for triggering EMT along the anterior-posterior axis of the embryo, such as BMP and WNT signals. In addition, there are differences in transcription factors expressed in the NC at each axial level that may account for differences in behavior. For instance, Ets1 is only expressed in the cephalic NC and contributes to the collective dispersion observed during NC delamination in the head (Theveneau et al., 2007). Nevertheless, many of the major transcriptional regulators that drive EMT, and therefore contribute to the overall morphological changes necessary for delamination, and subsequent migration, are conserved across species. These aspects are briefly highlighted in this section.

While residing in the NPB, premigratory NC cells exist in a polarized, epithelial sheet, and are tightly associated with one another through adherens junctions. One of the first events to occur during EMT is the dissolution of these cell-cell interactions to promote a more motile state. This involves a switch in cadherin-based cell adhesion from type I cadherins (E-cadherin, N-cadherin), which promote strong cell-cell interactions and stabilization of an epithelial phenotype, to type II cadherins (Cadherins 6b/7/11), which are associated with increased motility (Obrink, 1986). NC specifiers, Snail1 and Snail2 are well-characterized mediators of cadherin-switching, and function as transcriptional repressors that downregulate type I cadherins, most notably E-cadherin (Cano et al., 2000). Other NC specifiers work cooperatively with Snail factors to facilitate cadherin-switching, either through upregulation or downregulation of type I and type II cadherins, including FoxD3, Sox10 and Twist1 (Barriga et al., 2013; Cheung et al., 2005), thus shifting the balance toward reducing overall cell adhesion.

Concurrently, to fully detach from the neuroepithelium, delaminating NC cells must decrease their adhesion to the ECM that comprises the basement membrane. This is achieved by either reducing cell-ECM interactions or remodeling the ECM, and both can be modulated by metalloproteases (MMP), tissue inhibitors of MMPs (TIMP), and disintegrin and metalloproteases (ADAM). For instance, ADAM10 and ADAM13, are proteases that cleave the extracellular domains of transmembrane proteins associated with ECM, and play important roles in ECM remodeling. ADAM proteases are expressed in cranial NC cells and have been shown to cleave fibronectin substrates during initial emigration from the neuroectoderm (Alfandari et al., 2001). Interestingly, this same study also found that ADAM-mediated ECM remodeling was important for downstream migration in a stream-dependent manner, and proposed a model in which the first cranial NC cells to emerge might leave a path of remodeled ECM behind them that subsequent cells could follow. In addition, ADAM proteases are capable of cleaving the extracellular domain of cadherin proteins (McCusker et al., 2009), further reducing cell-cell adhesion leading to detachment and dispersal.

Snail factors, particularly Snail2, also appear to promote cell dispersion by controlling actin dynamics through upregulation of RhoB, a member of the Rho family of GTPases (del Barrio and Nieto, 2002), and inhibition of RhoB activity prevents NC cell delamination from chick neural tube explants (Liu and Jessell, 1998). Subcellular localization and levels of Rho activity have the ability to regulate actin polymerization and actin-mediated attachment to the cell membrane, thus facilitating cell dispersion (Sit and Manser, 2011). Accordingly, a more recent study using Rho biosensors to track *in vivo* dynamics in live zebrafish found Rho and Rho-kinase (ROCK) signaling to be enriched

apically in delaminating NC cells (Clay and Halloran, 2013). This led to changes in filamentous actin (F-actin) localization, actomyosin contractility and tension that resulted in apical detachment from the neuroepithelium, and cell retraction toward the basal lamina. Retracting cells also exhibited a blebbing phenotype with Rho activity restricted to the protruding edge, resulting in initial forward motility upon detachment from the neuroepithelium. Together, the EMT effector program, driven by NC specifiers can regulate diverse downstream outputs that orchestrate cellular changes necessary to transform tightly adherent, epithelial cells into loose, motile cells that are capable of undergoing directed migration.

NC migration and guidance

Following EMT, NC cells invade the space between the epidermal layer and the underlying mesenchyme, and migrate throughout the embryo guided along stereotypical pathways by external guidance cues. As a whole the NC can be divided into subpopulations based on their site of origination along the anterior-posterior body axis: cranial, vagal, trunk, and sacral. NC cells in each subpopulation initially emerge as a sheet-like wave, but are quickly divided into distinct streams depending on their axial origin. In addition, the distinct microenvironments and signals that the NC cells encounter as they migrate, as well as their final destination, have the ability to influence their cell fate. Cranial NC, which only migrate throughout the embryonic head, emerge from the hindbrain (rhombomere segments r1-r7) and are divided into 3 streams: (1) cells emerging from r1 and r2 will migrate to the frontonasal process and first pharyngeal arch where they form the skeletal elements of the face, and bones of the ear, (2) cells from r4

populate the second pharyngeal arch, giving rise to the cartilage of the neck, and (3) cells emerging from r6 populate the third and fourth pharyngeal arches, where they contribute to forming the thymus, parathyroid and thyroid glands (Le Lievre and Le Douarin, 1975). In addition, a subset of NC cells from r6, termed the cardiac NC, will continue to migrate toward the heart where they contribute to parts of the septum of the outflow tract (Waldo et al., 1998). The vagal NC, a transitional population found between the cranial and trunk NC, emerges from the hindbrain region adjacent to somites 1-7 and contributes to the smooth muscle that lines the aortic arch arteries and portions of the enteric nervous system, among other derivatives (Hutchins et al., 2018). The trunk NC emerges between somites 8-27, and splits into 2 discrete streams: (1) a dorsolateral stream in which NC cells move between the epidermis and the somites to colonize skin and hair follicles, giving rise to melanocytes, and (2) a ventral stream in which migration is restricted to the anterior portion of the somites. The NC cells that migrate along the ventral pathway contribute to sympathetic and dorsal root ganglia, adrenomedullary cells, and Schwann cells (Le Douarin and Teillet, 1974). Lastly, the sacral NC, which contributes to the enteric nervous system, arises posterior of somite 28 (Pomeranz et al. 1991).

Migratory routes are defined by positive and negative guidance cues, as well as permissive ECM molecules, which ensure that the NC cells remain on track. We will briefly focus on these guidance mechanisms in the cranial and trunk NC as it is most relevant to the work presented in this dissertation. In the head, cranial NC cells are directed into three distinct streams by establishing NC-free zones adjacent to r3 and r5. This is achieved through the inhibitory action of eph/ephrins and semaphorin/neuropilin/plexin signaling pathways. In mouse, cranial NC cells express a complex combination of ephrins and Eph

receptors (Davy et al., 2004), which when coupled with ephrin and Eph receptor distribution in the surrounding mesenchyme results in a “code” that promotes proper cranial NC patterning by preventing the streams from mixing (Baker and Antin, 2003). Cranial NC cells also express neuropilins 1 and 2, and plexinA, which are receptors sensitive to class3-semaphorin ligands secreted from surrounding tissues, specifically r3, r5 and the otic vesicle, which also acts as a physical barrier influencing migratory patterning (Eickholt et al., 1999; Gammill et al., 2007). Both signaling pathways contribute to maintaining NC-free zones by causing cell protrusions to collapse upon contact, and disruption of signaling leads to ectopic migration outside the specified routes.

While negative guidance cues keep the streams distinct, a variety of positive regulators direct the cranial NC cells toward their final destinations. Some of the most characterized include FGF, VEGF, PDGF signaling, all of which have been implicated in driving the migratory NC toward the frontonasal process, and into the pharyngeal arches (Kubota and Ito, 2000; McLennan et al., 2010; Sato et al., 2011; Smith and Tallquist, 2010; Trokovic et al., 2005). Another positive regulator is the chemokine Stromal cell-derived factor 1 (SDF1, also known as CXCL12), which is secreted by the pharyngeal endoderm and the epibranchial placodes (Olesnicky Killian et al., 2009; Theveneau et al., 2010). *In vivo* and *in vitro* studies have shown that binding of SDF1 to its receptor, CXCR4, is sufficient to attract cranial NC cells as they migrate ventrally away from the neuroectoderm and into the pharyngeal arches during migration in *Xenopus* (Theveneau et al., 2010). In addition, SDF1/CXCR4 signaling serves to stabilizes cell protrusions through activation of Rac1, a small GTPase, thus promoting directed migration.

In trunk NC cells, directed migration along the ventral pathway is controlled by negative regulators expressed on the posterior portion of the somites, which serves to restrict movement along the anterior half. Establishing this NC-free zone is mediated by the similar signaling pathways as described for the cranial NC, including Eph/ephrin and neuropilin/semaphorin signaling. Trunk NC cells express EphA/B receptors, and neuropilin1/2, while the posterior half of the somites expresses Ephrin-B ligands, and Semaphorin F. Disruption of these signaling cues leads to unsegmented migration and fusion of the peripheral ganglia (Baker and Antin, 2003; De Bellard et al., 2002; Gammill et al., 2006; Schwarz et al., 2009) Slit/Robo signaling also ensures that the migratory cells are guided along their respective pathways by selectively preventing trunk NC from entering the gut, while concurrently allowing the vagal NC passage (De Bellard et al., 2003). Finally, trunk NC cells are responsive to SDF1/CXCR4 signaling, but in a species-specific manner as trunk NC cells expressing CXCR4 give rise to dorsal root ganglia in the mouse (Belmadani et al., 2005), but sympathetic ganglia in chick (Kasemeier-Kulesa et al., 2010), and in both cases, of SDF1/CXCR4 lead to aberrant ganglia formation.

Eph/ephrin, Slit/Robo, and endothelin signaling regulate trunk NC cells as they migrate along the dorsolateral pathway. Trunk NC cells exhibit differential expression of Eph, Robo and endothelin receptors depending on the timing of emigration from the neural tube, which dictates if they continue along the dorsolateral or ventral path (Harris et al., 2008; Jia et al., 2005; Pla et al., 2005; Santiago and Erickson, 2002). The first wave of trunk NC cells tend to express EphB3, Robo1/2, and endothelin receptor B, and are forced toward the ventral pathway, where they will contribute to neural derivatives. However, trunk NC precursors in subsequent waves express EphB2 and endothelin

receptor B, which respond positively to surrounding ephrin and endothelin signals, thus promoting continued migration along the dorsolateral pathway. These NC cells will go on to colonize the skin giving rise to melanocytes. Although, species-specific variation in determining pathway preference has been observed. For instance, melanocyte precursors in zebrafish and frog can travel along either the dorsolateral or ventral pathway, indicating that there are a portion of trunk NC cells that may be controlled by other unidentified guidance cues (Collazo et al., 1993).

While guidance cues help to establish a defined route, positive and negative guidance cues alone are not enough to account for the high degree of directionality observed during NC cell migration. As a collective, NC precursors will migrate in chains or as clusters of cells, and directionality is mediated through transient cell-cell interactions in a process known as contact inhibition of locomotion (CIL). During CIL, collision between two cells leads to retraction of protrusions at the site of contact. This results in a shift in cell polarity that restricts more stable protrusions to a new leading edge within the cell, thus providing the means to elicit a change in direction (Mayor and Carmona-Fontaine, 2010). This process relies on homotypic binding of N-cadherin and reciprocal non-canonical Wnt/PCP signaling at the site of contact, which control the activity of small GTPases Rac1 and RhoA. Collision activates RhoA and inhibits Rac1, thus resulting in cytoskeletal rearrangement and cell repolarization (Carmona-Fontaine et al., 2008; Theveneau et al., 2010). RhoA activity is associated with the back or trailing edge of a cell, where it controls stress fiber contractility associated with focal adhesions. In contrast, Rac1 is crucial for stabilizing the dynamics of the actin cytoskeleton at the front or leading edge of a cell (Ridley and Hall, 1992). The combined action of both RhoA and Rac1 are

required for directed migration, and if either are disrupted CIL is inhibited and cells produce ectopic protrusions. In that light, CIL also mediates cell dispersion by preventing migrating NC cells from overlapping one another.

Furthermore, the dispersive effect of CIL is counteracted by a process known as co-attraction. In this mechanism, migrating NC cells secrete complement factor C3a, but also express its receptor, C3aR. Reciprocal, paracrine signaling produces a localized C3 gradient that pulls migratory NC cells toward one another. Binding of C3a to its receptor activates Rac1, thus repolarizing the cells and establishing a new leading edge. This changes the direction of the cells such that they move back toward the collective (Carmona-Fontaine et al., 2008). In this way, migratory NC cells never stray too far away from their respective stream, and are able to maintain a collective state as they migrate throughout the embryo. When taken as a whole, robust directed migration in the NC is mediated by the combined efforts of cell dispersion and co-attraction, as well as repulsive and permissive environmental guidance cues. Together these mechanism drive migratory NC cells toward their final sites of arrest within the embryo, where they ultimately differentiate into a variety of derivatives.

Diversification in the NC

Cell fate determination in the NC is a multistep process that unfolds gradually over time, in which NC cells undergo a series of morphological and behavioral transformations to attain cell type-specific function. While NC cells are exposed to a variety of cues during migration that may bias differentiation capacity toward a particular cell fate, several studies have shown that a majority of the NC cells remain multipotent up until this point,

both *in vitro* (Baroffio et al., 1991; Bronner-Fraser and Fraser, 1988; Sieber-Blum and Cohen, 1980; Trentin et al., 2004), and *in vivo* (Baggiolini et al., 2015; Bronner-Fraser and Fraser, 1988, 1989; McKinney et al., 2013; Serbedzija et al., 1990). How NC cells lose their multipotent potential as they undergo differentiation continues to be an area of active investigation.

As migrating NC cells begin to colonize regions of the embryo, they will transition from migratory streams to forming cell aggregates, which interact with surrounding cell populations to form various tissues and structures (Bronner and Le Douarin, 2012). As a whole, the NC has the remarkable capacity to give rise to a multitude of diverse cell types. However, specific derivatives are predominantly determined by where NC cells originated from along the length of the embryo, with exception of melanocytes, which are derived at all axial levels (Le Douarin, 1982).

Cranial NC cells give rise to a larger diversity of differentiated cell types compared to other NC cell populations, and are considered a major contributor to the formation of the vertebrate head. The cranial NC cells uniquely give rise to cartilage and bone that comprise the craniofacial skeleton, including the upper and lower jaw (Couly et al., 1998), bones in the middle ear (Anthwal and Thompson, 2016) and odontoblasts of the dental papilla (Chai et al., 2000). In addition, they contribute to connective tissues, such as the stroma of the thymus, parathyroid and thyroid glands (Le Lievre and Le Douarin, 1975), and the cornea endothelial and stromal cells of the eye, as well as the ciliary muscles of the anterior segment (Gage et al., 2005). They also give rise to the adipocytes of the face and neck (Billion et al., 2007), and the smooth muscle cells that line the blood vessels found in the face and forebrain (Etchevers et al., 2001). Lastly, cranial NC cells also

contribute to some of the cranial ganglia (superior and jugular ganglia, Thompson et al., 2010; ciliary ganglion, Lee et al., 2003) and portions of the facial, trigeminal, glossopharyngeal and vagal nerves, as well as the glial cells that myelinate them (Couly et al., 1998).

Trunk NC cells contribute to the different types of dorsal root ganglia, together enabling sensation of touch, temperature, and pain stimuli, and proprioception. They also give rise the sympathetic and parasympathetic ganglia, Schwann cells, and adrenomedullary cells (Le Douarin and Teillet, 1974). Finally, the vagal NC cells contribute to portions of the heart and enteric nerves of the gut (Hutchins et al., 2018), while sacral NC largely contribute to the enteric nervous system (Pomeranz et al. 1991).

Distinct gene regulatory modules associated with different NC cell derivatives have been established. Our current understanding of these circuits is centered around the contribution of NC specifiers, for instance Sox10 for the neural lineages, and Sox9 for chondrogenesis, and known signaling inputs from surrounding tissues. However, they are incomplete, as many questions still remain concerning the direct regulatory interactions that mediate the transition toward a particular cell fate (Betancur et al., 2010; Meulemans and Bronner-Fraser, 2004). In the sections that follow we will briefly discuss some of the regulatory mechanisms that contribute to the differentiation of ectodermal and mesoectodermal derivatives, with a specific focus on peripheral gangliogenesis, and the formation of the craniofacial skeleton.

Peripheral neurogenesis

NC cells give rise to components of the PNS, which include sensory and autonomic neurons, including sympathetic and parasympathetic ganglia, as well as Schwann cells. In general, sensory neurons function to sense external stimuli, such as touch, pain and temperature, and relay that information to the CNS. During sensory neurogenesis in dorsal root ganglia, migratory trunk NC cells undergo differentiation in three waves, where each give rise to a different sensory neuron subtype. In the first wave, trunk NC cells form large diameter proprioceptive and mechanoreceptive neurons, which sense touch, limb movements and position. These neurons express the neurotrophic tyrosine receptors TrkB (NTRK2) and TrkC (NTRK3), and respond to neurotrophic factors brain-derived neurotrophic factor (BDNF) and Neurotrophin 3 (NT-3) for survival. The second wave produces small diameter nociceptive neurons, responsible for sensing pain, as well as more TrkB/TrkC neurons. Based on their expression of TrkA (NTRK1), nociceptive neurons can be classified as peptidergic (TrkA+) or non-peptidergic (TrkA-).

In the mouse, waves of neuronal differentiation begin at E8.5, but full maturation of the neurons doesn't occur until much later in embryonic development. During that time the various subtypes are further specified through activation of a cascade of transcriptional regulators driven by WNT signaling (Ikeya et al., 1997). First, neurogenin1 and 2 (Ngn1/2) are expressed, which bias the neurons along the sensory lineage, rather than the autonomic lineage (Perez et al., 1999; Zirlinger et al., 2002). Ngn1 appears to specify TrkA+ neurons, although it has been shown to play minor roles in specification of the other neuronal cell types, as well. Ngn2 is expressed predominantly in TrkB+/TrkC+ cells, albeit transiently, as it is downregulated over time. Ngn1/2 activates expression of

the Neuronal Differentiation (NeuroD) family of transcription factors, as well as Forkhead Box S1 (Foxs1), Brain-Specific Homeobox/POU Domain Protein 3A (Brn3a), Runt-Related Transcription Factor 1 or 3 (Runx1/3) and Ret Proto-Oncogene (Ret), which promote terminal differentiation depending on the levels of Runx1/3 and Ret. Specifically, TrkB+/TrkC+ cells will become mechanoreceptive in the presence of Runx3 and Ret, but low levels of Ret specify the proprioceptive cell fate. Finally, diversification into TrkA+ peptidergic neurons requires Ret, but expression of Ret and Runx1 promotes generation of TrkA- non-peptidergic neurons (reviewed in Marmigère and Ernfors, 2007).

Moreover, studies have showed that as Ngn factors are increasingly expressed, Sox10, which was expressed in the migratory NC, is downregulated (Zirlinger et al., 2002). Sox10 expression is not necessary for dorsal root gangliogenesis, but does play a crucial role in the development of Schwann cells. Schwann cells not only myelinate the dorsal root ganglia, but they provide trophic support essential for survival. Accordingly, dorsal root ganglion formation occurs normally in Sox10-null mice, however the neurons undergo apoptosis shortly thereafter (McKeown et al., 2005; Sonnenberg-Riethmacher et al., 2001). Thus, activation of Ngn promotes sensory neuron differentiation by activating a downstream cascade of gene expression events leading to subtype specification, and by repressing competing fate programming.

Sympathetic ganglia, on the other hand, are responsible for maintaining homeostasis by regulating hormone release, heart rate and blood pressure. In the trunk, BMP signaling cooperates with Sox10 to induce a sympathetic cell fate through induction of Achaete-Scute Family BHLH Transcription Factor 1 (Ascl1) and Paired Mesoderm Homeobox Protein 2B (Phox2b) (Kim et al., 2003; Morikawa et al., 2009). These

transcriptional regulators activate Paired Mesoderm Homeobox Protein 2A (Phox2a), GATA Binding Protein 2 and 3 (GATA2/3), Heart And Neural Crest Derivatives Expressed 2 (Hand2), and Insulinoma-Associated Protein 1 (Insm1), which cross-regulate each other to mediate survival and further differentiation (Huber, 2006; Rohrer, 2011). Mature sympathetic neurons express TFAP2a, which interacts with Phox2b to activate tyrosine hydroxylase (TH), and dopamine beta hydroxylase (Kim et al., 1998), leading to production of norepinephrine, which contributes to activation of the "flight-or-fight" response in times of stress.

Currently, much of our understanding of the GRN underlying peripheral gangliogenesis is derived from studies of trunk NC (Betencur et al., 2010), and we have limited information about the mechanisms that drive this process in the head. Cranial NC cells contribute sensory neurons to the proximal ganglia of the facial, glossopharyngeal and vagal nerves, as well as the trigeminal ganglia in conjunction with placodal cells (D'Amico-Martel and Noden, 1983). Projections from the cranial NC-derived ganglia innervate the spinal trigeminal tract (Harlow et al., 2011; Harlow and Barlow, 2007), in order to relay sensory information regarding touch, pain, and temperature. In that light, cranial ganglia are similar to dorsal root ganglia in the trunk, and therefore may share similar mechanisms during differentiation in the head.

It has been shown that proper cranial ganglia assembly requires the interaction between migrating cranial NC cells and placodal cells (reviewed in Steventon et al., 2014). During gastrulation, placodal cells are induced in a domain adjacent to the NC within in the neuroectoderm. As development progresses, the ectoderm thickens and invaginates to form cranial placodes that contribute to sensory neurons and paired

sensory organs. Studies have shown that ablation of premigratory NC cells abolishes placode formation, and a loss of placodal ectoderm inhibits NC cell migration (Theveneau et al., 2013). In addition, migrating NC cells appear to form a tunnel through which placodal neuroblast cells will travel just prior to coalescence, and ablating the cranial NC results in displaced ganglia and abnormal projections to the CNS (Begbie and Graham, 2001). Finally, altered cranial NC migration in mice due to a loss of neuropilin2 results in fusion of ganglia, and ectopic neuron formation (Schwarz et al., 2008). Therefore, it is thought that the cranial NC cells provide a scaffold for integrating the two populations together to mediate proper condensation and positioning in order to facilitate full ganglion assembly.

Chondrogenesis in the cranial NC

During facial skeletogenesis, the streams of migrating cranial NC cells first colonize the frontonasal prominence and pharyngeal arches, then differentiate to form specific types of cartilage that eventually contribute to the skeletal elements of the face and throat (reviewed in D'Souza et al., 2010). NC cells that migrate into the frontonasal prominence give rise to the skeletal elements of the forehead, nose, upper lip and primary palate. Those that migrate into the first pharyngeal arch are separated into the maxillary and mandibular prominences, which contribute to the formation of the upper and lower jaw, respectively, among other elements. NC cells within the mandibular prominence form the Meckel's cartilages, which provide a scaffold for development of the lower jaw, and the malleus and incus of the ear. Those that migrate into the second arch contribute to the stapes of the ear, in addition to the hyoid bone, in conjunction with NC cells found

within the third pharyngeal arch. Finally, NC cells that migrate into the fourth pharyngeal arch give rise the thyroid cartilage.

Once migrating cells are recruited to sites of prospective skeletal element formation, chondrogenic differentiation unfolds in a series of well-described steps (reviewed in Bobick et al., 2009; Ray and Chapman, 2015). First, progenitor cells, which are initially dispersed and randomly organized, quickly aggregate to form condensations. Aggregation is mediated by increased cell-cell interactions, and changes in cell shape in which migrating cells will exchange their stellate, motile morphology for a cuboidal one, indicative of the chondroprogenitor state. Together, these changes trigger overt chondrogenic differentiation characterized by increased production of cartilage-specific matrix molecules, including various types of collagen, and proteoglycans, such as aggrecan. As chondrocytes mature they continue to synthesize and remodel the ECM, thus contributing to the integrity of the cartilaginous framework. In addition, cranial NC cells can give rise to osteogenic cells fates in response to signals derived from the pharyngeal epithelia (Hall, 1980).

Finally, craniofacial bone formation in the head occurs through both endochondral and intramembranous processes (reviewed in D'Souza et al., 2010). Ossification of the hyoid and thyroid cartilages, and bones of the ear occur through an endochondral process in which mature chondrocytes differentiate toward a terminal hypertrophic state and undergo apoptosis, thus allowing infiltration of osteoblasts that facilitate bone mineralization (Mackie et al., 2008). In contrast, the mandible and other facial skeletal elements undergo intramembranous ossification. Concerning mandible development specifically, a portion of NC cells differentiate into osteoblasts which lay down a

mineralized bone matrix that surrounds and replaces the Meckel's cartilages (Bhaskar et al. 1953; Chai et al., 2000; Funato et al., 2009; Radlanski et al., 2003; Tomo et al., 1997). However, secondary mandibular condylar cartilages, which serve as a growth center for the mandible at later stages of development, undergo endochondral ossification (Silbermann and Frommer, 1972).

Controlling chondrogenesis in the cranial NC is a transcriptional circuit regulated by the NC specifier, Sox9. In mouse, Sox9 regulates the expression of Sox5 and Sox6 (Akiyama et al., 2002), which then cooperate with Sox9 to directly activate the expression of collagen type 2a1 (Col2a1) and aggrecan (Bell et al., 1997; Lefebvre et al., 1998; Ng et al., 1997). Sox9 transcriptional activity is dependent on histone acetyltransferase CREB-binding protein (CBP)/p300 (Tsuda et al., 2003), and maximal expression is mediated through synergistic binding of not one, but multiple enhancers often located far upstream of the target gene (Liu and Lefebvre, 2015). In addition, Sox9-mediated gene expression can be enhanced through interactions with additional binding partners, such as SMAD3, a transcriptional mediator of TGFβ signaling pathway (Furumatsu et al., 2005). Moreover, the Sox9 and Sox5/6 trio has also been shown to regulate a number of other genes involved in chondrogenesis, including ECM components, Col9a2 and Col11a2 (Bi et al., 1999), and may be involved in repressing genes associated with the hypertrophic state, such as Col10a1 (Wang et al., 2013) and Runx2 (Liu and Lefebvre, 2015). Consequently, a loss of Sox9 in in murine cranial NC cells results in a reduction in the ability to form chondrogenic nodules, increased expression of hypertrophic markers Runx2 and Col10a1, and severe craniofacial defects due to an absence of endochondral cartilage and bone elements in the face (Mori-Akiyama et al., 2003).

Other transcription factors involved in regulating chondrogenesis are the Runt-related transcription factors Runx1 and Runx2. While both Runx1 and Runx2 transcription factors are known to regulate chondrogenesis during skeletal development, they do so in a stage-specific manner. Runx1 is highly expressed in mesenchymal condensations observed early in the differentiation process (Wang et al., 2005), and enhances cartilage matrix production in cooperation with Sox9 (Yano et al., 2019). In addition, Runx1 expression suppresses the hypertrophic state, partly through its repression of Bapx1 (also known as Nkx3.2; Yano et al., 2019), thus supporting the continued maintenance of the pre-hypertrophic state. In contrast, Runx2 plays an essential role in promoting the terminal hypertrophic state by directly activating osteocalcin (Ducy et al., 1997), Col10a1 (Li et al., 2011), and MMP13 (Hirata et al., 2012), all of which are involved in ECM remodeling and mineralization associated with bone formation. Accordingly, terminal differentiation was delayed in Runx2 knockout mice, and this was coupled with a complete loss of hypertrophic chondrocytes (Yoshida et al., 2004).

One common theme inherent to the transcriptional network underlying chondrogenesis is the reciprocal antagonism that exists between the factors associated with either the pre-hypertrophic or hypertrophic state. While we have a fundamental understanding of a handful of regulators that control the early and terminal stages of chondrogenesis, we currently lack information regarding regulation of the intermediate pre-hypertrophic state - the factors that maintain it, thus preserving the integrity of the cartilaginous framework, and those that might shift the balance toward chondrocyte hypertrophy and bone formation. In the developing embryo, chondrocytes differentiate and mature over time and the progression through each step depends on the interplay

between cell-intrinsic programming and external signaling. Discovering the transcriptional regulators, and upstream signaling inputs, driving the intermediate stages would not only yield a more comprehensive understanding of the GRN driving chondrogenic differentiation, but it would provide insight into how misregulation of these factors contribute to the formation of cranial NC-related craniofacial defects.

Thesis statement:

The current regulatory paradigms for NC differentiation along the ectodermal and mesoectodermal lineages focus primarily on the terminally differentiated state while overlooking the intermediate stages of the process (reviewed in Martik and Bronner, 2017). Moreover, much of our knowledge regarding the overall transcriptomic control of peripheral gangliogenesis or chondrogenesis is not obtained from the cranial NC, but from similar cell types, such as dorsal root ganglia derived from the trunk NC, or chondrogenesis in mesoderm-derived stem cells or tissues. One possible explanation for this gap in knowledge is that the cranial NC is a rare and transient population of cells, and the intermediate stages of differentiation are difficult to capture *in vivo*.

While methods for isolating and expanding NC cells *in vitro* have been developed, characterization of the cultures is limited to validation of cell identity and differentiation potential, and therefore lacking pertinent information regarding how NC cells differentiate into a particular cell type over time. In order to address essential questions regarding the molecular mechanisms that govern this time-sensitive and stepwise process, we established a culture system modeling the temporal progression of mammalian NC cell differentiation. We present a detailed characterization of the morphological and

behavioral changes that occur as NC cells differentiate along the neural and chondrogenic lineages. The temporal benchmarks that constitute each differentiation timeline allowed for detection and enrichment of cells within the intermediate stages of differentiation, thus enabling dissection of the transcriptional programming underlying their progression.

Using this culture system, we explicitly interrogated cranial NC cells to uncover the dynamic gene expression changes that occur over the course of neurogenesis and chondrogenesis. Our analysis revealed distinct transcriptional signatures corresponding to the intermediate stages, as well as putative regulators that drive the differentiation process over time. We also demonstrate that despite being two very different cell types, peripheral neurons and cartilage-matrix producing chondrocytes share many features in common, including morphological and behavioral changes during differentiation, and the transcriptional programming that governs key biological processes and pathways underlying those changes. These results provide crucial insight into the mechanisms that drive neurogenesis and chondrogenesis in the developing head. In addition, the work presented here serves as a platform to uncover novel cellular and molecular mechanisms that contribute to the etiology and pathogenesis of cranial NC-related structural and functional birth defects and disorders.

Chapter II

Materials and Methods

Experimental animals

All animal procedures were conducted according to NIH's Guide for the Care and Use of Laboratory Animals and approved by the Institutional Animal Care and Use Committee (IACUC) at the University of Wisconsin-Milwaukee. *Sox9*-cre mice, in which an IRES-Cre-pA cassette was inserted within the 3'UTR of the endogenous Sox9 gene, were a kind gift from Dr. Benoit de Crombrugghe (Akiyama et al., 2005). *B6.129X1-Gt(ROSA)26Sor* $^{tm1(EYFP)Cos}$*/J* mice (Srinivas et al., 2001), henceforth designated as *R26R-EYFP*, were obtained from Jackson Laboratory (Bar Harbor, ME). Timed matings between homozygous mice from each strain were conducted to produce *Sox9cre; R26R-EYFP* embryos. The presence of a vaginal plug on the following morning was counted as embryonic day (E) 0.5.

Neural crest cell culture

Primary cranial and trunk NC cells were cultured using protocols adapted and modified from Stemple and Anderson, 1992; Bixby et al., 2002; Ishii et al., 2012.

Basal medium

The basal medium was prepared as previously described (Bixby et al., 2002). Basal medium comprised: Dulbecco's Modified Eagle's Medium (DMEM)- Low glucose,

pyruvate (Gibco), 30% Neurobasal-A Medium (Gibco), 15% Chick embryo extract (prepared as described in (Stemple and Anderson, 1992), 55 mM 2-mercaptoethanol (Gibco), 1% N2 supplement (Gibco), 2% B27 supplement (Gibco), 100 U/mL penicillin and 100 μg/mL streptomycin (Corning). Basal medium was sterile filtered (0.22 μm pore size) and supplemented with 25 ng/mL recombinant human basic fibroblast growth factor (bFGF; R&D Systems), 20 ng/mL recombinant human insulin-like growth factor 1 (IGF1; Gibco) and 35 ng/mL retinoic acid (Sigma).

Isolation and expansion

Cranial or trunk tissues were specifically dissected from at minimum 6 *Sox9cre; R26R-EYFP* mouse embryos at E9.5. Cranial tissues were dissected rostral of the otic vesicle, excluding the pharyngeal arches and frontonasal process, and trunk tissues were dissected between somite 8 and somite 24 to avoid isolation of the vagal NC. Dissection of cranial or trunk tissues took place in ice cold phosphate-buffered saline (PBS) with no calcium and magnesium. Upon dissociation, four cranial or trunk tissues were pooled into one well of a 24-well plate, and tissues were enzymatically digested in 400 uL Accumax (STEMCELL Technologies) for no more than 15 minutes with agitation on a nutator. Reactions were quenched in 10% heat inactivated fetal calf serum (HI-FCS; Gemini Bio-Products) in DMEM (Gibco), and pelleted at 300g for 5 minutes. After aspirating the supernatant, cell pellets were resuspended in 250 uL fresh 10% HI-FCS/DMEM. Cranial or trunk cell suspensions were subjected to fluorescence activated cell sorting (FACS; BD FACSAria III flow cytometer, equipped with a 70 μm nozzle) in order to isolate EYFP-positive cranial or trunk NC cells.

Live, EYFP-positive cranial or trunk NC cells were grown in basal medium at 37ºC, 5% CO_2 on tissue culture-treated plates/flasks coated with 50 μg/mL Poly-D-Lysine (Sigma) and 150 μg/mL Fibronectin (Akron Biotechnology). Cells were seeded at 30,000 cells/cm^2 and passaged every 4 days. Approximately half of the basal medium was exchanged every other day. Primary cells isolated via FACS were defined as passage 0 (P0), and each cycle of trypsinization and re-seeding was considered to be an additional passage.

For subculturing, cells were rinsed with PBS and treated with 0.25% trypsin-EDTA (Gibco) at 37°C for 3 min. Cells were neutralized in 10% HI-FCS (Gemini Bio-Products) in DMEM and counted prior to re-seeding onto freshly coated plates/flasks. Cultures were typically diluted 2 to 3 times with a target seeding density of 30,000 cells/cm^2. Under these conditions, the primary cranial and trunk NC cells maintained logarithmic growth for an extended period of time.

Quantification of doubling time

Doubling time was determined as cells were passaged every 4 days (96 hours) over the course of a 20-day period. At each passage, cells were initially seeded at a density of 30,000 cells/cm^2, then after 4 days, cells were detached and final, live cell counts were determined using the Trypan Blue exclusion method. Initial and final cell concentrations at each passage were calculated by normalizing against surface area. Doubling time at each passage was determined using an online doubling time calculator (Roth, 2006).

Differentiation of NC cultures

For all derivatives, cultured cells were expanded for 3 passages prior to differentiation. Each differentiation experiment was carried out in duplicate and repeated using at minimum three independent cell isolates, for a total of six replicates.

Generation of neuronal cells

Primary cranial or trunk NC cells were seeded at 10,000 cells/cm^2 onto tissue culture-treated glass slides coated with 50 μg/mL Poly-D-Lysine (Sigma) and 10 μg/mL Laminin (Corning). Cells were grown in neuronal differentiation medium: Neurobasal-A medium (Gibco), 2 mM GlutaMAX (Gibco), 2% SM1 neuronal supplement (STEMCELL Technologies), 100 U/mL penicillin and 100 μg/mL streptomycin (Corning). Medium was sterile filtered, then supplemented with 100 ng/mL mouse nerve growth factor 2.5S (NGF; MilliporeSigma) and 50 ng/mL recombinant human neurotrophin-3 (NT3; MilliporeSigma). Half the medium was exchanged every other day.

Generation of glial cells

Primary cranial or trunk NC cells were seeded at 12,000 cells/cm^2 onto tissue culture-treated glass slides coated with 50 μg/mL Poly-D-Lysine (Sigma) and 10 μg/mL Laminin (Sigma). Cells were grown in glial differentiation medium, as previously described (Ishii et al., 2012): DMEM/F12 (Gibco), 1% HI-FCS (Gemini Bio-Products), 2 mM GlutaMAX (Gibco), 2% B27 supplement (Gibco), 100U/mL penicillin and 100 μg/mL streptomycin (Corning). Medium was sterile filtered, then supplemented with 50 ng/mL recombinant human bone morphogenetic protein 2 (BMP2; Gibco) and 50 ng/mL

recombinant human leukemia inhibitory factor (LIF; MilliporeSigma). Half the medium was exchanged every other day.

Generation of chondrocytes

Chondrogenic differentiation was induced using methods adapted from those previously described (Ishii et al., 2012). Primary cranial or trunk NC cells were initially cultured as a monolayer (30,000 cells/cm^2) on tissue culture-treated plates coated with 50 μg/mL Poly-D-Lysine (Sigma) and 150 μg/mL Fibronectin (Akron Biotechnology). Cells were grown for 3 days in osteogenic differentiation medium: α-MEM (Corning), 10% HI-FCS (Gemini Bio-Products), 0.1 μM Dexamethasone (Sigma), 10 mM β-glycerophosphate (Sigma), 50 μg/mL L-ascorbic acid (Sigma), 100 U/mL penicillin and 100 μg/mL streptomycin (Corning). Medium was sterile filtered, then supplemented with 100 ng/mL recombinant human bone morphogenetic protein 2 (BMP2; Gibco). Then on Day 4, cells were harvested and cultured as a micromass (Zhang et al., 2010). Briefly, cells were resuspended at 2x10^7 cells/mL in a 10 μL droplet. One droplet was placed in the center of each well in a 4-well plate. Cells were allowed to adhere at 37°C for 1 hour, prior to the addition of 400 μL chondrogenic differentiation medium (Ishii et al., 2012): α-MEM (Corning), 5% HI-FCS (Gemini Bio-Products), 0.1 μM Dexamethasone (Sigma), 50μg/mL L-ascorbic acid (Sigma), 1% ITS+ Premix (Corning), 1mM sodium pyruvate (Gibco), 100 U/mL penicillin and 100 μg/mL streptomycin (Corning). Medium was sterile filtered, then supplemented with 10 ng/mL recombinant human bone morphogenetic protein 2 (BMP2; Gibco) and 10 ng/mL human recombinant transforming growth factor-beta 3 (TGF-β3; Invitrogen). Half the medium was exchanged every other day.

Generation of smooth muscle cells

Primary cranial or trunk NC cells were seeded at 30,000 cells/cm^2 onto tissue culture-treated plates coated with 50 μg/mL Poly-D-Lysine (Sigma) and 150 μg/mL Fibronectin (Akron Biotechnology). Cells were grown in smooth muscle differentiation medium for 7 days, as previously described (Ishii et al., 2012): DMEM (Gibco), 10% HI-FCS (Gemini Bio-Products),100U/mL penicillin and 100μg/mL streptomycin (Corning). Medium was sterile filtered prior to use. Half the medium was exchanged the day after seeding, then the medium remained unchanged for the duration of the 7-day differentiation process.

Generation of adipocytes

Primary cranial or trunk NC cells were seeded at 50,000 cells/cm^2 onto tissue culture-treated plates coated with 50 μg/mL Poly-D-Lysine (Sigma) and 150 μg/mL Fibronectin (Akron Biotechnology). Cells were expanded in basal medium for 3 days to achieve 80-90% confluency, prior to culturing in Complete MesenCult™ Adipogenic Medium (Mouse; STEMCELL Technologies) for an additional 14 days. Half the medium was exchanged every 3 days.

Generation of melanocytes

Melanogenic differentiation was induced using a method adapted from those previously described (Maurer et al., 2007). Primary cranial or trunk NC cells were seeded at 20,000 cells/cm^2 onto tissue culture-treated plates coated with 50 μg/mL Poly-D-Lysine (Sigma) and 150 μg/mL Fibronectin (Akron Biotechnology). Cells were grown for 10 days

in melanogenic differentiation medium: Dulbecco's Modified Eagle's Medium (DMEM)-Low glucose, pyruvate (Gibco), 2% Chick embryo extract (prepared as described in Stemple and Anderson, 1992), 10% HI-FCS (Gemini Bio-Products), 1% N2 supplement (Gibco), 2% B27 supplement (Gibco), 100 U/mL penicillin and 100 μg/mL streptomycin (Corning). Medium was sterile filtered and supplemented with 1 ng/mL recombinant human basic fibroblast growth factor (bFGF; R&D Systems), 10 ng/mL recombinant human insulin-like growth factor 1 (IGF1; Gibco) and 100nM Endothelin 3 (ET3; Sigma). Half the medium was exchanged every other day.

Gene expression analysis by qRT-PCR

Quantitative reverse-transcriptase polymerase chain reaction (qRT-PCR) was performed to assess the relative expression of several markers against their expression in the reference tissue (Fig 3: *AP-2α*, *Snail1*, *Sox9*, *Nestin*: whole/unsorted E9.5 mouse embryo; *Sox10*: adult murine brain; Fig. 23: undifferentiated cranial NC). *Gapdh* was used as a housekeeping gene in all experiments. Primers were both designed and checked for specificity using Primer-BLAST (NCBI), then empirically validated prior to use (Table 1).

Total RNA was extracted using the RNeasy Micro kit, which included a DNase-treatment step (Qiagen). RNA concentration and purity were quantified using QuBit fluorometer (Invitrogen) and NanoDrop ND2000 spectrophotometer (Thermo Scientific), respectively. RNA integrity was determined using a 2100 Bioanalyzer (Agilent). Only samples with RNA integrity numbers (RIN) of 8.0 or greater were used for downstream analysis. A mixed primer strategy (Oligo dT_{20} and Random Primer) was used to generate cDNA from 250 ng of high-quality RNA from each sample using the qScript Flex cDNA

Synthesis kit (Quantabio), following the manufacture's protocol. cDNA used as a template in a 20 μL reaction containing 10 μL Fast SYBR Green Master Mix (Applied Biosciences) and 125 nmol forward and reverse primers. All qRT-PCR reactions were performed in duplicate on CFX96 Touch Real-Time PCR Detection System (BioRad). Reactions were amplified using a 2-stage protocol: 95°C for 5 min, followed by 34 cycles of 95°C for 15 s, and 60°C for 1 min. After the last cycle, a melt-curve was generated in order to verify that amplification produced a single, specific product. Fold change in gene expression relative to the reference tissue was calculated for each primer set using the [$2^{-\Delta\Delta Ct}$] method (Livak and Schmittgen, 2001).

Mesodermal gene expression analysis by RT-PCR

The expression of pan-mesodermal marker, *brachyury (T),* and axial mesoderm marker, *Tbx6*, was assessed in cultured cranial and trunk NC cells using reverse transcriptase-PCR (RT-PCR). NC markers, *Snail1* and *Sox9,* and housekeeping gene, *Gapdh*, served as positive controls. Primers were both designed and checked for specificity using Primer-BLAST (NCBI), then empirically validated prior to use (Table 1).

Total RNA was isolated from cultured cranial and trunk NC cells after three passages, or from whole/unsorted E9.5 mouse embryos. RNA was extracted and quality was assessed prior to transcribing cDNA using 250 ng of high-quality RNA, as described above. cDNA was diluted 1:2 prior to being used as a template in a 20 μL reaction containing 10 μL 2X GoTaq® Green Master Mix (Promega) and 500 nmol forward and reverse primers. Reactions were amplified on Mastercycler® Gradient thermal cycler (Eppendorf) using the following protocol: 95°C for 2 min, followed by 30 cycles of 95°C

for 1 min, 60°C for 1 min, and 72°C for 1 min, with a final extension step of 72°C for 10 min. Gene expression was assessed by standard gel electrophoresis. Images were taken upon ultraviolet transillumination (UVP) using a Camedia Wide Zoom 5.1Mp digital camera (Olympus), and processed using Photoshop Elements 2018 software (Adobe).

Table 1. qRT-PCR primers

Gene	NCBI Gene ID	Accession number	Primer sequence	
			Forward	Reverse
Brachyury (T)	20997	NM_009309.2	5'-CCAGCTCTAAGGAACCACCG-3'	5'-AAAGAACTGAGCTCCCAGCC-3'
Cabin1	104248	NM_172549.3	5'-GCTCTCCTACACCTCTGTGACC-3'	5'-CTTTGCTGTCTCTCCACTTTCC-3'
Col2a1	12824	NM_001113515.2	5'-TGGTGCTCGGGGTAACGAT-3'	5'-GGCTCCAGGAATACCATCAGT-3'
Dlx6	13396	NM_010057.2	5'-CCGAACTGGCTGCTTCCTTA-3'	5'-CAGAAACGTCCCACACTGGA-3'
Gapdh	14433	NM_001289726.1	5'-GCTCATGACCACAGTCCATGC-3'	5'-GTTGGGATAGGGCCTCTCTTG-3'
Hand2	15111	NM_010402.4	5'-CACCAGCTACATCGCCTACC-3'	5'-CTGTCCGGCCTTTGGTTTTC-3'
MEF2C	17260	NM_001170537.1	5'-GTGGTTTCCGTAGCAACTCC-3'	5'-AACTGACTGAGGGCAGATGG-3'
Nestin	18008	NM_016701.3.1	5'-AACAGAGATTGGAAGGCCGC-3'	5'-GCCACTTCCAGACTAAGGGAC-3'
Snail1	20613	NM_011427.2.1	5'-CTGCACGACCTGTGGAAAG-3'	5'-GCCTGGCACTGGTATCTCTT-3'
Sox10	20665	NM_011437.1.1	5'-TTCAGGCTCACTACAAGAGTGC-3'	5'-ATTACCTCGTGGCTGATCTCC-3'
Sox9	20682	NM_011448.4.1	5'-AGTCGGTGAAGAACGGACAA-3'	5'-CCCTCTCGCTTCAGATCAACT-3'
Tbx6	21389	NM_011538.2	5'-TGAAGATCGCAGCCAATCCC-3'	5'-TGAAAAGCGGCAGGGTGTAG-3'
TFAP2a	21418	NM_001122948.1.1	5'-CACTCCTTACCTCACGCCAT-3'	5'-GCCACCGTGACCTTGTACTT-3'

Table 1. All primers were designed to span an intron and produce a 150-300 base pair amplicon using Primer-BLAST (NCBI). Primers were tested via RT-PCR to ensure amplification of a single product.

Immunocytochemistry

Cultures were fixed with 4% paraformaldehyde for 30 minutes at room temperature and washed three times with PBS prior to immunostaining. Cultures were then washed two times with PBS with 0.1% Tween 20 (PBST, Sigma), blocked in 5% normal goat serum (Gibco)/PBST for 1 hour and incubated with primary antibodies overnight at 4ºC. The cultures were washed three times with PBST prior to incubation with fluorophore-conjugated secondary antibodies for 1 hour at room temperature. After incubation cultures were washed an additional six time in PBST to reduce non-specific background, followed by two washes in PBS in preparation for either 4,6-diamidino-2-phenylindole (DAPI) staining, or coverslipping with Vectasheild mounting medium (Vector

Laboratories). Cultures counterstained with DAPI were incubated with 300 nM DAPI dilactate (Invitrogen) in PBS for 4 minutes, then rinsed with PBS several times prior to imaging. Primary and secondary antibodies can be found on Table 2.

Single focal plane images were acquired with a Zeiss AxioZoom.V16 fluorescence stereomicroscope equipped with an Orca R2 CCD camera, a Zeiss ApoTome, and appropriate filter sets. The objective (PlanNeoFluar Z 2.3x size) on the AxioZoom.V16 has a 0.57 numerical aperture (NA). Fluorescent images were pseudocolored, as indicated in figure legends, merged using ZEN 2011 software (Zeiss), and exported to TIFF format using AxioVisionSE64 rel 4.9.1. (Zeiss). Overlapping images were taken in order to obtain a representative field of view of the entire culturing surface (1 cm^2 in an 8-well slide). Images were aligned and stitched using the open source Fiji software (Preibisch et al., 2009). All images were processed using Photoshop Elements 2018 software (Adobe) using Photoshop Elements 2018 software (Adobe).

Alcian blue staining

Chondrogenic micromass cultures were fixed with 4% paraformaldehyde for 30 minutes at room temperature and washed three times with PBS prior to incubation with a *0.1%* solution of Alcian blue 8GX (Sigma) dissolved in acidic ethanol (5% concentrated hydrochloric acid, 70% ethanol*)* overnight at 4ºC. After incubation, cultures were destained in acidic ethanol, washed with distilled water and imaged using light microscopy. All images were processed using Photoshop Elements 2018 software (Adobe).

Table 2. Primary and secondary antibodies used for immunocytochemistry

Primary antibodies

Antibody	Species	Dilution	Vendor	Catalog number
αSMA	mouse	1:500	eBiosciences	14-9760-80
Cabin1	rabbit	1:500	Abcam	ab3349
Col2a1	rabbit	1:500	Abcam	ab34712
ErbB3	mouse	1:500	Thermo Fisher Scientific	MA1-860
GFAP	mouse	1:1000	Sigma	G3893
HuC/D	mouse	1:1000	Invitrogen	A-21271
MEF2C	mouse	1:500	Thermo Fisher Scientific	MA5-17119
TUJ1	mouse	1:500	STEMCELL Technologies	60052

Fluorophore-conjugated secondary antibodies

Antibody	Species	Dilution	Vendor	Catalog number
AlexaFluor 546	goat	1:1000	Invitrogen	A11030 or A11035
AlexaFluor 633	goat	1:1000	Invitrogen	A21052 or A21071

Abbreviations: αSMA, alpha smooth muscle actin; Cabin1, calcineurin binding protein 1; Col2a1, collagen, type II, alpha 1; ErbB3, erb-b2 receptor tyrosine kinase 3; GFAP, glial fibrillary acidic protein; HuC/D, ELAV-like RNA binding proteins; MEF2, myocyte enhancer factor 2; TUJ1, neuron-specific class III β-tubulin.

Quantification of nodule number

Overlapping images of Alcian blue stained cultures were taken in order to obtain a representative field of view of the entire culturing surface of a well (2 cm^2) in a 4-well plate. Four images from each well were aligned and stitched using the open source Hugin software (d'Angelo, 2007). Nodule number was determined at each time point in duplicate using the particle analysis tool in ImageJ (Schneider et al., 2012). The results from three independent cultures were used to calculate the average number of nodules at each time point.

Alcian blue extraction

Cartilage-matrix accumulation was assessed by extracting specifically bound Alcian blue dye from the micromass cultures, as previously described (Paulsen et al.,

1988). Micromass cultures were solubilized in 4 M guanidine hydrochloric acid, pH 5.8 (GuHCl) overnight at 4ºC. Following incubation, absorbance at 600nm was measured using a spectrometer (Eppendorf BioPhotometer). Absorbance values were normalized against those measured at Day 0. The results from three independent cultures were used to determine the net amount of cartilage-matrix present at each time point.

Oil red O staining

Adipogenic differentiation was assessed by staining with Oil Red O (Humason, 1962; Thermo Fisher Scientific). Cultures were fixed with 4% paraformaldehyde at room temperature for 30 minutes, washed three times with PBS, then incubated in 60% isopropanol for 2 minutes. Cultures were then incubated with a 3:2 solution of 30% Oil red O dissolved in isopropanol:deionized water for 5 minutes at room temperature. After incubation, the cultures were washed with distilled water and imaged using light microscopy. Overlapping images were taken in order to obtain a representative field of view of the entire culturing surface of a well (2 cm^2) in a 4-well plate. In this case, four images from each well were aligned and stitched using the open source Hugin software (d'Angelo, 2007). All images were processed using Photoshop Elements 2018 software (Adobe).

L-DOPA reaction assay

Melanogenic differentiation was assessed by 3,4-Dihydroxy-L-phenylalanine (L-DOPA) reaction assay (Tsuchiyama et al., 2013). Briefly, primary cells were fixed with 4% paraformaldehyde at room temperature for 30 minutes, washed three times with PBS,

then incubated with 5 mM L-DOPA (Sigma) in PBS at 37°C for 8 hours in the dark. After incubation, the cells were washed with distilled water and imaged using light microscopy. Overlapping images were taken in order to obtain a representative field of view of the entire culturing surface of a well (2 cm^2) in a 4-well plate. In this case, four images from each well were aligned and stitched using the open source Hugin software (d'Angelo, 2007). All images were processed using Photoshop Elements 2018 software (Adobe).

HuC/D localization

Images of neurons differentiated from cranial and trunk NC cultures subjected to HuC/D immunofluorescence staining as described above were quantified with respect to the percentage of neurons extending HuC/D positive neurites. Five images were obtained from differentiated cultures in each biological replicate, and each image was separately analyzed by two blinded observers. Cells with neurites were identified in the green channel (EYFP). These cells were then assessed for HuC/D expression in the red channel to calculate the percentage of neurons with HuC/D in processes. Each dot represents one observation of one image, color-coded by biological replicate and observer.

Assessing Cabin1 nuclear localization

Nuclear localization was quantified using images of cranial NC cultures fixed at several time points over the course of chondrogenesis (Undifferentiated (Day 0), and after 4 and 14 days in chondrogenic differentiation medium), and subjected to Cabin1/DAPI immunofluorescence staining, as described above. At each time point, four representative

images were taken per well in duplicate. Each image was then divided equally into four fields of view using Photoshop Elements 2018 software (Adobe). Mean fluorescence intensity (MFI) of Cabin1 staining within the nuclei in each field of view was obtained using the particle analysis tool in Fiji (Schindelin et al, 2012), a distribution of ImageJ (Schneider et al., 2012). Specifically, fields of view taken in the blue channel (DAPI) were used to count and outline total nuclei. Nuclei outlines were then overlaid onto the corresponding field of view taken in the red channel (Cabin1) to calculate MFI per nuclei. Each dot represents MFI within one nucleus, color-coded by biological isolate.

Co-immunoprecipitation and immunoblotting

Nuclear lysates were extracted from cranial NC cells cultured in basal medium for three passages. Total protein was determined using a DC protein assay (BioRad). 50 µg of protein, prepared in 16.7 mM Tris-HCl (pH 8.1, Invitrogen), 1.1% Triton X-100 (Sigma), 0.01% SDS (Invitrogen), 167 mM NaCl (Thermo Fisher Scientific), and 1X protease inhibitor (Thermo Fisher Scientific), was incubated overnight with 10 µg of either Cabin1 (Abcam, ab3349) or MEF2C (Santa Cruz Biotechnology, sc-365862) antibody in the presence of 50uL protein A dynabeads (Invitrogen). Beads were collected magnetically and protein complexes were eluted in 2x Laemmli buffer (BioRad) with 55 mM 2-mercaptoethanol (1:20, Gibco) at 95°C for 5 minutes. In addition, 50ug of nuclear lysate was prepared in a similar solution and denatured at 95°C for 5 minutes.

All lysates were resolved using SDS-Page. Proteins were separated on 7.5% Mini-PROTEAN TGX Stain-Free gels (Bio-Rad) using the PowerPac Basic apparatus (BioRad) for 1 hour at 150V. Proteins were transferred to 0.2 µm PVDF membranes (Thermo Fisher

Scientific) for 1 hour at 100V. Membranes were blocked in 5% milk in tris-buffered saline (TBS) with 0.05% Tween 20 (TBST), and then incubated overnight at 4°C with an antibody against Cabin1 (1:1000, Abcam, ab3349) or MEF2C (1:1000, Thermo Fisher Scientific, #MA5-17119). Membranes were then washed several times in TBST prior to a 1 hour and 30 minute incubation with the corresponding secondary antibody conjugated with horseradish peroxidase (1:2000, Cell Signaling Technologies, Mouse Anti-Rabbit IgG (Light-Chain Specific) (D4W3E) mAb (HRP Conjugate) #93702; Rabbit Anti-Mouse IgG (Light Chain Specific) (D3V2A) mAb (HRP Conjugate) #58802). Membranes were again washed several times in TBST, and stored in TBS until imaged. Proteins were detected using Clarity Western ECL Chemiluminescent Substrate (BioRad) on a Syngene G:BOX XT4: Chemiluminescence and Fluorescence Imaging System with GeneSys software (Syngene). Images were processed using Photoshop Elements 2018 software (Adobe).

Statistical Analyses

All statistical analyses and graphical representations for the data presented were computed using GraphPad Prism, Version 7.0b for Mac OS X (GraphPad Software, La Jolla, CA, USA, http://www.graphpad.com). Significant differences between groups were determined using either repeated measures one-way analysis of variance (ANOVA; Figs. 2, 24), two-way ANOVA (Figs. 3, 8, 20), or unpaired t-tests (Fig. 23), as indicated. Comparisons between means were carried out using Tukey's post hoc multiple comparison test. Results are reported as mean ± SEM (Figs. 2, 3, 8, 23, 24) or as the

grand mean across replicates (Fig. 20). For all experiments, *p values* < 0.05 were considered statistically significant.

RNA-seq data generation

Cell isolation

Temporal changes in gene expression as cultured primary murine cranial NC cells differentiated over time into either neurons or chondrocytes were identified using RNA-seq. Undifferentiated cranial NC cells were expanded for three passages (12 days in culture) prior to being grown under either neuronal or chondrogenic differentiation conditions, as described above. Gene expression was interrogated in undifferentiated cranial NC cells, and in differentiating cultures at two time points: (1) an early time point representing a population of intermediate cells (Day 2 and Day 4 for neurogenesis and chondrogenesis, respectively), and (2) a late time point representing a population of differentiated cells (Day 6 and Day 14 for neurogenesis and chondrogenesis, respectively).

Specific methods were employed to enrich for intermediate progenitors or differentiated cells at each time point. For neurogenesis FACS (BD FACSAria III flow cytometer, equipped with a 100 μm nozzle) was used to exclude already differentiated neuronal cells at Day 2, which have a notably smaller cell size compared to the rest of the cells exposed to differentiation conditions, thus enabling enrichment of an intermediate cell population. FACS was utilized again at Day 6 to isolate differentiated peripheral neurons employing the same size differences. For chondrogenesis, whole cultures were processed at Day 4 as they were enriched for chondroprogenitors, which

display the characteristic cuboidal morphology. Enrichment of differentiated chondrocytes at Day 14 was carried out by picking individual chondrogenic nodules from our cultures. These nodules, which contain condensed, differentiated chondrocytes, were readily visualized throughout the cultures without the need for additional staining, and nodules were easily lysed in preparation for RNA extraction.

RNA isolation

Total RNA was extracted from differentiating neurons or chondrocytes at the early and late time points, and from an equivalent sample of undifferentiated cranial NC cells set aside prior to differentiation as a control using the using the RNeasy Micro kit, which included a DNase-treatment step (Qiagen). RNA concentration and purity were quantified using QuBit fluorometer (Invitrogen) and NanoDrop ND2000 spectrophotometer (Thermo Scientific), respectively. RNA integrity was determined using a 2100 Bioanalyzer (Agilent). Only samples with RNA integrity numbers (RIN) of 8.0 or greater were used for downstream analysis. To increase RNA yield from sorted neurogenic samples specifically, RNA amplification was performed using the MessageAmp™ II aRNA Amplification Kit (Ambion), following the manufacture's protocol. Briefly, 133 ng of RNA from each time point was reverse transcribed to produce single-stranded cDNA using a T7 Oligo (dT) primer. After second strand synthesis and purification, the double-stranded cDNA was used as a template for *in vitro* transcription with T7 RNA polymerase to generate multiple copies of amplified RNA. Amplified RNA was purified using an RNA clean and concentrator kit (Zymo Research) following the manufacture's protocol, and quality tested as described above, prior to being submitted for sequencing.

Library preparation and sequencing

For each lineage, three biological replicates from each time point were sent to University of Wisconsin Biotechnology Center (UWBC) for library preparation and sequencing. cDNA libraries were generated using TruSeq Stranded Total RNA Sample Prep Kits, (Illumina), which included an rRNA suppression step. Each cDNA library was indexed for multiplexing, and subsequently sequenced on one lane of a S1 flow cell of the Illumina NovaSeq device. Libraries were sequenced at 100 bp, and yielded 48 million paired-end reads/sample.

Bioinformatic analysis

Bioinformatics analysis closely followed the approach from Dhara et al. (2019). Briefly, after merging technical replicates of RNA-seq samples across lanes, adapter sequences were trimmed (TrimGalore v0.4.4, --stringency 3 -q 20, paired-end mode) and sequence quality was assessed (FastQC v0.11.5). The Kallisto pipeline (Bray et al., 2016) was used to perform pseudoalignment against the mouse transcriptome (GRCm38.p6 Mus musculus assembly, Genome Reference Consortium Mouse Build 38, patch release 6, annotation). Kallisto was also used to quantify transcript abundances using 500 bootstrap samples, which controls for variability in estimates due to read alignment.

Differentially expressed (DE) transcripts were identified using Sleuth (v0.29.0; Pimentel e al., 2017). A “full” model, including a factor for each time point, was estimated for each transcript, and a Wald test was calculated for each coefficient to identify significant differences using the undifferentiated cranial NC cells as the baseline. The Benjamini-Hochberg (Benjamini and Hochberg, 1995) approach was used in order to

control the false discovery rate (FDR) at 5% within each comparison. Beta values from the model were used as a biased estimator of log-fold change. Expression heatmaps were generated based on Z-scores calculated for log transcripts per million [TPM] estimates using ComplexHeatmap (v1.17.1; Gu et al., 2016). Transcript clusters were identified using the K-means algorithm, and hierarchical clustering (Euclidean distance, complete linkage) was used to organize transcripts within clusters. Temporal clusters were analyzed for enrichment of molecular and functional gene networks within the DE gene sets (FDR<0.05) at each time point using PantherGO (Version 14.1, released 2019-03-12; Mi et al., 2013, Thomas et al., 2003), ShinyGO (v0.61, Ge et al., 2020) and gprofiler (Raudvere et al., 2019) open source tools.

DE transcription factors at each time point were derived by comparing the overall list of DE genes to a recently published comprehensive list of known human transcription factors (Lambert et al., 2018). Identified transcription factors were clustered based on their temporal differential gene expression profiles, and functional relationships between the temporally clustered genes were inferred using PantherGO (Version 14.1, released 2019-03-12; Mi et al., 2013, Thomas et al., 2003), ShinyGO (v0.61, Ge et al., 2020) and gprofiler (Raudvere et al., 2019) open source tools.

CHAPTER III

Establishment of a murine culture system modeling the temporal progression of cranial and trunk neural crest cell differentiation[1]

Abstract

The neural crest (NC) is a transient population of embryonic progenitor cells that are implicated in a diverse range of congenital birth defects and pediatric syndromes. The broad spectrum of NC-related disorders can be attributed to the wide variety of differentiated cell types arising from the NC. *In vitro* models of NC cell development provide a powerful platform for testing the relative contributions of intrinsic and extrinsic factors mediating NC differentiation under normal and pathogenic conditions. Although differentiation is a dynamic process that unfolds over time, until recently, we lacked a well-defined chronology that characterizes the *in vitro* progression of NC differentiation towards specific cell fates. In this chapter, we present optimized culture conditions for expansion of primary murine NC cells that give rise to both ectodermal and mesoectodermal derivatives, even after multiple passages. Significantly, we have also established highly reproducible timelines that include distinct intermediate stages for lineage-specific NC differentiation *in vitro*. Specifically, our results define characteristic

[1] This chapter is a modified version of the published manuscript. Supplementary information can be found in Appendices A-G.

Replogle, M.R., Sreevidya, V.S., Lee, V.M., Laiosa, M.D., Svoboda, K.R., Udvadia, A.J., 2018. Establishment of a murine culture system for modeling the temporal progression of cranial and trunk neural crest cell differentiation. Dis Model Mech 11.

changes in cell morphology and behavior that track the temporal progression of NC cells as they differentiate along the neuronal, glial, and chondrogenic lineages *in vitro*. These benchmarks constitute a chronological baseline for assessing how genetic or environmental disruptions may facilitate or impede NC differentiation. Introducing a temporal dimension substantially increases the power of this platform for screening drugs or chemicals for developmental toxicity or therapeutic potential.

Introduction

As developmental precursors, the neural crest (NC) uniquely contributes to a wide variety of tissues and structures in vertebrate animals. Differences in spatiotemporal patterning during development direct the transition from multipotent, embryonic progenitor through the eventual acquisition of specific cell fates. Some of the factors influencing NC cell differentiation *in vivo* include the site of origination along the anterior-posterior neuraxis, the timing of emigration, the migratory pathway, and the final sites of arrest within the embryo (reviewed in Betancur et al., 2010; Bhatt et al., 2013; Simões-Costa and Bronner, 2015). The remarkable plasticity of the NC allows it to give rise to cell types as diverse in structure and function as neurons of the peripheral nervous system and cartilage-matrix producing cells found within cephalic structures (Le Douarin, 1982). Given their broad contribution to a range of tissues, disruption in any stage of NC cell development can result in pleiotropic structural and functional anomalies (Bolande, 1997). Thus, understanding the molecular mechanisms that regulate the normal growth and differentiation of the NC is necessary for fully comprehending the etiology underlying a plethora of birth defects.

The ability to manipulate isolated NC cells *in vitro* is highly advantageous, particularly for the purpose of testing the relative contributions of intrinsic and extrinsic factors mediating self-renewal and differentiation. For example, *in vivo*, the cranial NC normally gives rise to differentiated cells of both ectodermal and mesoectodermal cell fates, while trunk NC produces mainly ectodermal derivatives. However, directed differentiation of trunk NC *in vitro* demonstrates that trunk NC cells have the capacity to give rise to both ectodermal and mesoectodermal cell types (recently reviewed in Dupin et al., 2018). Direct comparisons of the two cell populations *in vitro,* would allow us to tease apart any intrinsic differences in cell behavior or response to environmental cues. In addition, *in vitro* models of NC development are beneficial for elucidating protein-protein and protein-gene interactions that regulate the transcriptional programs underlying NC growth and differentiation along distinct lineages. In such studies, *in vitro* expansion of the NC is valuable as the number of NC cells per developing embryo is very low in comparison to the millions of cells needed to investigate molecular function using biochemical assays, such as co-immunoprecipitation and ChIP-seq analysis.

While methods for isolating, expanding and differentiating both avian (Baroffio et al., 1991; Calloni et al., 2009; Cohen and Konigsberg, 1975; Etchevers, 2011; Kerosuo et al., 2015; Sieber-Blum and Cohen, 1980; Trentin et al., 2004) and rodent (Bixby et al., 2002; Etchevers, 2011; Ishii et al., 2012; Maurer et al., 2007; Pfaltzgraff et al., 2012; Stemple and Anderson, 1992) NC cells *in vitro* have been established, characterization of the cultured NC cells is limited to validation of cell identity and differentiation potential. However, reproducible landmarks that define the temporal progression of differentiation towards a particular cell fate *in vitro* have not been previously characterized. Since

directed differentiation of NC cells *in vitro* occurs over several days, delineating temporal differences could enhance the experimental dynamic range for assessing the impacts of genetic or environmental manipulations of the cultured cells. Therefore, our aim was to establish a culture system of the NC that will enable future investigations assessing how genetic or environmental perturbations may facilitate or impede NC cell differentiation along various cell lineages.

Previous reports suggest a difficulty in long-term maintenance of murine NC cells in culture, prompting the development of murine NC cell lines. Two murine NC cell lines have been previously established (Ishii et al., 2012; Maurer et al., 2007). One cell line, O9-1, was clonally-derived from cranial NC isolated from *Wnt1cre; R26R/EYFP* transgenic mouse embryos (Ishii et al., 2012). The second cell line, JoMa1, was established from clonally-derived trunk NC immortalized with the oncogene, c-myc (Maurer et al., 2007). Although established cell lines do overcome the obstacle of long-term maintenance, one inherent drawback is the phenotypic instability that occurs over time in culture (Geraghty et al., 2014; Ishii et al., 2012; Rao and Anderson, 1997). In addition, the O9-1 cells have diminished differentiation capacity as they lack the ability to give rise to neurons. Furthermore, it is not possible to directly compare cranial and trunk NC cell behavior using these cell lines because they were derived from different genetic backgrounds and are propagated under different conditions. Therefore, to conduct our temporal analysis of *in vitro* NC differentiation, we optimized conditions for propagating primary murine cultures of cranial and trunk NC cells.

Here we have established methods for primary murine NC cell culture that maintains both self-renewal capabilities and broad differentiation potential over an

extended period of time. Furthermore, we present a detailed characterization of cranial and trunk NC cells in culture, including the molecular and morphological changes that occur as the cells differentiate along the neuronal, glial, and chondrogenic lineages over time. Specifically, we compared directed differentiation of cranial and trunk NC cells isolated from *Sox9cre; R26R/EYFP* transgenic mouse embryos using fluorescence activated cell sorting (FACS). Through our characterization, we have defined reproducible benchmarks that track the progression of differentiation *in vitro,* many of which mimic well-documented changes described during these processes *in vivo*. In addition, since we isolated the cranial and trunk NC cells from the same embryos, we were able to directly compare differentiation within the two cell populations. This enabled us, in some cases, to detect subtle differences in cell morphology and behavior as cells differentiated. By establishing a chronological baseline for how the primary cranial and trunk NC cells differentiate under normal conditions, this culture system provides a platform for future investigations assessing how genetic manipulation or exposure to environmental toxins might disrupt the timing of NC differentiation.

Results

Cranial and trunk NC cells maintain expression of genes associated with NC cell identity and self-renewal in vitro over time.

Primary cranial and trunk NC cells were separately isolated from E9.5 mouse embryos on the basis of Sox9 reporter gene expression. Cranial tissues were dissected rostral of the otic vesicle, excluding the pharyngeal arches and frontonasal process, and trunk tissues were dissected between somite 8 and somite 24 to avoid isolation of the

vagal NC (Fig. 2A, *dashed lines*). Cranial and trunk tissues isolated from several embryos were separately pooled and dissociated into single cells prior to fluorescence activated cell sorting (FACS). Sorted, EYFP-positive cells cultured in basal medium exhibited a mesenchymal, stellate cell morphology (Figs. 2B, 2C), as previously described for NC cells in culture (Ishii et al., 2012; Maurer et al., 2007).

Once in culture, both NC cell populations expanded relatively quickly while maintaining their characteristic morphology. Cells were passaged every four days over a 20-day period. Although cranial NC cell growth was variable during the first four days in culture, the cells maintained consistent growth over subsequent passages (Fig. 2D). The trunk NC cells maintained consistent growth throughout the 20-day period (Fig. 2E). On average, cranial and trunk NC cultures doubled approximately every 40 hours and maintained high viability (93% $\pm$ 4.49%) based on trypan blue exclusion. Overall, the mesenchymal, stellate cell morphology was retained as cells were passaged during the same time period (Fig. 3A), although, we sporadically observed isolated cells exhibiting short processes and neuronal morphology. We typically isolate approximately 9,000 cranial and 3,000 trunk NC cells/embryo. Given the average doubling times of the cells, over 7 million cranial and 5 million trunk NC cells can be obtained from an average litter size of 9 embryos after just three passages (12 days in culture; Appendix A). Thus, *Sox9*-positive NC cells isolated and cultured in this manner display a robust capacity for survival and expansion *in vitro*.

Furthermore, the cultured cells retained their NC cell identity and capacity for self-renewal over time. We used RT-qPCR to assess the relative expression of several well-described markers of NC cell fate, including *AP-2*α, *Snail1*, *Sox9* and *Sox10*, and stem

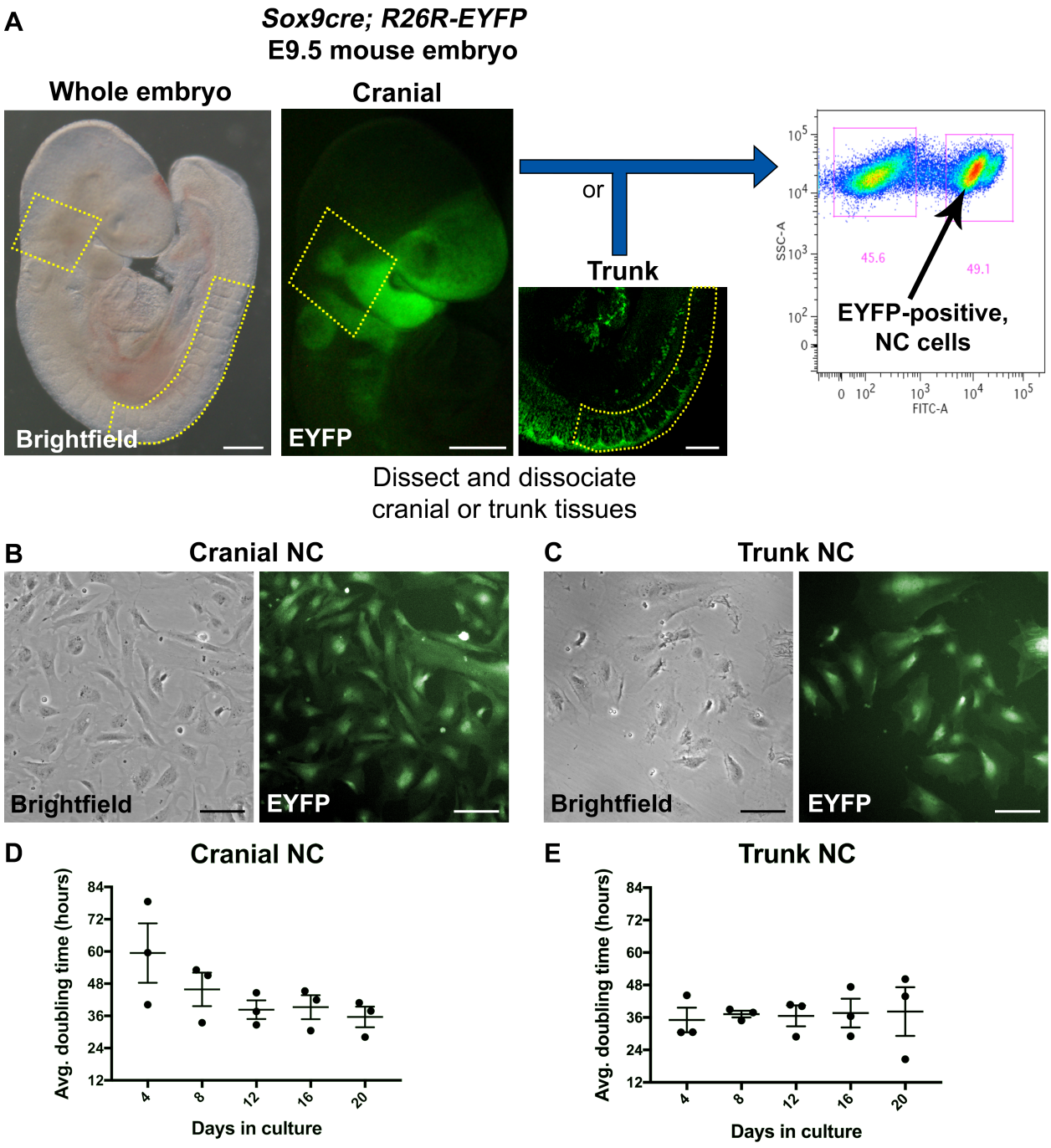

Figure 2. Isolation and growth profile for primary cranial and trunk NC cells in culture. **(A)** Workflow for isolating primary NC cells via fluorescence-activated cell sorting (FACS). Cranial or trunk tissues were dissected *(dashed lines)* from *Sox9cre; R26R-EYFP* mouse embryos at E9.5. Tissues were dissociated into single cells and sorted via FACS. Sorted, EYFP+ NC cells were cultured in basal medium and passaged every 4 days: **(B)** cranial and **(C)** trunk NC cells. **(D, E)** Doubling time for cultured cranial and trunk NC cells was calculated over 5 passages. Average doubling time was 44 and 39 hours for cranial and trunk NC, respectively. Neither cell population showed a statistically significant difference in doubling time across the five passages (repeated measures one-way ANOVA). All cells are derived from *Sox9cre; R26R-EYFP* mice and express EYFP (*green*). Values represent mean ± SEM (n=3). Scale bars: (A) 200μm; (B, C) 100μm.

cell-like marker, *Nestin*. Expression analysis was performed using RNA extracted from a sampling of the cultured cranial or trunk NC cells every four days, as cells were passaged over a 20-day period (Fig. 3A). Using this approach, we found that neither cell population exhibited a statistically significant change in the relative expression of these genes across the various time points (Figs. 3B, 3C). Together with the growth profile and morphological observations of the cultured cells, these results indicate that NC cell identity and self-renewal capacity is maintained as cells are expanded over a three-week period.

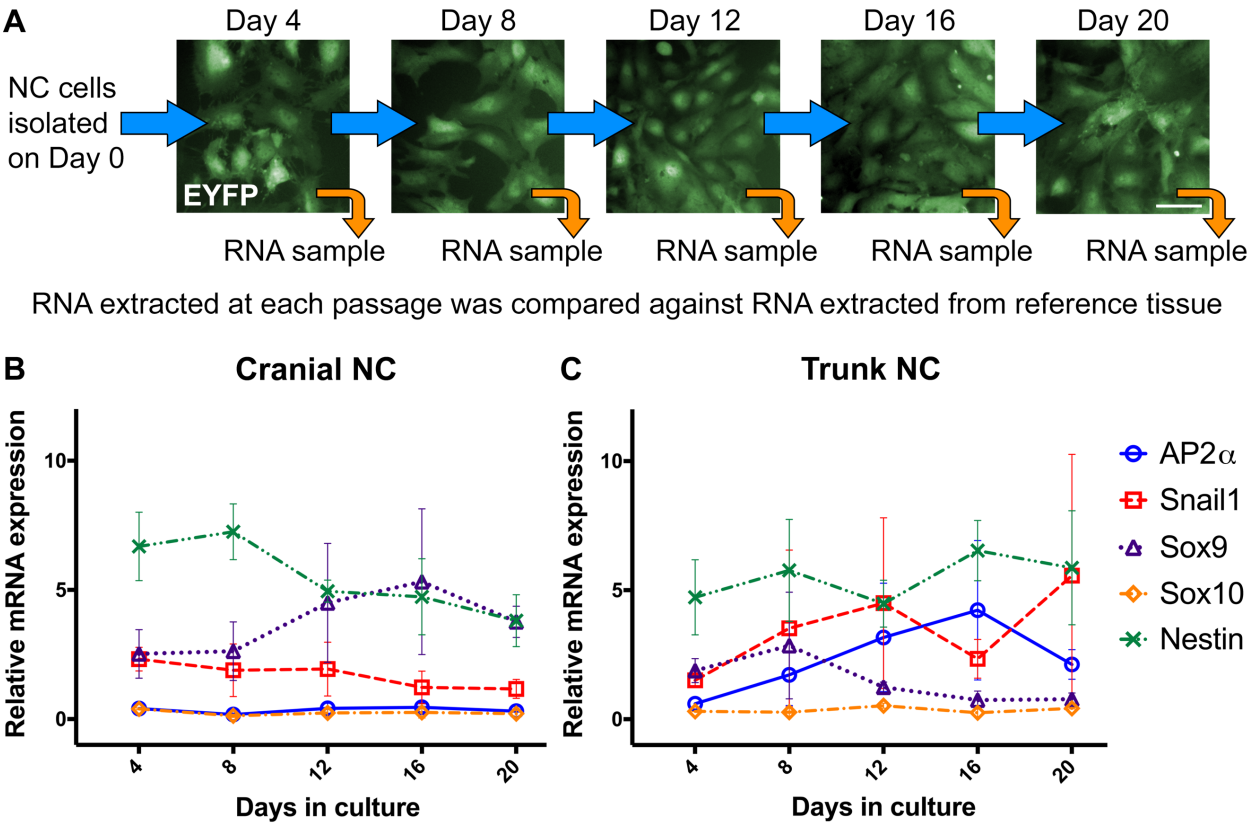

Figure 3. Maintenance of gene expression associated with NC cell identity and self-renewal.
(A) Workflow for quantitative reverse transcriptase-polymerase chain reaction (RT-qPCR) analysis. RNA was extracted from a sampling of cells at each passage. Expression of NC cell markers (*AP2α*, *Snail1*, *Sox9*, *Sox10*), and stem cell-like marker (Nestin), were assessed every four days as cells were passaged over 20 days in culture. The cultured NC cells displayed a mesenchymal morphology at each time point across three independent cell isolates. Neither the cranial **(B)** nor the trunk **(C)** NC cells showed a statistically significant change in the relative expression of these genes across 5 passages (two-way ANOVA). All cells are derived from *Sox9cre; R26R-EYFP* mice and express EYFP (*green*). Values represent mean ± SEM (n=6; three independent cell isolates carried out in duplicate). Scale bar: 50μm.

Cranial and trunk NC cells differentiate into multiple NC derivatives in vitro.

A hallmark of NC cells *in vivo* is their ability to give rise to a diverse range of cell types including ectodermal and mesoectodermal derivatives (Le Douarin, 1982). Therefore, we tested the ability of cultured *Sox9*-positive cranial and trunk NC cells to produce various cell types when exposed to lineage specific differentiation conditions. Our results show that both cell populations could be induced to generate a broad array of NC cell derivatives *in vitro*, including neuronal cells (Figs. 4A, 4B, Appendix B), glial cells (Figs. 4C, 4D), smooth muscle cells (Figs. 4E, 4F, Appendix C), chondrocytes (Figs. 4G, 4H, Appendix D), adipocytes (Figs. 4I, 4J, Appendix D), and melanocytes (Figs. 4K, 4L, Appendix D). For consistency, differentiation potential was assessed after passaging the cells three times (12 days in culture), however, we have been successful in inducing differentiation of ectodermal and mesoectodermal derivatives at both earlier and later passages as well (data not shown).

To ensure that differentiation into mesoectodermal derivatives was not due to inadvertent expansion of mesodermal cells, we tested for the expression of canonical mesodermal markers, *T (brachyury)* and *Tbx6*. We did not detect expression of either marker in cultured cranial or trunk NC cells (Appendix E). Together, these data demonstrate that the cultured *Sox9*-positive cranial and trunk NC cells maintain a broad differentiation potential *in vitro*, as would be expected from this multipotent cell population. Expanding on these findings, we next sought to establish reproducible benchmarks exhibited by the primary cranial and trunk NC cells as they differentiated towards the neuronal, glial and chondrogenic cell fate *in vitro* over time.

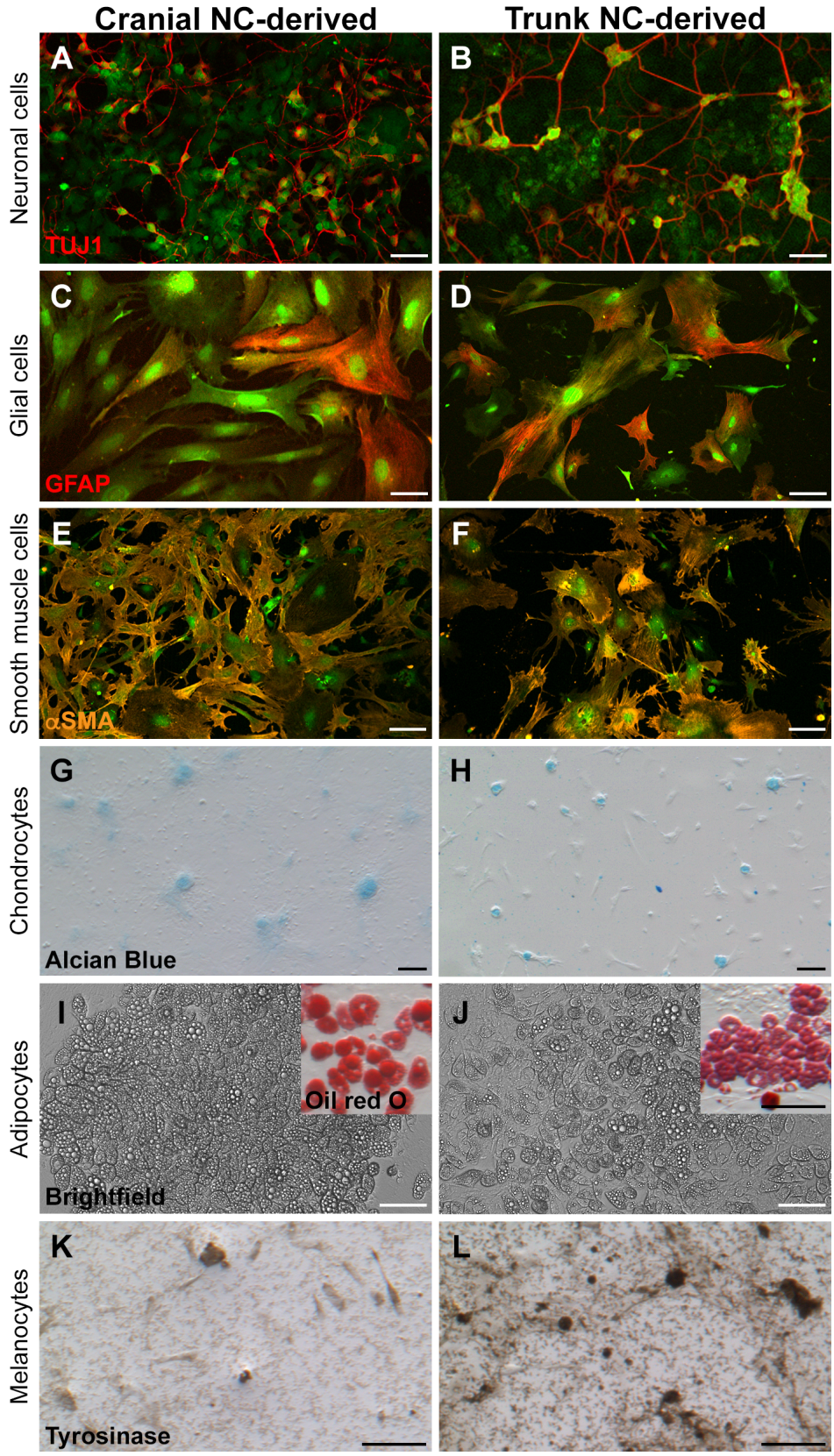

Figure 4. See next page for legend.

Figure 4. Differentiation potential of cultured primary cranial and trunk NC cells. Both cranial and trunk NC cells gave rise to known NC derivatives when grown under conditions reported to induce lineage-specific differentiation. Representative images of differentiated cells: neuronal cells **(A, B**; TUJ1, *red*; 4 days in differentiation medium containing NT3 and NGF**)**, glial cells **(C, D**; GFAP, *red*; 8 days in differentiation medium containing BMP2 and LIF**)**, smooth muscle cells **(E, F**; αSMA, *orange*; 7 days in differentiation medium containing FCS**)**, chondrocytes **(G, H**; Alcian blue staining; 6 days (G) and 14 days (H) in differentiation medium containing TGF-β3**)**, adipocytes **(I, J**; Brightfield, **Inset:** Oil red O staining; 14 days in Adipogenic Medium from STEMCELL Technologies**)**, and melanocytes **(K, L**; Tyrosinase, *brown*; 10 days in differentiation medium containing ET3**)**. All cells are derived from *Sox9cre; R26R-EYFP* mice and express EYFP (*green*). Cells were expanded for 3 passages (12 days in culture) prior to differentiation. Differentiation into each of the derivatives was consistent across replicates (n=6; duplicate cultures from each of three independent cell isolates). Scale bars: (A – D) 50μm; (E – L) 100μm.

Cranial and trunk NC cells exhibit reproducible, temporal changes in morphology and behavior during neuronal differentiation in vitro.

Neuronal differentiation was characterized by assessing the expression of neuron-specific class III β-tubulin (TUJ1) and ELAV-like RNA binding proteins (HuC/D) at several time points along the 8-day differentiation process (Figs. 5 and 6). Robust expression of both markers was observed as early as 2 days in neuronal differentiation medium (Figs. 5A, 5B; 6A, 6B). In addition, there was an observable decrease in soma size in differentiated cells, as illustrated in cultures immunostained with TUJ1 (Figs. 5A, 5B). Specifically, TUJ1-negative cells displayed a stellate, mesenchymal morphology (Figs. 5A', 5B'; *white lines*), similar to the morphology seen in undifferentiated cells shown previously (Figs. 2B, 2C). In contrast, TUJ1-positive cells exhibited neuronal-like morphology with a compacted soma (Figs. 5A'', 5B''; *cyan lines*), as well as the extension of neuritic processes.

Neuritic outgrowth continued in both cell populations as differentiation progressed through Day 4 (Figs. 5C, 5D) and Day 6 (Figs. 5E, 5F), however under these culture conditions, we observed clear differences in cell aggregation. After 4 days in differentiation medium, TUJ1-positive cells derived from the trunk NC began to coalesce

in distinct regions, forming dense aggregations (Figs. 5D, Appendix B, *arrowheads*). Similar coalescence was not observed in TUJ1-positive cells derived from the cranial NC until Day 6. In addition, the aggregates formed by cranial NC were more loosely formed and amorphous (Fig. 5E, *arrowheads*) compared to those observed in cultures of trunk NC. Aggregates observed at Day 6 in cranial NC resembled those observed at Day 2 in cells derived from the trunk NC (Fig. 5B, *cyan dashed box*). The loose aggregation of TUJ1-positive cells and moderate neuritic outgrowth, remained characteristic of the cranial NC-derived cells as differentiation progressed through Day 8 (Figs. 5G, Appendix B). This was in stark contrast to the aggregates formed from trunk NC-derived positive cells, which were more compact and well-defined at Day 6 (Figs. 5F, 6F) and Day 8 (Figs. 5H, 6H, Appendix B) and displayed extensive neuritic outgrowth. The changes in morphology and timing of aggregation were consistently observed over multiple replicates (n=8) from several different cell isolates (n=4). Therefore, these characteristics can all be used to assess the temporal progression of neuronal differentiation *in vitro*.

Another difference detected in neurons derived from trunk NC was the localization of ELAV-like RNA binding proteins HuC and HuD. After 4 days in differentiation medium, HuC/D was localized to the soma and neuritic processes in most of the cranial NC-derived cells (85.89 +/- 13.12%; Figs. 6C, 6C', 6C''; *arrowheads;* quantified in Appendix F). In comparison, HuC/D expression was observed in the soma in trunk NC-derived cells, and mostly absent from the neuritic processes (8.51 +/- 12.91%; Figs. 6D, 6D', 6D''; *arrowheads;* quantified in Appendix F). Differential HuC/D localization persisted through Day 8 (6E, 6F, 6G, 6H). This axial difference suggests that HuC/D is not necessary for neuritic outgrowth during trunk NC-derived neuronal differentiation. Having the ability to

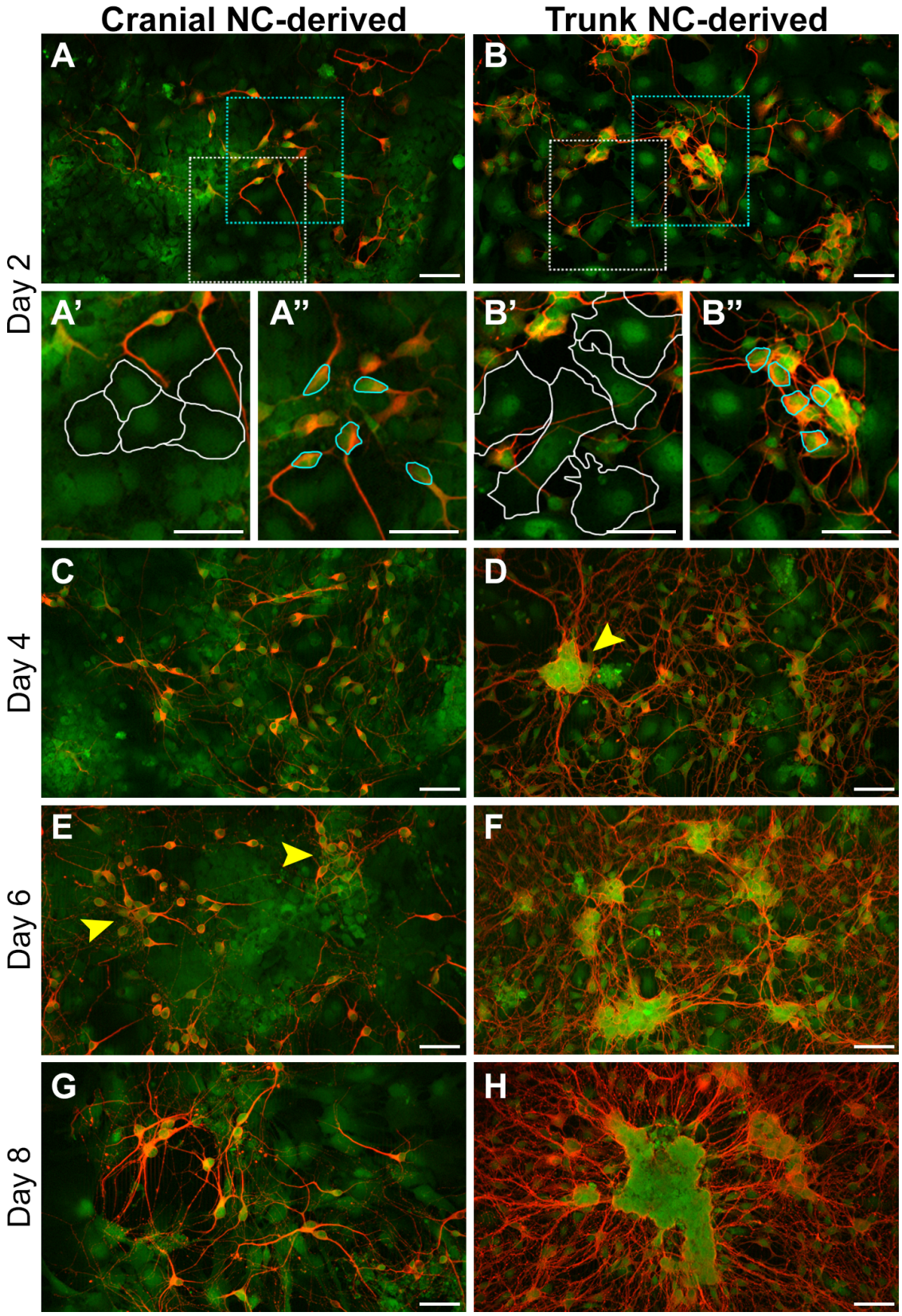

Figure 5. See next page for legend.

Figure 5. Temporal progression of neuronal differentiation in cultured cranial and trunk NC cells. Neuronal differentiation was assessed at various time points via immunostaining for TUJ1, a neuron-specific class III β-tubulin. Robust expression of TUJ1 was observed at Day 2 **(A, B)**. Higher magnification of boxed regions show an observable decrease in soma size when comparing TUJ1-negative cells displaying a mesenchymal morphology **(A', B'**; *white lines***)** and cells positive for TUJ1 that display a neuronal-like morphology **(A'', B''**; *cyan lines***)**. Neuritic outgrowth continued through Day 4 in both cell populations **(C, D)**. In addition, in trunk NC-derived cells, TUJ1-positive cells formed discrete aggregates **(D;** *arrowhead***)**, however similar aggregation was not observed in cells derived from the cranial NC at this time point. By Day 6, the difference in aggregation between the cell populations became more apparent **(E, F)**. While TUJ1-positive aggregates derived from the trunk NC were tightly compacted **(F)**, TUJ1-positive aggregates derived from the cranial NC were loosely formed **(E**; *arrowheads***)**. At Day 8, TUJ1-positive cells derived from the cranial NC maintained a similar phenotype as seen in Day 6 **(G)**. In contrast, TUJ1-positive cells derived from the trunk NC displayed enhanced aggregation, coupled with extensive neuritic outgrowth **(H)**. Phenotypic characteristics of the cells at each time point were consistently observed (n=6; duplicate cultures from each of three independent cell isolates). All cells are derived from *Sox9cre; R26R-EYFP* mice and express EYFP (*green*). Red staining = TUJ1. Scale bars: 50μm.

detect such differences allows further investigation to determine the specific role of HuC/D, and other RNA binding proteins, during neuritogenesis in the peripheral nervous system.

Cranial and trunk-derived NC cells differentiated in culture display distinct morphological transitions characteristic of glial differentiation in vivo.

The temporal progression underlying glial differentiation was determined utilizing the expression of glial fibrillary acidic protein (GFAP, Fig. 7; Jessen and Mirsky, 1984). After 4 days, robust GFAP expression could be seen in both cranial and trunk NC cells (Figs. 7A, 7B), with most cells displaying a stellate, mesenchymal morphology comparable to undifferentiated cells shown previously (Figs. 2B, 2C). After 10 days in glial differentiation medium, the cells exhibited a more diversified range of cell morphologies. Specifically, some of the GFAP-positive cells displayed flattened, sheet-like processes (Figs. 7C, 7D; *asterisks*), similar to those formed by Schwann cell precursors, while other cells had adopted an elongated, spindle-like morphology (Figs.

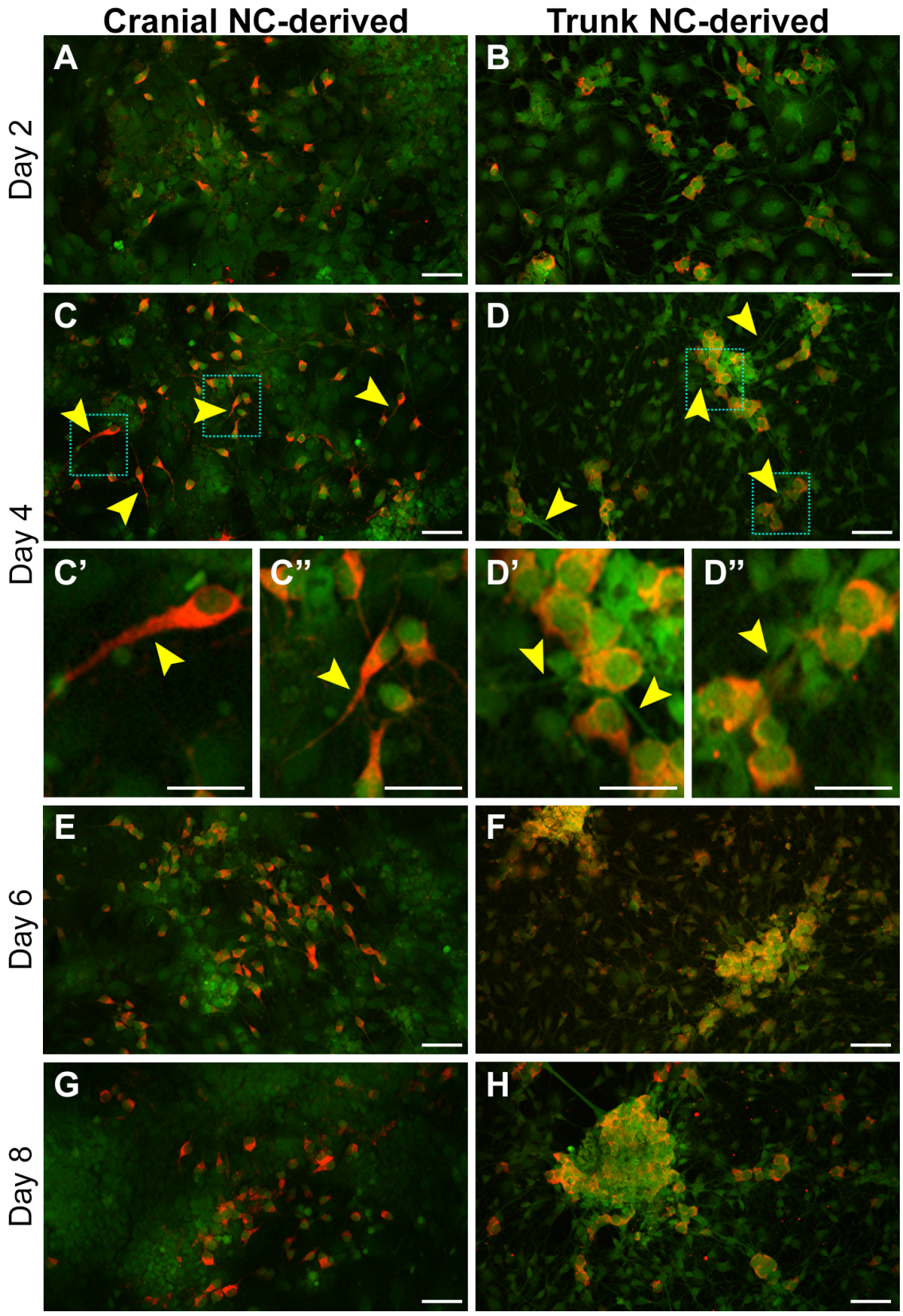

Figure 6. See next page for legend.

Figure 6. Cultured cranial and trunk NC cells exhibit differential HuC/D localization during neuronal differentiation. Neuronal differentiation was assessed at various time points via immunostaining for HuC/D, a pan-neuronal marker recognizing neuron-specific RNA binding proteins. Robust HuC/D expression was observed after 2 days in differentiation medium **(A, B)**. By Day 4, a difference in HuC/D localization in neuritic processes between the cell populations was observed **(C, D**; *arrowheads***)**. Higher magnification of boxed regions show HuC/D localized to the soma and neuritic process of cells derived from the cranial NC **(C', C''**; *arrowheads***)**, however HuC/D expression was only observed in the soma of cells derived from the trunk NC, and absent from the neuritic processes **(D', D''**; *arrowheads***)**. Differences in HuC/D localization between the cell populations persisted through Day 8 **(E – H)**. Phenotypic characteristics of the cells at each time point were consistently observed (n=6; duplicate cultures from each of three independent cell isolates). All cells are derived from *Sox9cre; R26R-EYFP* mice and express EYFP (*green*). Red staining = HuC/D. Scale bars: (A – D; E – H) 50μm; (C', C'', D', D'') 25μm.

7C, 7D, *arrowheads*), indicative of immature Schwann cells. By Day 14, most GFAP-positive cells derived from either cell population displayed an elongated morphology, with extension of bipolar processes (Figs. 7E, 7F). Moreover, flattened, sheet-like processes noted at earlier time points were only observed sporadically throughout the cultures at Day 14. Similar observations were also made using a marker of Schwann cell differentiation, Erb-B2 Receptor Tyrosine Kinase 3 (Erb-B3, Riethmacher et al., 1997; Appendix G).

The transition from flattened, sheet-like processes to elongation of bipolar processes is considered a hallmark of differentiation during Schwann cell development (Dong et al., 1999; Jessen et al., 2015; Maurer et al., 2007; Thaxton et al., 2011). *In vivo*, further maturation is dependent on environmental context as immature Schwann cells will either become a myelinating or non-myelinating Schwann cell depending on the size of the associated axon. In absence of peripheral axons, we conclude that the primary cranial and trunk NC cells are able to give rise to immature Schwann cells *in vitro*. Moreover, changes in cell morphology over the 14-day differentiation time course were highly consistent between cultures (n=6) derived from different cell isolates (n=3). Therefore, the temporal transition in cell shape, specifically between 10 and 14 days in differentiation

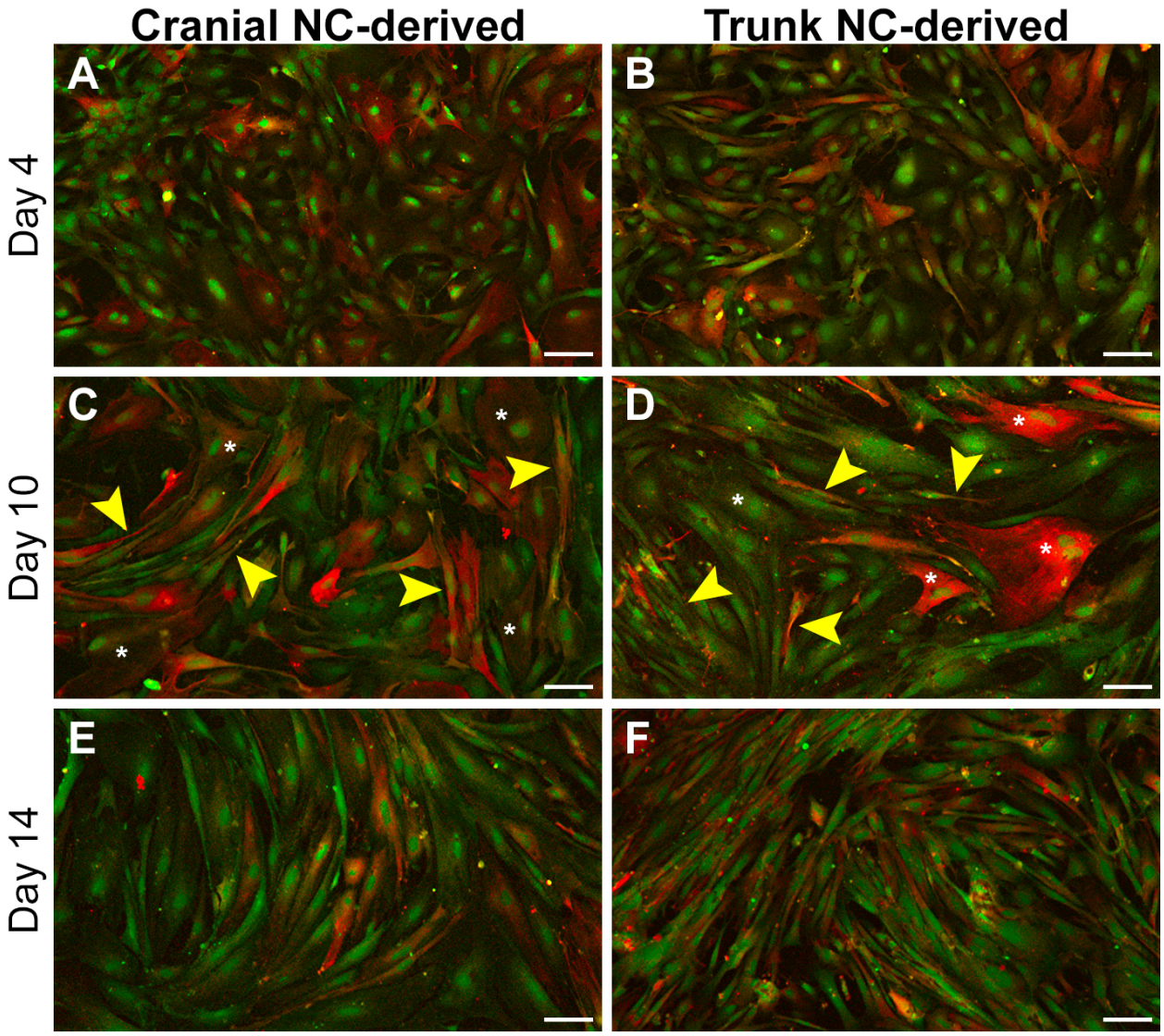

Figure 7. Primary cranial and trunk NC cells display distinct morphological transitions during the temporal progression of glial differentiation *in vitro*. Glial differentiation was assessed via immunostaining for glial fibrillary acidic protein (GFAP) after 4, 10 or 14 days in differentiation medium. GFAP-positive cells were observed in both cranial and trunk NC cell populations at Day 4 **(A, B)**. By Day 10, some of the GFAP-positive cells extended flattened, sheet-like processes **(C, D**; *asterisks***)** while the other GFAP-positive cells displayed an elongated, spindle-like morphology **(C, D**; *arrowheads***)**. After 14 days, most GFAP-positive cells in both populations exhibited an elongated, bipolar morphology and cells extending flattened, sheet-like processes were only occasionally observed **(E, F)**. Phenotypic characteristics of the cells at each time point were consistently observed (n=6; duplicate cultures from each of three independent cell isolates). All cells are derived from *Sox9cre; R26R-EYFP* mice and express EYFP (*green*). Red staining: GFAP. Scale bars: 100μm.

medium, could act as a reproducible gauge of differentiation towards the glial cell fate *in vitro*. We further conclude that both the primary cranial and trunk NC cells exhibit a similar capacity to differentiate into glial cells, and that differentiation occurs along a similar temporal progression.

Cranial NC-derived chondrocytes form distinct nodules and secrete measurable cartilage matrix proteins when cultured as a micromass.

Cranial NC-derived chondrogenic differentiation was assessed by documenting changes in protein expression and cell morphology at several time points over a 2-week differentiation window. These characteristics were determined utilizing expression of Type II collagen (Col2a1), an established marker of articular chondrocyte differentiation (Lefebvre et al., 1997), as well as Alcian blue staining, a common dye used to stain the acidic glycosaminoglycans and sulfated glycoproteins secreted by chondrocytes during chondrogenesis (Mello and Tuan, 1999; Paulsen et al., 1988; Paulsen and Solursh, 1988). *In vivo*, chondroprogenitors initially exhibit a stellate, mesenchymal morphology, and subsequently transition to a cuboidal shape as differentiation progresses (reviewed in Woods et al., 2007). In addition, they begin to produce cartilage matrix proteins, including Col2a1, and highly sulfated proteoglycans, such as aggrecan (reviewed in Woods et al., 2007). The production of cartilage matrix proteins promotes aggregation, which results in the formation of chondrogenic condensations, a hallmark of overt differentiation (reviewed in Hall and Miyake, 2000). *In vitro,* we demonstrate that our cultured cells undergo similar transitions in cell morphology, condensation, and cartilage matrix secretion as described for chondrogenic progenitors *in vivo.*

After 4 days in differentiation medium, many of the cultured cells positive for Col2a1 had transitioned from a mesenchymal morphology (Figs. 8A, 8A'; *white lines*) to a cuboidal one (Figs. 8A, 8A''; *cyan lines*). However, at this time point, parallel cultures displayed only faint Alcian blue staining (Fig. 8E). This suggests that early Col2a1 expression may be promoting morphological changes necessary to begin the differentiation process, but the robust secretion of cartilage matrix proteins has not yet occurred.

We first observed distinct chondrogenic nodules after 6 days in differentiation medium (Figs. 8B, 8F; *arrowheads*). Nodules could be visualized using both Col2a1 and Alcian blue staining, indicating that cartilage matrix proteins were being produced and secreted. Furthermore, the timing of nodule formation was consistent across multiple replicates (n=6) from several distinct cell isolates (n=3).

By Day 8, cartilage matrix-producing chondrocytes were observed extending from the nodules (Figs. 8C, 8G; *arrows*), a phenotypic characteristic which became more prominent as differentiation progressed through Day 14 (Figs. 8D, 8H; *arrows*). Higher magnification of boxed regions in Figures 8C and 8D show chondrocytes which appeared to align and form chains of cells that emanate from the nodules at Day 8 (Fig. 8C', *cyan lines*) and Day 14 (Fig. 8D', *cyan lines*).

Based on our observations, increases in nodule number and cartilage matrix accumulation over time can serve as a measurable benchmark of chondrogenic differentiation *in vitro*. Lower magnification views at Day 6 revealed that chondrogenic nodule formation occurred in localized regions of the cultures (Fig. 8I). However, by Day 14, nodules were observed throughout the cultures (Fig. 8J). Further quantification of

temporal changes in nodule number and cartilage matrix accumulation were analyzed in Alcian blue stained cultures. Consistent with our histological observations, our results showed a statistically significant increase in both nodule number (Fig. 8K) and cartilage matrix accumulation (Fig. 8L) over time when compared to the undifferentiated cells. Together, these data reveal several reproducible characteristics that define the temporal progression of cranial NC-derived chondrogenic differentiation *in vitro*, including the timing of detectable Alcian blue staining, nodule formation and secretion of cartilage matrix proteins.

Discussion

In this chapter, we demonstrate a reliable method for establishing a robust *in vitro* model system of the mammalian NC. We successfully isolated primary cranial and trunk NC cells from E9.5 mouse embryos by FACS, using Sox9 as marker. Once in culture, both NC cell populations expanded relatively quickly while maintaining NC cell identity and stem cell-like properties, even as they were passaged over the course of a 3-week time period. We have also shown that our cultured cells can be reproducibly differentiated into a multitude of NC derivatives, including neuronal cells, glial cells, smooth muscle cells, chondrocytes, adipocytes and melanocytes. Based on our characterization of differentiation markers, cell morphology and cell behavior, we also established reproducible benchmarks that define the temporal progression of NC differentiation into neurons, glia and chondrocytes. This allowed us to detect similarities and differences between the cranial and trunk NC cells as they transitioned through intermediate stages of differentiation, comparable to those described *in vivo.* These temporal benchmarks

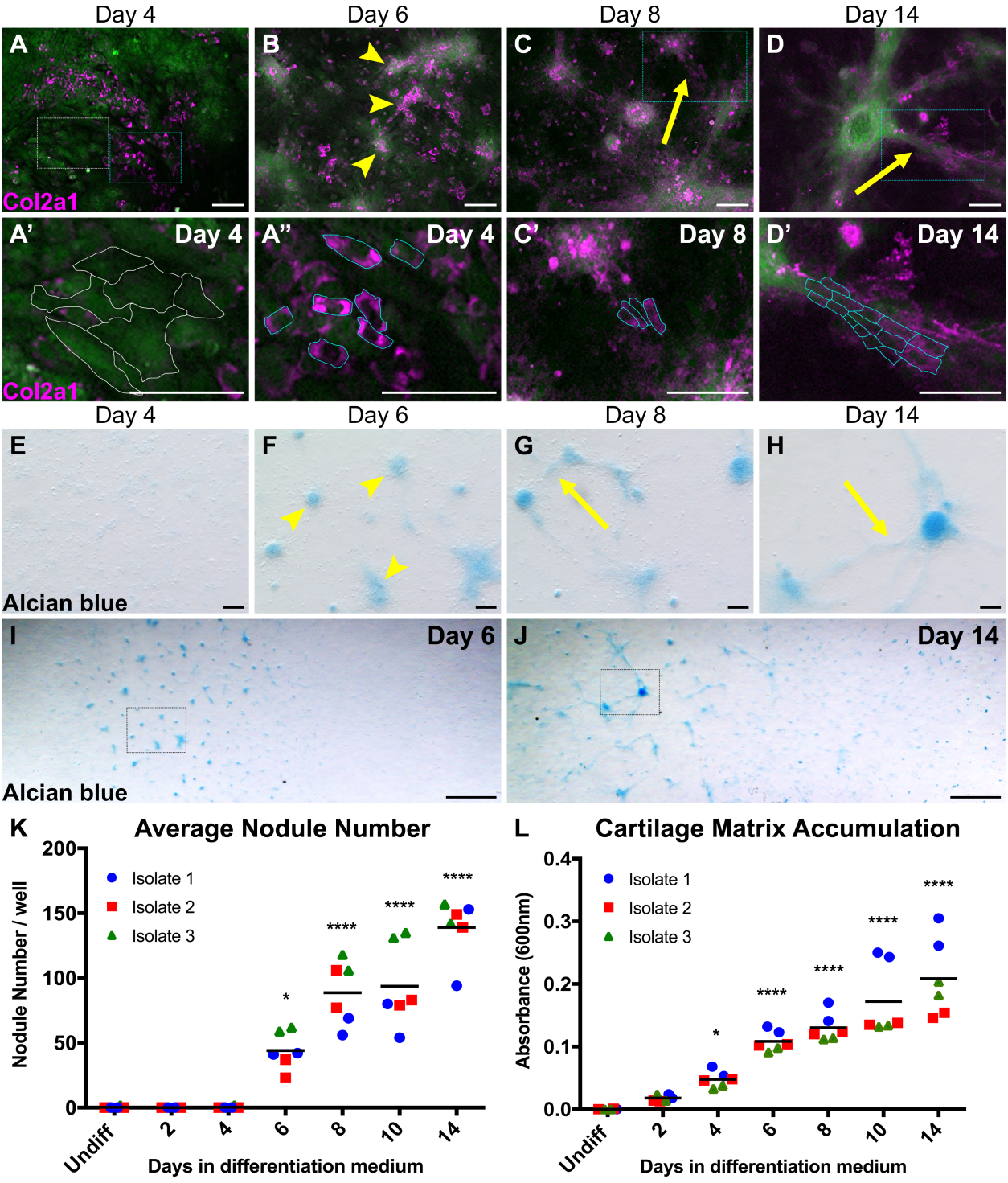

Figure 8. Cranial NC-derived chondrocytes form distinct nodules and produce cartilage matrix *in vitro* over time. Cell morphology and cartilage matrix production were analyzed at various time points via immunostaining for Type II collagen (Col2a1) **(A – D),** and Alcian blue staining **(E - J)**. After 4 days in differentiation medium, Col2a1-positive cells displayed a cuboidal morphology **(A)**. Higher magnification of boxed region highlights the difference between Col2a1-negative cells displaying a mesenchymal morphology (**A'**; *white lines*) and cells positive for Col2a1 that display a cuboidal morphology **(A''**; *cyan lines*). At this same time point, parallel cultures showed faint Alcian blue staining **(E)**. By Day 6, Col2a1-

positive cells began to form chondrogenic nodules that stained positive for Alcian blue **(B, F**; *arrowheads***)**. At later stages of chondrogenic differentiation, chains of chondrocytes producing cartilage matrix could be seen emanating from the nodules **(C, D, G, H**; *arrows***)**. Higher magnification of boxed regions shows chondrocytes which appear aligned, forming chains of cells that emanate from the nodules at Day 8 and Day 14 **(C', D'**; *cyan lines***)**. In addition, the number of chondrogenic nodules increased over time. **(I, J)** In order to obtain a representative field of view of the entire culturing surface, four images from overlapping fields of view were aligned and stitched using the open source Hugin software (d'Angelo, 2007). Nodules were first observed in distinct regions of the well at Day 6 **(I)**, but by Day 14, had spread throughout the well **(J)**. Boxed regions in **I** and **J** correspond to the higher magnification images in **F** and **H**, respectively. Quantification of chondrogenic nodule number **(K)** and cartilage matrix accumulation **(L)** further demonstrates the increase in nodule formation over time. Experiments were repeated from three independent cell isolates, each in duplicate. Each dot represents one technical replicate, grouped by biological isolate. Black horizontal line indicates grand mean across replicates. $*p < 0.05$, $****p < 0.0001$ vs. undifferentiated cells (two-way ANOVA). All cells are derived from *Sox9cre; R26R-EYFP* mice and express EYFP (*green*). Magenta staining = Col2a1. Scale bars: (A – H) 100μm; (I, J) 1mm.

constitute a valuable addition to existing criteria for assessing the impacts of genetic or environmental perturbations on the timing of NC differentiation.

Our method for isolating murine NC cells via FACS differs from previously established protocols in which NC cells are collected after emigrating from neural tube explants dissected at E8.5. At E8.5, isolating premigratory NC cells via FACS alone does not yield enough cells to establish successful growth in culture. Using Wnt1 as a marker, FACS has been used to further select NC cells isolated from E8.5 neural tube explants and expanded in culture (Ishii et al., 2012). Although Wnt1 is commonly used as a marker for selecting the NC (Druckenbrod and Epstein, 2005; Ishii et al., 2012; Pfaltzgraff et al., 2012; Wong et al., 2006), Wnt1 is expressed throughout the cranial dorsal neural tube where it is a marker for both NC and non-NC derivatives (Lewis et al., 2013; McMahon and Bradley, 1990; Pietri et al., 2003). This makes it difficult to specifically isolate cranial NC cells directly from the embryo by FACS using Wnt1 as a marker. In contrast, our method isolates *Sox9*-positive NC cells from specific tissues dissected at E9.5, where Sox9 is a well-established marker for both premigratory and migratory NC cells (Cheung and Briscoe, 2003). In addition, by isolating primary NC cells at this later developmental

time point, we were able to consistently isolate enough purified NC cells to establish successful cultures without the need for an intermediate *in vitro* expansion step prior to selection (Ishii et al., 2012).

We also demonstrate that the cultured primary cranial and trunk NC cells can be induced to differentiate into a broad range of NC derivatives (Fig. 4). As previously described, the cultured cells can give rise to a larger repertoire of derivatives than would be expected from the same cells *in vivo*, when exposed to appropriate differentiation factors. For example, cultured trunk NC cells grown under conditions which simulate the endogenous microenvironment during differentiation could give rise to chondrocytes (Ido and Ito, 2006; Maurer et al., 2007; McGonnell and Graham, 2002) and adipocytes (Billon et al., 2007), albeit with less efficiency compared to the cranial NC. This innate ability to generate multiple cell fates suggests that at least some NC cells possess an inherent plasticity concerning fate determination that can be influenced by exposure to the appropriate environmental cues.

Moreover, while the cultured NC cells were able to produce all the differentiated cell types tested, we also observed subtle, but reproducible differences in the extent of differentiation between the cranial and trunk NC. For instance, melanocyte differentiation appeared more robust in trunk NC cultures, while chondrogenic differentiation appeared more robust in cranial NC cultures. The subtle variations in the extent of differentiation observed between cranial and trunk NC could indicate an intrinsic difference in the way these two populations respond to environmental cues. Alternatively, these differences may reflect mixtures of progenitors with varying differentiation potential as has been described previously (Morrison et al., 1999; Stemple and Anderson, 1992). In support of

this explanation, recent studies have revealed that a large majority of premigratory/migratory murine trunk NC cells are multipotent, both as single cells, and as a population (Baggiolini et al., 2015). However, the number of derivatives formed by each single cell varied, consistent with the premise that NC cells exhibit diverse multipotent potentials.

Distinguishing how cell intrinsic factors and cell environment contribute to the broad, but varied, differentiation potential of NC cells is critical to understanding embryonic development and NC-related diseases. Gene regulatory networks governing NC specification, migration and differentiation demonstrate that NC specifier genes can play multiple roles over the course of NC development (recently reviewed in Martik and Bronner, 2017). For example, Sox9 plays important roles in premigratory and migratory NC, and is also a key regulator of chondrogenic differentiation in cranial NC. Although we demonstrate broad potential for differentiation of Sox9-positive NC cells, it is possible that our primary cultures may select for a population of cells that have a special propensity for Sox9-dependent differentiated cell types. Alternatively, it is possible that Sox9, which is co-expressed broadly in migrating NC cells with other NC specifiers, is later re-expressed in a more limited population during differentiation. We anticipate the isolation and expansion methods we have described could also be applied to embryos from the broad array of NC reporter lines (recently reviewed in Debbache et al., 2018). Genomic and proteomic analyses of NC cells isolated based on expression of different NC specifiers may help determine if expression of different specifiers select for distinct subpopulations with variations in differentiation potential.

Our comparison of cranial and trunk NC isolated from the same animals has also

enabled us to detect axial differences in behavior, morphology and protein localization during the differentiation process. One of the most significant axial differences we noted was in the ability of cells to aggregate during neuronal differentiation. While we observed aggregation in both cell populations, the neurons derived from the trunk NC formed distinct cell aggregates sooner in culture that were more compact and well-defined compared to the cranial NC, suggesting that they have a greater propensity for aggregation (Figs. 5, Appendix B). *In vivo*, aggregation is a common behavior observed between the cranial and trunk NC during gangliogenesis, however there are inherent differences in cell-environment interactions during this process. While the dorsal root ganglia arise exclusively from the trunk NC, neurons in the cranial ganglia are largely derived from placodal ectoderm in the head with contributions from the NC (D'Amico-Martel and Noden, 1983). To date, the specific signals involved in regulating interactions between NC and placodal ectoderm involved in cranial ganglion assembly are still under investigation (Kurosaka et al., 2015). Future studies may exploit the differences we observe *in vitro* between cranial and trunk cultures by using genomic and proteomic analyses to identify cell intrinsic factors that contribute to gangliongenesis at each axial level *in vivo*.

Another difference we detected was in the cellular localization of the HuC/D RNA binding proteins in neurons derived from cranial or trunk NC. While HuC/D was present in the soma and neurites of neurons derived from cranial NC, it was present only in the soma of neurons derived from trunk NC (Fig. 6). This suggests that axonal trafficking or local translation within peripheral axons arising from neurons in the head and trunk may be governed by different mechanisms. In vertebrates, HuC and HuD proteins bind to AU-

rich regulatory sequences in the 3' UTR of target gene transcripts, leading to mRNA stability (reviewed in Dêschenes-Furry et al., 2006). Overexpression of HuC or HuD accelerates neurite outgrowth in cultured PC12 cells (Akamatsu et al., 1999, Anderson et al., 2000), E19 rat cortical neurons and retinoic acid-induced embryonic stem cells (Anderson et al., 2001), and stabilizes growth-associated mRNAs localized to the growth cones of PC12 cells (Smith et al., 2004). Given that we observe HuC/D in neurites of neurons derived from cranial NC, but not from trunk NC, it is possible that another type of RNA-binding protein stabilizes growth-associated mRNAs in the trunk NC. Our culture model provides a means for isolating neurites from the different populations in order to address this possibility. In addition, these cultures may also be used to screen pharmacological agents that promote or disrupt these same processes.

A unique contribution of the current study is our temporal characterization of differentiation along the neuronal, glial, and chondrogenic lineages. Through this analysis, we reproducibly identified distinct intermediate stages during differentiation that mimicked those previously described *in vivo*. We envision future studies that will elucidate gene regulatory changes that accompany these transitions, which could identify cell intrinsic drivers of stage-specific progression along differentiation pathways. Such drivers would serve as important targets for screening potential therapeutic agents useful in stem cell therapies. For example, agents that promote condensation of cells during chondrogenic differentiation may be useful for improving the efficiency of direct programming protocols, enabling more effective generation of resting chondrocytes that could be used to combat the progression of cartilage degeneration associated with osteoarthritis, or restore head and facial tissues disrupted in craniofacial syndromes. In addition, our temporal

characterization of differentiation *in vitro* provides a basis for more comprehensive testing of industrial compounds, personal use products, and therapeutic drugs for developmental toxicity. Although whole animal testing remains the standard for assessing developmental toxicity, the cost and time involved in *in vivo* testing has resulted in a large backlog of compounds to be tested (Woodruff et al., 2011; Mitro et al., 2015). *In vitro* assays that include intermediate endpoints in neuronal, glial, and chondrogenic differentiation could serve as a valuable preliminary screen to prioritize compounds for further *in vivo* analysis.

Another potential application of this culture system is to examine cell intrinsic mechanisms of NC differentiation in the context of various mouse models of human NC-related disorders. Disruption of NC development underlies many pediatric syndromes and has been associated with deletions in multiple genes affecting various aspects of NC development. In many neurocristopathies, patients with identical deletions present with widely disparate symptoms or with varying severity of symptoms (reviewed in Noack Watt and Trainor, 2014). This suggests that a critical interplay between genetic and environmental factors can contribute to the severity of NC-related disorders. *In vitro* methods, such as ours, enables the characterization of cell intrinsic contributions of specific mutations, which can subsequently be assessed in the context of controlled environmental manipulations. For example, the *LgDel* mouse model of chromosome 22q11 deletion syndrome displays many of the hallmarks of the pediatric syndrome including dysphagia (Karpinski et al., 2014). These mice display defects in both cranial nerve development and orofacial morphology, suggesting an impact of the deletion on neuronal and chondrogenic development. However, *in vivo*, it is difficult to separate the direct effects of the deletion on each tissue from the potential of the neural defect to

secondarily impact orofacial development. Furthermore, the ability to partially rescue of the phenotype by manipulation of retinoic acid synthesis suggests the potential for environmental disrupters to further modify the effects of the deletion. *In vitro* analysis of differentiation along both the neural and chondrogenic lineages could help to distinguish the direct impact of the deletions on differentiation of each lineage separately, while providing a platform to investigate environmental contributions.

In accordance with our primary objectives, we have developed methods for effective isolation, expansion, and directed differentiation of murine NC cells. With this method, we are able to reliably obtain enough cells for biochemical analyses, such as co-immunoprecipitation and ChIP-seq, after only a short expansion in culture, thus advancing our ability to elucidate novel protein-protein and protein-gene interactions that regulate NC growth and differentiation. Additionally, since we isolate both cranial and trunk NC cells from the same embryos, this culture system offers a foundation to tease apart the intrinsic and extrinsic factors that contribute to cell fate acquisition in an axial level-specific manner. Finally, we established reproducible benchmarks that define the temporal progression of neural and chondrogenic differentiation *in vitro.* These benchmarks significantly enhance our ability to determine how subtle alterations in the timing of differentiation due to genetic mutation or toxicological exposures contribute to NC-related birth defects and disorders.

CHAPTER IV

Chronological transcriptomic analysis of cranial neural crest cell differentiation along neurogenic and chondrogenic lineages

Abstract

Abnormal cranial neural crest (NC) development can result in a broad spectrum of congenital malformations, many of which are often associated with pediatric syndromes. As multipotent progenitors, cranial NC cells contribute to a diverse array of ectodermal and mesoectodermal cell types, from neurons and glia of the peripheral nervous system to the cartilage and bone of the face. To transition from a progenitor state to a specific cell type, developing cranial NC cells must undergo a sequential series of time-sensitive changes in morphology and behavior driven by concurrent changes in gene expression. However, we currently have a limited understanding of the molecular programming underlying the progression through the intermediate stages of cranial NC differentiation along a specific lineage. Recently, we established a murine culture system modeling cranial NC cell differentiation along the neurogenic and chondrogenic lineages. Systematic characterization of the cultured cells identified reproducible timelines for changes in cell shape, protein expression and aggregation behavior that mimic the progression of neurogenic and chondrogenic differentiation *in vivo*. Using this culture system, we have delineated transcriptional changes that accompany the transition of cranial NC cells to (1) intermediate progenitors, and (2) differentiated peripheral neurons or cartilage matrix-producing chondrocytes. Our results reveal that the temporal

progression of differentiation toward either cell fate is governed by both shared and lineage-specific gene expression patterning that together drive distinct, yet partially overlapping biological processes and pathways. In addition, we have identified distinct transcriptional signatures indicative of the intermediate state, as well as candidate transcriptional regulators that potentially coordinate cell fate acquisition in a stepwise and time-sensitive manner. Together, these data provide a platform for further investigation into the hierarchical, cell-intrinsic circuitry contributing to the plasticity and developmental potential of the cranial NC, and serve as a valuable tool for discovering the molecular targets of genetic and environmental factors that lead to cranial NC-related birth defects and disorders.

Introduction

Disruption of cranial neural crest (NC) cell development can manifest as a wide variety of human congenital birth defects, including craniofacial skeleton malformations, and facial or trigeminal nerve hypoplasia, but can also contribute to predisposition to aggressive types of cancer, such as melanoma and neuroblastoma. Of these, craniofacial abnormalities alone account for one-third of all birth defects and are a leading cause of infant mortality (Gorlin et al., 1990). Despite their prevalence, the etiology underlying many cranial NC-related defects remains poorly understood. Contributing to the diversity of anomalies is the ability of the cranial NC to give rise to both ectodermal cell types, such as sensory ganglia and peripheral glia, and mesoectodermal cell types, including the cartilage, bone, and connective tissues of the face. Proper formation of these derivatives is mediated by a dynamic, multistep process that involves temporal changes in cell

morphology and behavior, both of which play a crucial role in determining cell type-specific function. However, despite their critical contribution to the developing vertebrate head, little is known about the genetic programming that explicitly governs the temporal progression of cranial NC differentiation. Specifically, there is limited information regarding the molecular mechanisms governing the initial transition toward a specific cell type, and the subsequent progression through the intermediate stages of differentiation in that cell type. This gap in knowledge impedes our understanding of how genetic perturbations or environmental toxins may impact the process of differentiation as it unfolds during embryonic development. Elucidation of the dynamic intrinsic programming that governs the temporal progression of cranial NC differentiation will provide a platform for discovering novel molecular targets of genetic and environmental factors that lead to cranial NC-related malformations.

In order to understand the complex molecular programming regulating cranial NC differentiation, it is necessary to obtain a global representation of the transcriptional changes that occur as cranial NC transition toward a specific cell fate. Over the last decade, cumulative information gathered from genome-wide analyses and gene perturbation studies across various vertebrate models has led to the assembly of a putative GRN for the different phases of cranial NC cell development: specification, migration, and differentiation (reviewed in Martik and Bronner, 2017). The overall GRN is characterized by a cascade of regulatory modules for each phase that combines our current understanding of the signaling and transcriptional inputs shown to drive activation of downstream gene batteries. To date, most of the information compiled focuses on the regulatory logic controlling cranial NC specification and migration. Although modules for

lineage-specific differentiation have been formulated, the information is limited to the terminally differentiated state. Consequently, this static, endpoint assessment of cranial NC diversification lacks pertinent information regarding the progression through the intermediate stages of cranial NC differentiation toward a particular cell fate in a stepwise and time-sensitive manner. Disruption or mis-wiring of the temporal circuitry leading to either accelerated or delayed cranial NC differentiation may contribute to the formation of cranial NC-related defects. Introducing a temporal dimension into our current understanding of the GRNs driving differentiation would enable development of improved strategies for diagnosing and treating patients with structural and functional deficits resulting from perturbation of this process.

Advances in high-throughput genomic sequencing technologies have provided the opportunity to assess the dynamically changing regulatory landscape controlling cranial NC differentiation, thus increasing our resolution of the current GRNs. However, the mammalian cranial NC is a transient, rare population of cells and the intermediate stages of differentiation toward a specific cell fate are difficult to isolate and assess *in vivo*. Recently, we have established a primary murine culture system modelling the temporal progression of cranial NC differentiation along the ectodermal (neurogenic) and mesoectodermal (chondrogenic) lineages (Replogle et al., 2018). Detailed characterization of the cultured cells identified reproducible timelines for stepwise changes in morphology and behavior that mimic those described during neurogenesis and chondrogenesis *in vivo*. Importantly, having the ability to capture these intermediate stages of differentiation allows us to determine the precise transcriptional programming that governs cranial NC cell fate acquisition in a stepwise and time-sensitive manner.

Taking advantage of this culture system, we set out to determine the specific transcriptional signatures associated with the intermediate stages of neurogenesis or chondrogenesis in the cranial NC. Specifically, we utilized RNA-seq to identify temporal changes in gene expression that accompany cultured cranial NC cells as they transition to (1) intermediate progenitors, and then (2) differentiated peripheral neurons or cartilage matrix-producing chondrocytes. We chose to focus our studies on these two lineages based on their relevance to human cranial NC-related malformations, but also because we observed similar changes in cell shape and aggregation formation during the differentiation process *in vitro*, that are also known to occur *in vivo*. For instance, during neurogenesis in the developing peripheral nervous system, migratory NC cells are directed into discrete streams, which promotes aggregation and subsequent differentiation characterized by soma compaction and extension of neuritic processes (reviewed in Marmigère and Ernfors, 2007). We observed the same cell shape changes in neurons derived from the cultured cranial NC, coupled with aggregation and neuritic outgrowth over time (Replogle et al., 2018). During limb bud morphogenesis *in vivo*, mesenchymal progenitors will transition first to chondroprogenitors, which display a cuboidal morphology, then produce various cartilage matrix proteins, thus promoting condensation which is crucial for further differentiation and maturation of the chondrocytes (reviewed in Bobick et al., 2009). We observe similar transitions in cell shape and condensation in our cultured cranial NC cells as they differentiate into cartilage matrix-producing chondrocytes over time (Replogle et al., 2018). The apparent similarities in cellular changes between these two distinctly different cell fates raises the intriguing possibility that there may be a degree of overlapping programming shared between

neurogenesis and chondrogenesis, at least during the initial stages of cranial NC differentiation. Deciphering transcriptional relationships mediating the formation of peripheral neurons and chondrocytes in the developing head, may provide crucial insight into the mechanisms that contribute to multisystemic phenotypes often associated with cranial NC-related disorders.

In this chapter, we present a comprehensive analysis of gene expression changes detected at early and late time points over the course of neuronal and chondrogenic differentiation in the cranial NC. Significantly, we detected distinct transcriptional signatures corresponding to the intermediate neuroprogenitor or chondroprogenitor state. To our knowledge, our study is the first to systematically profile the transient, intermediary cells associated with peripheral gangliogenesis or chondrogenesis in the cranial NC. Moreover, comparison of the transcriptional signatures between the two cell fates revealed a combination of both common and lineage-specific gene expression modules that together govern distinct, yet partially overlapping biological processes and pathways mediating the progression toward a differentiated state. We also discovered putative transcriptional regulators that potentially drive the stage-specific transitions during the differentiation process. Elucidation of these temporally dynamic, stage-specific gene modules represents a crucial first step in elaborating upon the current GRNs underlying the progression of differentiation along the neurogenic or chondrogenic lineages in the cranial NC.

Results

Temporally-clustered transcriptional signatures reveal common and lineage-specific programming

In order to identify transcription profiles indicative of the intermediate state we utilized RNA-seq to assess changes in gene expression that accompanied cultured primary murine cranial NC cells as they differentiated over time into either neurons or chondrocytes. Transcriptomic comparisons were carried out at two specific time points relative to the undifferentiated cranial NC (Day 0). Cells at the earlier time points, Day 2 for neurogenesis and Day 4 for chondrogenesis, represent a target population of transient intermediates progressing toward a differentiated state. Cells at the later time points, Day 6 for neurogenesis and Day 14 for chondrogenesis, represent a population enriched for differentiated cells (Fig. 9, Appendix H). These time points were chosen as they correspond to well-characterized lineage-specific changes in morphology and behavior that define the progression of neurogenic or chondrogenic differentiation, both observed *in vitro*, and reported *in vivo*.

Our overall transcriptomic analysis revealed lineage-specific changes in the expression of over a thousand transcripts in at least one time point relative to their expression in the undifferentiated cranial NC. However, to determine if the differentially expressed (DE) transcripts followed a temporally dynamic pattern of expression across the time points, we identified the timing of their peak expression over the course of neurogenesis or chondrogenesis. Peak expression was determined by comparing transcript counts of individual transcripts in each sample against the mean derived from all biological replicates across all time points. Transcripts were then grouped based on

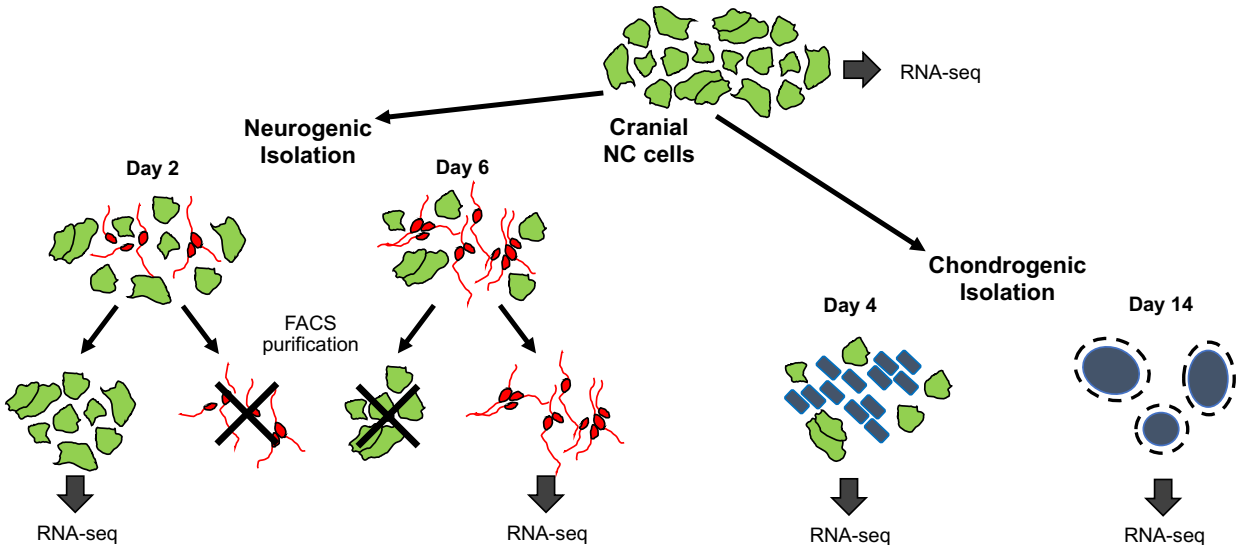

Figure 9. Workflow for isolation of target populations for RNA-seq. Total RNA was extracted for each lineage at 2 time points, as well as from cranial NC cells set aside prior to differentiation. Concerning neurogenic differentiation, at Day 2 differentiated neurons (red cells) represent a small proportion of the overall culture, while a majority of the remaining cells maintain a stellate morphology (green cells). In contrast, at Day 6 a larger proportion of the culture contains mature neurons. This suggests the presence of neuronal intermediate progenitors undergoing the initial stages of differentiation at the earlier time point. FACS purification was used to enrich for target populations at each time point based on cell size differences, thus eliminating the small number of differentiated neurons at Day 2 and stellate cranial NC cells at Day 6. Concerning chondrogenic differentiation, at Day 4 whole cultures were processed as they are enriched for chondroprogenitors (blue cells), which display the characteristic cuboidal morphology. At Day 14, chondrogenic nodules (blue circles) containing condensed, differentiated chondrocytes are readily visualized throughout the cultures. To enrich for differentiated cells at Day 14, chondrogenic nodules were individually picked and dissociated for downstream analyses.

the temporal patterning of Z-scores using K-means clustering. This enabled detection of several distinct clusters of transcripts that displayed peak expression at each one of the time points assessed for both neuronal and chondrogenic differentiation (Fig. 10A) Specifically, we identified a subset of transcripts with peak expression in the intermediate cells, potentially playing a role in driving the transition from multipotent cranial NC cell toward either lineage. We also observed a subset of transcripts that displayed peak expression in both populations at time points corresponding to a mature, differentiated state. As expected, lineage-specific markers were present in these data sets, including the transcriptional regulators Ascl1 and NeuroD1 for neurogenesis, and Sox9 and Runx1

for chondrogenesis. Finally, we observed a subset of transcripts that displayed peak expression in the undifferentiated cranial NC, and were subsequently downregulated over time. Together, these clusters represent distinct modules of gene expression that control the progression through the various stages of diversification toward these two specific cell fates.

One surprising, but not completely unexpected finding was that 420 DE transcripts were shared between neurogenesis and chondrogenesis. Of the those identified, 183 transcripts (43.6%, Appendix I) were commonly upregulated, and 237 transcripts (56.4%, Appendix J) were commonly downregulated as the cranial NC cells progressed through these differentiation processes. The shared expression of these transcripts may be connected to subtle similarities in cellular changes that we observed during neuronal or chondrogenic differentiation in our culture system. Notably, cranial NC cells directed toward either lineage will first reduce cell size, then form aggregations over time, and this progression was coupled with robust differentiation (Replogle et al., 2018). To determine which biological processes were enriched in each of these groups we performed gene ontology (GO) analysis. We detected 12 biological processes that were commonly controlled either through upregulation or downregulation of gene expression (Figs. 10B, 10C). Consistent with the shared behaviors we observed over the course of differentiation *in vitro,* we found many of the processes to be associated with cellular and cytoskeletal reorganization, as well as those related to cell-cell and cell-matrix interactions (Fig. 10B). Moreover, commonly downregulated transcripts were predominantly associated with cell

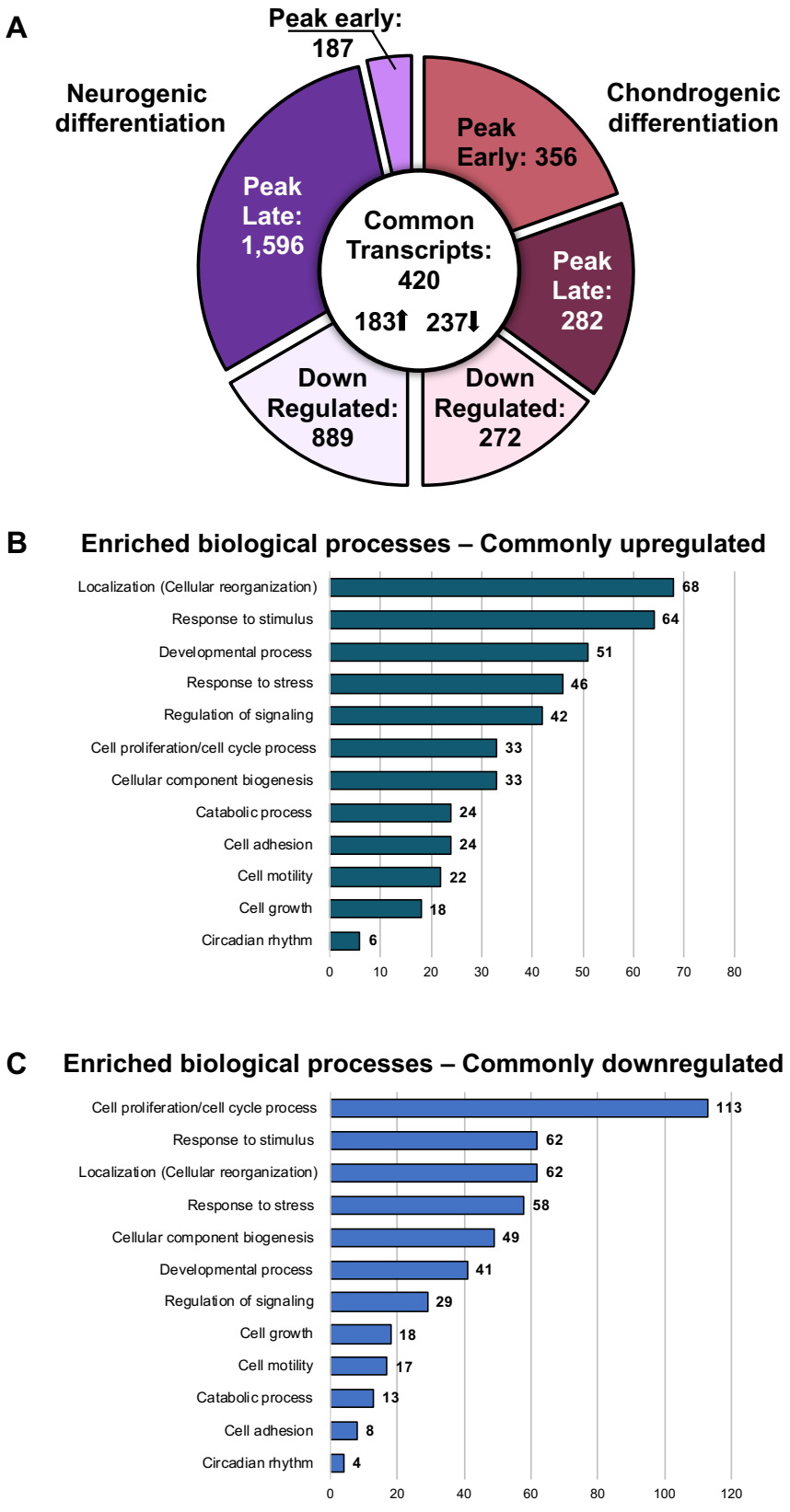

Figure 10. See next page for legend.

Figure 10. Differentially expressed transcripts cluster temporally to reveal common and lineage-specific differentiation programs. (A) Summary of RNA-seq data generated from cells isolated at time points corresponding to the intermediate state (early time points) and differentiated state (late time points) relative to the undifferentiated cranial NC. Differentially expressed transcripts demonstrate stage-specific gene expression patterning during neurogenic (shades of orange) or chondrogenic differentiation (shades of purple). Of these, the expression of 420 transcripts was shared between neurogenesis and chondrogenesis, where 183 transcripts were commonly upregulated, and 237 transcripts were commonly downregulated over the course of differentiation. **(B, C)** GO analysis of commonly upregulated (B) and downregulated (C) transcripts showed enrichment for 12 distinct biological processes. Number of transcripts associated with each biological process is noted.

cycle progression and cell proliferation (Fig. 10C). Interestingly, cross-referencing these transcripts against the Mouse Genome Informatics (MGI) Human Disease database revealed a subset of genes implicated in congenital birth defects and human genetic diseases, including microcephaly, Alport syndrome, Bloom syndrome, Charcot-Marie-Tooth disease, and increased cancer susceptibility**.** Together, these findings indicate that there is a degree of overlapping programming that is shared between these two cell fates that drive similar morphological and behavioral changes over the course of differentiation. In addition, reducing the expression of genes associated with cell cycle progression is consistent with the idea that in order to achieve a differentiated state, progenitor cells must first suppress programming associated with maintenance of stem cell-like properties, such as self-renewal. We further conclude that differentially expressed transcripts not found in common between the two processes are likely to be ones driving the fate-specific differentiation programs.

Temporal gene expression patterning drives stage-specific biological processes and pathways over the course of neuronal differentiation in the cranial NC.

To specifically interrogate gene expression patterning and associated biological processes over the course of neurogenesis in the cranial NC, we focused our analysis on

DE transcripts identified at early (Day 2) and late (Day 6) time points relative to their expression in the undifferentiated cultures (Day 0). Our transcript list was further refined by excluding the 420 transcripts found in common with chondrogenesis, thus revealing 2,672 DE transcripts specifically associated with the progression of neurogenesis. Peak expression of these transcripts was again used to generate temporal clusters using K-means clustering analysis. We detected 5 different clusters of transcripts, each of which exhibited a distinct pattern of peak expression corresponding to the time points assessed (Fig. 11A). For instance, 187 DE transcripts (70.0%) displayed peak expression explicitly at Day 2, and were subsequently downregulated in the differentiated peripheral neurons. Since this time point represents the intermediate state, the genes expressed in this cluster may be those promoting commitment to the neuronal cell fate by driving the initial transition from a multipotent state toward a differentiated one. In comparison, we identified 1,596 DE transcripts (59.7%) that displayed peak expression at Day 6, corresponding to differentiated peripheral neurons. Interestingly, closer analysis revealed two discrete patterns of expression for the DE transcripts in this category: one representing transcripts that gradually increased as the undifferentiated cells progressed toward the differentiated state (602 DE transcripts; 22.5% of the total transcripts), and another characterized by an apparent downregulation of expression in the intermediate cell population, followed by peak expression in the differentiated neurons (994 DE transcripts; 37.2% of the total transcripts). These differences in gene expression signatures accentuate two separate programs working together to promote lineage restriction, one that contributes to the gradual transition from intermediate neuroprogenitor to differentiated neuron, and one that is involved in maintenance of the

terminally differentiated state. The remaining 889 DE transcripts (33.3%) were grouped across two clusters, both of which displayed peak expression in the undifferentiated cells, remained highly expressed through the intermediate state, but showed marked reduction of expression in the differentiated neurons. Since the overall pattern of expression was very similar between these two groups, the transcripts in these clusters were merged prior to downstream analysis. Taken as whole, our results delineate the temporally dynamic genetic program driving the progression through the intermediate and differentiated stages of neurogenesis in cranial NC, and highlight specific subsets of genes that may be crucial for the initial transition along the ectodermal lineage, as well as those potentially required for commitment and maintenance of the differentiated state.

We next queried the temporally clustered transcripts for evidence of stage-specific biological processes and pathways that underlie the progression of neuronal differentiation in the cranial NC. Our results revealed that diversification along the neurogenic lineage is mediated by a chronological series of distinct, but partially overlapping biological events, which together delineate the stepwise transition toward a neuronal cell fate (Fig. 11B). As expected, many of the transcripts with peak expression in the differentiated state were enriched for biological processes and pathways known to be associated with nervous system development and maturation, including neuronal projection organization, synapse formation, and neurotransmitter release. In addition, transcripts that were specifically downregulated over time were primarily involved in cell cycle progression, DNA replication and DNA repair, a gene signature indicative of differentiated cells.

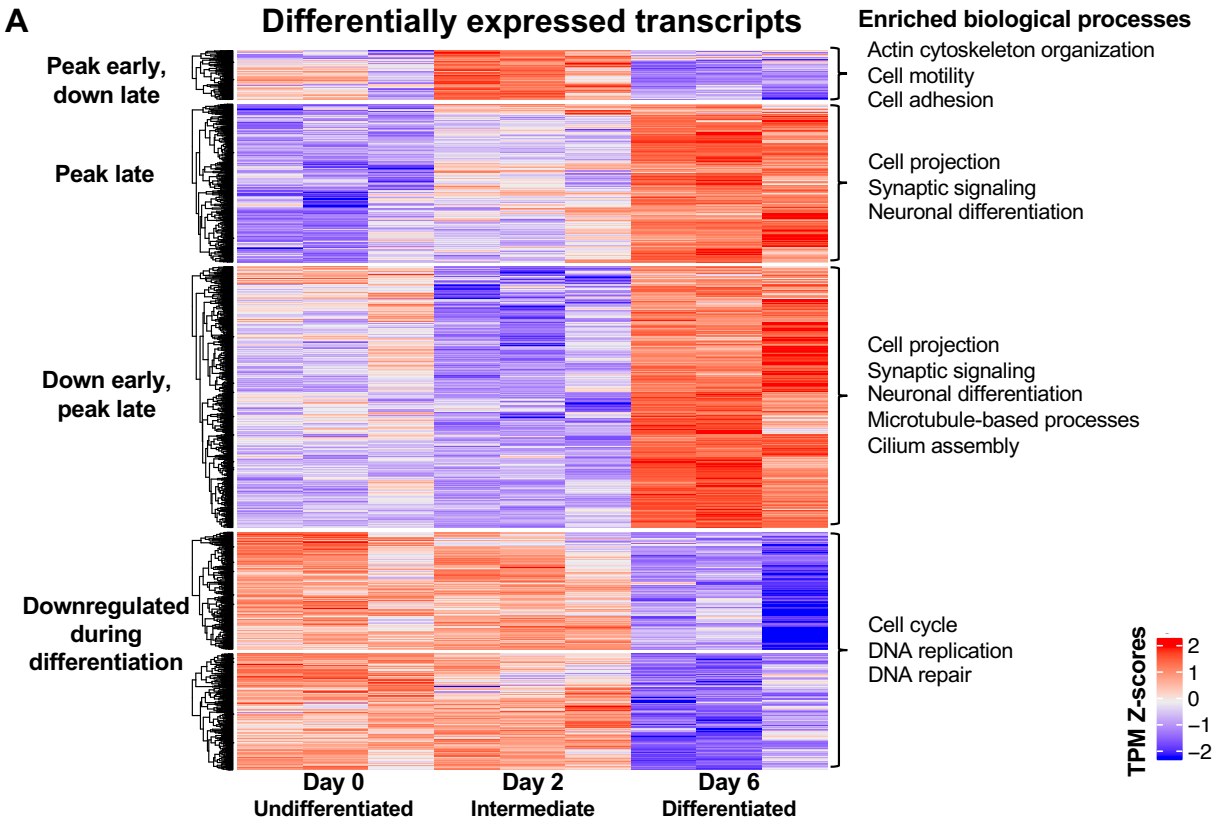

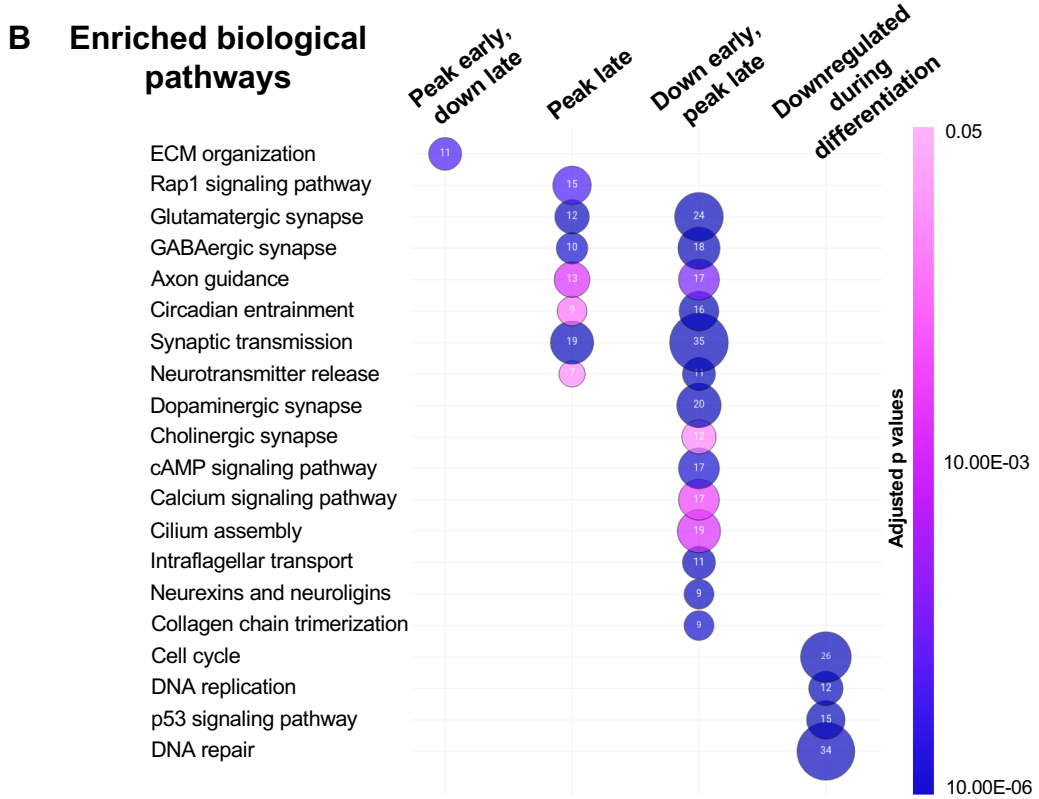

Figure 11. See next page for legend.

Figure 11. Temporally dynamic gene expression modules govern stage-specific biological process and pathways over the course of neuronal differentiation in the cranial NC. (A) Temporally clustered transcripts reveal distinct gene expression modules corresponding to the intermediate and differentiated stages of neurogenesis. Transcripts within each cluster display stage-specific enrichment of biological processes underlying the progression of differentiation. Expression heatmap was produced from Z-scores (calculated using transcript per millions [TPM] estimates) of 2,672 differentially expressed transcripts with adjusted p values <0.01. Mean normalized transcript counts were generated for each transcript across all samples at all time points. Each row represents a single transcript. Each column represents one of the three biological replicates for each time point. Red and blue indicate standard deviation above and below the mean, respectively. GO analysis was used to determine enrichment of biological process associated with cluster-specific transcripts. **(B)** Stage-specific enrichment of biological pathways associated with temporally clustered transcripts. Color scale represents adjusted p values. Circle size represents number of transcripts associated with each biological process, where the specific value appears within each circle.

There were also several biological processes that emerged as potentially defining features associated with the progression towards a neuronal phenotype. Notably, pathways involved in actin cytoskeletal reorganization were significantly enriched in the intermediate cell population, and subsequently downregulated in the differentiated cells. In our culture system we observed soma compaction to be one of the earliest events associated with acquisition of a neuronal morphology (Replogle et al., 2018). Therefore, the genes associated with this process may be those contributing to cell remodeling needed to reduce cell size, and also promote initial axon sprouting (reviewed in Compagnucci et al., 2016). Transcripts found associated with the intermediate state were also enriched in pathways corresponding to ECM organization. *In vitro* studies have shown that lineage specification in mesenchymal stem cells (MSCs) can be solely directed by extracellular matrix elasticity or “stiffness” to produce a range of derivatives from neurons to bone (Engler et a., 2006; Swift et al., 2013), suggesting an important contribution of microenvironment composition in influencing cell fate decisions. Accordingly, pathways involved in cell adhesion were enriched in transcripts that gradually peaked in expression in the differentiated state, potentially playing a role in

facilitating cell-cell and cell-ECM interactions that promote aggregation, and further maturation of the neurons.

We further identified circadian entrainment as a significantly enriched pathway associated with transcripts that were downregulated in the intermediate cell population, but upregulated in the differentiated neurons. In the mammalian brain, the suprachiasmatic nucleus (SCN) of the hypothalamus is recognized as the master regulator of circadian rhythm, although locally generated rhythmicity can be synchronized in peripheral tissues by external cues in order to coordinate cell-type specific gene expression (recently reviewed in Astiz et al., 2019). However, this process has not been previously investigated in the cranial NC or its derivatives. Additionally, we observed pathways associated with cilium assembly and intraflagellar transport enriched in transcripts exhibiting the same trend, suggesting a temporal dependence on primary cilia assembly and signaling in both NC development and peripheral neurogenesis. Interestingly, NC-specific perturbation of cilium function results in aberrant NC patterning and development (reviewed in Chang et al., 2015), however the specific role of primary cilia in neurons derived from the cranial NC is not well understood. Furthermore, misregulation of the transcripts identified in this particular cluster have been implicated in a number of ciliopathies, such as Bardet-Biedl syndrome and Kartagener's syndrome. In addition, we detected many transcripts in a cluster-wide analysis associated with various neurological and neurodevelopmental disorders, as well as neurodegenerative disease. Taken together, our data demonstrates that temporal changes in transcriptional programming govern stage-specific biological processes corresponding to the progression of peripheral gangliogenesis in the cranial NC.

Temporal gene expression patterning drives stage-specific biological processes and pathways over the course of chondrogenic differentiation in the cranial NC.

Similar trends in temporal gene expression patterning were evident as cultured cranial NC cells transitioned along the chondrogenic lineage. Exclusion of the transcripts found in common with neurogenesis enabled detection of 910 DE transcripts specifically associated with the early (Day 4) and late (Day 14) time points of chondrogenesis, with respect to their expression in the undifferentiated cultures (Day 0). These transcripts were then grouped based on their pattern of peak expression, revealing 3 specific clusters (Fig 12A). In one cluster we observed 356 DE transcripts (39.1%) that were downregulated in the undifferentiated cultures, but exhibited peak expression in the intermediate cell population, and remained highly expressed as differentiation continued. It is possible that transcripts within this cluster are those that not only bias cranial NC cell fate decisions toward the mesoectodermal lineage, but reinforce the initial programming necessary to promote a chondroprogenitor state. We also identified 282 DE transcripts (31.0%) that displayed peak expression specifically in differentiated cells found within the chondrogenic nodules, and therefore are likely contributing to maturation and maintenance of the cartilage matrix-producing chondrocytes. Lastly, we detected 272 DE transcripts (29.9%) with peak expression in the undifferentiated cranial NC cells that displayed a gradual downregulation as the cultures differentiated into chondrocytes over time, thus contributing to refining the transcriptional programming that promotes the overall differentiation process. Comparable to our observations during neurogenesis, these data demonstrate that the temporal progression of chondrogenic differentiation in the cranial NC is mediated by stage-specific gene expression modules, which together

drive the stepwise transition from multipotent cranial NC progenitor toward a specialized differentiated cell type.

Subsequent GO analysis of the cluster-specific transcripts identified key biological processes and pathways corresponding to structural and behavioral changes known to mediate the progression through the intermediate stages of chondrogenesis (Fig. 12B). Of note, processes associated with cellular reorganization, cell motility, and cellular homeostasis were found to be enriched in transcripts that were initially upregulated in the intermediate cells, but remained highly expressed as differentiation progressed. Some of the same processes were also enriched in transcripts displaying peak expression in the differentiated cells consistent with continued involvement of these gene products during chondrocyte maturation. Moreover, we observed cell-cell communication, regulation of signal transduction, and pathways associated with ECM organization and collagen formation to be significantly enriched in the differentiated cells. We also detected enrichment of transcripts associated with hypoxia-inducible factor 1 (HIF1) signaling and circadian rhythm in the differentiated chondrocytes. While both of these pathways have been implicated in regulating endochondral ossification during mesoderm-derived skeletogenesis (Amarilio et al., 2007; Takarada et al., 2012), neither have been investigated for their cell autonomous regulation specifically in cranial NC-derived chondrocytes that form the craniofacial skeleton. Lastly, as expected for differentiated cell types, transcripts that were downregulated over time were found to be involved with cell cycle progression, DNA replication and DNA repair, similar to as seen during neurogenesis.

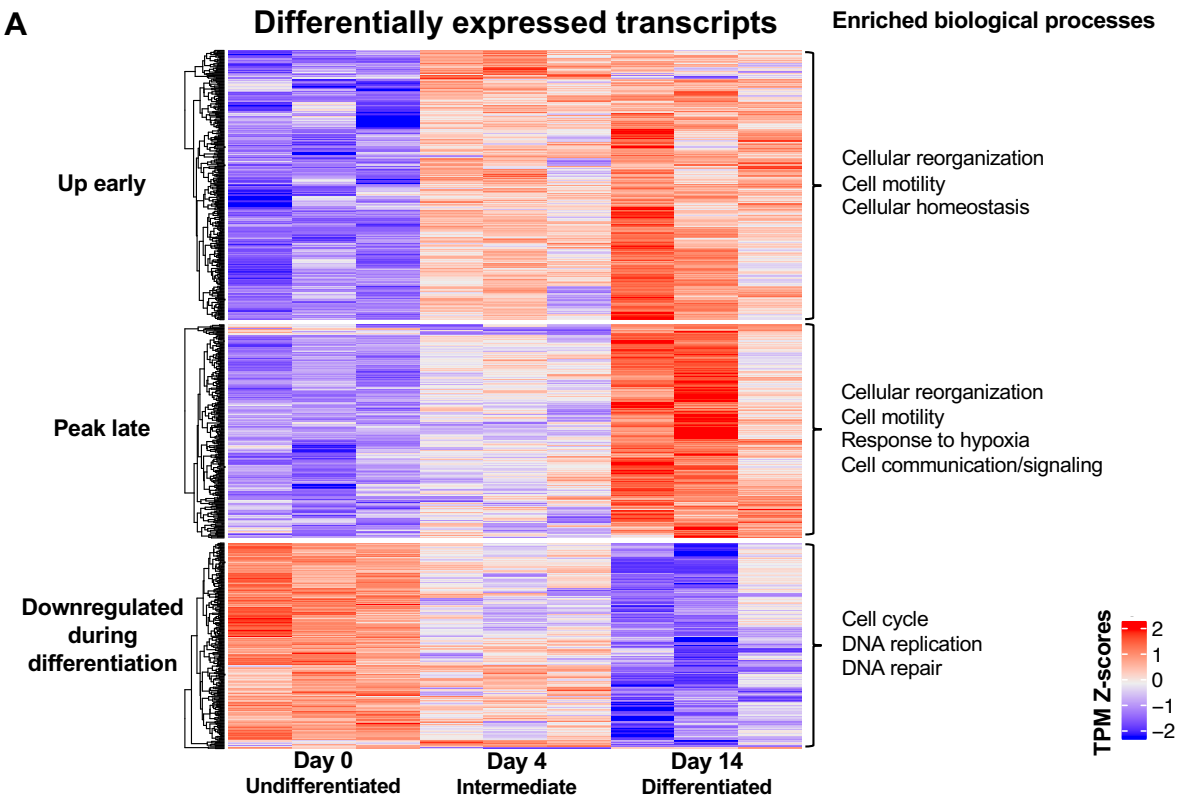

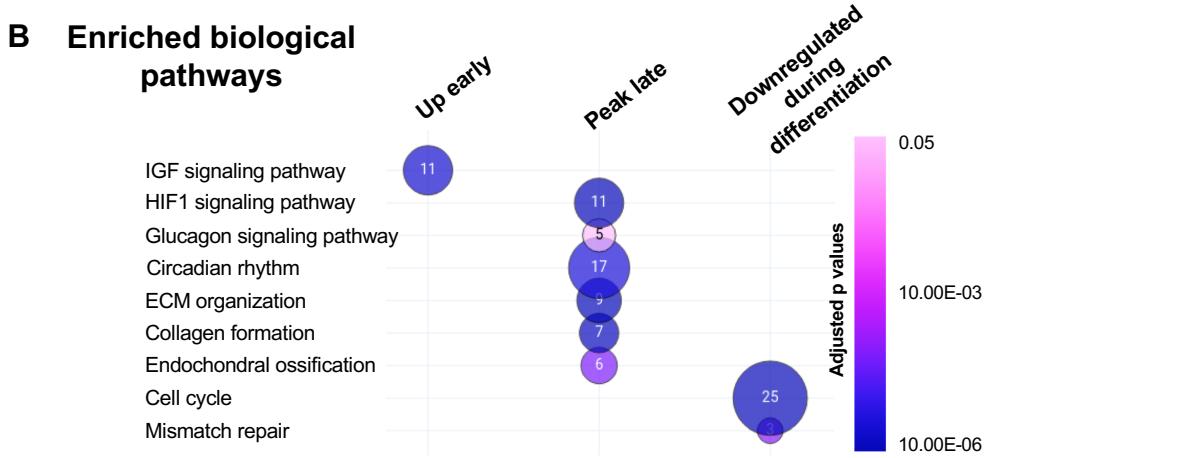

Figure 12. Temporally dynamic gene expression modules govern stage-specific biological processes and pathways over the course of chondrogenic differentiation in the cranial NC. (A) Temporally clustered transcripts reveal distinct gene expression modules corresponding to the intermediate and differentiated stages of chondrogenesis. Transcripts within each cluster display stage-specific enrichment of biological processes underlying the progression of differentiation. Expression heatmap was produced from Z-scores (calculated using transcript per millions [TPM] estimates) of 910 differentially expressed transcripts with adjusted p values <0.01. Mean normalized transcript counts were generated for each transcript across all samples at all time points. Each row represents a single transcript. Each column represents one of the three biological replicates for each time point. Red and blue indicate standard deviation above and below the mean, respectively. GO analysis was used to determine enrichment of biological process associated with cluster-specific transcripts. **(B)** Stage-specific enrichment of biological pathways associated with temporally clustered transcripts. Color scale represents adjusted p values. Circle size represents number of transcripts associated with each biological process, where the specific value appears within each circle.

The processes and pathways identified correlate with well-described, sequential changes in cell shape and condensation behavior that occur in chondroprogenitors as they progress toward a differentiated state, both *in vivo* and *in vitro*. First, cytoskeletal reorganization leads to acquisition of a cuboidal morphology, which in turn promotes cellular organization, including dynamic changes in nuclear shape and intercellular location of organelles. Stabilization of this new cellular equilibrium triggers an increase in cell-cell and cell-ECM interactions, as well as ECM deposition, all of which are necessary for subsequent condensation of the dispersed cells, ECM establishment and ECM maintenance. Importantly, disruption of either morphogenic process inhibits overt chondrogenic differentiation (Ray and Chapman, 2015). Along those lines, many DE transcripts identified in our chondrogenic signatures have been implicated in human genetic diseases and syndromes characterized by multi-symptom phenotypes, including facial dysmorphism. Importantly, we have also identified circadian rhythm and hypoxia signaling as potentially novel pathways involved in this process. While mechanisms underlying these two pathways have been shown to regulate mesoderm-derived skeletogenesis, they have not been investigated specifically for their role in regulating chondrogenic differentiation in the cranial NC. Thus, our analysis provides new avenues for exploration into the similarities and differences in these mechanisms and how they might be applicable to cartilage formation in the developing head. Moreover, we conclude that the temporal progression of chondrogenesis in the cranial NC is governed by dynamically changing gene expression modules, which drive distinct, yet partially overlapping biological processes and pathways important for proper formation of the craniofacial skeleton.

Stage-specific transcriptional regulators drive the temporal progression of neurogenesis and chondrogenesis in the cranial NC.

Our transcriptomic analysis revealed both common and unique gene expression signatures that together promote the transition and subsequent lineage-specific differentiation in the cranial NC in a stepwise and time-sensitive manner. Not surprisingly, many of the gene sets corresponded to biological processes and pathways expected to underlie the progression toward each cell fate. Others were novel, and warrant further investigation in the context of cranial NC. In addition, we identified several reoccurring processes and pathways that were shared between neurogenesis and chondrogenesis, including cell motility, cell-cell and cell-ECM interactions, ECM organization and circadian rhythm. While many of the associated transcripts were found to be commonly expressed between the two cell fates, we also detected distinct suites of genes for each process that were expressed in a lineage-specific manner. This suggests a potential interplay between common and unique transcriptional programming in mediating the gradual shift toward fate commitment, possibly through regulatory interactions between transcription factors found in each program.

To address this, we next wanted to determine the key regulators responsible for driving the dynamic changes in transcriptional programming over the course of neurogenesis or chondrogenesis. By comparing our transcriptomic data to a recently published catalog of known human transcription factors (Lambert et al., 2018), we were able to compile a list of 198 transcription factor-encoding transcripts that displayed differential expression at any time point during the differentiation process (Fig. 13A). Of these transcripts, 18 (9.1%) were found to be either commonly upregulated or

downregulated over the course of differentiation (Fig. 13B). Interestingly, we identified Klf9 and Pura as commonly upregulated genes associated with circadian rhythm (Petsakou et al., 2015; Spörl et al., 2012), suggesting an important role for these regulators in driving this process in both neurogenesis and chondrogenesis. Consistent with previous observations, many of the commonly downregulated transcripts encoded gene products involved in controlling stem cell renewal (Tead2) or proliferation (Mxd3, Foxm1, Mybl2, Dach1). Unexpectedly, only two C2H2 zinc finger proteins, Zbtb16 and Zbtb20, have been reported to play dual roles in regulating cell fate decisions along ectodermal and mesoectodermal lineages. In fact, many of the commonly identified factors are only known to modulate differentiation toward one fate or the other. Moreover, very few have been investigated in the context of the cranial NC, highlighting new avenues of exploration to uncover the function of these transcriptional regulators in governing lineage-specific cell fate acquisition.

The remaining transcripts were unique to neurogenesis and chondrogenesis, respectively, and displayed temporal expression pattering similar to that seen when assessing peak DE transcript expression for either time course as a whole (Figs. 13C, 13D; Appendix K, Appendix L). Representatives from each cluster revealed potential drivers of the stage-specific gene expression modules. Notably, for neurogenesis, only two definitive transcriptional regulators were detected in the cluster displaying peak expression in the intermediate stage: Pa2g4 and Six4.

Pa2g4, also known as ErbB3-binding protein, regulates global gene expression through its repression of SUV39H1-mediated histone H3K9 trimethylation, and the gene

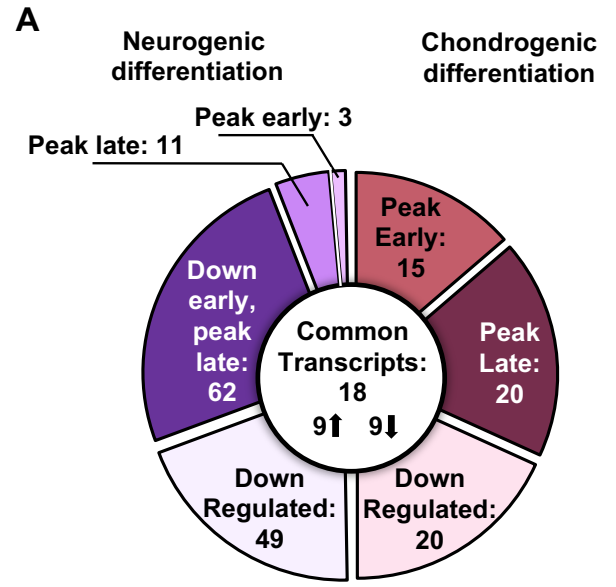

B **Commonly upregulated transcription factors**

Transcript ID	Gene abbreviation	Gene name	DBD
ENSMUST00000107893.8	Atf5	Activating transcription factor 5	bZIP
ENSMUST00000024954.10	Epas1	Endothelial PAS domain protein 1	bHLH
ENSMUST00000106307.8	Hivep3	HIV type I enhancer binding protein 3	C2H2 ZF
ENSMUST00000036884.2	Klf9	Kruppel-like factor 9	C2H2 ZF
ENSMUST00000003870.14	Mxi1	MAX interactor 1, dimerization protein	bHLH
ENSMUST00000051301.5	Pura	Purine rich element binding protein A	Unknown
ENSMUST00000000579.2	Sox9	SRY (sex determining region Y)-box 9	HMG/Sox
ENSMUST00000093852.4	Zbtb16	Zinc finger and BTB domain containing 16	C2H2 ZF
ENSMUST00000114694.8	Zbtb20	Zinc finger and BTB domain containing 20	C2H2 ZF

Commonly downregulated transcription factors

Transcript ID	Gene abbreviation	Gene name	DBD
ENSMUST00000014747.2	Alx3	Aristaless-like homeobox 3	Homeodomain
ENSMUST00000026662.7	Cbx2	Chromobox 2	AT hook
ENSMUST00000069334.7	Dach1	Dachshund family transcription factor 1	Unknown
ENSMUST00000073316.12	Foxm1	Forkhead box M1	Forkhead
ENSMUST00000041183.6	Meox2	Mesenchyme homeobox 2	Homeodomain
ENSMUST00000021941.7	Mxd3	MAX dimerization protein 3	bHLH
ENSMUST00000018005.9	Mybl2	Myeloblastosis oncogene-like 2	Myb/SANT
ENSMUST00000000095.6	Tbx2	T-box 2	T-box
ENSMUST00000033060.13	Tead2	TEA domain family member 2	TEA

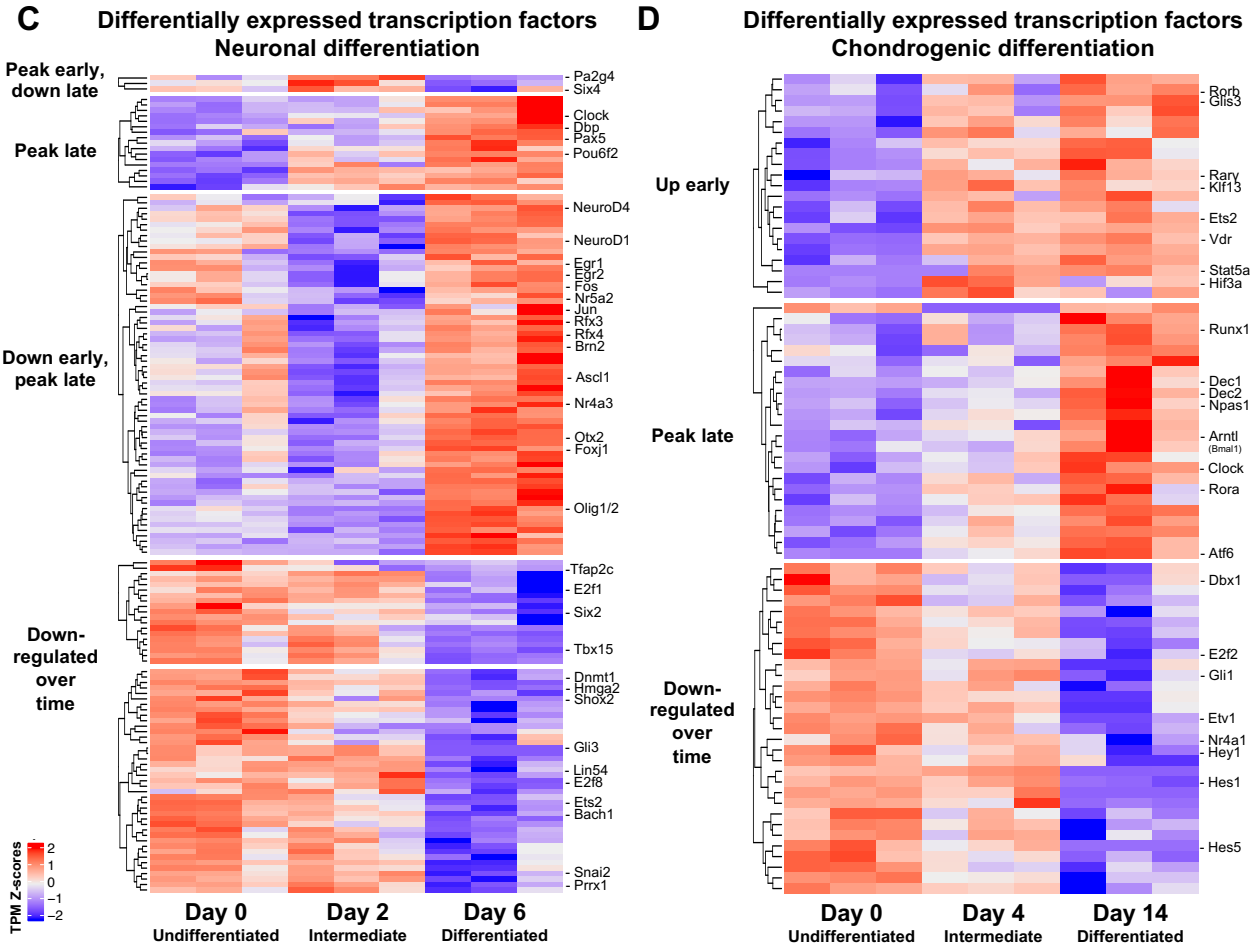

Figure 13. See next page for legend.

Figure 13. Stage-specific transcriptional regulators associated with common and lineage-specific transcriptional programming. (A) Transcription factor-encoding transcripts demonstrate stage-specific gene expression patterning over the course of neurogenic (shades of orange) or chondrogenic differentiation (shades of purple). **(B)** 18 transcriptional regulators were shared between neurogenesis and chondrogenesis, where 9 were commonly upregulated, and 9 were commonly downregulated over the course of differentiation. **(C, D)** Temporally clustered transcripts reveal transcriptional regulators uniquely associated with the intermediate and differentiated stages of neurogenesis (C, 125 transcripts) or chondrogenesis (D, 55 transcripts). Each row represents a single transcript. Each column represents one of the three biological replicates for each time point. Red and blue indicate standard deviation above and below the mean, respectively. GO analysis was used to determine enrichment of biological process associated with cluster-specific transcripts. bHLH, basic helix-loop-helix; bZIP, basic leucine zipper; C2H2 ZF, Cys2-His2 zinc finger; DBD, DNA-binding domain; HMG/Sox, sex-determining region Y-related, high mobility group-box.

encoding DNMT1, a DNA methyltransferase (Ko et al., 2019). Loss of Pa2g4 in mice results in neuron apoptosis and significant brain malformations (Ko et al., 2019). Pa2g4 has also been identified as a downstream regulator of sympathetic neuronal proliferation, survival and differentiation in response to neuregulin signaling (Kwon and Ahn, 2010). Interestingly, DNMT1 appears in our list of transcripts that are downregulated in differentiated cells, indicating that Pa2g4-mediated repression of DNMT1, and other epigenetic modifiers, may be important for initiating a cascade of gene regulatory changes that ultimately promote neuronal cell fate in the cranial NC.

More specific to cranial peripheral neuron development is Six4, a member of the Six-class homeobox gene family. Six4 is highly expressed in developing trigeminal ganglia in an overlapping pattern with Six1, and mice deficient for both transcription factors displayed aberrant gangliogenesis characterized by reduced sensory neuron number and increased apoptosis (Konishi et al., 2006). Early trigeminal sensory neurons are derived from a mixture of NC and placodal cells, and therefore Six4, as well as other Six factors, are promising candidate regulators mediating the intermediate step of peripheral neurogenesis in the developing head.

As expected, many canonical drivers associated with differentiation along the neuronal lineage were found to be upregulated in the differentiated cells, including NeuroD1, NeuroD4, Fos, Jun and Ascl1. We also identified Clock, a fundamental circadian regulator, exhibiting peak expression in the differentiated neurons. In addition, two other circadian-associated factors, Dbp and Egr1, were detected, but their expression was specifically downregulated in the intermediate cell population, and upregulated in the differentiated neurons. While Clock and its interacting partner, Arntl (also known as Bmal1), are most well-described for their rhythmic regulation of target gene expression, Dbp participates in forming a feedback loop that stabilizes the oscillations within a particular period length (Yoshitane et al., 2019). Egr1 was also shown to modulate oscillatory period length, and Egr1 null mice exhibit defects in daily Clock:Bmal1-induced rhythmicity, as well as altered body temperature regulation (Riedel et al., 2018). This suggests that modulating the length of circadian oscillations may be important for differentiated peripheral neurons. In addition, it is an example of how potential interactions between multiple transcriptional regulators with different gene expression patterns might coordinate to control a specific cellular output.

Several transcripts encoding regulators of cilium assembly, including Rfx3, Rfx4 and Foxj1, were also detected as being downregulated in the intermediate cells, but upregulated in differentiated neurons. Both Rfx transcription factors and Foxj1 are expressed during early brain development, and cooperatively regulate a number of genes associated with different aspects of cilia biogenesis ranging from formation of the basal body and axoneme to components of intraflagellar transport machinery (reviewed in Choksi et al, 2014). Moreover, NC-specific ablation of ciliary function in mice resulted in

a loss of cell polarity, failure to respond to hedgehog signaling, and altered ventral forebrain morphogenesis (Schock and Brugmann, 2017). This study predicted that the changes in cilia-mediated cell polarity within the NC negatively influenced overall neuroectoderm morphology, thus resulting in defective forebrain formation. Identification of these transcriptional regulators in our data supports the need for further investigation into the cell intrinsic contribution of ciliogenesis during neuronal differentiation in the cranial NC, potentially providing insight into how misregulation of this process during peripheral neurogenesis might also impact overall brain morphogenesis.

Rounding out the stage-specific regulators for neurogenesis were those that were downregulated over time. Not surprisingly, many of these transcripts were associated with cell cycle progression and stem cell maintenance. We also detected TFAP2c and Snail2 in this cluster, suggesting that these NC specifiers are not needed for maturation of neurons derived from the cranial NC. Interestingly, we identified a number of transcripts encoding regulators with known roles in mesodermal differentiation, indicating an important role for proper suppression of competing programs in order to realize robust neuronal differentiation.

For chondrogenesis, we identified several transcription factors that were significantly upregulated in the intermediate cells that have been implicated in MSC differentiation, including Glis3, Stat5a, Hivep3 and the vitamin D receptor, Vdr (Fig. 12D). In addition, we identified Hif3a, a hypoxia-inducible factor, as an important regulator of the intermediary step in the progression. The HIF family of transcription factors, which also includes Hif1a and Epas1 (also known as Hif2a), is known to control gene expression associated with robust ECM synthesis in human articular chondrocytes in response to

low oxygen levels (Lafont et al., 2007; Markway et al., 2015). Interestingly, we identified Epas1 as a commonly upregulated transcript, and genes involved in the HIF1 signaling pathway were found to be enriched in differentiated chondrocytes. Together, these data accentuate an interplay between shared and early lineage-specific programming in mediating downstream hypoxia-induced gene expression associated with the progression of chondrogenic differentiation.

We also detected several transcriptional activators and repressors involved in regulating the later stage of chondrogenesis. Surprisingly, 9 of the 20 transcripts upregulated specifically in the differentiated cells encode canonical transcriptional factors associated with circadian rhythm, emphasizing a significant role for this process in differentiating chondrocytes derived from the cranial NC. In support of these findings, a recent study showed that Bmal1, a master clock transcription factor, is crucial for controlling postnatal growth of cranial cartilage elements, as Bmal1-deficient mice have smaller, shorter mandibles due to decreased calcification (Yu et al., 2020). Circadian control of mandibular cartilage development was found to be regulated by Hedgehog signaling, however the precise mechanism of circadian regulation in cranial NC cells over the course of chondrogenic differentiation has not been specifically investigated.

Peripheral circadian clocks found in various adult human and mouse limb cartilages are known to be important for regulating cartilage homeostasis, and dysregulation of rhythmicity leads to matrix degradation and osteoarthritis-like damage (Dudek et al., 2016; Gossan et al., 2013). We predict that similar mechanisms for controlling cartilage homeostasis are operating in differentiating chondrocytes derived from the cranial NC. Consistent with this idea, we detected downregulation of Notch

signaling effectors, Hes5, Hes1 and Hey1, in our chondrogenic cultures over time. Initial decreases in expression of these transcriptional repressors is required in order to promote chondrogenic maturation (Karlsson et al., 2007), and subsequent upregulation over time promotes a hypertrophic state, characterized by reduced Sox9 expression and cartilage matrix degradation (Rutkowski et al., 2016). While it is not known if these effectors lie downstream of the circadian rhythm pathway, these studies indicate that their timely downregulation not only contributes to the overall progression of chondrogenesis, but helps to coordinate the balance between cartilage matrix production and degradation needed for maintaining a stable chondrogenic phenotype.

Discussion

As a stem cell-like population with the capacity to give rise to a plethora of diverse cell types, the cranial NC serves as an excellent model for addressing essential questions regarding the complex intrinsic mechanisms regulating cell fate determination. Diversification of the cranial NC is a highly dynamic process involving sequential morphological and behavioral transformations that gradually unfold as an embryo develops over time. Underlying these cellular changes is a highly regulated, transcriptional program that guides cranial NC progenitors through a series of decisions ultimately leading to acquisition of a specific cell fate. However, the precise genetic control mediating the initiation of fate-specifying programming, and how it changes as cranial NC cells gradually transition toward a specific differentiated state remains poorly understood.

In this chapter, we demonstrate that stage-specific transcriptional modules facilitate the progression through the different phases of neurogenesis or chondrogenesis

in the cranial NC. Each module drives distinct, yet partially overlapping biological processes and pathways that accompany gradual differentiation into either peripheral neurons or cartilage-matrix producing chondrocytes. Closer analysis revealed commonalities in gene expression patterning corresponding to shared cellular and behavioral changes observed between the two cell fates, both *in vivo* and *in vitro*, in addition to unique lineage-specific programming. In accordance with our goal, we delineated specific transcriptional signatures corresponding to the intermediate neuroprogenitors or chondroprogenitor state. Significantly, we also identified candidate transcriptional regulators that dictate the timing of this progression *in vitro*, including those that may contribute to early commitment toward either lineage, as well as those that promote maturation of the differentiated state. Elucidation of the temporally-regulated gene modules governing cranial NC differentiation enables discovery of novel molecular targets of genetic and environmental factors that might contribute to cranial NC-related malformations, as well as development of potential therapeutic treatments.

Shared transcriptional programs underlie lineage-specific outcomes.

One significant finding of our transcriptomic analysis was the existence of both common and lineage-specific gene expression signatures that appear to work together in a stepwise and time-sensitive manner to promote differentiation toward a neuronal or chondrogenic cell fate in the cranial NC. For instance, many of the transcripts identified to be commonly regulated between the two cell fates were associated with cellular and cytoskeletal reorganization, as well as cell-cell and cell-matrix interactions. As cranial NC cells differentiated over time, we observed continued enrichment of these shared

processes, however the corresponding transcripts were unique for each cell type, and their expression changed in a stage-specific manner. We predict that the transcripts corresponding to these shared biological processes are regulating similar changes in cell shape and aggregation potential observed during differentiation both in *in vitro* and *in vivo*. Specifically, acquisition of a bipolar neuronal morphology, and the transition to a cuboidal chondroprogenitor, are characterized by an initial reduction of cell size, and both peripheral neurons and chondrocytes are known to coalesce to form aggregations as differentiation progresses. Recent studies have implicated regulation of cytoskeletal dynamics as important influencers of cell fate determination (Chen et al., 1997; Mammoto et al., 2011; Mammoto and Ingber, 2009; McBeath et al., 2004), and highlight signaling pathways involving Rho family of small GTPases as key regulators of changes in cortical cytoskeleton architecture that occur during neurogenesis and chondrogenesis (Gonzalez-Billault et al., 2012; Ray and Chapman, 2015). Interestingly, cytoskeletal rearrangement is not only necessary for controlling cell shape, but also plays crucial roles in modulating organelle localization, and intracellular transport, as well as interactions between cells and with their microenvironment, such as those involved in formation of focal adhesions, adherens junctions or actin bridges (reviewed in Mammoto and Ingber, 2010). Cell-cell and cell-ECM interactions are crucial for mediating proper coalescence of both developing cranial ganglion and chondrogenic mesenchyme in the head, and disruption of adhesion-mediated mechanisms results in disorganized cranial ganglion assembly (Shaiu and Bronner-Fraser, 2010), and inhibition of chondrogenic condensation (Ray and Chapman, 2015), respectively. In that light, the mechanisms controlling reduction in cell size and aggregation capabilities in both neurons and chondrocytes may be more closely

linked than previously appreciated. Finally, changes in cytoskeletal architecture facilitate the direct association between cell membrane and nucleus, which has been shown to influence downstream gene expression, and transcription factor availability, in a cell-type specific manner (Mammoto et al., 2011; Percipalle, 2013; Swift et al., 2013; Wang et al., 2009). Given this information, our results reveal a crucial role for proper expression of genes associated with cytoskeletal dynamics during the earliest stages of differentiation in the cranial NC. In addition, they provide insight into how commonly regulated transcripts, which appear to be important for two very different cell fates, can potentially coordinate subsequent lineage-specific outcomes. Future studies that manipulate the expression of these genes early in the differentiation process, and then assess downstream changes in gene expression, morphology and behavior will be able to determine their precise contribution to the formation of these derivatives in the cranial NC.

The expression pattern of transcripts associated with circadian rhythm and entrainment represent another example of the interplay between common and lineage-specific programming during neurogenesis and chondrogenesis. While circadian rhythm is an evolutionarily conserved biological feature found in most cells, it has not been directly investigated in the context of the cranial NC or in the formation of its derivatives. In mammals, a global 24-hour circadian cycle is established through the central pacemaker located in the SCN of the hypothalamus, which translates external stimuli, such as light/dark input from the retina, into temporal signals that are then communicated to other clocks within the brain, and peripheral tissues. Tissue-specific peripheral clocks can be further modulated or entrained by other external cues (known as *zeitgebers*), including hormones, exercise, stress, drugs, and food entraining factors, such as glucose

and insulin. At the level of the single cell, circadian clocks are responsible for generating oscillatory expression patterns through cell-autonomous transcription-translation feedback loops involving canonical clock components, Bmal1, Clock, Per and Cry. Integration of the master feedback loop with others creates an endogenous circadian network that has the ability to control rhythmic chromatin transitions (Ripperger and Schibler, 2006), as well the expression of over 40% of murine protein-coding RNA, and over a thousand non-coding RNAs in a tissue-specific manner (Zhang et al., 2014). Additionally, the timing underlying the expression of an oscillatory transcript is typically synchronized with the biological pathway involving its gene product, highlighting a time-dependent relationship between the peak expression of circadian-regulated transcripts and pathway output (Panda et al., 2002).

In our study, we identified several transcripts associated with circadian rhythm to be shared during neurogenesis and chondrogenesis, but we also observed a distinct suite of transcripts that seemed to propagate this process in a lineage-specific manner. We predict that the commonly regulated transcripts provide the foundation needed for initial establishment of the circadian clock in differentiating cranial NC cells, but then the circadian transcriptional profile is tailored as cells diversify into either peripheral neurons or cartilage-matrix producing chondrocytes in order to orchestrate cell-type specific function. For instance, synchronizing environmental signals throughout the systemic circadian network is achieved through the autonomic nervous system and the endocrine system, and coordinated communication is crucial for driving a wide range of physiological and behavioral responses, including sleep cycles, feeding behavior, metabolic function, body temperature regulation, and hormone release (reviewed in Xie

et al., 2019). Since cranial NC-derived ganglia in the head are a component of the autonomic nervous system, establishment of circadian rhythmicity during differentiation may be governing the transcriptional programming necessary for integrating SCN output in order to facilitate synchronization of other peripheral clocks. In support of this, the transcripts enriched over the course of neuronal differentiation were those known to be associated with clock-to-clock synchronization, including GABA and glutamate sensors (Moore et al., 1993; Liu et al., 2000; Meijer and Schwartz, 2003), and modulators of the adenosine monophosphate/adenosine triphosphate (AMP/ATP) ratio (Lamia et al., 2009). Interestingly, the AMP/ATP ratio is also an indicator of the cell's metabolic state, and AMP-dependent activation of AMP kinase (AMPK), which acts as a central sensor of metabolic signals in many cell types, including neurons, has also been implicated in regulating nutrient-mediated clock entrainment in the liver (Lamia et al., 2009), suggesting a relationship between metabolic homeostasis and circadian rhythm that warrants further exploration in the context of cranial NC differentiation.

In contrast, circadian rhythm in articular chondrocytes is known to play important roles in maintaining cartilage homeostasis and integrity by controlling the delicate balance between ECM synthesis and degradation. Accordingly, mouse models exhibiting a loss of key clock genes, such as Bmal1, have ectopic ossification of cartilage, reduced bone growth, altered bone volume and increased susceptibility to inflammatory joint diseases such as osteoarthritis and rheumatoid arthritis (Dudek et al., 2016; Gossan et al., 2013; Yu et al., 2020). Unexpectedly, we found that nearly half of the transcriptional regulators exhibiting peak expression in differentiated chondrocytes were associated with control of circadian rhythm, indicating a significant role for clock-related gene regulation in the

cranial NC during chondrogenic differentiation. In addition, we observed enrichment of glucagon and IGF1 signaling pathways over the course of chondrogenic differentiation. Recently, both serum glucagon and IGF1 levels were identified as novel factors in the entrainment of the circadian clock in the liver (Ikeda et al., 2018), thus suggesting a potentially novel role for these same factors in entrainment of the chondrogenic clock during cranial NC-derived chondrogenesis. When taken as a whole, the results of our transcriptomic analysis reveal key differences in circadian requirements between neurogenesis and chondrogenesis, but also highlight circadian-controlled maintenance of cellular homeostasis as a potential similarity underlying the differentiated state. We envision future studies using targeted genetic approaches to assess the definitive roles of both commonly regulated circadian transcripts, particularly Klf9 and Pura, and lineage-specific ones, will advance our understanding of the rhythmic mechanisms that not only control cell fate acquisition, but maintenance of the differentiated state during neurogenesis and chondrogenesis in the cranial NC.

Lineage-specific biological processes coordinate gene expression associated with progression of differentiation, and the maintenance of the differentiated state.

Having the ability to detect environmental stimuli, like microenvironment or signaling pathway outputs, and then translate that information to achieve a cell-type dependent physiological or behavioral response is crucial for proper cell fate acquisition. Accordingly, our analysis also pinpointed transcripts associated with ECM organization, cilium assembly and hypoxia signaling as potential integrators of extrinsic cues involved not only in the stepwise progression of differentiation in a cell-type dependent manner,

but the continued maintenance of the differentiated state. Interestingly, we observed ECM organization as a shared biological process between neurogenesis and chondrogenesis, however each cell type displayed a unique combination of transcripts, which likely contribute to differences in microenvironment composition that promotes lineage specification. This is consistent with several studies demonstrating that the physical attributes of extracellular matrices, such as composition, concentration and elasticity, can have a direct effect on fate specification (Engler et al., 2006, Swift et al., 2013; Yang et al., 2016). Matrix elasticity can be mimicked *in vitro* using either collagen-coated polyacrylamide gels or hydrogels engineered to exhibit a range of matrix flexibilities. Subsequently, naïve MSCs exposed to identical media conditions will differentiate into neurons when grown on softer matrices, and osteoblasts when grown on more rigid matrices. Elasticity-directed differentiation was disrupted upon the addition of instructive medium that conflicted with the matrix stiffness, suggesting that synchrony in microenvironment and instructive cues is crucial for robust differentiation into a particular cell type. Interestingly, variations in matrix mechanisms were found to influence focal adhesion structure and cytoskeletal dynamics through non-muscle myosin II (Engler et al., 2006), as well as nuclear lamina stabilization via mechanical stress-induced changes in lamin-A levels (Swift et al., 2013). In both cases, these mechanical signals facilitated changes in transcriptional and proteomic profiles that enhanced lineage-specific differentiation, thus emphasizing a significant role for the combined effect of ECM composition, cytoskeleton remodeling, nuclear membrane stability, and cell-ECM interactions in coordinating gene expression outcomes associated with cell fate acquisition.

Enrichment of transcripts associated with cilium assembly were detected in both undifferentiated cranial NC cultures, and differentiated peripheral neurons. Primary cilia are essential for reception and internal processing of outputs from multiple molecular signaling pathways, including Hedgehog, WNT and Notch signaling (Bangs and Anderson, 2017; Reiter and Leroux, 2017; May-Simera et al., 2017; Pala et al., 2017). Once the axoneme of a cilium is established, signaling components are transported along microtubules via intraflagellar transport, allowing the cilium to act as a cellular antenna. Primary cilia are typically extended in quiescent cells and are found in most cell types, including NC cells and many PNS derivatives, although the specific role of primary cilia in neurons derived from the cranial NC has not been previously investigated. Interestingly, transgenic mouse mutants exhibiting a loss of cilia specifically in the NC failed to respond to hedgehog signaling emanating from the ventral forebrain, and this resulted in disruption of cell polarity in both NC cells and ventral forebrain neuroectoderm (Schock and Brugmann, 2017). These findings suggest a crucial role for reciprocal signaling between NC and surrounding tissues during brain development. Future work focusing on how cilia interpret molecular signals in order to direct downstream cellular outputs mediating tissue morphogenesis, and the specific contribution of ciliated cranial ganglia to this process, may provide insight into the etiology underlying ciliopathies.

Lastly, we detected stage-specific expression of transcripts associated with the hypoxia signaling pathway specifically during chondrogenesis. Hypoxia-inducible factors are key mediators of the cellular response to limiting oxygen conditions, responsible for activating transcriptional programming associated with tissue protection and homeostasis. Cartilage is an avascular tissue, and therefore chondrocytes are inherently

adapted to hypoxic conditions. In this context, stabilization of HIFs trigger enhanced ECM deposition, as well as increased Sox9, Col2a1 and aggrecan expression, all of which is associated with a robust articular chondrocyte phenotype (Murphy and Polak, 2004; Robins et al., 2005; Lafont et al.,2007). In addition, chondrogenic nodules formed during the initial stages of chondrogenic differentiation in developing limb buds were found to be hypoxic (Schipani et al., 2001; Amarilio et al., 2007), suggesting a similar environmental condition, and requirement for HIF signaling, in chondrocytes derived from the cranial NC. During skeletogenesis *in vivo*, condensing chondrocytes will first maintain a pre-hypertrophic state, characterized by continued ECM deposition and maintenance, but they will eventually transition toward a terminal hypertrophic state, which results in ECM degradation, calcification and bone formation. In our transcriptomic analysis, we observe Hif3a as an early regulator of hypoxia-induced gene expression that persists through the later stages of differentiation. Interestingly, progressive increases in Hif3a expression in healthy human articular chondrocytes *in vivo* or differentiated MSCs *in vitro*, was found to be associated with low levels of hypertrophic markers, Col10a1 and MMP13. In contrast, human articular cartilage harvested from patients with osteoarthritis, exhibited low levels of Hif3a, and high hypertrophic gene expression (Markway et al., 2015). We do not detect expression of Col10a1 or MMP13 in our cultured chondrocytes indicating that they have not progressed toward a hypertrophic state, and therefore represent resting, pre-hypertrophic chondrocytes. In this light, it is possible that hypoxia-induced gene expression may help to preserve cartilage homeostasis through maintenance of the resting chondrogenic state, partly by regulating the timing of hypertrophy.

New paradigm for diversification along the ectodermal or mesoectodermal lineages in the cranial NC.

When taken together, the results of our transcriptomic analysis suggest a new paradigm for cranial NC diversification along the ectodermal or mesoectodermal lineages in which specific cell fate acquisition is mediated by two, partially overlapping transcriptional programs (Fig. 14). The first is a cell type-independent program commonly initiated in the cranial NC progenitor cells undergoing neuronal or chondrogenic differentiation. Significantly, we identified transcripts associated with cytoskeletal reorganization, cell-cell and cell-ECM interactions, and circadian rhythm to be shared between developing neurons and chondrocytes. These processes have been implicated in regulating cellular changes corresponding to those observed early in the differentiation process for both cell types, however they also have the potential to directly influence downstream gene expression in a lineage-specific manner. Accordingly, transcripts associated with common programming may be instrumental in establishing an overall differentiation-competent state, thus providing an intrinsic foundation from which intermediate neuroprogenitors or chondroprogenitors can elicit lineage-specific physiological or behavioral outputs in response to external cues.

Subsequently, the progression through the intermediate state toward a differentiated one is mediated by a second, cell type-dependent program, characterized by distinct, stage-specific gene expression modules that appear to work synergistically with the common programming to control the precise cellular changes required for function of either peripheral neurons or pre-hypertrophic chondrocytes. Of note, we identified unique transcripts associated with ECM organization, cilium assembly and

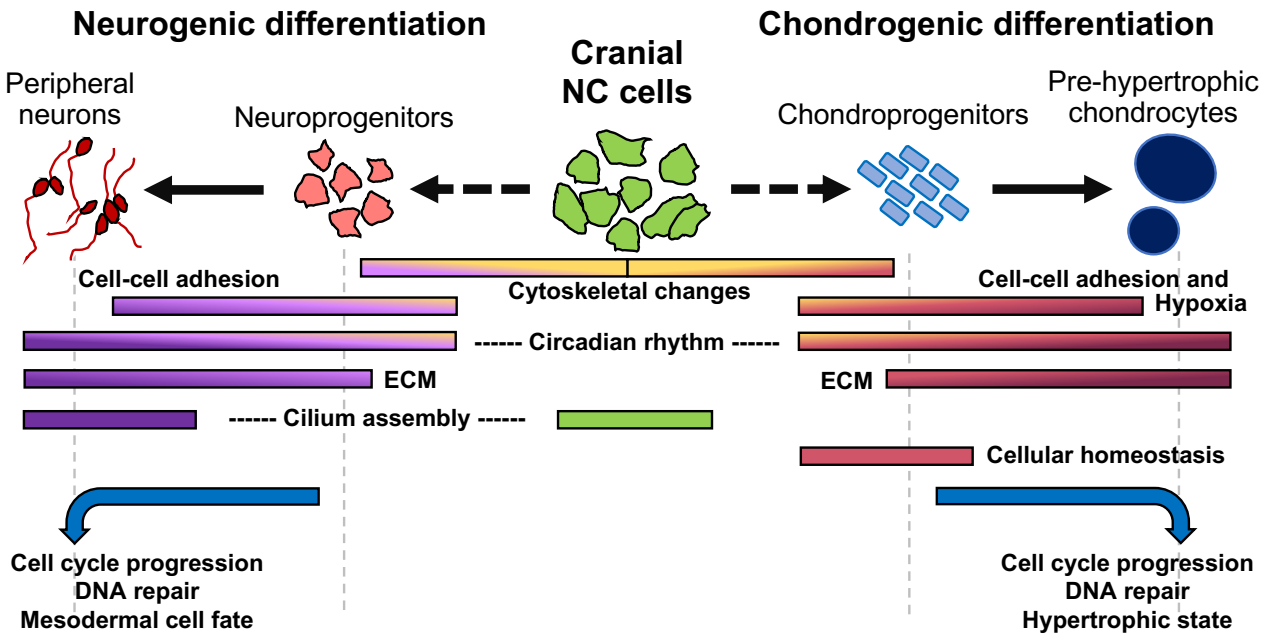

Figure 14. Schematic representation of cranial NC diversification along the neurogenic and chondrogenic lineages. The transition from multipotent, cranial NC progenitor (green cells) to a differentiated peripheral neuron (red cells) or pre-hypertrophic chondrocyte (blue circles) is mediated by two partially overlapping programs. The first, a cell type-independent program (yellow), is commonly initiated in progenitor cells as they begin to transition toward neuroprogenitor (pink cells) or chondroprogenitor (light blue cells) state. Enriched biological processes corresponding to the commonly regulated transcripts are associated with shared morphological and behavior changes known to occur in the early stages of the differentiation along either lineage. Transcripts associated with the common programming likely promote an overall differentiation-competent state, which lays the intrinsic foundation for subsequent lineage-specific differentiation. The second program is characterized by stage-specific gene expression modules that are unique to each cell fate. Transcripts associated with this program are enriched for biological processes capable of driving the transition through the intermediate stages of differentiation, but are also the continued maintenance of the differentiated state. Robust differentiation is achieved through cooperation of both programs in a stepwise and time-sensitive manner, as well as concurrent downregulation of competing programs (blue arrows), such as those involved in self-renewal, conflicting cell fates, or progression toward alternative fates. Temporal dynamics of stage-specific biological process and pathways are represented by each bar. Colors denote common (yellow) or lineage-specific programming for neurogenesis (shades of purple) or chondrogenesis (shades of magenta).

hypoxia response over the course of either neurogenesis or chondrogenesis. One common feature underlying the mechanisms corresponding to these processes is the inherent ability to sense and integrate external inputs to produce transcriptional outputs that would influence cell type-specific function. In that light, these processes may not only play an important role in mediating the temporal progression of differentiation by translating spatiotemporal cues into stage-specific changes in gene expression, but

potentiate the maintenance of the differentiated state. Finally, robust differentiation is achieved through concurrent suppression of competing programs, including those associated with stem cell-like properties, such as self-renewal and DNA repair, those that promote conflicting fate programs, or those that propagate inevitable states of maturation outside the scope of our culture system.

Our results provide strong evidence that cranial NC diversification along the neurogenic or chondrogenic lineage is mediated through gradual coordination of both common and lineage-specific programming, as well as concurrent downregulation of competing cell fate modules. These findings are similar to a recent study which observed that increased synchronization of fate-specific programming and concurrent repulsion of competing non-relevant programming promoted gradual biases favoring either the ectodermal or mesoectodermal lineage in pre- and post-migratory murine cranial NC cells (Soldatov et al., 2019). In addition, they support the idea that determination of a specific cell fate is coordinated, rather than stochastic, and mediated through the interplay between intrinsic programming and extrinsic signals which together promote gradual shifts toward commitment (Soldatov et al., 2019; Hu et al., 1997). However, identification of common programming shared between neurogenesis and chondrogenesis challenges the current view of differentiation where acquisition of a particular cell fate is thought to be achieved upon activation of a single, mutually exclusive lineage-specific program. Consequently, this model does not account for potential overlap in transcriptional signatures as multipotent, cranial NC progenitor cells transition toward a differentiated state, nor their potential contribution to the developmental progression. Our findings support the incorporation of this shared module into the overall model of cell differentiation

in the cranial NC, thus expanding the depth and complexity of the transcriptional logic controlling the formation of these derivatives in the developing embryo.

Nevertheless, one limitation to our transcriptomic approach is that the populations captured at the early time points for both neurogenesis and chondrogenesis likely represent a mixture of cells transitioning toward a differentiated state, and those that may never differentiate, even when grown in an instructive environment. Our stringent criteria for denoting significant changes in differential gene expression revealed pertinent programming mediating the intermediate steps. However, it is also possible that subtle, yet equally relevant changes remain undetected in our analysis due to the heterogeneity. A logical future approach would be to employ single-cell RNA-seq to catalog cell-to-cell variation in transcriptional profiles over the course of neuronal or chondrogenic differentiation. Similar analyses have been used to elegantly capture spatiotemporal biasing in early cell fate choices toward the ectodermal or mesoectodermal lineages in FACS purified pre- and post-migratory murine cranial and trunk NC cells *in vivo* (Soldatov et al., 2019). One caveat to this approach for assessing differentiation *in vivo* is that computational reconstruction of single-cell data only predicts lineage relationships, and our current interpretation of these data are largely founded on information derived from non-cranial NC sources. However, *in vitro* studies utilizing single-cell profiling at multiple time points over the course of directed differentiation would enable identification of distinct changes in gene expression that are coupled with observable morphological, cellular and behavioral transformations characteristic of neuroprogenitors or chondroprogenitors, as well as other intermediate stages, during cranial NC diversification. These findings would not only provide a higher resolution map of the molecular programming identified in this

study, but contribute to more accurate interpretation of subsequent *in vivo* single-cell assessment.

The findings of our transcriptomic analysis represent a crucial first step in establishing a comprehensive regulatory network detailing the temporally dynamic genetic program that directs the transitions through the intermediate stages of differentiation in the cranial NC. Our immediate next step would be to utilize our culture system to validate the results of our transcriptomic analysis via RT-qPCR, and a combination of conventional and novel immunolabeling techniques, such as SABER (Kishi et al., 2019). SABER allows for multiplexed amplification of signals from oligo-based fluorescent *in situ* hybridization (FISH) probes targeting up to 17 different transcripts simultaneously with high resolution. Such a technique would not only allow for visual confirmation of the distinct temporal gene expression patterns we observed at the level of the single cell *in vitro*, but it can also be applied *in vivo* as well, allowing incorporation of spatial patterning of the DE transcripts in the context of the developing mouse embryo. In addition, targeted manipulation of the transcripts identified would illuminate how disruption of the programming might accelerate or delay the progression of cranial NC cell differentiation, thus contributing to cranial NC-related defects and disease.

The ultimate long-term goal of this work would be integration of our findings into the current GRNs underlying cranial NC diversification. Significantly, our transcriptomic analysis has identified several candidate regulatory factors that may coordinate changes in gene expression over the course of cranial NC differentiation, however differential expression alone is not enough to definitively establish their regulatory role during these

processes. It is important to recognize that transcription factor activity may be influenced by a number of variables, including chromatin accessibility, interaction with various co-factors, and/or binding partners, as well as post-translational modification. In addition, recent studies demonstrate that gene regulatory programs directing changes in cell state, such as those associated with lineage specification, are controlled through the combinatorial binding of transcription factors and chromatin regulators to distal gene enhancers (Attanasio et al., 2013; Velasco et al., 2017). Therefore, to truly incorporate this information we must first decipher the shared *cis*-regulatory modules that drive stage-specific gene expression during neuronal and chondrogenic differentiation in the cranial NC. To achieve this, we intend to use ATAC-seq (Buenrostro et al., 2013) in order to identify transcriptionally accessible regions of chromatin that correspond to putative DNA regulatory sequences (promoters, enhancers, and insulators) in cultured cranial NC cells as they transition through the intermediate stages of neurogenic and chondrogenic differentiation. Motif analysis enrichment would be performed to determine transcription factor binding sites within the temporally clustered enhancers, thus uncovering key transcriptional regulators mediating each step of the differentiation process. We would also expect to decipher co-regulatory binding sites within temporally clustered enhancer sequences which, when coupled with our temporal gene expression profiles, would enable identification of combinatorial transcriptional activity controlling the stepwise, lineage-specific gene expression changes as cranial NC cells transition toward the neurogenic or chondrogenic cell fate. Similar approaches have been used to identify key transcriptional regulators driving the stepwise progression of optic nerve regeneration in zebrafish (Dhara et al., 2019), as well as those involved in direct programming of human

embryonic stem cells (hESCs) into motor neurons (Velasco et al., 2017). It is expected that data from these combined temporal analyses could be used to build a high resolution, comprehensive roadmap of the unique lineage-specific regulatory mechanisms driving cranial NC differentiation.

The temporal, transcriptomic data presented in this chapter serves as an excellent resource for further exploration into the dynamic intrinsic control of the progression of neurogenic and chondrogenic differentiation in the cranial NC. Interrogation of the stage-specific transcriptional modules elucidated both expected and novel biological processes and pathways that govern the initial transition and subsequent transformation through the intermediate stages of differentiation. We also uncovered unique transcriptional signatures indicative of the intermediate stages, as well as putative transcriptional regulators that mediate the progression, including those that may contribute to early commitment toward either lineage, and those that promote maturation of the differentiated state. Significantly, our results suggest a crucial interplay between common and lineage-specific programming over the course of differentiation in the cranial NC. We expect that future studies using targeted genetic manipulation of the genes associated with each program may yield insight into how they work together in a stepwise and time-sensitive manner to coordinate appropriate downstream physiological and behavioral responses during differentiation. In that light, our findings provide a valuable platform for discovering previously unknown mechanisms underlying a range of cranial NC-related malformations including, but not limited to, craniofacial defects and neuroblastoma. We expect the findings of such studies will enhance our understanding of the etiology underlying the pleiotropic structural and functional anomalies that often accompany pediatric syndromes

arising from defects in the cranial NC. Finally, assessing how genetic mutations or developmental exposure to environmental toxins impact the temporal regulation of cranial NC differentiation would enable discovery of novel molecular targets of genetic and environmental factors that might contribute to cranial NC-related malformations. This information would not only facilitate the development of effective therapeutic interventions, but also strategies for prevention with the long-term goal of reducing the overall incidence of cranial NC-related defects in the population.

CHAPTER V

General Discussion

Summary of key findings and future directions

The work that comprises this dissertation provides several tools for uncovering the specific mechanisms that govern the progressive acquisition of cell fate in the NC. In order to investigate the temporal regulation of this process we established a robust *in vitro* model system of mammalian cranial and trunk NC cell differentiation. We demonstrate reproducible methods for isolation and long-term expansion of both primary cranial and trunk NC cells obtained from the same animals. Both populations maintained their multipotency in culture, as demonstrated by their ability to be directly differentiated into neurons, glia, melanocytes, chondrocytes, adipocytes and smooth muscle cells. Characterization of directed differentiation along the neural and chondrogenic lineages revealed reproducible, temporal benchmarks indicative of the intermediate stages underlying the progression. Using this culture system, we explicitly interrogated cranial NC cells to uncover the dynamic gene expression changes that occur over the course of neurogenesis and chondrogenesis. Our analysis revealed that cranial NC cell diversification toward either fate is mediated through gradual coordination of both common and lineage-specific programming, as well as concurrent suppression of competing cell fates. We further identified distinct transcriptional signatures corresponding to the intermediate state, as well as putative regulators that govern the overall progression in a stage-specific and time-sensitive manner.

Lineage-specific transcriptional signatures that delineate the intermediate stage of differentiation in the cranial NC.

The current GRNs describing NC cell diversification lack specific modules that represent the progression through the intermediate stages of differentiation toward a particular cell type. One significant finding of the work presented was the identification of key candidate transcriptional activators and repressors that control the transition from multipotent progenitor to an intermediate neuroprogenitor and chondroprogenitor state. Upon validation, and functional assessment, these regulators would represent a new module in hierarchical regulation of NC cell development (Fig. 15).

Notably, for neurogenesis, we specifically identified Pa2g4 and Six4, both of which regulate gene expression associated with sensory neuron survival (Ko et al., 2019; Konishi et al., 2006; Kwon and Ahn, 2010). As a direct repressor of the methyltransferase DNMT1, and suppressor of SUV39H1-mediated histone H3K9 trimethylation (Ko et al., 2019), Pa2g4 may play a crucial role in promoting global changes in chromatin accessibility, thereby promoting activation of downstream genes associated with sensory neuron development. Targeted manipulation of Pa2g4 in our cultures, followed by RNA-seq would clarify which genes might be under the control of Pa2g4-mediated activation, and therefore crucial for the initial transition toward the sensory neuron cell fate. A similar approach could be used to determine downstream gene targets of Six4. Six1/Six4-deficient mice displayed aberrant gangliogenesis due to increased apoptosis (Konishi et al., 2006), however the loss of Six1/Six4 was not specific to the cranial NC. Six factors are expressed in placodal cells, which also contribute to trigeminal ganglion formation. Therefore, such analysis would shed light on the specific effect of Six4 in the cranial NC

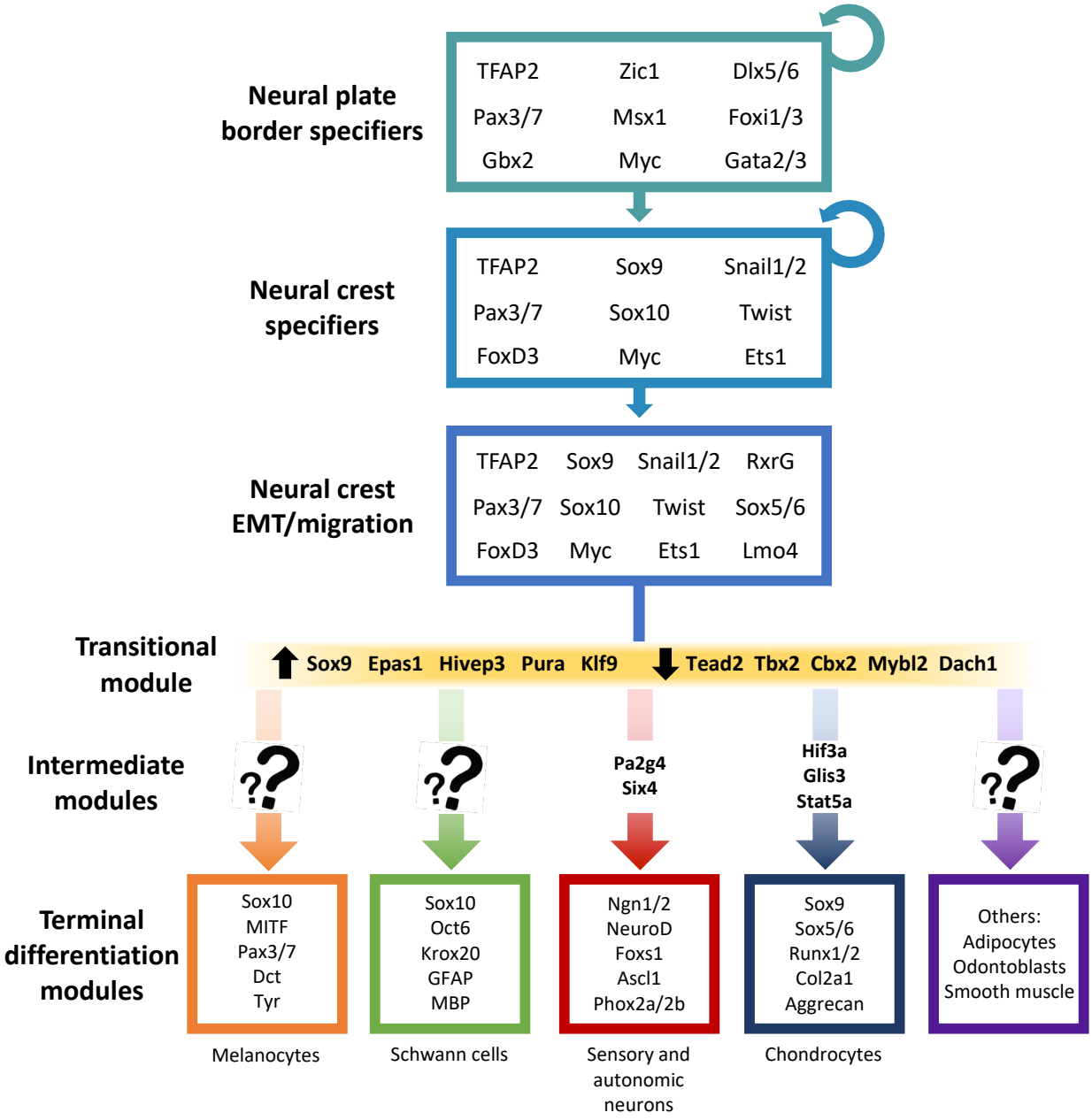

Figure 15: Incorporation of putative transitional and intermediate modules into the current GRN for neural crest cell differentiation. Transcriptional regulators that are shared between neurogenesis and chondrogenesis comprise a novel Transitional module (yellow). Commonly upregulated and downregulated transcription factors mediate the initial transition toward either cell fate by driving shared cellular and behavioral changes observed during the earliest stages of differentiation along either the neuronal or chondrogenic lineage, and may play similar roles in driving the transition toward other cell fates, as well. Intermediate modules for neurogenesis (red arrow) and chondrogenesis (dark blue arrow) include novel transcriptional regulators that specifically control the progression through the intermediate neuroprogenitor or chondroprogenitor state. Regulators found within intermediate modules likely drive downstream gene expression batteries associated with robust lineage-specific differentiation and maturation.

during neurogenesis.

For chondrogenesis, the transcription factors upregulated in the intermediate stage were those known to play roles during MSC differentiation, as well as Hif3a and Epas1, which are associated with hypoxia-induced signaling. In healthy human articular chondrocytes, Hif3a and Epas1 control robust ECM synthesis and a stable pre-hypertrophic phenotype, characterized by high Sox9 expression, and low levels of hypertrophic markers Col10a1, and MMP13 (Lafont et al., 2007; Markway et al., 2015). We do not detect significant Sox9 expression, or Alcian blue-positive ECM synthesis in our cultures until the differentiated cells condense to form chondrogenic nodules, which have been described as a hypoxic environment (Amarillio et al., 2007; Schipini et al., 2001). Therefore, it is possible that expression of Hif3a and Epas1 in the intermediate cells may be the first step in establishing a robust response which allows chondrocytes to adapt to low oxygen conditions at the later stages of differentiation. Consistent with this, we observe enrichment of additional genes associated with the HIF1 signaling pathway in the differentiated cells found within chondrogenic nodules.

Even though the cultured chondrocytes used in this study were grown under normoxic conditions, we were able to detect enrichment of transcripts associated with hypoxia-related signaling. Therefore, our culture system serves as a tool to further investigate the role of hypoxia-induced gene expression during chondrogenesis in the cranial NC. Moreover, growing cultures in the presence of low oxygen tension using a hypoxia chamber may uncover hypoxia-related mechanisms or factors involved in the progression of chondrogenic differentiation that are not readily detectable under normoxia. Together, these findings would inform future strategies for improving

chondrogenic culture conditions, enabling advancement of stem-cell based therapies to treat congenital and acquired craniofacial deformities, such as craniofacial tissue repair.

Enriched biological processes and pathways reveal potential mechanisms of cell fate determination in the cranial NC

The results of our analysis further revealed common and lineage-specific programming that governs distinct, but partially overlapping biological processes and pathways that may have important roles to play in cell fate determination in the cranial NC. While this work provides a snapshot into the cell intrinsic mechanisms that direct differentiation over time, diversification *in vivo* is also dependent on spatial and temporal extrinsic factors, such as paracrine and autocrine signaling molecules, ECM composition, and physical interaction with surrounding tissues. However, how migratory NC cells integrate this information in order to activate downstream gene expression modules associated with a particular cell fate is not well understood. We hypothesize that common programming shared between developing peripheral neurons and chondrocytes poises the cells to sense and respond to various environmental contexts in a lineage-specific manner. A question then becomes: what are the mechanisms by which a common regulatory program can drive a cell type-specific differentiation response?

In our study, we found that common transcriptional signatures were associated with cytoskeletal reorganization, changes in cell-cell and cell-ECM interactions and circadian rhythm (Fig. 15). We also detected lineage-specific gene expression associated with these processes as the cells progressed toward a differentiated state. The interplay between these two programs in driving the shared processes is consistent with our

observations that a reduction in cell size, and aggregation formation were some of the earliest changes displayed by differentiating cranial NC cells, no matter their future fate. We predict that the mechanisms underlying these early cellular changes are crucial for determining downstream lineage-specific outcomes.

Consistent with this idea a recent study investigating the timing of skeletal element formation in the developing avian head found that cytoskeletal rearrangement associated with changes in cell shape were required for condensation formation, and overt chondrogenic differentiation (Ray and Chapman, 2015). Cytoskeletal remodeling was facilitated by RhoA/ROCK-driven actomyosin contractions and non-muscle myosin II (NMII)-mediated changes in cell cortex tension. Disruption of F-actin remodeling, RhoA/ROCK-driven actomyosin contractility or NMII-generated tension via treatment with Cytochalasin D, ROCK inhibitor Y27632, or Blebbistatin, respectively, prevented overt differentiation, as indicated by a loss of Sox9 expression, dysregulated TGFβ/SMAD2, BMP2, and FGF signaling, and a lack of condensations. This illustrates a direct connection between changes in cytoskeletal architecture and the regulation of downstream gene expression, at least concerning Sox9, and signaling dynamics associated with robust chondrogenic differentiation.

Accordingly, we predict that global disruption in cell shape changes as the cells begin to transition toward either the neurogenic or chondrogenic fate would inhibit differentiation. However, we would also expect that targeted manipulation of specific factors associated with cytoskeletal organization identified in our study would have a differential impact on neuronal and/or chondrogenic differentiation depending on whether they were detected in the common or lineage-specific programming. We identified Ezrin

as a possible regulator of cytoskeletal dynamics in both peripheral neurons and chondrocytes. Ezrin regulates membrane tension by linking the plasma membrane to the actomyosin cortex, and by switching between active and inactive states it can impact cellular morphology (Doherty and McMahon, 2008). Activated Ezrin results in increased tension, and cell spreading, while the inactive form promotes cell contraction, and the conformational switch in activity is mediated through Rho kinase signaling (Matsui et al., 1998). Since Ezrin was found in common between the two cell fates we would expect that inhibition of Ezrin activity would impact both neurogenesis and chondrogenesis during development. Importantly, by identifying potential cytoskeletal regulators that are shared between both cell types, our analysis enables discovery of genes that may contribute to multisymptom phenotypes often associated with cranial NC-related disorders.

It is also possible that the regulators found within the common programming are conserved across other NC cell derivatives. For instance, we observed that cranial and trunk NC cells undergoing glial differentiation exhibited distinct morphological transformations over time. For both cell populations, NC cells initially displayed flattened, sheet-like morphology but transitioned toward an elongated, bipolar morphology, indicative of immature Schwann cells, as differentiation progressed. Therefore, it would be advantageous to conduct a temporal transcriptional analysis for gliogenesis, as we have described for neurongenesis and chondrogenesis. This would not only enable identification of regulators that control the distinct morphological transitions, but also provide insight into the overall transcriptional programming that governs the progression toward a glial cell fate.

One potential mechanism for transducing actomyosin-mediated mechanical forces into regulatory signals that direct lineage-specific gene expression would be through modulation of nuclear stability and stiffness. In the study referenced above, Ray and Chapman (2015) found that temporal cytoskeletal remodeling not only impacted overall cell morphology, but the shape of the nucleus and cell-cell/cell-ECM interactions, as well. At first, they observed irregularly-shaped cells transforming to a characteristic cuboidal chondrocyte morphology. This change was coupled with increased F-actin homogeneity, and a significant decrease in nuclear circularity, resulting in a similarly cuboidal nuclear shape. Then, as the chondrocytes condensed, their overall morphology, and nuclear shape, relaxed to become more rounded. Concurrently, they observed increased focal adhesion formation, thus fixing the condensing cells to extracellular substrate. Several studies have shown that external mechanical forces, such as those associated with morphological transformation, can lead to nuclear deformation and altered levels of euchromatin and heterochromatin (Bank and Gruenbaum, 2011; Stephens et al., 2018; Swift et al., 2013). Since higher order chromatin structure is partly controlled through its attachment to the nuclear periphery (Guelen et al., 2008; Harr et al., 2015), it is possible that subtle changes in cellular mechanics can have a significant impact on overall chromatin accessibility and enhancer-promoter interactions that regulate transcriptional programming during differentiation.

Changes in the tensile forces due to cytoskeletal reorganization and modulation of ECM adhesion are propagated into the nucleus through the nuclear lamina via Lamin-A (Swift et al., 2013). Nuclear lamins are intermediate filaments that comprise a meshwork found just inside the nuclear envelope, and are responsible for regulating nuclear stability

(De Vos et al., 2011). Varying levels of Lamin-A were shown to enhance tissue-specific differentiation *in vitro*, and this effect was mediated by matrix elasticity. Higher levels of Lamin-A were induced in cells grown on stiffer matrices, and this was associated with cell spreading and bone formation. In contrast, softer matrices were correlated with low Lamin-A levels, and were associated with adipocyte formation, which display a more rounded phenotype.

Interestingly, we detected upregulation of the gene for Lamin-A/C (LMNA) in the intermediate chondroprogenitors, indicating a viable role for this mechanism in promoting chondrogenic differentiation in the cranial NC. In contrast, Lamin-A expression was not found to be differentially expressed over the course of neurogenesis. This is consistent with studies that have shown that MSCs grown on softer matrices preferentially give rise to neurons (Engler et al., 2006), and therefore Lamin-A suppression may be necessary in order to drive cranial NC cells toward a neuronal cell fate. Characterizing Lamin-A dynamics and changes in nuclear stabilization over the course of differentiation would provide insight into the differential role of mechanotransduction during lineage specification in the cranial NC. Future temporal analyses utilizing chromatin capture techniques, coupled with RNA-seq and ATAC-seq, could uncover how changes higher order chromatin architecture due to mechanical forces generated upon morphological transformation are correlated with dynamic changes in chromatin landscape and gene expression, thus potentiating acquisition of a particular cell fate. We would expect these aspects to be unique to each cell type, and therefore dysregulation of these processes could result in either delayed or ectopic differentiation, thus contributing to the etiology underlying cranial NC-related birth defects and disorders.

Outside the cell, extracellular matrices play an integral role in promoting lineage diversification by acting as an instructive, mechanical switch that initiates mechanotransduction pathways (Engler et al., 2006, Swift et al., 2013; Yang et al., 2016). Matrix elasticity alone can direct naïve MSCs toward a neuronal or chondrogenic cell fate, yet there are many unanswered questions regarding the precise composition, concentration and organization of matrices that these cells are exposed to during differentiation, and how they together mediate robust differentiation.

Our transcriptional analysis revealed specific suites of genes associated with ECM organization that were uniquely expressed in either differentiating peripheral neurons or chondrocytes. These transcripts were significantly enriched in the intermediate stage and then continued to be expressed in the differentiated cells. We predict that gradual expression of these transcripts over time serves two purposes. First, they promote aggregation of the intermediary cells by providing a scaffold that fixes the cells spatially, which in the developing embryo would contribute to position and patterning of the future tissue or structure. Second, by bringing the differentiating cells in close contact, ECM composition facilitates cell-cell communication that triggers downstream transcriptional events, including expression of genes necessary for continued production and reorganization of the ECM. By continuing to tailor the surrounding microenvironment in a cell type-specific manner, the cranial NC cells could promote robust differentiation by stabilizing the programming associated with a distinct cell fate. We expect that closer examination of the genes associated with ECM organization identified in this study will greatly contribute to our understanding of how the microenvironment drives lineage diversification in the cranial NC.

Interestingly, stabilization of matrix-mediated lineage-specific programming may be achieved through regulation of circadian rhythm. A recent study found that ECM stiffness can directly influence circadian dynamics (Yang et al., 2017). Here, mammary epithelial cells cultured on extremely stiff matrices displayed dampened circadian rhythmicity, but softer matrices promoted a 7-fold increase in the amplitude of the oscillations. Differences in circadian activity were found to be associated with vinculin, a tension sensing adhesion molecule that is downstream of the Rho/ROCK signaling pathway. This raises the intriguing possibility that a similar interplay between mechanotransduction and circadian rhythm may be occurring during neuronal and chondrogenic differentiation in the cranial NC.

In our analysis we identified key differences in circadian transcriptional signatures between differentiated peripheral neurons and chondrocytes, and hypothesize that circadian-controlled gene expression plays a role in maintaining cellular homeostasis, albeit in two different ways. In differentiated neurons the transcripts identified were associated with clock synchronization and metabolic homeostasis, while circadian rhythm-related transcripts in differentiated chondrocytes have been implicated in regulating the balance between cartilage synthesis and degradation. Given that ECM-mediated mechanotransduction has the potential to direct downstream gene expression changes, it is possible that the microenvironment may play a previously unappreciated role in tailoring circadian dynamics to coordinate lineage-specific physiological and functional output, thus promoting maintenance of the differentiated state. Regulation of circadian rhythm is often studied in the context of ageing, and disease, such as osteoarthritis. Therefore, future studies focusing on discovering the chemical and

biomechanical inputs that govern circadian dynamics, and the downstream clock-controlled genes that regulate neuronal or chondrogenic differentiation, will be able to clarify the contribution of this process to cranial NC cell development. In addition, information gathered from these studies may be directly applicable to understanding the pathogenesis of circadian-related disease progression, thus enabling development of potential therapies and strategies for disease prevention.

Concluding remarks

Our primary murine culture system modeling NC cell differentiation provides a powerful tool for investigating the cell intrinsic mechanisms that coordinate the progression of cell fate acquisition. Given their broad contribution to a range of tissues, disruption of NC cell development can result in pleiotropic structural and functional anomalies. The well-characterized differentiation timelines described in this work constitute a temporal baseline for assessing how genetic or environmental disruptions may facilitate or impede NC differentiation, thus contributing to these defects. In addition, our transcriptomic analyses enable discovery of novel genes that may contribute to multisymptom phenotypes often associated with cranial NC-related disorders. Future studies can build on this work by interrogating cranial or trunk NC undergoing differentiation toward other cell fates, such as the gliogenic or melanogenic lineages. Such information would broaden our understanding of the similarities and differences in programming that govern NC cell diversification, as well as their potential contribution to NC-related defects and disorders, thus enabling development of novel therapeutic interventions, and strategies for prevention.

REFERENCES

Akiyama, H., Chaboissier, M.C., Martin, J.F., Schedl, A., de Crombrugghe, B., 2002. The transcription factor Sox9 has essential roles in successive steps of the chondrocyte differentiation pathway and is required for expression of Sox5 and Sox6. Genes Dev 16, 2813-2828.

Akiyama, H., Kim, J.E., Nakashima, K., Balmes, G., Iwai, N., Deng, J.M., Zhang, Z., Martin, J.F., Behringer, R.R., Nakamura, T., de Crombrugghe, B., 2005. Osteo-chondroprogenitor cells are derived from Sox9 expressing precursors. Proc Natl Acad Sci U S A 102, 14665-14670.

Alfandari, D., Cousin, H., Gaultier, A., Smith, K., White, J.M., Darribere, T., DeSimone, D.W., 2001. Xenopus ADAM 13 is a metalloprotease required for cranial neural crest-cell migration. Curr Biol 11, 918-930.

Amarilio, R., Viukov, S.V., Sharir, A., Eshkar-Oren, I., Johnson, R.S., Zelzer, E., 2007. HIF1alpha regulation of Sox9 is necessary to maintain differentiation of hypoxic prechondrogenic cells during early skeletogenesis. Development 134, 3917-3928.

Anderson, K.D., Sengupta, J., Morin, M., Neve, R.L., Valenzuela, C.F., Perrone-Bizzozero, N.I.,2001. Overexpression of HuD accelerates neurite outgrowth and increases GAP-43 mRNA expression in cortical neurons and retinoic acid-induced embryonic stem cells in vitro. Exp Neurol 168, 250-258.

Anthwal, N., Thompson, H., 2016. The development of the mammalian outer and middle ear. J Anat 228, 217-232.

Aoki, Y., Saint-Germain, N., Gyda, M., Magner-Fink, E., Lee, Y.H., Credidio, C., Saint-Jeannet, J.P., 2003. Sox10 regulates the development of neural crest-derived melanocytes in Xenopus. Dev Biol 259, 19-33.

Astiz, M., Heyde, I., Oster, H., 2019. Mechanisms of Communication in the Mammalian Circadian Timing System. Int J Mol Sci 20.

Attanasio, C., Nord, A.S., Zhu, Y., Blow, M.J., Li, Z., Liberton, D.K., Morrison, H., Plajzer-Frick, I., Holt, A., Hosseini, R., Phouanenavong, S., Akiyama, J.A., Shoukry, M., Afzal, V., Rubin, E.M., FitzPatrick, D.R., Ren, B., Hallgrimsson, B., Pennacchio, L.A., Visel, A., 2013. Fine tuning of craniofacial morphology by distant-acting enhancers. Science 342, 1241006.

Aybar, M.J., Nieto, M.A., Mayor, R., 2003. Snail precedes slug in the genetic cascade required for the specification and migration of the Xenopus neural crest. Development 130, 483-494.

Baggiolini, A., Varum, S., Mateos, J.M., Bettosini, D., John, N., Bonalli, M., Ziegler, U., Dimou, L., Clevers, H., Furrer, R., Sommer, L., 2015. Premigratory and migratory neural crest cells are multipotent in vivo. Cell Stem Cell 16, 314-322.

Baker, R.K., Antin, P.B., 2003. Ephs and ephrins during early stages of chick embryogenesis. Dev Dyn 228, 128-142.

Bangs, F., Anderson, K.V., 2017. Primary Cilia and Mammalian Hedgehog Signaling. Cold Spring Harb Perspect Biol 9.

Bank, E.M., Gruenbaum, Y., 2011. The nuclear lamina and heterochromatin: a complex relationship. Biochem Soc Trans 39, 1705-1709.

Baroffio, A., Dupin, E., Le Douarin, N.M., 1991. Common precursors for neural and mesectodermal derivatives in the cephalic neural crest. Development 112, 301-305.

Barriga, E.H., Maxwell, P.H., Reyes, A.E., Mayor, R., 2013. The hypoxia factor Hif-1alpha controls neural crest chemotaxis and epithelial to mesenchymal transition. J Cell Biol 201, 759-776.

Begbie, J., Graham, A., 2001. Integration between the epibranchial placodes and the hindbrain. Science 294, 595-598.

Bell, D.M., Leung, K.K., Wheatley, S.C., Ng, L.J., Zhou, S., Ling, K.W., Sham, M.H., Koopman, P., Tam, P.P., Cheah, K.S., 1997. SOX9 directly regulates the type-II collagen gene. Nat Genet 16, 174-178.

Belmadani, A., Tran, P.B., Ren, D., Assimacopoulos, S., Grove, E.A., Miller, R.J., 2005. The chemokine stromal cell-derived factor-1 regulates the migration of sensory neuron progenitors. J Neurosci 25, 3995-4003.

Benjamini, Y., Hochberg, Y., 1995. Controlling the False Discovery Rate - a Practical and Powerful Approach to Multiple Testing. J R Stat Soc B 57, 289-300.

Betancur, P., Bronner-Fraser, M., Sauka-Spengler, T., 2010. Assembling neural crest regulatory circuits into a gene regulatory network. Annu Rev Cell Dev Biol 26, 581-603.

Bhaskar, S.N., Weinmann, J.P., Schour, I., 1953. Role of Meckel's cartilage in the development and growth of the rat mandible. J Dent Res 32, 398-410.

Bhatt, S., Diaz, R., Trainor, P.A., 2013. Signals and switches in Mammalian neural crest cell differentiation. Cold Spring Harb Perspect Biol 5.

Bi, W., Deng, J.M., Zhang, Z., Behringer, R.R., de Crombrugghe, B., 1999. Sox9 is required for cartilage formation. Nat Genet 22, 85-89.

Billon, N., Iannarelli, P., Monteiro, M.C., Glavieux-Pardanaud, C., Richardson, W.D., Kessaris, N., Dani, C., Dupin, E., 2007. The generation of adipocytes by the neural crest. Development 134, 2283-2292.

Bixby, S., Kruger, G.M., Mosher, J.T., Joseph, N.M., Morrison, S.J., 2002. Cell-intrinsic differences between stem cells from different regions of the peripheral nervous system regulate the generation of neural diversity. Neuron 35, 643-656.

Bobick, B.E., Chen, F.H., Le, A.M., Tuan, R.S., 2009. Regulation of the chondrogenic phenotype in culture. Birth Defects Res C Embryo Today 87, 351-371.

Bolande, R.P., 1997. Neurocristopathy: its growth and development in 20 years. Pediatr Pathol Lab Med 17, 1-25.

Bray, N.L., Pimentel, H., Melsted, P., Pachter, L., 2016. Near-optimal probabilistic RNA-seq quantification. Nat Biotechnol 34, 525-527.

Bronner, M.E., LeDouarin, N.M., 2012. Development and evolution of the neural crest: an overview. Dev Biol 366, 2-9.

Bronner-Fraser, M., Fraser, S., 1989. Developmental potential of avian trunk neural crest cells in situ. Neuron 3, 755-766.

Bronner-Fraser, M., Fraser, S.E., 1988. Cell lineage analysis reveals multipotency of some avian neural crest cells. Nature 335, 161-164.

Buenrostro, J.D., Giresi, P.G., Zaba, L.C., Chang, H.Y., Greenleaf, W.J., 2013. Transposition of native chromatin for fast and sensitive epigenomic profiling of open chromatin, DNA-binding proteins and nucleosome position. Nat Methods 10, 1213-1218.

Calloni, G.W., Le Douarin, N.M., Dupin, E., 2009. High frequency of cephalic neural crest cells shows coexistence of neurogenic, melanogenic, and osteogenic differentiation capacities. Proc Natl Acad Sci U S A 106, 8947-8952.

Cano, A., Perez-Moreno, M.A., Rodrigo, I., Locascio, A., Blanco, M.J., del Barrio, M.G., Portillo, F., Nieto, M.A., 2000. The transcription factor snail controls epithelial-mesenchymal transitions by repressing E-cadherin expression. Nat Cell Biol 2, 76-83.

Carmona-Fontaine, C., Matthews, H.K., Kuriyama, S., Moreno, M., Dunn, G.A., Parsons, M., Stern, C.D., Mayor, R., 2008. Contact inhibition of locomotion in vivo controls neural crest directional migration. Nature 456, 957-961.

Chai, Y., Jiang, X., Ito, Y., Bringas, P., Jr., Han, J., Rowitch, D.H., Soriano, P., McMahon, A.P., Sucov, H.M., 2000. Fate of the mammalian cranial neural crest during tooth and mandibular morphogenesis. Development 127, 1671-1679.

Chang, C.F., Schock, E.N., Attia, A.C., Stottmann, R.W., Brugmann, S.A., 2015. The ciliary baton: orchestrating neural crest cell development. Curr Top Dev Biol 111, 97-134.

Chen, C.S., Mrksich, M., Huang, S., Whitesides, G.M., Ingber, D.E., 1997. Geometric control of cell life and death. Science 276, 1425-1428.

Cheung, M., Briscoe, J., 2003. Neural crest development is regulated by the transcription factor Sox9. Development 130, 5681-5693.

Cheung, M., Chaboissier, M.C., Mynett, A., Hirst, E., Schedl, A., Briscoe, J., 2005. The transcriptional control of trunk neural crest induction, survival, and delamination. Dev Cell 8, 179-192.

Choksi, S.P., Lauter, G., Swoboda, P., Roy, S., 2014. Switching on cilia: transcriptional networks regulating ciliogenesis. Development 141, 1427-1441.

Clay, M.R., Halloran, M.C., 2013. Rho activation is apically restricted by Arhgap1 in neural crest cells and drives epithelial-to-mesenchymal transition. Development 140, 3198-3209.

Cohen, A.M., Konigsberg, I.R., 1975. A clonal approach to the problem of neural crest determination. Dev Biol 46, 262-280.

Collazo, A., Bronner-Fraser, M., Fraser, S.E., 1993. Vital dye labelling of Xenopus laevis trunk neural crest reveals multipotency and novel pathways of migration. Development 118, 363-376.

Compagnucci, C., Piermarini, E., Sferra, A., Borghi, R., Niceforo, A., Petrini, S., Piemonte, F., Bertini, E., 2016. Cytoskeletal dynamics during in vitro neurogenesis of induced pluripotent stem cells (iPSCs). Mol Cell Neurosci 77, 113-124.

Couly, G., Grapin-Botton, A., Coltey, P., Ruhin, B., Le Douarin, N.M., 1998. Determination of the identity of the derivatives of the cephalic neural crest: incompatibility between Hox gene expression and lower jaw development. Development 125, 3445-3459.

D'Amico-Martel, A., Noden, D.M., 1983. Contributions of placodal and neural crest cells to avian cranial peripheral ganglia. Am J Anat 166, 445-468.

d'Angelo, P., 2007. Hugin - Panorama Photo Stitcher.

D'Souza, R. N., Ruest, L. B., Hinton, R. J., Svoboda, K. K. H., 2010. Development of the craniofacial complex. In Bone and Development: Topics in Bone Biology 6 (eds. F. Bronner, M. C. Farach-Carson, H. I. Roach), pp. 153-181. London: Springer.

Danielian, P.S., Muccino, D., Rowitch, D.H., Michael, S.K., McMahon, A.P., 1998. Modification of gene activity in mouse embryos in utero by a tamoxifen-inducible form of Cre recombinase. Curr Biol 8, 1323-1326.

Davidson, E.H., 2010. Emerging properties of animal gene regulatory networks. Nature 468, 911-920.

Davy, A., Aubin, J., Soriano, P., 2004. Ephrin-B1 forward and reverse signaling are required during mouse development. Genes Dev 18, 572-583.

De Bellard, M.E., Ching, W., Gossler, A., Bronner-Fraser, M., 2002. Disruption of segmental neural crest migration and ephrin expression in delta-1 null mice. Dev Biol 249, 121-130.

De Bellard, M.E., Rao, Y., Bronner-Fraser, M., 2003. Dual function of Slit2 in repulsion and enhanced migration of trunk, but not vagal, neural crest cells. J Cell Biol 162, 269-279.

De Vos, D., Bruggeman, F.J., Westerhoff, H.V., Bakker, B.M., 2011. How molecular competition influences fluxes in gene expression networks. PLoS One 6, e28494.

del Barrio, M.G., Nieto, M.A., 2002. Overexpression of Snail family members highlights their ability to promote chick neural crest formation. Development 129, 1583-1593.

Dhara, S.P., Rau, A., Flister, M.J., Recka, N.M., Laiosa, M.D., Auer, P.L., Udvadia, A.J., 2019. Cellular reprogramming for successful CNS axon regeneration is driven by a temporally changing cast of transcription factors. Sci Rep 9, 14198.

Doherty, G.J., McMahon, H.T., 2008. Mediation, modulation, and consequences of membrane-cytoskeleton interactions. Annu Rev Biophys 37, 65-95.

Dong, Z., Sinanan, A., Parkinson, D., Parmantier, E., Mirsky, R., Jessen, K.R., 1999. Schwann cell development in embryonic mouse nerves. J Neurosci Res 56, 334-348.

Dottori, M., Gross, M.K., Labosky, P., Goulding, M., 2001. The winged-helix transcription factor Foxd3 suppresses interneuron differentiation and promotes neural crest cell fate. Development 128, 4127-4138.

Druckenbrod, N.R., Epstein, M.L., 2005. The pattern of neural crest advance in the cecum and colon. Dev Biol 287, 125-133.

Duband, J.L., Thiery, J.P., 1982. Distribution of fibronectin in the early phase of avian cephalic neural crest cell migration. Dev Biol 93, 308-323.

Ducy, P., Zhang, R., Geoffroy, V., Ridall, A.L., Karsenty, G., 1997. Osf2/Cbfa1: a transcriptional activator of osteoblast differentiation. Cell 89, 747-754.

Dudek, M., Gossan, N., Yang, N., Im, H.J., Ruckshanthi, J.P., Yoshitane, H., Li, X., Jin, D., Wang, P., Boudiffa, M., Bellantuono, I., Fukada, Y., Boot-Handford, R.P., Meng, Q.J., 2016. The chondrocyte clock gene Bmal1 controls cartilage homeostasis and integrity. J Clin Invest 126, 365-376.

Dupin, E., Calloni, G.W., Le Douarin, N.M., 2010. The cephalic neural crest of amniote vertebrates is composed of a large majority of precursors endowed with neural, melanocytic, chondrogenic and osteogenic potentialities. Cell Cycle 9, 238-249.

Dushane, G. P., 1938. Neural fold derivatives in the amphibia: Pigment cells, spinal ganglia and Rohon-Beard cells. J. Exp. Zool. 78, 485-503.

Eickholt, B.J., Mackenzie, S.L., Graham, A., Walsh, F.S., Doherty, P., 1999. Evidence for collapsin-1 functioning in the control of neural crest migration in both trunk and hindbrain regions. Development 126, 2181-2189.

Engler, A.J., Sen, S., Sweeney, H.L., Discher, D.E., 2006. Matrix elasticity directs stem cell lineage specification. Cell 126, 677-689.

Etchevers, H., 2011. Primary culture of chick, mouse or human neural crest cells. Nat Protoc 6, 1568-1577.

Etchevers, H.C., Vincent, C., Le Douarin, N.M., Couly, G.F., 2001. The cephalic neural crest provides pericytes and smooth muscle cells to all blood vessels of the face and forebrain. Development 128, 1059-1068.

Funato, N., Chapman, S.L., McKee, M.D., Funato, H., Morris, J.A., Shelton, J.M., Richardson, J.A., Yanagisawa, H., 2009. Hand2 controls osteoblast differentiation in the branchial arch by inhibiting DNA binding of Runx2. Development 136, 615-625.

Furumatsu, T., Tsuda, M., Taniguchi, N., Tajima, Y., Asahara, H., 2005. Smad3 induces chondrogenesis through the activation of SOX9 via CREB-binding protein/p300 recruitment. J Biol Chem 280, 8343-8350.

Gans, C., Northcutt, R. G., 1983. Neural crest and the origin of vertebrates: a new head. Science 220, 268-273.

Gammill, L.S., Gonzalez, C., Bronner-Fraser, M., 2007. Neuropilin 2/semaphorin 3F signaling is essential for cranial neural crest migration and trigeminal ganglion condensation. Dev Neurobiol 67, 47-56.

Gammill, L.S., Gonzalez, C., Gu, C., Bronner-Fraser, M., 2006. Guidance of trunk neural crest migration requires neuropilin 2/semaphorin 3F signaling. Development 133, 99-106.

Garnett, A.T., Square, T.A., Medeiros, D.M., 2012. BMP, Wnt and FGF signals are integrated through evolutionarily conserved enhancers to achieve robust expression of Pax3 and Zic genes at the zebrafish neural plate border. Development 139, 4220-4231.

Ge, S.X., Jung, D., Yao, R., 2020. ShinyGO: a graphical gene-set enrichment tool for animals and plants. Bioinformatics 36, 2628-2629.

Geraghty, R.J., Capes-Davis, A., Davis, J.M., Downward, J., Freshney, R.I., Knezevic, I., Lovell-Badge, R., Masters, J.R., Meredith, J., Stacey, G.N., Thraves, P., Vias, M., Cancer Research, U.K., 2014. Guidelines for the use of cell lines in biomedical research. Br J Cancer 111, 1021-1046.

Gonzalez-Billault, C., Munoz-Llancao, P., Henriquez, D.R., Wojnacki, J., Conde, C., Caceres, A., 2012. The role of small GTPases in neuronal morphogenesis and polarity. Cytoskeleton (Hoboken) 69, 464-485.

Gorlin, R.J., Cohen, M. M., Levin, L. S., 1990. Syndromes of the head and neck. Oxford, UK: Oxford University Press.

Gossan, N., Zeef, L., Hensman, J., Hughes, A., Bateman, J.F., Rowley, L., Little, C.B., Piggins, H.D., Rattray, M., Boot-Handford, R.P., Meng, Q.J., 2013. The circadian clock in murine chondrocytes regulates genes controlling key aspects of cartilage homeostasis. Arthritis Rheum 65, 2334-2345.

Groves, A.K., LaBonne, C., 2014. Setting appropriate boundaries: fate, patterning and competence at the neural plate border. Dev Biol 389, 2-12.

Gu, Z., Eils, R., Schlesner, M., 2016. Complex heatmaps reveal patterns and correlations in multidimensional genomic data. Bioinformatics 32, 2847-2849.

Guelen, L., Pagie, L., Brasset, E., Meuleman, W., Faza, M.B., Talhout, W., Eussen, B.H., de Klein, A., Wessels, L., de Laat, W., van Steensel, B., 2008. Domain organization of human chromosomes revealed by mapping of nuclear lamina interactions. Nature 453, 948-951.

Haldin, C.E., LaBonne, C., 2010. SoxE factors as multifunctional neural crest regulatory factors. Int J Biochem Cell Biol 42, 441-444.

Hall, B.K., 1980. Tissue interactions and the initiation of osteogenesis and chondrogenesis in the neural crest-derived mandibular skeleton of the embryonic mouse as seen in isolated murine tissues and in recombinations of murine and avian tissues. J Embryol Exp Morphol 58, 251-264.

Hall, B.K., 2000. The neural crest as a fourth germ layer and vertebrates as quadroblastic not triploblastic. Evol Dev 2, 3-5.

Hanahan, D., Weinberg, R.A., 2011. Hallmarks of cancer: the next generation. Cell 144, 646-674.

Harlow, D.E., Barlow, L.A., 2007. Embryonic origin of gustatory cranial sensory neurons. Dev Biol 310, 317-328.

Harlow, D.E., Yang, H., Williams, T., Barlow, L.A., 2011. Epibranchial placode-derived neurons produce BDNF required for early sensory neuron development. Dev Dyn 240, 309-323.

Harr, J.C., Luperchio, T.R., Wong, X., Cohen, E., Wheelan, S.J., Reddy, K.L., 2015. Directed targeting of chromatin to the nuclear lamina is mediated by chromatin state and A-type lamins. J Cell Biol 208, 33-52.

Harris, M.L., Hall, R., Erickson, C.A., 2008. Directing pathfinding along the dorsolateral path – the role of EDNRB2 and EphB2 in overcoming inhibition. Development 135, 4113-4122.

Hirata, M., Kugimiya, F., Fukai, A., Saito, T., Yano, F., Ikeda, T., Mabuchi, A., Sapkota, B.R., Akune, T., Nishida, N., Yoshimura, N., Nakagawa, T., Tokunaga, K., Nakamura, K., Chung, U.I., Kawaguchi, H., 2012. C/EBPbeta and RUNX2 cooperate to degrade cartilage with MMP-13 as the target and HIF-2alpha as the inducer in chondrocytes. Hum Mol Genet 21, 1111-1123.

His, W., 1868. *Untersuchungen über die erste Anlage des Wirbelthierleibes: die erste Entwickelung des Hü hnchens im Ei*. Leipzig: F.C.W. Vogel.

Hörstadius, S., 1950. The neural crest: its properties and derivatives in the light of experimental research. New York, London: Oxford University Press.

Hörstadius, S. and Sellman, S., 1941. Experimental studies on the determination of the chondrocranium in Amblystoma mexicanum. Ark. Zool. A 33, 1-8.

Hu, M., Krause, D., Greaves, M., Sharkis, S., Dexter, M., Heyworth, C., Enver, T., 1997. Multilineage gene expression precedes commitment in the hemopoietic system. Genes Dev 11, 774-785.

Huber, K., 2006. The sympathoadrenal cell lineage: specification, diversification, and new perspectives. Dev Biol 298, 335-343.

Humason, G.L., 1962. Animal tissue techniques. W.H. Freeman, San Fancisco.

Hutchins, E.J., Kunttas, E., Piacentino, M.L., Howard, A.G.A.t., Bronner, M.E., Uribe, R.A., 2018. Migration and diversification of the vagal neural crest. Dev Biol 444 Suppl 1, S98-S109.

Ido, A., Ito, K., 2006. Expression of chondrogenic potential of mouse trunk neural crest cells by FGF2 treatment. Dev Dyn 235, 361-367.

Ikeda, Y., Kamagata, M., Hirao, M., Yasuda, S., Iwami, S., Sasaki, H., Tsubosaka, M., Hattori, Y., Todoh, A., Tamura, K., Shiga, K., Ohtsu, T., Shibata, S., 2018. Glucagon and/or IGF-1 Production Regulates Resetting of the Liver Circadian Clock in Response to a Protein or Amino Acid-only Diet. EBioMedicine 28, 210-224.

Ikeya, M., Lee, S.M., Johnson, J.E., McMahon, A.P., Takada, S., 1997. Wnt signalling required for expansion of neural crest and CNS progenitors. Nature 389, 966-970.

Ishii, M., Arias, A.C., Liu, L., Chen, Y.B., Bronner, M.E., Maxson, R.E., 2012. A stable cranial neural crest cell line from mouse. Stem Cells Dev 21, 3069-3080.

Jessen, K.R., Mirsky, R., 1984. Nonmyelin-forming Schwann cells coexpress surface proteins and intermediate filaments not found in myelin-forming cells: a study of Ran-2, A5E3 antigen and glial fibrillary acidic protein. J Neurocytol 13, 923-934.

Jessen, K.R., Mirsky, R., Lloyd, A.C., 2015. Schwann cells: Development and role in nerve repair. Cold Spring Harb Perspect Biol 7, a020487.

Kalcheim, C., Burstyn-Cohen, T., 2005. Early stages of neural crest ontogeny: formation and regulation of cell delamination. Int J Dev Biol 49, 105-116.

Karlsson, C., Jonsson, M., Asp, J., Brantsing, C., Kageyama, R., Lindahl, A., 2007. Notch and HES5 are regulated during human cartilage differentiation. Cell Tissue Res 327, 539-551.

Kasemeier-Kulesa, J.C., McLennan, R., Romine, M.H., Kulesa, P.M., Lefcort, F., 2010. CXCR4 controls ventral migration of sympathetic precursor cells. J Neurosci 30, 13078-13088.

Kerosuo, L., Nie, S., Bajpai, R., Bronner, M.E., 2015. Crestospheres: Long-term maintenance of multipotent, premigratory neural crest stem cells. Stem Cell Reports 5, 499-507.

Khudyakov, J., Bronner-Fraser, M., 2009. Comprehensive spatiotemporal analysis of early chick neural crest network genes. Dev Dyn 238, 716-723.

Kim, H.S., Seo, H., Yang, C., Brunet, J.F., Kim, K.S., 1998. Noradrenergic-specific transcription of the dopamine beta-hydroxylase gene requires synergy of multiple cis-acting elements including at least two Phox2a-binding sites. J Neurosci 18, 8247-8260.

Kim, J., Lo, L., Dormand, E., Anderson, D.J., 2003. SOX10 maintains multipotency and inhibits neuronal differentiation of neural crest stem cells. Neuron 38, 17-31.

Kishi, J.Y., Lapan, S.W., Beliveau, B.J., West, E.R., Zhu, A., Sasaki, H.M., Saka, S.K., Wang, Y., Cepko, C.L., Yin, P., 2019. SABER amplifies FISH: enhanced multiplexed imaging of RNA and DNA in cells and tissues. Nat Methods 16, 533-544.

Ko, H.R., Hwang, I., Jin, E.J., Yun, T., Ryu, D., Kang, J.S., Park, K.W., Shin, J.H., Cho, S.W., Lee, K.H., Ye, K., Ahn, J.Y., 2019. Roles of ErbB3-binding protein 1 (EBP1) in embryonic development and gene-silencing control. Proc Natl Acad Sci U S A 116, 24852-24860.

Konishi, Y., Ikeda, K., Iwakura, Y., Kawakami, K., 2006. Six1 and Six4 promote survival of sensory neurons during early trigeminal gangliogenesis. Brain Res 1116, 93-102. Kubota, Y., Ito, K., 2000. Chemotactic migration of mesencephalic neural crest cells in the mouse. Dev Dyn 217, 170-179.

Kurosaka, H., Trainor, P.A., Leroux-Berger, M., Iulianella, A., 2015. Cranial nerve development requires co-ordinated Shh and canonical Wnt signaling. PLoS One 10, e0120821.

Kwon, I.S., Ahn, J.Y., 2011. p48 Ebp1 acts as a downstream mediator of Trk signaling in neurons, contributing neuronal differentiation. Neurochem Int 58, 215-223.

Lafont, J.E., Talma, S., Murphy, C.L., 2007. Hypoxia-inducible factor 2alpha is essential for hypoxic induction of the human articular chondrocyte phenotype. Arthritis Rheum 56, 3297-3306.

Lambert, S.A., Jolma, A., Campitelli, L.F., Das, P.K., Yin, Y., Albu, M., Chen, X., Taipale, J., Hughes, T.R., Weirauch, M.T., 2018. The Human Transcription Factors. Cell 175, 598-599.

Lamia, K.A., Sachdeva, U.M., DiTacchio, L., Williams, E.C., Alvarez, J.G., Egan, D.F., Vasquez, D.S., Juguilon, H., Panda, S., Shaw, R.J., Thompson, C.B., Evans, R.M., 2009. AMPK regulates the circadian clock by cryptochrome phosphorylation and degradation. Science 326, 437-440.

Landacre, F. L., 1921. The fate of the neural crest in the head of the urodeles. J. Comp. Neurol. 33, 1-43.

Le Douarin, N., 1982. The Neural Crest. Cambridge University Press, Cambridge.

Le Douarin, N.M., Teillet, M.A., 1974. Experimental analysis of the migration and differentiation of neuroblasts of the autonomic nervous system and of neurectodermal mesenchymal derivatives, using a biological cell marking technique. Dev Biol 41, 162-184.

Le Lievre, C.S., Le Douarin, N.M., 1975. Mesenchymal derivatives of the neural crest: analysis of chimaeric quail and chick embryos. J Embryol Exp Morphol 34, 125-154.

Lee, M., Goodall, J., Verastegui, C., Ballotti, R., Goding, C.R., 2000. Direct regulation of the Microphthalmia promoter by Sox10 links Waardenburg-Shah syndrome (WS4)-associated hypopigmentation and deafness to WS2. J Biol Chem 275, 37978-37983.

Lee, V.M., Sechrist, J.W., Luetolf, S., Bronner-Fraser, M., 2003. Both neural crest and placode contribute to the ciliary ganglion and oculomotor nerve. Dev Biol 263, 176-190.

Lefebvre, V., Huang, W., Harley, V.R., Goodfellow, P.N., de Crombrugghe, B., 1997. SOX9 is a potent activator of the chondrocyte-specific enhancer of the pro alpha1(II) collagen gene. Mol Cell Biol 17, 2336-2346.

Lefebvre, V., Li, P., de Crombrugghe, B., 1998. A new long form of Sox5 (L-Sox5), Sox6 and Sox9 are coexpressed in chondrogenesis and cooperatively activate the type II collagen gene. EMBO J 17, 5718-5733.

Lewis, A.E., Vasudevan, H.N., O'Neill, A.K., Soriano, P., Bush, J.O., 2013. The widely used Wnt1-Cre transgene causes developmental phenotypes by ectopic activation of Wnt signaling. Dev Biol 379, 229-234.

Li, F., Lu, Y., Ding, M., Napierala, D., Abbassi, S., Chen, Y., Duan, X., Wang, S., Lee, B., Zheng, Q., 2011. Runx2 contributes to murine Col10a1 gene regulation through direct interaction with its cis-enhancer. J Bone Miner Res 26, 2899-2910.

Light, W., Vernon, A.E., Lasorella, A., Iavarone, A., LaBonne, C., 2005. Xenopus Id3 is required downstream of Myc for the formation of multipotent neural crest progenitor cells. Development 132, 1831-1841.

Liu, C., Reppert, S.M., 2000. GABA synchronizes clock cells within the suprachiasmatic circadian clock. Neuron 25, 123-128.

Liu, C.F., Lefebvre, V., 2015. The transcription factors SOX9 and SOX5/SOX6 cooperate genome-wide through super-enhancers to drive chondrogenesis. Nucleic Acids Res 43, 8183-8203.

Liu, J.P., Jessell, T.M., 1998. A role for rhoB in the delamination of neural crest cells from the dorsal neural tube. Development 125, 5055-5067.

Livak, K.J., Schmittgen, T.D., 2001. Analysis of relative gene expression data using real-time quantitative PCR and the 2(-Delta Delta C(T)) Method. Methods 25, 402-408.

Mackie, E.J., Ahmed, Y.A., Tatarczuch, L., Chen, K.S., Mirams, M., 2008. Endochondral ossification: how cartilage is converted into bone in the developing skeleton. Int J Biochem Cell Biol 40, 46-62.

Mammoto, A., Ingber, D.E., 2009. Cytoskeletal control of growth and cell fate switching. Curr Opin Cell Biol 21, 864-870.

Mammoto, T., Ingber, D.E., 2010. Mechanical control of tissue and organ development. Development 137, 1407-1420.

Mammoto, T., Mammoto, A., Torisawa, Y.S., Tat, T., Gibbs, A., Derda, R., Mannix, R., de Bruijn, M., Yung, C.W., Huh, D., Ingber, D.E., 2011. Mechanochemical control of mesenchymal condensation and embryonic tooth organ formation. Dev Cell 21, 758-769.

Markway, B.D., Cho, H., Zilberman-Rudenko, J., Holden, P., McAlinden, A., Johnstone, B., 2015. Hypoxia-inducible factor 3-alpha expression is associated with the stable chondrocyte phenotype. J Orthop Res 33, 1561-1570.

Marmigere, F., Ernfors, P., 2007. Specification and connectivity of neuronal subtypes in the sensory lineage. Nat Rev Neurosci 8, 114-127.

Martik, M.L., Bronner, M.E., 2017. Regulatory Logic Underlying Diversification of the Neural Crest. Trends Genet 33, 715-727.

Marusich, M.F., Furneaux, H.M., Henion, P.D., Weston, J.A., 1994. Hu neuronal proteins are expressed in proliferating neurogenic cells. J Neurobiol 25, 143-155.

Matsui, T., Maeda, M., Doi, Y., Yonemura, S., Amano, M., Kaibuchi, K., Tsukita, S., Tsukita, S., 1998. Rho-kinase phosphorylates COOH-terminal threonines of ezrin/radixin/moesin (ERM) proteins and regulates their head-to-tail association. J Cell Biol 140, 647-657.

Matsuo-Takasaki, M., Matsumura, M., Sasai, Y., 2005. An essential role of Xenopus Foxi1a for ventral specification of the cephalic ectoderm during gastrulation. Development 132, 3885-3894.

Matsuoka, T., Ahlberg, P.E., Kessaris, N., Iannarelli, P., Dennehy, U., Richardson, W.D., McMahon, A.P., Koentges, G., 2005. Neural crest origins of the neck and shoulder. Nature 436, 347-355.

Maurer, J., Fuchs, S., Jager, R., Kurz, B., Sommer, L., Schorle, H., 2007. Establishment and controlled differentiation of neural crest stem cell lines using conditional transgenesis. Differentiation 75, 580-591.

May-Simera, H., Nagel-Wolfrum, K., Wolfrum, U., 2017. Cilia - The sensory antennae in the eye. Prog Retin Eye Res 60, 144-180.

Mayor, R., Carmona-Fontaine, C., 2010. Keeping in touch with contact inhibition of locomotion. Trends Cell Biol 20, 319-328.

McBeath, R., Pirone, D.M., Nelson, C.M., Bhadriraju, K., Chen, C.S., 2004. Cell shape, cytoskeletal tension, and RhoA regulate stem cell lineage commitment. Dev Cell 6, 483-495.

McCusker, C., Cousin, H., Neuner, R., Alfandari, D., 2009. Extracellular cleavage of cadherin-11 by ADAM metalloproteases is essential for Xenopus cranial neural crest cell migration. Mol Biol Cell 20, 78-89.

McGonnell, I.M., Graham, A., 2002. Trunk neural crest has skeletogenic potential. Curr Biol 12, 767-771.

McKeown, S.J., Lee, V.M., Bronner-Fraser, M., Newgreen, D.F., Farlie, P.G., 2005. Sox10 overexpression induces neural crest-like cells from all dorsoventral levels of the neural tube but inhibits differentiation. Dev Dyn 233, 430-444.

McKinney, M.C., Fukatsu, K., Morrison, J., McLennan, R., Bronner, M.E., Kulesa, P.M., 2013. Evidence for dynamic rearrangements but lack of fate or position restrictions in premigratory avian trunk neural crest. Development 140, 820-830.

McLarren, K.W., Litsiou, A., Streit, A., 2003. DLX5 positions the neural crest and preplacode region at the border of the neural plate. Dev Biol 259, 34-47.

McLennan, R., Teddy, J.M., Kasemeier-Kulesa, J.C., Romine, M.H., Kulesa, P.M., 2010. Vascular endothelial growth factor (VEGF) regulates cranial neural crest migration in vivo. Dev Biol 339, 114-125.

McMahon, A.P., Bradley, A., 1990. The Wnt-1 (int-1) proto-oncogene is required for development of a large region of the mouse brain. Cell 62, 1073-1085.

Meijer, J.H., Schwartz, W.J., 2003. In search of the pathways for light-induced pacemaker resetting in the suprachiasmatic nucleus. J Biol Rhythms 18, 235-249.

Mello, M.A., Tuan, R.S., 1999. High density micromass cultures of embryonic limb bud mesenchymal cells: an in vitro model of endochondral skeletal development. In Vitro Cell Dev Biol Anim 35, 262-269.

Meulemans, D., Bronner-Fraser, M., 2004. Gene-regulatory interactions in neural crest evolution and development. Dev Cell 7, 291-299.

Mi, H., Muruganujan, A., Thomas, P.D., 2013. PANTHER in 2013: modeling the evolution of gene function, and other gene attributes, in the context of phylogenetic trees. Nucleic Acids Res 41, D377-386.

Miller, C.T., Swartz, M.E., Khuu, P.A., Walker, M.B., Eberhart, J.K., Kimmel, C.B., 2007. mef2ca is required in cranial neural crest to effect Endothelin1 signaling in zebrafish. Dev Biol 308, 144-157.

Moore, R.Y., Speh, J.C., 1993. GABA is the principal neurotransmitter of the circadian system. Neurosci Lett 150, 112-116.

Mori-Akiyama, Y., Akiyama, H., Rowitch, D.H., de Crombrugghe, B., 2003. Sox9 is required for determination of the chondrogenic cell lineage in the cranial neural crest. Proc Natl Acad Sci U S A 100, 9360-9365.

Morikawa, Y., Zehir, A., Maska, E., Deng, C., Schneider, M.D., Mishina, Y., Cserjesi, P., 2009. BMP signaling regulates sympathetic nervous system development through Smad4-dependent and -independent pathways. Development 136, 3575-3584.

Morrison, S.J., White, P.M., Zock, C., Anderson, D.J., 1999. Prospective identification, isolation by flow cytometry, and in vivo self-renewal of multipotent mammalian neural crest stem cells. Cell 96, 737-749.

Mundell, N.A., Labosky, P.A., 2011. Neural crest stem cell multipotency requires Foxd3 to maintain neural potential and repress mesenchymal fates. Development 138, 641-652. Murphy, C.L., Polak, J.M., 2004. Control of human articular chondrocyte differentiation by reduced oxygen tension. J Cell Physiol 199, 451-459.

Murisier, F., Guichard, S., Beermann, F., 2007. The tyrosinase enhancer is activated by Sox10 and Mitf in mouse melanocytes. Pigment Cell Res 20, 173-184.

Ng, L.J., Wheatley, S., Muscat, G.E., Conway-Campbell, J., Bowles, J., Wright, E., Bell, D.M., Tam, P.P., Cheah, K.S., Koopman, P., 1997. SOX9 binds DNA, activates transcription, and coexpresses with type II collagen during chondrogenesis in the mouse. Dev Biol 183, 108-121.

Nikitina, N., Sauka-Spengler, T., Bronner-Fraser, M., 2008. Dissecting early regulatory relationships in the lamprey neural crest gene network. Proc Natl Acad Sci U S A 105, 20083-20088.

Noack Watt, K. E.,Trainor, P. A., 2014. Neurocristopathies: The etiology and pathogenesis of disorders arising from defects in neural crest cell development. In Neural Crest Cells: Evolution, Development and Disease (ed. P.A. Trainor), pp. 361-394. New York: Elsevier.

Obrink, B., 1986. Epithelial cell adhesion molecules. Exp Cell Res 163, 1-21.

Olesnicky Killian, E.C., Birkholz, D.A., Artinger, K.B., 2009. A role for chemokine signaling in neural crest cell migration and craniofacial development. Dev Biol 333, 161-172. Pala, R., Alomari, N., Nauli, S.M., 2017. Primary Cilium-Dependent Signaling Mechanisms. Int J Mol Sci 18.

Pan, F., Means, A.R., Liu, J.O., 2005. Calmodulin-dependent protein kinase IV regulates nuclear export of Cabin1 during T-cell activation. EMBO J 24, 2104-2113.

Panda, S., Antoch, M.P., Miller, B.H., Su, A.I., Schook, A.B., Straume, M., Schultz, P.G., Kay, S.A., Takahashi, J.S., Hogenesch, J.B., 2002. Coordinated transcription of key pathways in the mouse by the circadian clock. Cell 109, 307-320.

Paulsen, D.F., Langille, R.M., Dress, V., Solursh, M., 1988. Selective stimulation of in vitro limb-bud chondrogenesis by retinoic acid. Differentiation 39, 123-130.

Paulsen, D.F., Solursh, M., 1988. Microtiter micromass cultures of limb-bud mesenchymal cells. In Vitro Cell Dev Biol 24, 138-147.

Percipalle, P., 2013. Co-transcriptional nuclear actin dynamics. Nucleus 4, 43-52. Perez, S.E., Rebelo, S., Anderson, D.J., 1999. Early specification of sensory neuron fate revealed by expression and function of neurogenins in the chick embryo. Development 126, 1715-1728.

Petsakou, A., Sapsis, T.P., Blau, J., 2015. Circadian Rhythms in Rho1 Activity Regulate Neuronal Plasticity and Network Hierarchy. Cell 162, 823-835.

Pimentel, H., Bray, N.L., Puente, S., Melsted, P., Pachter, L., 2017. Differential analysis of RNA-seq incorporating quantification uncertainty. Nat Methods 14, 687-690.

Pfaltzgraff, E.R., Mundell, N.A., Labosky, P.A., 2012. Isolation and culture of neural crest cells from embryonic murine neural tube. J Vis Exp, e4134.

Pietri, T., Eder, O., Blanche, M., Thiery, J.P., Dufour, S., 2003. The human tissue plasminogen activator-Cre mouse: a new tool for targeting specifically neural crest cells and their derivatives in vivo. Dev Biol 259, 176-187.

Pla, P., Alberti, C., Solov'eva, O., Pasdar, M., Kunisada, T., Larue, L., 2005. Ednrb2 orients cell migration towards the dorsolateral neural crest pathway and promotes melanocyte differentiation. Pigment Cell Res 18, 181-187.

Platt, J. B., 1893. Ectodermic origin of the cartilages of the head. Anat. Anz. 8, 506-509.

Platt, J. B., 1897. The Development of the Cartilaginous Skull and of the Branchial and Hypoglossal Musculature in Necturus. Morphol. Jahrb. 25, 377-464.

Pomeranz, H.D., Sherman, D.L., Smalheiser, N.R., Tennyson, V.M., Gershon, M.D., 1991. Expression of a neurally related laminin binding protein by neural crest-derived cells that colonize the gut: relationship to the formation of enteric ganglia. J Comp Neurol 313, 625-642.

Prasad, M.S., Sauka-Spengler, T., LaBonne, C., 2012. Induction of the neural crest state: control of stem cell attributes by gene regulatory, post-transcriptional and epigenetic interactions. Dev Biol 366, 10-21.

Preibisch, S., Saalfeld, S., Tomancak, P., 2009. Globally optimal stitching of tiled 3D microscopic image acquisitions. Bioinformatics 25, 1463-5.

Radlanski, R.J., Renz, H., Klarkowski, M.C., 2003. Prenatal development of the human mandible. 3D reconstructions, morphometry and bone remodelling pattern, sizes 12-117 mm CRL. Anat Embryol (Berl) 207, 221-232.

Rao, M.S., Anderson, D.J., 1997. Immortalization and controlled in vitro differentiation of murine multipotent neural crest stem cells. J Neurobiol 32, 722-746.

Raudvere, U., Kolberg, L., Kuzmin, I., Arak, T., Adler, P., Peterson, H., Vilo, J., 2019. g:Profiler: a web server for functional enrichment analysis and conversions of gene lists (2019 update). Nucleic Acids Res 47, W191-W198.

Ray, P., Chapman, S.C., 2015. Cytoskeletal Reorganization Drives Mesenchymal Condensation and Regulates Downstream Molecular Signaling. PLoS One 10, e0134702.

Reiter, J.F., Leroux, M.R., 2017. Genes and molecular pathways underpinning ciliopathies. Nat Rev Mol Cell Biol 18, 533-547.

Replogle, M.R., Sreevidya, V.S., Lee, V.M., Laiosa, M.D., Svoboda, K.R., Udvadia, A.J., 2018. Establishment of a murine culture system for modeling the temporal progression of cranial and trunk neural crest cell differentiation. Dis Model Mech 11.

Ridley, A.J., Hall, A., 1992. Distinct patterns of actin organization regulated by the small GTP-binding proteins Rac and Rho. Cold Spring Harb Symp Quant Biol 57, 661-671.

Riedel, C.S., Georg, B., Jorgensen, H.L., Hannibal, J., Fahrenkrug, J., 2018. Mice Lacking EGR1 Have Impaired Clock Gene (BMAL1) Oscillation, Locomotor Activity, and Body Temperature. J Mol Neurosci 64, 9-19.

Ripperger, J.A., Schibler, U., 2006. Rhythmic CLOCK-BMAL1 binding to multiple E-box motifs drives circadian Dbp transcription and chromatin transitions. Nat Genet 38, 369-374.

Robins, J.C., Akeno, N., Mukherjee, A., Dalal, R.R., Aronow, B.J., Koopman, P., Clemens, T.L., 2005. Hypoxia induces chondrocyte-specific gene expression in mesenchymal cells in association with transcriptional activation of Sox9. Bone 37, 313-322.

Roellig, D., Tan-Cabugao, J., Esaian, S., Bronner, M.E., 2017. Dynamic transcriptional signature and cell fate analysis reveals plasticity of individual neural plate border cells. Elife 6.

Rohrer, H., 2011. Transcriptional control of differentiation and neurogenesis in autonomic ganglia. Eur J Neurosci 34, 1563-1573.

Roth, V., 2006. Doubling time computing.

Rutkowski, T.P., Kohn, A., Sharma, D., Ren, Y., Mirando, A.J., Hilton, M.J., 2016. HES factors regulate specific aspects of chondrogenesis and chondrocyte hypertrophy during cartilage development. J Cell Sci 129, 2145-2155.

Santiago, A., Erickson, C.A., 2002. Ephrin-B ligands play a dual role in the control of neural crest cell migration. Development 129, 3621-3632.

Sato, A., Scholl, A.M., Kuhn, E.N., Stadt, H.A., Decker, J.R., Pegram, K., Hutson, M.R., Kirby, M.L., 2011. FGF8 signaling is chemotactic for cardiac neural crest cells. Dev Biol 354, 18-30.

Sauer, B., Henderson, N., 1988. Site-specific DNA recombination in mammalian cells by the Cre recombinase of bacteriophage P1. Proc Natl Acad Sci U S A 85, 5166-5170. Sauka-Spengler, T., Bronner-Fraser, M., 2008. A gene regulatory network orchestrates neural crest formation. Nat Rev Mol Cell Biol 9, 557-568.

Schindelin, J., Arganda-Carreras, I., Frise, E., Kaynig, V., Longair, M., Pietzsch, T., Preibisch, S., Rueden, C., Saalfeld, S., Schmid, B., Tinevez, J.Y., White, D.J., Hartenstein, V., Eliceiri, K., Tomancak, P., Cardona, A., 2012. Fiji: an open-source platform for biological-image analysis. Nat Methods 9, 676-682.

Schipani, E., Ryan, H.E., Didrickson, S., Kobayashi, T., Knight, M., Johnson, R.S., 2001. Hypoxia in cartilage: HIF-1alpha is essential for chondrocyte growth arrest and survival. Genes Dev 15, 2865-2876.

Schneider, C.A., Rasband, W.S., Eliceiri, K.W., 2012. NIH Image to ImageJ: 25 years of image analysis. Nat Methods 9, 671-675.

Schock, E.N., Brugmann, S.A., 2017. Discovery, Diagnosis, and Etiology of Craniofacial Ciliopathies. Cold Spring Harb Perspect Biol 9.

Schock, E.N., Brugmann, S.A., 2017. Neural crest cells utilize primary cilia to regulate ventral forebrain morphogenesis via Hedgehog-dependent regulation of oriented cell division. Dev Biol 431, 168-178.

Schwarz, Q., Maden, C.H., Davidson, K., Ruhrberg, C., 2009. Neuropilin-mediated neural crest cell guidance is essential to organise sensory neurons into segmented dorsal root ganglia. Development 136, 1785-1789.

Schwarz, Q., Vieira, J.M., Howard, B., Eickholt, B.J., Ruhrberg, C., 2008. Neuropilin 1 and 2 control cranial gangliogenesis and axon guidance through neural crest cells. Development 135, 1605-1613.

Serbedzija, G.N., Fraser, S.E., Bronner-Fraser, M., 1990. Pathways of trunk neural crest cell migration in the mouse embryo as revealed by vital dye labelling. Development 108, 605-612.

Sieber-Blum, M., Cohen, A.M., 1980. Clonal analysis of quail neural crest cells: they are pluripotent and differentiate in vitro in the absence of noncrest cells. Dev Biol 80, 96-106.

Silbermann, M., Frommer, J., 1972. The nature of endochondral ossification in the mandibular condyle of the mouse. Anat Rec 172, 659-667.

Simões-Costa, M., Bronner, M.E., 2015. Establishing neural crest identity: a gene regulatory recipe. Development 142, 242-257.

Simões-Costa, M., Tan-Cabugao, J., Antoshechkin, I., Sauka-Spengler, T., Bronner, M.E., 2014. Transcriptome analysis reveals novel players in the cranial neural crest gene regulatory network. Genome Res 24, 281-290.

Sit, S.T., Manser, E., 2011. Rho GTPases and their role in organizing the actin cytoskeleton. J Cell Sci 124, 679-683.

Smith, C.L., Tallquist, M.D., 2010. PDGF function in diverse neural crest cell populations. Cell Adh Migr 4, 561-566.

Soldatov, R., Kaucka, M., Kastriti, M.E., Petersen, J., Chontorotzea, T., Englmaier, L., Akkuratova, N., Yang, Y., Haring, M., Dyachuk, V., Bock, C., Farlik, M., Piacentino, M.L., Boismoreau, F., Hilscher, M.M., Yokota, C., Qian, X., Nilsson, M., Bronner, M.E., Croci, L., Hsiao, W.Y., Guertin, D.A., Brunet, J.F., Consalez, G.G., Ernfors, P., Fried, K., Kharchenko, P.V., Adameyko, I., 2019. Spatiotemporal structure of cell fate decisions in murine neural crest. Science 364.

Sonnenberg-Riethmacher, E., Miehe, M., Stolt, C.C., Goerich, D.E., Wegner, M., Riethmacher, D., 2001. Development and degeneration of dorsal root ganglia in the absence of the HMG-domain transcription factor Sox10. Mech Dev 109, 253-265.

Spörl, F., Korge, S., Jurchott, K., Wunderskirchner, M., Schellenberg, K., Heins, S., Specht, A., Stoll, C., Klemz, R., Maier, B., Wenck, H., Schrader, A., Kunz, D., Blatt, T., Kramer, A., 2012. Kruppel-like factor 9 is a circadian transcription factor in human epidermis that controls proliferation of keratinocytes. Proc Natl Acad Sci U S A 109, 10903-10908.

Srinivas, S., Watanabe, T., Lin, C.S., William, C.M., Tanabe, Y., Jessell, T.M., Costantini, F., 2001. Cre reporter strains produced by targeted insertion of EYFP and ECFP into the ROSA26 locus. BMC Dev Biol 1, 4.

Stemple, D.L., Anderson, D.J., 1992. Isolation of a stem cell for neurons and glia from the mammalian neural crest. Cell 71, 973-985.

Stephens, A.D., Liu, P.Z., Banigan, E.J., Almassalha, L.M., Backman, V., Adam, S.A., Goldman, R.D., Marko, J.F., 2018. Chromatin histone modifications and rigidity affect nuclear morphology independent of lamins. Mol Biol Cell 29, 220-233.

Steventon, B., Mayor, R., Streit, A., 2014. Neural crest and placode interaction during the development of the cranial sensory system. Dev Biol 389, 28-38.

Stewart, H.J., Morgan, L., Jessen, K.R., Mirsky, R., 1993. Changes in DNA synthesis rate in the Schwann cell lineage in vivo are correlated with the precursor--Schwann cell transition and myelination. Eur J Neurosci 5, 1136-1144.

Stolt, C.C., Wegner, M., 2016. Schwann cells and their transcriptional network: Evolution of key regulators of peripheral myelination. Brain Res 1641, 101-110.

Swift, J., Ivanovska, I.L., Buxboim, A., Harada, T., Dingal, P.C., Pinter, J., Pajerowski, J.D., Spinler, K.R., Shin, J.W., Tewari, M., Rehfeldt, F., Speicher, D.W., Discher, D.E., 2013. Nuclear lamin-A scales with tissue stiffness and enhances matrix-directed differentiation. Science 341, 1240104.

Takarada, T., Kodama, A., Hotta, S., Mieda, M., Shimba, S., Hinoi, E., Yoneda, Y., 2012. Clock genes influence gene expression in growth plate and endochondral ossification in mice. J Biol Chem 287, 36081-36095.

Thaxton, C., Bott, M., Walker, B., Sparrow, N.A., Lambert, S., Fernandez-Valle, C., 2011. Schwannomin/merlin promotes Schwann cell elongation and influences myelin segment length. Mol Cell Neurosci 47, 1-9.

Theveneau, E., Duband, J.L., Altabef, M., 2007. Ets-1 confers cranial features on neural crest delamination. PLoS One 2, e1142.

Theveneau, E., Marchant, L., Kuriyama, S., Gull, M., Moepps, B., Parsons, M., Mayor, R., 2010. Collective chemotaxis requires contact-dependent cell polarity. Dev Cell 19, 39-53.

Theveneau, E., Mayor, R., 2012. Neural crest delamination and migration: from epithelium-to-mesenchyme transition to collective cell migration. Dev Biol 366, 34-54.

Theveneau, E., Steventon, B., Scarpa, E., Garcia, S., Trepat, X., Streit, A., Mayor, R., 2013. Chase-and-run between adjacent cell populations promotes directional collective migration. Nat Cell Biol 15, 763-772.

Thiery, J.P., Duband, J.L., Delouvee, A., 1982. Pathways and mechanisms of avian trunk neural crest cell migration and localization. Dev Biol 93, 324-343.

Thomas, P.D., Kejariwal, A., Campbell, M.J., Mi, H., Diemer, K., Guo, N., Ladunga, I., Ulitsky-Lazareva, B., Muruganujan, A., Rabkin, S., Vandergriff, J.A., Doremieux, O., 2003. PANTHER: a browsable database of gene products organized by biological function, using curated protein family and subfamily classification. Nucleic Acids Res 31, 334-341.

Thompson, H., Blentic, A., Watson, S., Begbie, J., Graham, A., 2010. The formation of the superior and jugular ganglia: insights into the generation of sensory neurons by the neural crest. Dev Dyn 239, 439-445.

Tomo, S., Ogita, M., Tomo, I., 1997. Development of mandibular cartilages in the rat. Anat Rec 249, 233-239.

Trentin, A., Glavieux-Pardanaud, C., Le Douarin, N.M., Dupin, E., 2004. Self-renewal capacity is a widespread property of various types of neural crest precursor cells. Proc Natl Acad Sci U S A 101, 4495-4500.

Trokovic, N., Trokovic, R., Partanen, J., 2005. Fibroblast growth factor signalling and regional specification of the pharyngeal ectoderm. Int J Dev Biol 49, 797-805.

Tsuchiyama, K., Wakao, S., Kuroda, Y., Ogura, F., Nojima, M., Sawaya, N., Yamasaki, K., Aiba, S., Dezawa, M., 2013. Functional melanocytes are readily reprogrammable from multilineage-differentiating stress-enduring (muse) cells, distinct stem cells in human fibroblasts. J Invest Dermatol 133, 2425-2435.

Tsuda, M., Takahashi, S., Takahashi, Y., Asahara, H., 2003. Transcriptional co-activators CREB-binding protein and p300 regulate chondrocyte-specific gene expression via association with Sox9. J Biol Chem 278, 27224-27229.

Twitty, V. C., Bodenstein, D., 1941. Experiments on the determination problem I. The roles of ectoderm and neural crest in the development of the dorsal fin in Amphibia. II. Changes in ciliary polarity associated with the induction of fin epidermis. J. Exp. Zool. 86, 343-380.

Velasco, S., Ibrahim, M.M., Kakumanu, A., Garipler, G., Aydin, B., Al-Sayegh, M.A., Hirsekorn, A., Abdul-Rahman, F., Satija, R., Ohler, U., Mahony, S., Mazzoni, E.O., 2017. A Multi-step Transcriptional and Chromatin State Cascade Underlies Motor Neuron Programming from Embryonic Stem Cells. Cell Stem Cell 20, 205-217 e208.

Verzi, M.P., Agarwal, P., Brown, C., McCulley, D.J., Schwarz, J.J., Black, B.L., 2007. The transcription factor MEF2C is required for craniofacial development. Dev Cell 12, 645-652.

Waldo, K., Miyagawa-Tomita, S., Kumiski, D., Kirby, M.L., 1998. Cardiac neural crest cells provide new insight into septation of the cardiac outflow tract: aortic sac to ventricular septal closure. Dev Biol 196, 129-144.

Wang, N., Tytell, J.D., Ingber, D.E., 2009. Mechanotransduction at a distance: mechanically coupling the extracellular matrix with the nucleus. Nat Rev Mol Cell Biol 10, 75-82.

Wang, Y., Belflower, R.M., Dong, Y.F., Schwarz, E.M., O'Keefe, R.J., Drissi, H., 2005. Runx1/AML1/Cbfa2 mediates onset of mesenchymal cell differentiation toward chondrogenesis. J Bone Miner Res 20, 1624-1636.

Wang, J., Wang, X., Holz, J.D., Rutkowski, T., Wang, Y., Zhu, Z., Dong, Y., 2013. Runx1 is critical for pth-induced onset of mesenchymal progenitor cell chondrogenic differentiation. PLoS ONE 8(9): e74255. doi:10.1371/journal.pone.0074255

Wong, C.E., Paratore, C., Dours-Zimmermann, M.T., Rochat, A., Pietri, T., Suter, U., Zimmermann, D.R., Dufour, S., Thiery, J.P., Meijer, D., Beermann, F., Barrandon, Y., Sommer, L., 2006. Neural crest-derived cells with stem cell features can be traced back to multiple lineages in the adult skin. J Cell Biol 175, 1005-1015.

Xie, Y., Tang, Q., Chen, G., Xie, M., Yu, S., Zhao, J., Chen, L., 2019. New Insights Into the Circadian Rhythm and Its Related Diseases. Front Physiol 10, 682.

Yamauchi, Y., Abe, K., Mantani, A., Hitoshi, Y., Suzuki, M., Osuzu, F., Kuratani, S., Yamamura, K., 1999. A novel transgenic technique that allows specific marking of the neural crest cell lineage in mice. Dev Biol 212, 191-203.

Yang, C., DelRio, F.W., Ma, H., Killaars, A.R., Basta, L.P., Kyburz, K.A., Anseth, K.S., 2016. Spatially patterned matrix elasticity directs stem cell fate. Proc Natl Acad Sci U S A 113, E4439-4445.

Yang, J.H., Choi, J.H., Jang, H., Park, J.Y., Han, J.W., Youn, H.D., Cho, E.J., 2011. Histone chaperones cooperate to mediate Mef2-targeted transcriptional regulation during skeletal myogenesis. Biochem Biophys Res Commun 407, 541-547.

Yang, N., Williams, J., Pekovic-Vaughan, V., Wang, P., Olabi, S., McConnell, J., Gossan, N., Hughes, A., Cheung, J., Streuli, C.H., Meng, Q.J., 2017. Cellular mechano-environment regulates the mammary circadian clock. Nat Commun 8, 14287.

Yano, F., Ohba, S., Murahashi, Y., Tanaka, S., Saito, T., Chung, U.I., 2019. Runx1 contributes to articular cartilage maintenance by enhancement of cartilage matrix production and suppression of hypertrophic differentiation. Sci Rep 9, 7666.

Yoshida, C.A., Yamamoto, H., Fujita, T., Furuichi, T., Ito, K., Inoue, K., Yamana, K., Zanma, A., Takada, K., Ito, Y., Komori, T., 2004. Runx2 and Runx3 are essential for chondrocyte maturation, and Runx2 regulates limb growth through induction of Indian hedgehog. Genes Dev 18, 952-963.

Yoshitane, H., Asano, Y., Sagami, A., Sakai, S., Suzuki, Y., Okamura, H., Iwasaki, W., Ozaki, H., Fukada, Y., 2019. Functional D-box sequences reset the circadian clock and drive mRNA rhythms. Commun Biol 2, 300.

Youn, H.D., Liu, J.O., 2000. Cabin1 represses MEF2-dependent Nur77 expression and T cell apoptosis by controlling association of histone deacetylases and acetylases with MEF2. Immunity 13, 85-94.

Yu, S., Tang, Q., Xie, M., Zhou, X., Long, Y., Xie, Y., Guo, F., Chen, L., 2020. Circadian BMAL1 regulates mandibular condyle development by hedgehog pathway. Cell Prolif 53, e12727.

Yu, W.M., Feltri, M.L., Wrabetz, L., Strickland, S., Chen, Z.L., 2005. Schwann cell-specific ablation of laminin gamma1 causes apoptosis and prevents proliferation. J Neurosci 25, 4463-4472.

Zhang, L., Su, P., Xu, C., Yang, J., Yu, W., Huang, D., 2010. Chondrogenic differentiation of human mesenchymal stem cells: a comparison between micromass and pellet culture systems. Biotechnol Lett 32, 1339-1346.

Zhang, R., Lahens, N.F., Ballance, H.I., Hughes, M.E., Hogenesch, J.B., 2014. A circadian gene expression atlas in mammals: implications for biology and medicine. Proc Natl Acad Sci U S A 111, 16219-16224.

Zirlinger, M., Lo, L., McMahon, J., McMahon, A.P., Anderson, D.J., 2002. Transient expression of the bHLH factor neurogenin-2 marks a subpopulation of neural crest cells biased for a sensory but not a neuronal fate. Proc Natl Acad Sci U S A 99, 8084-8089.

Appendix A: Cell numbers and doubling rates for biological replicates

Biological isolates		Cranial NC					Trunk NC				
Pregnant dams	Number of embryos	Total cells recovered	Cells per embryo	Doubling rate (hours)	Cells per embryo by P3	Total number of cells by P3	Total cells recovered	Cells per embryo	Doubling rate	Cells per embryo by P3	Total number of cells by P3
3	28	2.77E+05	9.89E+03	44.6	8.69E+05	2.43E+07	7.26E+04	2.59E+03	40.0	3.81E+05	1.07E+07
2	18	1.20E+05	6.64E+03	42.9	6.97E+05	1.25E+07	5.19E+04	2.88E+03	42.6	3.12E+05	5.62E+06
1	7	7.50E+04	1.07E+04	44.9	9.14E+05	6.40E+06	3.00E+04	4.29E+03	32.6	1.96E+06	1.37E+07
average	8.83		9.08E+03	44.1	8.37E+05	7.39E+06		3.25E+03	38.4	5.89E+05	5.20E+06

Table 3. Cell numbers and doubling rates for biological replicates. Each primary isolate consisted of cells pooled from 1-3 litters of embryos (7-28 embryos total) depending on how many females set up for breeding were carrying E9.5 embryos on the day of dissection. *Method:* "Doubling rate" was determined using an online doubling time calculator (Roth, 2006). "Cells per embryo" was calculated by dividing the total number of cells recovered at isolation by the total number of embryos. "Cells per embryo by P3 (passage 3)" was calculated using the doubling rate formula (cells per embryo x $2^{(\text{hours in culture (288)/doubling rate})}$). "Total number of cells by P3" for each experiment was calculated by multiplying "number embryos" by "cells per embryo by P3". Average number of embryos per litter was calculated by dividing the total number of embryos recovered from the three biological replicates (53) by the total number of litters (6). Average "Cells per embryo" and "Doubling rate" were calculated by taking the average of the three biological replicates. Average "Cells per embryos by P3" was calculated was calculated using the doubling rate formula (average cells per embryo x $2^{(\text{hours in culture (288)/average doubling rate})}$). Average "Total number of cells by P3" was calculated by multiplying "average number embryos" by "average cells per embryo by P3".

Appendix B: Wide field comparisons of neuronal differentiation in cultures derived from cranial and trunk NC.

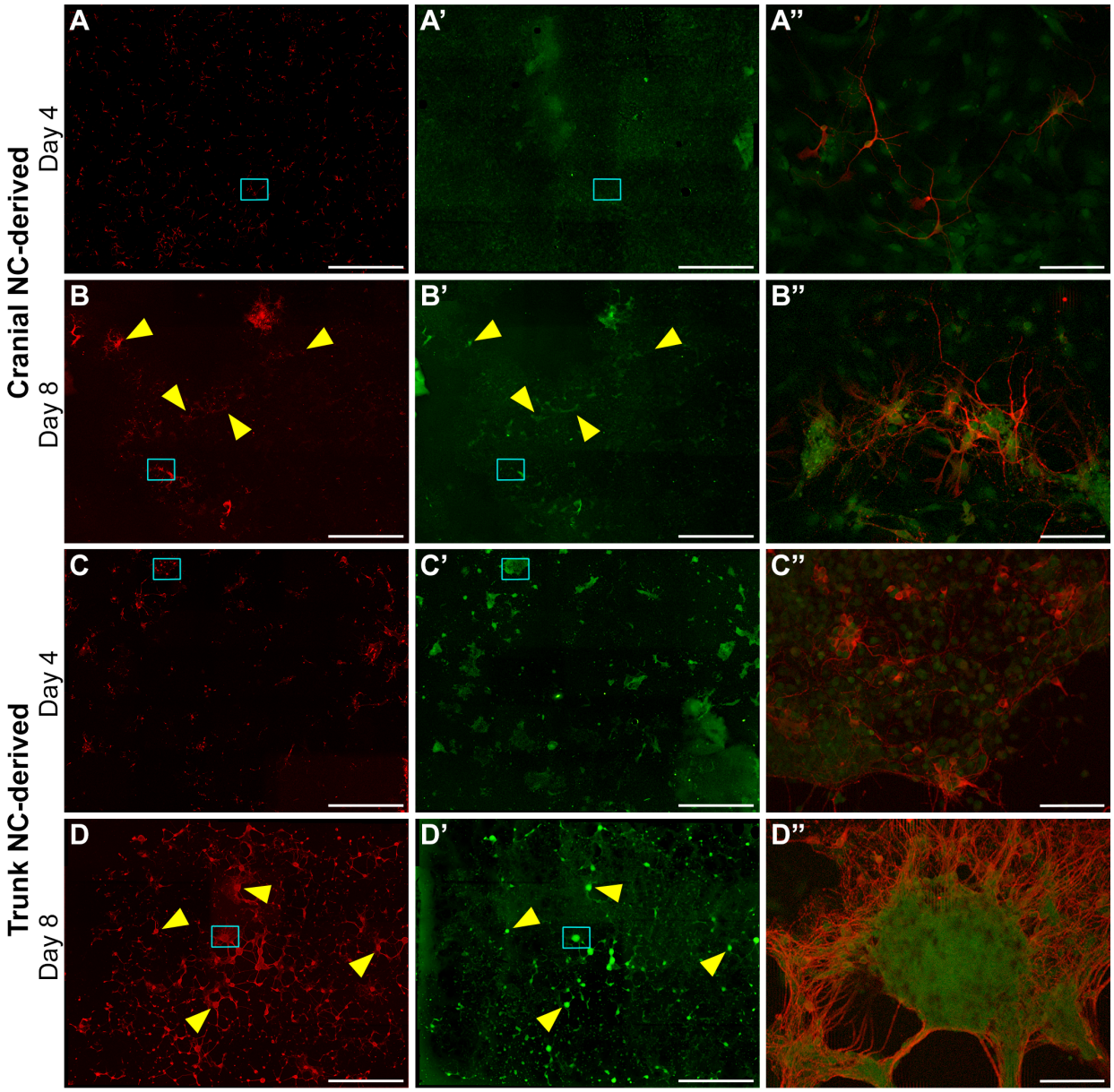

Figure 16. Wide field comparisons of neuronal differentiation in cultures derived from cranial and trunk NC. Neuronal differentiation of cranial- and trunk-derived NC cells was observed after four and eight days in in differentiation medium containing NT3 and NGF. Differentiation was assessed by immunostaining for TUJ1, a neuron-specific class III b-tubulin. In order to visualize the extent of differentiation within the cultures, we obtained overlapping, high resolution images spanning the entire culture well. **(A-D)** TUJ1 immunostaining. **(A'-D')** EYFP expression (lineage tracer in the NC cells). **(A"-D")** Higher magnification, merged images of the boxed regions in A-D' (TUJ1, red; EYFP, green). Images were aligned and stitched using the open source Fiji software (Preibisch et al.,

2009). Cells with neurites are observed throughout cultures from both cranial and trunk NC, however, aggregation of neurons is more prevalent in neurons derived from trunk NC at both time points. At day 4, individual neurons extending neurites were observed throughout the cranial NC culture **(A, A")**, while trunk NC-derived neurons are observed both singly and in small loosely formed aggregates **(C, C")**. By day 8, loose aggregates of cranial NC-derived neurons can also be observed (examples indicated by *arrowheads* and *boxed* region in **B,** and as magnified boxed region in **B"**), however, aggregates formed by trunk NC-derived neurons are more compact and well-defined with extensive neuritic outgrowth (examples indicated by *arrowheads* and *boxed* region in **D,** and magnified boxed region in **D"**). Scale bars: (A-D and A'-D') 2 mm; (A"-D") 100 μm.

Appendix C: Wide field comparisons of smooth muscle differentiation in cultures derived from cranial and trunk NC.

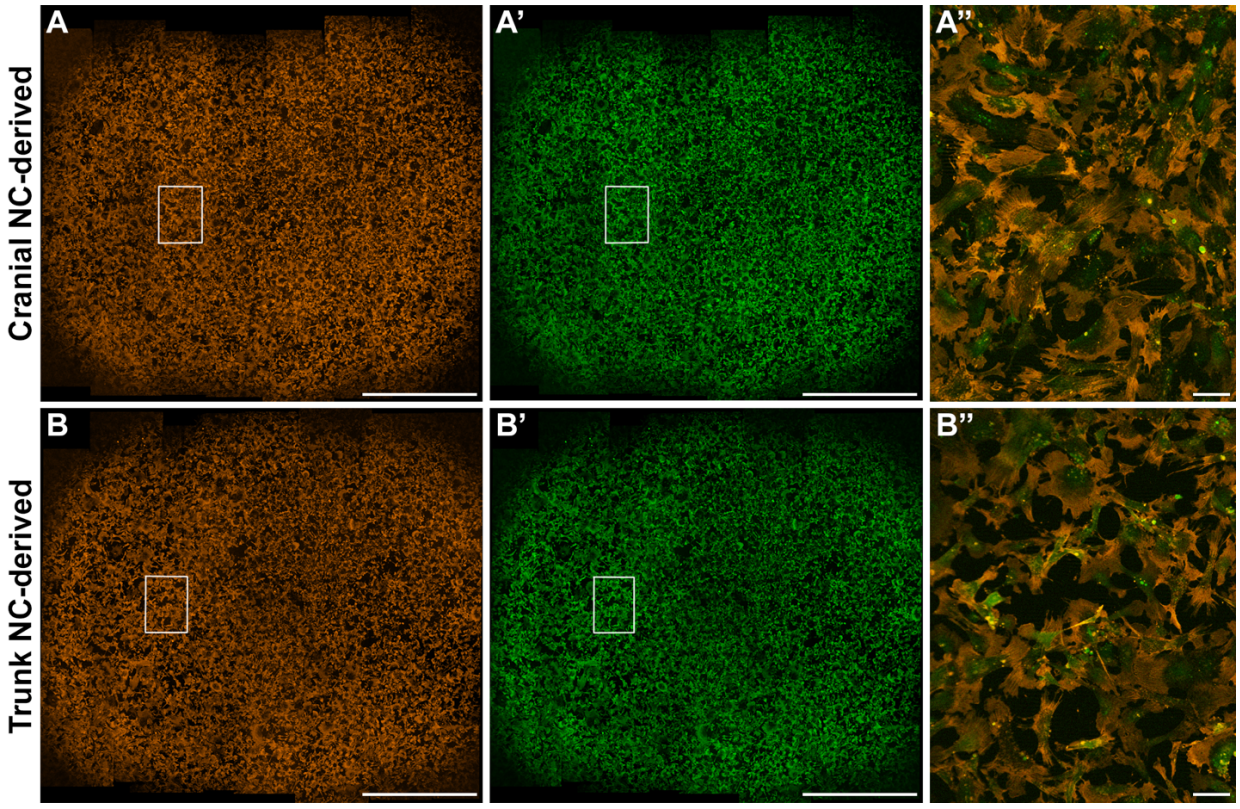

Figure 17. Wide field comparisons of smooth muscle differentiation in cultures derived from cranial and trunk NC. Smooth muscle differentiation of cranial- and trunk-derived NC cells was observed throughout the culture after seven days in differentiation medium containing FCS. Differentiation was assessed by immunostaining for alpha smooth muscle actin (αSMA). In order to visualize the extent of differentiation within the cultures, we obtained overlapping, high resolution images spanning the entire culture well. **(A, B)** αSMA immunostaining, **(A', B')** EYFP expression (lineage tracer in the NC cells). Images were aligned and stitched using the open source Fiji software (Preibisch et al., 2009). **(A", B")** Higher magnification, merged images of the boxed regions in A-B' (αSMA, orange; EYFP, green). Images were aligned, stitched and pseudocolored using the open source Fiji software (Preibisch et al., 2009). Scale bars: (A, B and A', B') 2 mm; (A", B") 100 μm.

Appendix D: Wide field comparisons of chondrogenic, adipogenic, and melanogenic differentiation in cultures derived from cranial and trunk NC.

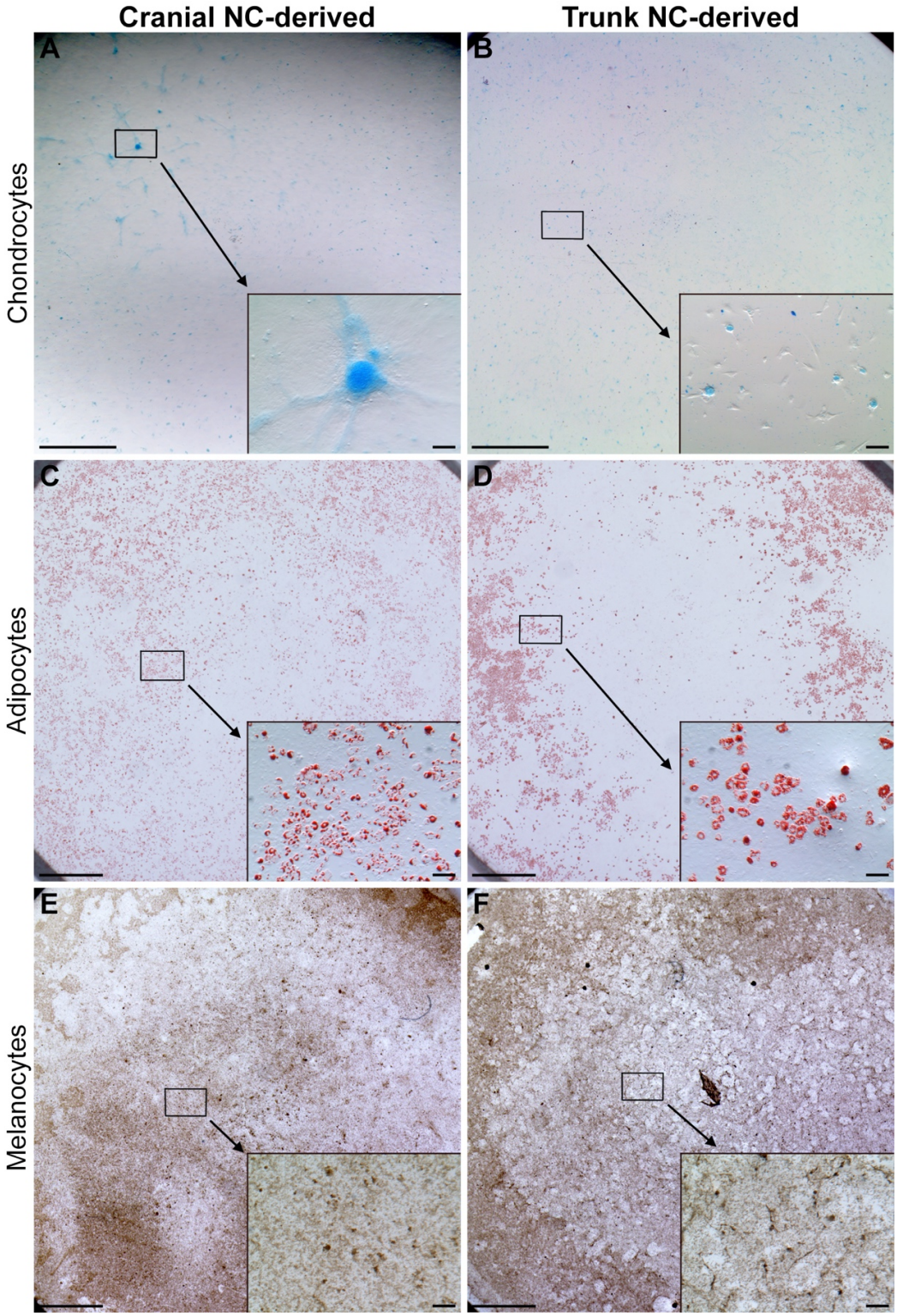

Figure 18. See next page for legend.

Figure 18. Wide field comparisons of chondrogenic, adipogenic, and melanogenic differentiation in cultures derived from cranial and trunk NC. Differentiation of cranial- and trunk-derived NC cells into chondrocytes, adipocytes and melanocytes was observed throughout the cultures (**A, B:** chondrocytes (*blue*) detected by Alcian blue staining after 14 days in differentiation medium containing TGF-β3; **C, D:** adipocytes *(red*) detected by Oil red O staining after 14 days in Adipogenic Medium from STEMCELL Technologies; and **E, F:** melanocytes (*brown*) detected based on tyrosinase activity after 10 days in differentiation medium containing ET3). In order to visualize the extent of differentiation within the cultures, we obtained overlapping, high resolution images spanning the entire culture well. Images were aligned and stitched using the open source Hugin software (d'Angelo, 2007). Higher magnification images of the boxed regions are shown in the insets. Scale bars: 2 mm; insets, 100 μm.

Appendix E: Mesodermal markers are not detected in cultured cranial and trunk NC cells.

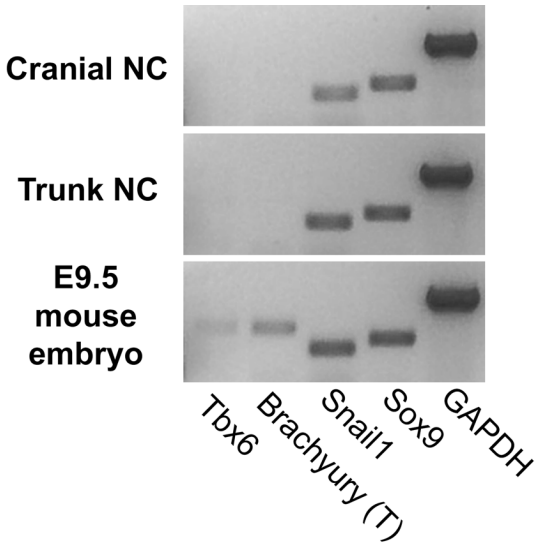

Figure 19. Mesodermal markers are not detected in cultured cranial and trunk NC cells. Cultured NC cells were compared with whole E9.5 embryos for the expression of a pan-mesodermal marker, Brachyury (T), or a marker for axial mesoderm, Tbx6, using reverse transcriptase PCR. NC markers, Snail and Sox9, and housekeeping gene, GAPDH, served as positive controls. A representative gel is shown; however, identical results were obtained from three independent biological samples.

Appendix F: Neuritic expression of HuC/D is more prevalent in neurons derived from cranial NC when compared to those derived from trunk NC.

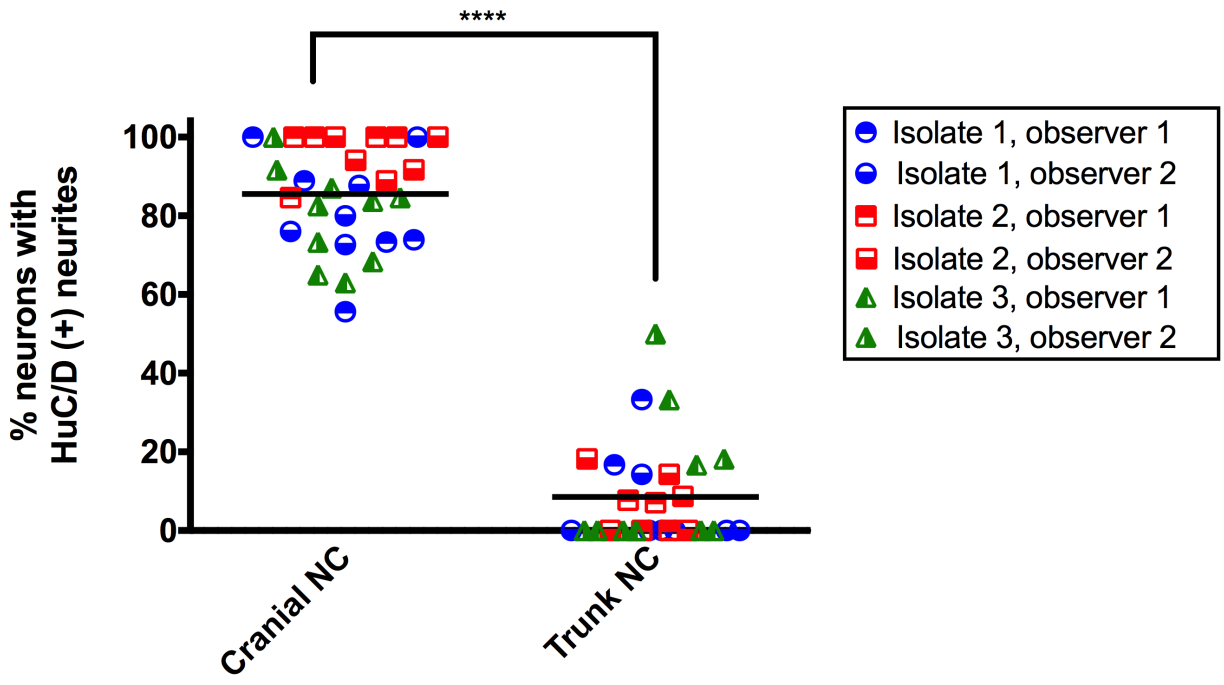

Figure 20. Neuritic expression of HuC/D is more prevalent in neurons derived from cranial NC when compared to those derived from trunk NC. Images of neurons differentiated from cranial and trunk-derived NC and subjected to HuC/D immunofluorescence staining for experiments described in Fig. 5 were quantified with respect to the percentage of neurons extending HuC/D positive neurites. Five images were obtained from differentiated cultures in each biological replicate. Cells with neurites were identified in the green channel (EYFP). These cells were then assessed for HuC/D expression in the red channel to calculate the percentage of neurons with HuC/D in processes. Each image was analyzed separately by two blinded observers, and both sets of observations are displayed in the graph. The Grubbs test was used to eliminate outliers in the cranial and trunk data sets from each observer, resulting in elimination of two points: (1) trunk, isolate 2, observer 1 and (2) trunk, isolate 1, observer 2. Two-way ANOVA analysis with Tukey's multiple testing correction determined no significant effects of observer or isolate, but a significant effect between cranial and trunk NC ($p<0.0001$). Each dot represents one observation of one image and is color-coded by biological replicate and observer as indicated. Black horizontal line indicates grand mean across replicates.

Appendix G: Primary cranial and trunk NC cells express Schwann cell marker, ErbB3, during glial differentiation.

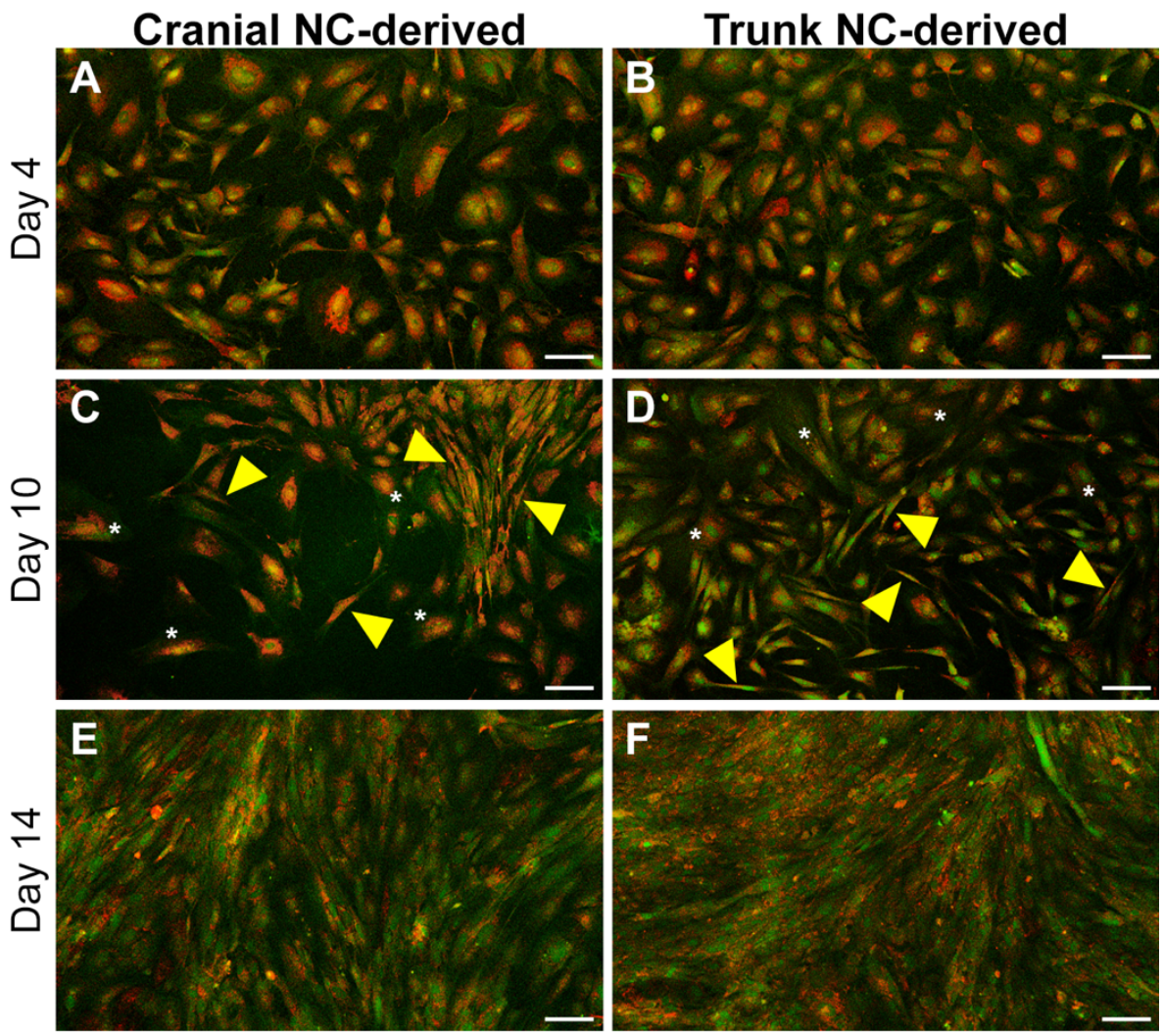

Figure 21. Primary cranial and trunk NC cells express Schwann cell marker, ErbB3, during glial differentiation. Schwann cell differentiation of cranial- and trunk-derived NC cells was observed after 4, 10 or 14 days in differentiation medium containing BMP2 and LIF. Differentiation was assessed by immunostaining for ErbB3, a receptor tyrosine kinase enriched in Schwann cell. ErbB3-positive cells were observed in both cranial and trunk NC cell populations at Day 4 **(A, B)**. By Day 10, some of the ErbB3-positive cells extended flattened, sheet-like processes **(C, D**; *asterisks*) while the other ErbB3-positive cells displayed an elongated, spindle-like morphology **(C, D**; *arrowheads*). After 14 days, most ErbB3-positive cells in both populations exhibited an elongated, bipolar morphology and cells extending flattened, sheet-like processes were only occasionally observed **(E, F)**. Phenotypic characteristics of the cells at each time point were consistently observed (n=6; duplicate cultures from each of three independent cell isolates). All cells are derived from *Sox9cre; R26R-EYFP* mice and express EYFP (*green*). Red staining: ErbB3. Scale bars: 100μm.

Appendix H: Enriching for intermediate and differentiated cell populations over the course of neurogenesis and chondrogenesis.

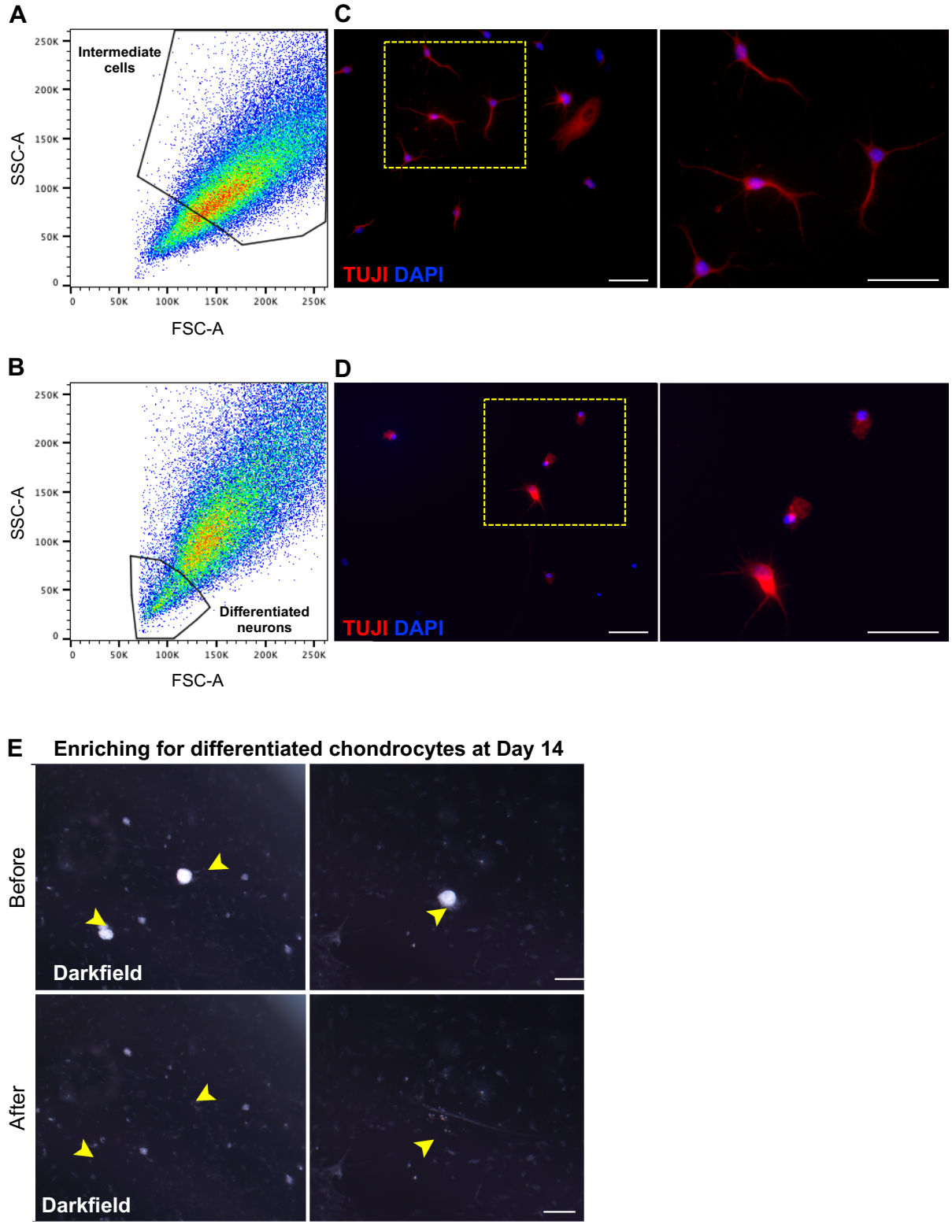

Figure 22. See next page for legend.

Figure 22: Enriching for intermediate and differentiated cell populations over the course of neurogenesis and chondrogenesis. Cranial NC cells were grown in neuronal differentiation medium for two and six days. FACS purification was used to enrich for intermediate neuroprogenitors or differentiated neurons distinguished by cell size. (**A**) Intermediate neuroprogenitors, corresponding to the larger cell population (*black polygon*), were isolated from cells grown for two days in neuronal differentiation medium. (**B**) Differentiated neurons, corresponding to the smaller cell population (*black polygon*), were isolated from cells grown for six days in neuronal differentiation medium. Cells collected and cultured from both populations appeared healthy and reattached to the culture dish, however, after one day in differentiation medium, the isolated differentiated neurons appeared stressed and were not extending neurites in contrast to the isolated intermediate cells (not pictured). (**C**) Many of the intermediate cells grown in neuronal differentiation medium for two days following FACS purification began to extend neurites. (**D**) Most of the differentiated neurons grown in neuronal differentiation medium for two days following FACS purification extended short, fine neuritic processes that appear as a TUJ1-positive halo around the cell body. Chondrogenic nodules (*arrowheads*) were individually picked from chondrogenic cultures at Day 14, and dissociated for downstream analysis. Representative images showing cultures before and after nodule selection. Red staining = TUJI. Blue staining = DAPI labelled nuclei. Scale bars: (C, D) 50 μm; (E) 200 μm.

Appendix I: Commonly upregulated transcripts over the course of neurogenesis and chondrogenesis.

Table 4. Commonly upregulated transcripts over the course of neurogenesis and chondrogenesis.

Ensembl transcript ID	Mouse gene symbol
ENSMUST00000043313.14	Nmnat2
ENSMUST00000146468.3	Lgals3
ENSMUST00000006669.5	Pdk1
ENSMUST00000107044.9	Plekhb1
ENSMUST00000002305.8	Kdm7a
ENSMUST00000006697.16	Itih3
ENSMUST00000027297.10	Plekhb2
ENSMUST00000027477.14	Ngef
ENSMUST00000070256.8	Kcnq3
ENSMUST00000047786.5	March4
ENSMUST00000029766.8	Bcar3
ENSMUST00000003870.14	Mxi1
ENSMUST00000004756.13	Wwox
ENSMUST00000070478.3	Sdc3
ENSMUST00000030915.10	Morn1
ENSMUST00000053355.5	Creg2
ENSMUST00000032201.7	Ret
ENSMUST00000046212.1	Slc16a1
ENSMUST00000102823.9	Ttc39b
ENSMUST00000034992.7	Nt5e
ENSMUST00000020586.6	Slc22a4
ENSMUST00000208605.1	Map6
ENSMUST00000090379.6	Usp53
ENSMUST00000038562.8	Spsb1
ENSMUST00000163230.7	Cd200
ENSMUST00000151894.8	Pfkp
ENSMUST00000022875.6	Ank
ENSMUST00000020497.13	Aldh1l2
ENSMUST00000163832.7	Gbe1
ENSMUST00000045557.9	Slc7a5
ENSMUST00000127492.1	Map6
ENSMUST00000039522.7	Apobr
ENSMUST00000093852.4	Zbtb16
ENSMUST00000032203.8	A2m
ENSMUST00000117077.7	Slc7a2
ENSMUST00000086559.6	Slc41a1
ENSMUST00000161017.7	Kif26b
ENSMUST00000051293.7	Gpr146
ENSMUST00000102813.1	Cfap157
ENSMUST00000121288.1	Fam167a
ENSMUST00000102549.9	Nipal3
ENSMUST00000109349.8	Dbndd2

ENSMUST00000005829.12	Ampd3
ENSMUST00000050958.8	Tmie
ENSMUST00000086465.5	Adora1
ENSMUST00000020500.13	Appl2
ENSMUST00000094456.9	Snph
ENSMUST00000238946.1	Aqp4
ENSMUST00000000608.7	Gm2a
ENSMUST00000025830.8	Apba1
ENSMUST00000047889.12	Atp1b2
ENSMUST00000077902.4	Gfap
ENSMUST00000156673.1	Als2cl
ENSMUST00000094569.10	Nfasc
ENSMUST00000067444.9	Gfap
ENSMUST00000027741.11	Xpr1
ENSMUST00000024988.14	C3
ENSMUST00000173287.7	Adamtsl3
ENSMUST00000002073.12	Ltbp2
ENSMUST00000163060.1	Hr
ENSMUST00000089332.4	Col8a1
ENSMUST00000034230.6	Cx3cl1
ENSMUST00000020399.5	Cpm
ENSMUST00000038188.13	Limch1
ENSMUST00000032342.2	Mgp
ENSMUST00000028815.14	Slc23a2
ENSMUST00000163623.2	Nedd9
ENSMUST00000058981.2	Lxn
ENSMUST00000118317.7	Hipk1
ENSMUST00000040914.2	Hist1h1c
ENSMUST00000026617.12	Phkg1
ENSMUST00000067854.9	1600014C10Rik
ENSMUST00000032272.12	Adipor2
ENSMUST00000031446.6	Tmem132b
ENSMUST00000102911.9	Slc44a1
ENSMUST00000160719.7	Mfap3l
ENSMUST00000028080.11	Nebl
ENSMUST00000036070.14	Fam107a
ENSMUST00000219435.1	Chchd10
ENSMUST00000023099.7	Slc38a2
ENSMUST00000218362.1	Ttc9
ENSMUST00000097425.9	Fndc1
ENSMUST00000091288.12	Prnp
ENSMUST00000113457.8	Col4a3
ENSMUST00000019734.10	Cyb561
ENSMUST00000009789.14	P4ha1
ENSMUST00000112747.1	Spp1
ENSMUST00000060251.7	Higd1a
ENSMUST00000014990.12	Tppp3

ENSMUST00000112748.7	Spp1
ENSMUST00000099396.2	Nt5dc3
ENSMUST00000000058.6	Cav2
ENSMUST00000009435.11	Pttg1ip
ENSMUST00000191805.6	Larp1b
ENSMUST00000027726.13	Cyb5r1
ENSMUST00000048116.14	Slc7a1
ENSMUST00000165027.8	Ifrd1
ENSMUST00000089959.6	Gch1
ENSMUST00000031243.14	Spp1
ENSMUST00000189137.6	Trpc1
ENSMUST00000100635.4	Lratd2
ENSMUST00000029326.5	Sucnr1
ENSMUST00000056416.8	Rbfox1
ENSMUST00000025363.6	Hbegf
ENSMUST00000236652.1	Rps14
ENSMUST00000031766.11	Asns
ENSMUST00000019445.5	Hsd17b1
ENSMUST00000121334.7	Sept8
ENSMUST00000080145.12	Adamts16
ENSMUST00000031122.8	Gabrb1
ENSMUST00000036884.2	Klf9
ENSMUST00000029188.7	Ccn5
ENSMUST00000084412.5	Ifitm10
ENSMUST00000046071.4	Klhdc8a
ENSMUST00000048432.5	Prelp
ENSMUST00000113585.8	Mgll
ENSMUST00000070070.7	Dnaja4
ENSMUST00000209208.1	Gm19935
ENSMUST00000018361.9	Pmp22
ENSMUST00000031646.7	Rasl11a
ENSMUST00000112933.1	Cntf
ENSMUST00000049095.5	Faah
ENSMUST00000039438.8	Ntrk3
ENSMUST00000032185.8	Slc6a6
ENSMUST00000038791.14	Gde1
ENSMUST00000046515.14	Nceh1
ENSMUST00000034905.8	Gclc
ENSMUST00000001824.6	Folh1
ENSMUST00000085412.6	Coch
ENSMUST00000027263.13	Stk17b
ENSMUST00000222970.1	Aspg
ENSMUST00000066708.6	Dmp1
ENSMUST00000156876.7	Mfsd6
ENSMUST00000009798.4	Oit3
ENSMUST00000118800.7	Afap1l2
ENSMUST00000069620.9	Per2

ENSMUST00000022616.13	Clu
ENSMUST00000091309.11	Cp
ENSMUST00000036653.4	Htr2a
ENSMUST00000016168.8	Lbp
ENSMUST00000108713.7	Epn2
ENSMUST00000063982.6	Fzd5
ENSMUST00000060989.8	Sorl1
ENSMUST00000046765.9	Kcnk1
ENSMUST00000105686.2	Slc25a33
ENSMUST00000121200.8	Palld
ENSMUST00000130310.7	Cpeb1
ENSMUST00000098786.2	1700029J07Rik
ENSMUST00000102955.10	Cetn4
ENSMUST00000000579.2	Sox9
ENSMUST00000021390.8	Galc
ENSMUST00000020234.13	Timp3
ENSMUST00000033933.6	Saraf
ENSMUST00000210490.2	Igip
ENSMUST00000043098.8	Gadd45a
ENSMUST00000164047.1	Ifrd1
ENSMUST00000134004.2	Ank
ENSMUST00000075980.11	Tmem107
ENSMUST00000051301.5	Pura
ENSMUST00000030056.11	Tnc
ENSMUST00000020223.7	Tcp11l2
ENSMUST00000105507.4	Ppil6
ENSMUST00000071986.12	Mia
ENSMUST00000018246.5	Hist1h2bc
ENSMUST00000230160.1	Clip4
ENSMUST00000064234.6	Ezr
ENSMUST00000107893.8	Atf5
ENSMUST00000106307.8	Hivep3
ENSMUST00000050584.9	Cystm1
ENSMUST00000207932.1	Prss23
ENSMUST00000027863.12	Atp1b1
ENSMUST00000080666.7	Ndrg4
ENSMUST00000153290.7	Htra1
ENSMUST00000155364.7	Mpc1
ENSMUST00000171970.2	Bmp6
ENSMUST00000114694.8	Zbtb20
ENSMUST00000087050.6	Col4a4
ENSMUST00000024954.10	Epas1
ENSMUST00000137948.1	Ankrd29
ENSMUST00000002885.7	Epdr1
ENSMUST00000226438.1	Retreg1
ENSMUST00000203574.1	Gm31520
ENSMUST00000033333.12	Tmem9b

Appendix J: Commonly downregulated transcripts over the course of neurogenesis and chondrogenesis.

Table 5. Commonly downregulated transcripts over the course of neurogenesis and chondrogenesis.

Ensembl transcript ID	Mouse gene symbol
ENSMUST00000014917.7	Dll1
ENSMUST00000021164.3	Pimreg
ENSMUST00000195957.4	Hgf
ENSMUST00000023353.3	Mcm4
ENSMUST00000093937.2	Cdc6
ENSMUST00000094339.2	Peg12
ENSMUST00000026461.7	Prim1
ENSMUST00000088248.12	Ube2c
ENSMUST00000027393.7	Bard1
ENSMUST00000028803.13	Knstrn
ENSMUST00000005607.8	Asf1b
ENSMUST00000060710.8	Cdc25c
ENSMUST00000101343.1	Mad2l1
ENSMUST00000086461.12	Rfc5
ENSMUST00000203220.2	Hnrnpa2b1
ENSMUST00000034205.4	Cenpn
ENSMUST00000105866.2	Aunip
ENSMUST00000172699.1	Mex3a
ENSMUST00000110621.2	Lrr1
ENSMUST00000052686.3	H2afx
ENSMUST00000021941.7	Mxd3
ENSMUST00000026661.3	Tk1
ENSMUST00000034830.8	Crabp1
ENSMUST00000130533.1	Cpxm1
ENSMUST00000102691.10	Cdca7
ENSMUST00000096482.9	Skp2
ENSMUST00000031838.8	Igf2bp3
ENSMUST00000104999.3	Nrarp
ENSMUST00000197962.1	Cenpa
ENSMUST00000045802.6	Pclaf
ENSMUST00000110382.8	Gmnn
ENSMUST00000119827.7	Cdk1
ENSMUST00000052140.2	Haspin
ENSMUST00000019907.7	Fbxo5
ENSMUST00000063531.4	Cdkn2c
ENSMUST00000110949.8	Arhgap11a
ENSMUST00000107415.7	Zfp618
ENSMUST00000166505.6	Pabpc4l
ENSMUST00000166117.3	Gen1
ENSMUST00000070326.13	Ttk
ENSMUST00000022218.5	Dhfr
ENSMUST00000081387.10	Birc5
ENSMUST00000069334.7	Dach1
ENSMUST00000030714.7	Sema3a

ENSMUST00000110057.2	Flrt3
ENSMUST00000026846.10	Tyms
ENSMUST00000022945.8	Shcbp1
ENSMUST00000100458.3	Suv39h2
ENSMUST00000024736.13	Sgo1
ENSMUST00000018744.14	Shmt1
ENSMUST00000117280.7	Smc2
ENSMUST00000020980.11	Rrm2
ENSMUST00000108324.3	Ccne2
ENSMUST00000237276.1	Ska1
ENSMUST00000041183.6	Meox2
ENSMUST00000047768.10	Neil3
ENSMUST00000034815.8	Kif23
ENSMUST00000022536.2	Ska3
ENSMUST00000047368.7	Mnd1
ENSMUST00000129195.7	Adamts20
ENSMUST00000029270.9	Ccna2
ENSMUST00000024840.11	Arhgap28
ENSMUST00000139460.1	Top2a
ENSMUST00000119026.7	Tmem132c
ENSMUST00000151815.7	Atad5
ENSMUST00000022612.9	Pbk
ENSMUST00000020794.5	Ska2
ENSMUST00000122091.7	Zwilch
ENSMUST00000038194.4	Atad2
ENSMUST00000229333.1	Atad2
ENSMUST00000080511.2	Hist1h1b
ENSMUST00000007296.11	Pole
ENSMUST00000200543.4	Adgrl2
ENSMUST00000071812.10	Iqgap3
ENSMUST00000096766.11	Eml4
ENSMUST00000033060.13	Tead2
ENSMUST00000048374.5	Cip2a
ENSMUST00000084828.4	Ncapg2
ENSMUST00000054917.11	Epb41
ENSMUST00000102611.9	Myh10
ENSMUST00000093321.11	Grb10
ENSMUST00000018506.12	Kpna2
ENSMUST00000025425.6	Cep192
ENSMUST00000045730.6	Akap12
ENSMUST00000168479.2	Nynrin
ENSMUST00000024599.13	Igf2r
ENSMUST00000093812.4	Cd109
ENSMUST00000168064.2	Vgll3
ENSMUST00000071750.12	Col12a1
ENSMUST00000023612.16	Ets2
ENSMUST00000074733.10	Sept11
ENSMUST00000216139.1	Akap12
ENSMUST00000212426.1	Mcm5

ENSMUST00000026150.14	Arhgap19
ENSMUST00000039949.4	Eme1
ENSMUST00000058011.7	Mcm2
ENSMUST00000033154.7	Plk1
ENSMUST00000073316.12	Foxm1
ENSMUST00000018005.9	Mybl2
ENSMUST00000027601.10	Mcm6
ENSMUST00000025486.8	Lmnb1
ENSMUST00000038131.9	Rfc3
ENSMUST00000043296.9	Dlgap5
ENSMUST00000108023.9	Ccne1
ENSMUST00000035651.5	Lrrc17
ENSMUST00000072119.14	Ccnb1
ENSMUST00000109140.9	Aurka
ENSMUST00000049348.8	Traip
ENSMUST00000110387.3	Ncaph
ENSMUST00000046916.8	Ckap2
ENSMUST00000005365.14	Spc25
ENSMUST00000105286.3	Kera
ENSMUST00000028329.12	Sapcd2
ENSMUST00000051594.11	Depdc1b
ENSMUST00000034278.5	Gins2
ENSMUST00000146520.4	Tyms
ENSMUST00000078259.7	Nsl1
ENSMUST00000045876.7	BC055324
ENSMUST00000223907.1	Kif20b
ENSMUST00000023666.10	Chaf1b
ENSMUST00000086423.5	Gm10184
ENSMUST00000014747.2	Alx3
ENSMUST00000001566.9	Tubb5
ENSMUST00000030674.7	Sytl1
ENSMUST00000070755.12	Rad54b
ENSMUST00000039725.11	Exo1
ENSMUST00000150006.8	Cdca2
ENSMUST00000029183.2	Fam83d
ENSMUST00000171808.7	Dbf4
ENSMUST00000093191.2	Spdl1
ENSMUST00000029170.7	Rbl1
ENSMUST00000044423.3	Brip1
ENSMUST00000028858.7	Bub1
ENSMUST00000045607.11	Melk
ENSMUST00000025965.11	Hells
ENSMUST00000052201.8	Mis18bp1
ENSMUST00000062893.11	Cenpe
ENSMUST00000022613.9	Esco2
ENSMUST00000068225.14	Nusap1
ENSMUST00000029482.15	Gpsm2
ENSMUST00000048518.15	Parpbp
ENSMUST00000155907.1	Adamts20

ENSMUST00000157040.7	Mest
ENSMUST00000026662.7	Cbx2
ENSMUST00000102744.3	Orc1
ENSMUST00000012587.3	Kif11
ENSMUST00000216689.1	Kif11
ENSMUST00000028000.12	Nuf2
ENSMUST00000040912.8	Anln
ENSMUST00000028802.2	Knl1
ENSMUST00000020579.8	Hmmr
ENSMUST00000225740.1	Epb41l3
ENSMUST00000171929.7	Cenpf
ENSMUST00000053266.10	Mcm3
ENSMUST00000035977.8	Ticrr
ENSMUST00000115390.4	Ccnf
ENSMUST00000035495.14	Fanca
ENSMUST00000021311.9	Kif18b
ENSMUST00000065896.8	Kif2c
ENSMUST00000022053.10	Trip13
ENSMUST00000000028.13	Cdc45
ENSMUST00000038341.7	Bub1b
ENSMUST00000031366.11	Kntc1
ENSMUST00000114426.9	Tacc3
ENSMUST00000025562.8	Incenp
ENSMUST00000040717.6	Kif15
ENSMUST00000048391.14	Clspn
ENSMUST00000109432.3	Fbln1
ENSMUST00000117396.2	Ncapg
ENSMUST00000059091.5	Clca3a1
ENSMUST00000199581.4	Hgf
ENSMUST00000000095.6	Tbx2
ENSMUST00000081314.10	Blm
ENSMUST00000024981.8	Jpt2
ENSMUST00000025704.2	Cdca5
ENSMUST00000076147.5	Ackr4
ENSMUST00000099349.9	Hspa12b
ENSMUST00000025595.4	Fam111a
ENSMUST00000027202.8	Sgo2a
ENSMUST00000156899.1	Tpm1
ENSMUST00000024851.9	Ndc80
ENSMUST00000053364.11	Aspm
ENSMUST00000126739.1	Hjurp
ENSMUST00000035164.9	Topbp1
ENSMUST00000033310.8	Mki67
ENSMUST00000082337.12	Mdc1
ENSMUST00000033283.9	Rrm1
ENSMUST00000054674.14	Hjurp
ENSMUST00000054607.15	Ahcy
ENSMUST00000017290.10	Brca1
ENSMUST00000051395.8	Prr11

ENSMUST00000068031.7	Top2a
ENSMUST00000028119.6	Mastl
ENSMUST00000129466.7	Tpm1
ENSMUST00000013559.2	Igf2bp1
ENSMUST00000045026.3	Spag5
ENSMUST00000070607.8	Haus6
ENSMUST00000043294.11	Asb4
ENSMUST00000231569.1	Ttc3
ENSMUST00000098942.5	Spc24
ENSMUST00000075550.3	Cenph
ENSMUST00000154332.7	Top2a
ENSMUST00000093346.5	H2afv
ENSMUST00000102647.9	Selenoh
ENSMUST00000024270.13	Cdca3
ENSMUST00000029679.3	Cks1b
ENSMUST00000125430.1	Mad2l1
ENSMUST00000075995.6	Cand2
ENSMUST00000021359.6	Pole2
ENSMUST00000084296.9	Cdca8
ENSMUST00000112221.7	Rad51ap1
ENSMUST00000174105.7	Chek1
ENSMUST00000225316.1	Epb41l3
ENSMUST00000117299.8	Selenoh
ENSMUST00000178997.7	Tpx2
ENSMUST00000067925.7	Hmgb2
ENSMUST00000034742.7	Ccnb2
ENSMUST00000028948.4	Gins1
ENSMUST00000072239.13	Tmpo
ENSMUST00000120272.7	Depdc1a
ENSMUST00000181026.1	Cox4i1
ENSMUST00000041045.13	H2afz
ENSMUST00000222156.1	Trip13
ENSMUST00000023598.14	Rfc4
ENSMUST00000110805.2	Oip5
ENSMUST00000222761.1	Ncapg2
ENSMUST00000144742.5	Cenpa
ENSMUST00000144800.1	Cthrc1
ENSMUST00000202314.2	Cthrc1
ENSMUST00000182402.7	2700099C18Rik
ENSMUST00000139147.1	Rad54l
ENSMUST00000107802.7	Trim59
ENSMUST00000075853.5	Cks2
ENSMUST00000099985.5	Cenpw
ENSMUST00000067426.5	Cdkn3
ENSMUST00000226621.1	Cdkn3
ENSMUST00000022227.7	Cenpk

Appendix K: Differentially expressed transcription factor encoding transcripts over the course of neurogenesis.

Table 6. Differentially expressed transcription factor encoding transcripts over the course of neurogenesis.

Ensembl transcript ID	Mouse gene symbol	q value
ENSMUST00000026425.12	Pa2g4	0.037074859
ENSMUST00000221541.1	E2f6	0.011229629
ENSMUST00000043208.7	Six4	0.0495181
ENSMUST00000114694.8	Zbtb20	2.27E-05
ENSMUST00000022304.9	Thrb	9.62E-12
ENSMUST00000051301.5	Pura	0.006341933
ENSMUST00000202651.3	Clock	0.003385927
ENSMUST00000114086.7	Klf7	0.025446458
ENSMUST00000080885.11	Dbp	0.00143505
ENSMUST00000063116.9	Msx1	0.002286702
ENSMUST00000014174.13	Pax5	6.55E-05
ENSMUST00000042352.10	Zmat4	0.028186784
ENSMUST00000107893.8	Atf5	0.000171867
ENSMUST00000139064.9	Pou6f2	0.001722898
ENSMUST00000141605.7	Hivep3	0.000485563
ENSMUST00000105637.7	Prdm16	0.034215109
ENSMUST00000036884.2	Klf9	4.57E-19
ENSMUST00000106307.8	Hivep3	0.000232794
ENSMUST00000210120.1	Dbp	0.025489191
ENSMUST00000024954.10	Epas1	0.007117976
ENSMUST00000174611.7	Zic4	0.016797667
ENSMUST00000048934.14	Tbr1	0.044821646
ENSMUST00000061571.4	Neurod4	0.001291819
ENSMUST00000003870.14	Mxi1	0.000120296
ENSMUST00000196324.1	Nhlh2	0.00399891
ENSMUST00000163727.3	St18	6.74E-08
ENSMUST00000030124.3	Tal2	0.003135712
ENSMUST00000211665.1	Zscan18	0.002306537
ENSMUST00000041099.4	Neurod1	2.18E-06
ENSMUST00000018842.13	Lhx1	6.64E-05
ENSMUST00000105238.9	Stat2	0.027075271
ENSMUST00000208230.1	Fosb	0.031214601
ENSMUST00000165033.1	Egr1	0.01465912
ENSMUST00000064795.5	Egr1	0.022408227
ENSMUST00000127820.1	Egr2	0.005492251
ENSMUST00000231082.1	Egr2	0.005492251
ENSMUST00000021674.6	Fos	0.003059529
ENSMUST00000027649.13	Nr5a2	0.037553714
ENSMUST00000098611.3	Lef1	0.023964961
ENSMUST00000107094.1	Jun	0.018848301
ENSMUST00000173161.1	Rfx3	0.023420476
ENSMUST00000205980.1	Sox6	0.045398148
ENSMUST00000109129.7	Zfp2	0.000560989
ENSMUST00000081162.5	Homez	0.046336946
ENSMUST00000183176.1	Mzf1	0.017366523
ENSMUST00000095388.4	Rfx4	0.011017416

ENSMUST00000178174.2	Pou3f2	0.016982133
ENSMUST00000207873.1	Zfp14	0.015766186
ENSMUST00000135523.4	Sall2	0.011231309
ENSMUST00000000579.2	Sox9	0.046674133
ENSMUST00000176383.2	Zfhx4	0.006679687
ENSMUST00000089257.5	Insm1	0.010597163
ENSMUST00000036328.8	Zfhx2	0.002689615
ENSMUST00000020243.9	Ascl1	0.002401149
ENSMUST00000175965.9	Onecut2	3.65E-05
ENSMUST00000109514.7	Bcl11a	8.96E-05
ENSMUST00000113132.8	Pbx3	0.031836646
ENSMUST00000205391.1	Cebpa	0.025625003
ENSMUST00000153369.1	Nr4a3	0.013392873
ENSMUST00000057950.8	Sall3	0.018055327
ENSMUST00000105494.7	Scml4	0.015821594
ENSMUST00000024159.7	Dlx2	0.010882032
ENSMUST00000140030.7	Camta1	2.57E-05
ENSMUST00000122912.7	Csrnp3	1.00E-13
ENSMUST00000118578.8	Otx2	0.041849927
ENSMUST00000053491.8	Pou3f1	0.0080492
ENSMUST00000036215.7	Foxj1	9.17E-06
ENSMUST00000206034.1	Sox6	0.030006111
ENSMUST00000130310.7	Cpeb1	0.013891018
ENSMUST00000078058.4	Purg	0.010746307
ENSMUST00000046870.12	Lhx9	0.009718447
ENSMUST00000216751.1	Myb	0.026804145
ENSMUST00000090813.5	Sp9	5.65E-08
ENSMUST00000111752.9	Cux2	0.004533237
ENSMUST00000093852.4	Zbtb16	0.008541476
ENSMUST00000188495.7	Myb	1.20E-10
ENSMUST00000105590.7	Esr1	1.56E-11
ENSMUST00000056882.6	Olig1	0.002789013
ENSMUST00000035608.9	Olig2	9.77E-08
ENSMUST00000129843.7	Myt1	6.87E-05
ENSMUST00000030489.8	Tal1	0.000336058
ENSMUST00000054244.6	Dbx2	0.000562862
ENSMUST00000145088.1	Dlx1	0.000378653
ENSMUST00000049784.16	Myt1l	1.42E-13
ENSMUST00000066384.6	Zic4	2.79E-11
ENSMUST00000028928.7	Gzf1	0.028954405
ENSMUST00000020982.6	Klf11	0.024282276
ENSMUST00000128406.7	Tfap2c	0.017668791
ENSMUST00000072566.4	Nme2	0.000467672
ENSMUST00000021941.7	Mxd3	6.82E-06
ENSMUST00000018005.9	Mybl2	0.009778572
ENSMUST00000103145.10	E2f1	0.008347907
ENSMUST00000073316.12	Foxm1	4.39E-06
ENSMUST00000000095.6	Tbx2	0.000265269
ENSMUST00000102923.9	Aebp1	0.005313408
ENSMUST00000163568.3	Six2	0.005042195
ENSMUST00000175984.1	Tsc22d1	0.022038383

ENSMUST00000129393.1	Smyd3	0.013139532
ENSMUST00000031017.10	Fosl2	0.045749144
ENSMUST00000112966.9	Lhx6	2.94E-07
ENSMUST00000014747.2	Alx3	0.005563884
ENSMUST00000102864.4	Rel	0.026836299
ENSMUST00000029462.9	Tbx15	3.05E-06
ENSMUST00000052946.11	Tbx20	0.000180055
ENSMUST00000042054.2	Foxf2	0.000481976
ENSMUST00000214964.1	Dnmt1	0.002449328
ENSMUST00000056924.13	Plagl2	0.002474876
ENSMUST00000072777.13	Hmga2	8.85E-61
ENSMUST00000162098.8	Shox2	6.78E-05
ENSMUST00000097216.4	Tead2	2.23E-06
ENSMUST00000124268.7	Rreb1	0.00169927
ENSMUST00000022646.8	Nkx3-1	0.000725587
ENSMUST00000159310.1	Hmga2	1.69E-06
ENSMUST00000026662.7	Cbx2	0.021209482
ENSMUST00000033060.13	Tead2	0.007675474
ENSMUST00000137093.7	Stat3	0.000843998
ENSMUST00000069334.7	Dach1	0.023916477
ENSMUST00000110510.3	Gli3	0.005826814
ENSMUST00000069536.11	Tcf7l1	0.033216635
ENSMUST00000070143.12	Zhx1	0.031575319
ENSMUST00000229748.1	Zhx1	0.031575319
ENSMUST00000144716.1	Lin54	0.020720846
ENSMUST00000119223.1	E2f8	2.42E-06
ENSMUST00000076521.6	Irf6	0.009893328
ENSMUST00000144742.5	Cenpa	0.006173902
ENSMUST00000003369.9	Plag1	0.018375568
ENSMUST00000197962.1	Cenpa	0.000119044
ENSMUST00000023612.16	Ets2	0.025721954
ENSMUST00000026703.5	Bach1	0.017142392
ENSMUST00000102820.8	Bnc2	9.18E-12
ENSMUST00000176971.1	Bnc2	0.000186192
ENSMUST00000187952.1	Plscr1	7.12E-08
ENSMUST00000093801.9	Plscr1	0.004409213
ENSMUST00000100043.2	Sp5	0.000131646
ENSMUST00000032768.14	Nr2f2	0.023978763
ENSMUST00000005279.7	Klf5	0.009858261
ENSMUST00000040536.5	Batf	0.000640377
ENSMUST00000113326.8	Foxp1	0.00716893
ENSMUST00000110835.2	Elf1	0.028562499
ENSMUST00000208474.1	Nr2f2	0.020551134
ENSMUST00000065360.4	Zic1	0.002356006
ENSMUST00000207153.1	Nr2f2	0.018522085
ENSMUST00000041183.6	Meox2	2.59E-05
ENSMUST00000023356.7	Snai2	0.00077003
ENSMUST00000021333.4	Foxg1	0.000351571
ENSMUST00000075805.12	Prrx1	0.031157801

Appendix L: Differentially expressed transcription factor encoding transcripts over the course of chondrogenesis.

Table 7. Differentially expressed transcription factor encoding transcripts over the course of chondrogenesis.

Ensembl transcript ID	Mouse gene symbol	q value
ENSMUST00000096430.10	Zhx2	0.03045774
ENSMUST00000112832.7	Rorb	0.037690499
ENSMUST00000162022.7	Glis3	0.024024999
ENSMUST00000114694.8	Zbtb20	0.012944301
ENSMUST00000106307.8	Hivep3	0.000347325
ENSMUST00000103112.7	Zhx3	0.007380018
ENSMUST00000108639.7	Zbtb4	0.018430829
ENSMUST00000102944.10	Creb3	0.002321999
ENSMUST00000043637.13	Mitf	0.01681401
ENSMUST00000043172.14	Rarg	0.044180782
ENSMUST00000109460.7	Zhx3	0.000947638
ENSMUST00000063694.9	Klf13	0.00079267
ENSMUST00000216150.1	Zbtb16	0.012208448
ENSMUST00000023612.16	Ets2	5.84E-05
ENSMUST00000093852.4	Zbtb16	1.02E-12
ENSMUST00000023119.14	Vdr	9.57E-13
ENSMUST00000036884.2	Klf9	1.53E-34
ENSMUST00000107893.8	Atf5	8.76E-05
ENSMUST00000004145.13	Stat5a	0.035531961
ENSMUST00000108492.8	Hif3a	1.43E-07
ENSMUST00000024954.10	Epas1	0.026372533
ENSMUST00000128282.3	Jazf1	0.015076474
ENSMUST00000130491.2	Cebpg	0.012429213
ENSMUST00000113956.9	Runx1	0.001018652
ENSMUST00000023673.13	Runx1	0.001647935
ENSMUST00000139491.7	Zbtb20	0.031988814
ENSMUST00000195612.1	Zbtb18	0.044222356
ENSMUST00000003870.14	Mxi1	0.025833874
ENSMUST00000032194.10	Bhlhe40	0.023204295
ENSMUST00000032386.10	Bhlhe41	4.33E-07
ENSMUST00000210748.1	Npas1	0.012311725
ENSMUST00000111703.1	Bhlhe41	7.64E-05
ENSMUST00000000579.2	Sox9	0.03698768
ENSMUST00000047321.8	Arntl	0.00079267
ENSMUST00000053484.7	Eea1	0.034021177
ENSMUST00000152594.7	Zbtb38	0.018512368
ENSMUST00000075159.4	Clock	0.002017165
ENSMUST00000046303.11	Crebl2	0.000130738
ENSMUST00000113624.2	Rora	0.032142853
ENSMUST00000048128.14	Zbtb7a	0.044136531

ENSMUST00000051301.5	Pura	0.006126644
ENSMUST00000211770.1	Arntl	0.00346531
ENSMUST00000202122.1	Clock	0.004380651
ENSMUST00000130310.7	Cpeb1	0.001626425
ENSMUST00000027974.6	Atf6	0.000920068
ENSMUST00000144742.5	Cenpa	0.022392889
ENSMUST00000032717.6	Dbx1	0.04109932
ENSMUST00000197962.1	Cenpa	0.0001589
ENSMUST00000174672.1	Zfp57	0.001273074
ENSMUST00000021941.7	Mxd3	0.023604982
ENSMUST00000018005.9	Mybl2	7.64E-05
ENSMUST00000073316.12	Foxm1	4.36E-05
ENSMUST00000107801.9	Tead2	2.89E-05
ENSMUST00000061721.5	E2f2	0.001210404
ENSMUST00000219808.1	Gli1	0.043851212
ENSMUST00000026474.4	Gli1	0.031881612
ENSMUST00000041183.6	Meox2	0.009514586
ENSMUST00000155821.1	Nfib	0.000933271
ENSMUST00000107246.1	Nfib	0.002378571
ENSMUST00000159334.7	Etv1	0.000362215
ENSMUST00000226960.1	Dzip1	0.037423673
ENSMUST00000231153.1	Nr4a1	0.045484727
ENSMUST00000192102.1	Hey1	0.042644997
ENSMUST00000192550.5	Hey1	0.024668126
ENSMUST00000215916.1	Csrnp1	0.001294471
ENSMUST00000161839.1	Hes1	2.23E-07
ENSMUST00000109795.1	Plagl2	0.000140655
ENSMUST00000023171.7	Hes1	0.017404777
ENSMUST00000000095.6	Tbx2	0.005778282
ENSMUST00000176161.7	Ebf2	0.001083613
ENSMUST00000014747.2	Alx3	0.043167409
ENSMUST00000049621.6	Hes5	8.63E-08
ENSMUST00000033060.13	Tead2	0.000559772
ENSMUST00000026662.7	Cbx2	0.011223377
ENSMUST00000069334.7	Dach1	0.00231894
ENSMUST00000177754.8	Dnmt1	0.00290074

Appendix M: Characterization of Cabin1 during chondrogenic differentiation in the cranial neural crest

Previous work in our lab discovered that transient reduction of Cabin1 expression in developing zebrafish embryos resulted in a distinct phenotype characterized by a range of developmental defects, including craniofacial deformities and abnormal cranial NC cell migration. During T-cell activation and muscle development, Cabin1 modulates the temporal expression of genes associated with differentiation through its interaction with a variety of proteins, including MEF2 (myocyte enhancer factor 2; Yang et al., 2011; Youn and Liu, 2000). One specific isoform of MEF2, MEF2C, is a well-established transcriptional regulator of chondrogenesis (Miller et al., 2007; Verzi et al., 2007), however it is not known if Cabin1 interacts with MEF2C in the cranial NC during the formation of the craniofacial skeleton. We hypothesize that Cabin1 regulates chondrogenic differentiation through its repression of MEF2C, thus inhibiting gene expression associated with this process during cranial NC cell migration. Here we demonstrate that Cabin1 and MEF2C directly interact in cultured cranial NC cells, and observe a reduction in Cabin1 protein during in vitro chondrogenic differentiation. Taken together, these observations support a novel role for Cabin1 in the cranial NC, paving the way future investigation into the definitive role of this transcriptional repressor during craniofacial development.

In order to determine if Cabin1 was expressed in the cranial NC we assessed Cabin1 protein expression in undifferentiated cranial NC cells grown for three passages (12 days in culture). Robust Cabin1 expression was observed in both the cytoplasmic and nuclear compartments of the undifferentiated cultures (Fig. 23A). Moreover, the expression of MEF2C, an isoform of MEF2 known to regulate chondrogenesis, was also observed in undifferentiated cranial NC cells (Fig. 23A'). MEF2C expression was localized to the nucleus, as we would expect for a transcriptional activator. Importantly, merged images of Cabin1 and MEF2C protein expression reveal co-expression of Cabin1 and MEF2C in the nucleus of the undifferentiated cranial NC cells (Fig. 23A''), thus increasing the possibility for a potential interaction between the two proteins.

Cabin1 is known to interact with MEF2 proteins during T-cell activation and skeletal myogenesis (Yang et al., 2011; Youn and Liu, 2000). During these processes, the presence of Cabin1 inhibits differentiation in general, however differentiation progressed upon dissociation of Cabin1 from MEF2. In order to determine if Cabin1 interacts with MEF2C in the cranial NC, we performed immunoprecipitation assays on nuclear lysate extracted from undifferentiated cranial NC cells grown for three passages (12 days in culture). Antibodies against Cabin1 and MEF2C were validated using immunoblotting in the same lysates, which also served to confirm the nuclear localization of these two proteins in the undifferentiated cultures. In support of our hypothesis, Cabin1 was detected in the immunoprecipitation of MEF2C (Fig. 23B; *red dashed boxes*). Conversely, MEF2C protein was also detected in the immunoprecipitation of Cabin1 (Fig 23C; *red dashed boxes*). In both cases, Cabin1 or MEF2C proteins were detected in the flow-through lysate. This suggests that both Cabin1 and MEF2C may also interact with other proteins in the undifferentiated cranial NC cells as they are known to do in other cell types. Nevertheless, these results indicate that Cabin1 and MEF2C interact in the nucleus of the undifferentiated cranial NC cells.

We next sought to determine how Cabin1 gene expression changed over the course of chondrogenic differentiation, and how the expression of MEF2C-target genes might be impacted as a result. To do this, we evaluated gene expression changes for Cabin1, and MEF2C-target genes, Dlx6 (direct target) and Hand2 (indirect target), between the undifferentiated cranial NC and over the course of chondrogenic differentiation using qRT-PCR. Cabin1 expression was still detectable after 4 days in chondrogenic differentiation, however we observed reduced Cabin1 gene expression in RNA extracted from chondrogenic nodules at Day 14 (Fig. 23D). Dlx6 expression did not change relative to its expression in the undifferentiated cultures, although reduced Cabin1 expression over time appeared to correlate with modest increases in Hand2 expression, both at Day 4 and Day 14. During cartilage formation in both mice and zebrafish, MEF2C activation results in expression of Dlx6 and Dlx5, which work cooperatively to activate Hand2 (Miller et al., 2007; Verzi et al., 2007). We predicted that a reduction in Cabin1 expression over time would be correlated with increases in MEFC-target genes. Our results do not support this relationship, although it does not preclude its ability to regulate other genes during chondrogenesis that have yet to be determined.

In human naïve T cells, the ability of Cabin1 to repress MEF2 gene activation is known to be modulated by nuclear export in response to increased calcium levels, which promotes expression of MEF2-target gene IL-2 during T-cell activation (Pan et al., 2005). To determine if Cabin1 localization changes during chondrogenesis, we evaluated differences in Cabin1 nuclear localization between undifferentiated cranial NC cells and those undergoing chondrogenic differentiation at an early (Day 4) and late (Day 14) time point. We observed Cabin1 protein in both the cytoplasmic and nuclear compartments at all time points tested, however Cabin1 nuclear localization decreased in cells undergoing chondrogenesis over time (Fig. 24). Specifically, there was a statistically significant reduction of Cabin1 in the nucleus of cells assessed after 4 days in chondrogenic differentiation medium when compared to undifferentiated cranial NC cultures (Figs. 24B, 24B’ compared to 24A, 24A’, quantified in Fig. 24D). A similar significant decrease was also detected in chondrocytes at Day 14 (Figs. 24C, 24C’ compared to 24A, 24A’, quantified in Fig. 24D), although Cabin1 nuclear localization was significantly higher at Day 14 compared to Day 4 (Fig. 24D). Most notably, we observed a marked reduction in Cabin1 immunostaining in regions of the well containing differentiated chondrocytes within chondrogenic nodules at this later time point (Figs. 24C, 24C’, 24C’’; *arrowheads*), although we are unable to rule out the possibility that antibody penetration may not have occurred equally across all the cells within the center of the nodules. We also noted that the presence of nuclear Cabin1 was significantly higher at Day 14 compared to Day 4, although it is possible that our data may represent an overestimation of the amount of Cabin1 in the nucleus at this later time point. At Day 14, the chondrocytes within the nodules are compacted, making it difficult to establish parameters that would definitively distinguish each individual nuclei of these cells within the nodules without increasing detection of artifacts/debris. Since some of the differentiated cells within the nodules were not being assessed, it is possible that the MFI values reported for Day 14 are higher than they would be had the analysis been able to account for those missing nuclei, or if it were more specific to the differentiated cells within the nodules. Despite these caveats, our results do indicate that the presence of Cabin1 in the nucleus decreases during chondrogenesis.

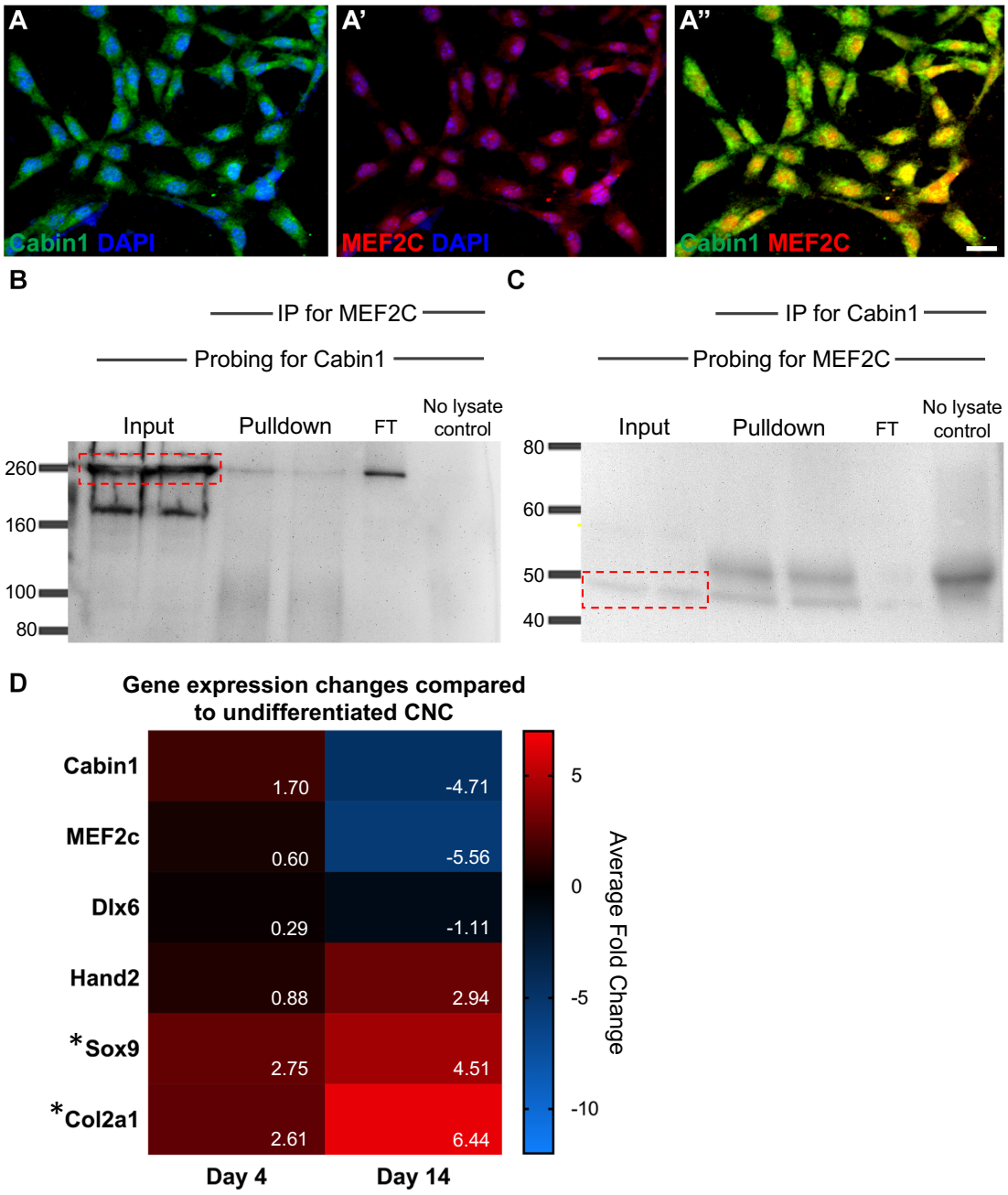

Figure 23: Cabin1 and MEF2C interact in the nucleus of undifferentiated cranial NC cells. (A, A', A'') Cabin1 (A) and MEF2C (A') were co-expressed in the nucleus of the undifferentiated cranial NC cells. Merged image of Cabin1 and MEF2C (A'') **(B)** Cabin1 (250 kDa; *red dashed box*) was detected in the immunoprecipitation of MEF2C from nuclear lysate extracted from undifferentiated cranial NC cells. **(C)** MEF2C (45 kDa; *red dashed box*) was detected in the immunoprecipitation of Cabin1 from nuclear lysate extracted from undifferentiated cranial NC cells. **(D)** Expression of Cabin1, MEF2C, MEF2C-target genes, Dlx6 and Hand2, and chondrogenic markers, Sox9 and Col2a1 were assessed in RNA extracted from cranial NC cells after 4 and 14 days in chondrogenic differentiation medium. Only Sox9 and Col2a1 showed a statistically significant change in relative expression between Day 4 and Day 14 when compared against the undifferentiated cultures. (*P<0.05, Unpaired t-test). Values represent mean ± SEM from 3 independent isolates of cranial NC. Green staining = Cabin1. Red staining = MEF2C. Blue staining = DAPI labelled nuclei. Scale bar: 25 µm.

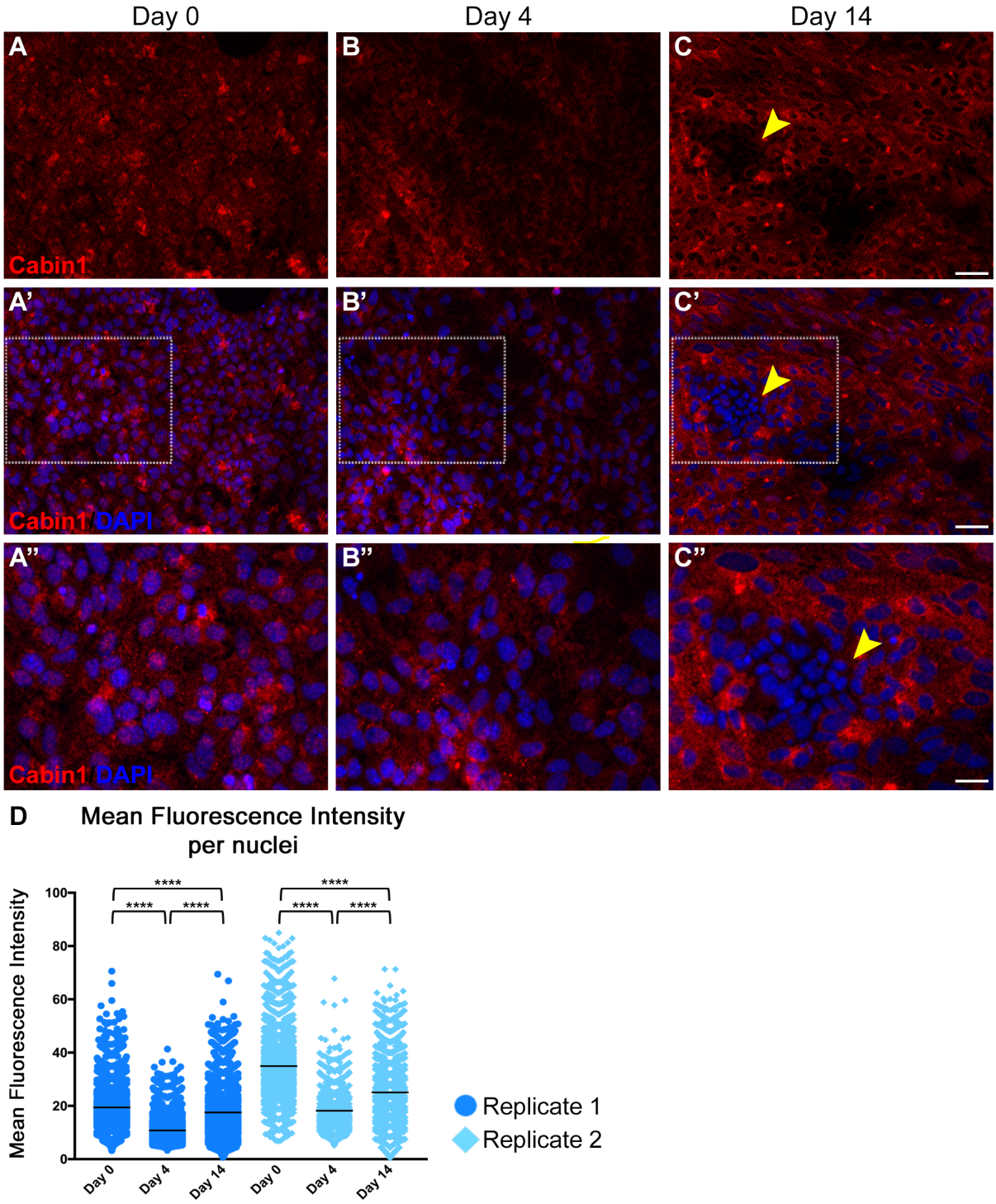

Figure 24: Reduced Cabin1 nuclear localization corresponds with progression of chondrogenesis *in vitro*. (A-C, A'-C') Cabin1 protein expression in undifferentiated cranial NC cells (Day 0), and after 4 and 14 days in chondrogenic differentiation medium. Cabin1 was observed in both the cytoplasm and nuclear compartments at all time points, however its nuclear localization decreased over time. A marked reduction of Cabin1 was detected in regions of the cultures containing chondrogenic nodules (arrowheads) **(A''-C'')** Higher magnification views of the boxed regions show changes in Cabin1 nuclear localization over time **(D)** Quantification of Cabin1 nuclear localization in undifferentiated (Day 0), and differentiated chondrocytes

over time. Each dot represents MFI within one nucleus, color-coded by biological isolate. Black horizontal lines represent mean ± SEM. (****P<0.0001. Unpaired t-test was used to assess replicates at each time point. One-way ANOVA was used to assess each replicate across time points). Red staining = Cabin1. Blue staining = DAPI labelled nuclei. Scale bars: (A, B, A', B', A'', B'') 50 μm; (C, C', C'') 25 μm.

CURRICULUM VITAE

Maria R. Replogle

CURRENT POSITION

University of Wisconsin – Milwaukee Milwaukee, WI
Dissertator/Ph.D. candidate – Advisor: Ava J. Udvadia August 2012 to May 2020
Teaching Assistant – Genetics Discussion (BioSci 325) August 2012 to May 2020

PREVIOUS EMPLOYMENT

SunHealth Research Institute Sun City, AZ
Research Technician – Laboratory of Neuroinflammation November 2003 to November 2004
Research Assistant – Center for Parkinson's Disease Research June 2002 to May 2003

EDUCATION

University of Wisconsin – Milwaukee Milwaukee, WI
B.S., Biologic al Sciences May 2012
Ph.D, Developmental and Molecular Neuroscience May 2020

RESEARCH EXPERIENCE

University of Wisconsin – Milwaukee Milwaukee, WI
Dissertator/Ph.D. candidate – Advisor: Ava J. Udvadia August 2012 to May 2020
Determining the gene regulatory mechanisms controlling ectodermal and mesoectodermal cell fate acquisition in the cranial neural crest

- Developed methods for isolating, expanding and directly differentiating primary murine cranial and trunk neural crest cells *in vitro*
- Established reproducible benchmarks that track the temporal progression of cranial and trunk neural crest differentiation along the neuronal, glial and chondrogenic lineages
- Assessed genome-wide changes in gene expression and chromatin accessibility in cultured cranial neural crest cells over the course of neurogenesis and chondrogenesis
- Investigated the role of Cabin1 in regulating the temporal progression of chondrogenesis in the cranial neural crest using various molecular biology techniques and biochemical assays
- Extensive experience in mouse and zebrafish husbandry and transgenic colony maintenance

University of Wisconsin – Milwaukee Milwaukee, WI
Undergraduate Researcher/Independent Researcher – Advisor: Ava J. Udvadia June 2011 to August 2012
Assessed the role of Cabin1 in auditory-vestibular system development in zebrafish

- Characterized Cabin1 protein localization in the developing zebrafish inner ear
- Investigated the effect of reduced Cabin1 expression on otolith size using Morphometric software on Alcian blue stained zebrafish larvae
- Gained experience in zebrafish husbandry and transgenic colony maintenance

SunHealth Research Institute Sun City, AZ

Research Technician – Laboratory of Neuroinflammation November 2003 to November 2004

- Investigated amyloid-beta peptide expression in sectioned brain tissue dissected from a mouse model of Alzheimer's disease
- Gained experience in mouse husbandry and transgenic colony maintenance

Research Assistant – Center for Parkinson's Disease Research June 2002 to May 2003

- Assessed the neuroprotective effect of D2/D3 receptor agonists on dopaminergic neuronal death in the substantia nigra of MPTP-treated mice

RELATED PROFESSIONAL EXPERIENCE

Marine Biological Laboratory Woods Hole, MA

Frontiers in Stem Cells and Regeneration, Advanced Training Course Fall 2017, 2018, 2019

Role: Research Facilitator

- Organized and prepared the laboratory section of the zebrafish optic nerve regeneration lecture
- Assisted in mentoring students of all professional levels in completing the lab, which included teaching how to perform optic nerve crush and retina dissection on euthanized zebrafish

AWARDS AND HONORS

2012 to 2019	Chancellor's Award, UW-Milwaukee Graduate School
April 2019	James J. Magnino, MD Scholarship, UW-Milwaukee
May 2018	Jeannette Seloover Johnson '62 and R. Douglas Johnson Women in Science & Technology Fellowship
April 2018	Biological Sciences Symposium – Best poster by a graduate student (tie)
April 2018	Ruth Walker Grant-in-Aid Award, UW-Milwaukee
April 2017	James D. Anthony Memorial Scholarship, UW-Milwaukee
April 2017	Biological Sciences Symposium – Best talk by a graduate student
April 2016	Ruth Walker Grant-in-Aid Award, UW-Milwaukee
June 2014	Society of Developmental Biology Travel Award
April 2014	Biological Sciences Symposium – Best talk by a graduate student
April 2013	Ruth Walker Grant-in-Aid Award, UW-Milwaukee
May 2012	Genetics Society of America Travel Award
April 2012	Ruth Walker Graduating Senior Award, UW-Milwaukee
2011 to 2012	SURF Award, Office of Undergraduate Research, UW-Milwaukee *Three time recipient – Summer 2011, Spring 2012, Summer 2012*
April 2011	Ruth Walker Tuition Award, UW-Milwaukee

PUBLICATIONS

Maria R. Replogle, Virinchipuram S. Sreevidya, Vivian M. Lee, Michael D. Laiosa, Kurt R. Svoboda, Ava J. Udvadia. 2018. *In vitro* model for characterizing the differentiation of primary murine cranial and trunk neural crest cells. Disease Models and Mechanisms. 11 (12): dmm.035097 doi:10.1242/dmm.035097 PMID: 30409814.

*Associated first author interview: Disease Models and Mechanisms (2018) 11:dmm038117 doi:10.1242/dmm038117

Jeffrey N. Joyce, T.C. Der, Lynn Renish, Tracy Osredkar, Diane Hagner, **Maria Replogle**, Shinichi Sakakibara, Shuichi Ueda. 2004. Loss of D3 receptors in the zitter mutant rat is not reversed by L-dopa treatment. Experimental Neurology. 187(1), 178-89. doi:10.1016/j.expneurol.2004.01.012 PMID: 15081599.

Jeffrey N. Joyce, T.C. Der, Lynn Renish, Tracy Osredkar, Diane Hagner, **Maria Replogle**, Shinichi Sakakibara, Shuichi Ueda. 2003. Neuroprotective effects of the novel D-3/D-2 receptor agonist and antiparkinson agent, S32504*, in vitro* against 1-methyl-4-phenylpyridinium (MPP+) and *in vivo* against 1-methyl-4-phenyl-1,2,3,6-tetrahydropyridine (MPTP): a comparison to ropinirole. Experimental Neurology. 184(1), 393-407. doi:10.1016/j.expneurol.2004.01.012 PMID: 14637109.

Alex V. Yarkov, Diane Hagner, **Maria Replogle**, Jeffrey N. Joyce. 2003. Behavioral effects of dopamine agonists and antagonists in MPTP-lesioned D-3 receptor knockout mice. Pharmacology Biochemistry and Behavior. 76(3-4), 551-562. doi:10.1016/j.pbb.2003.09.011 PMID: 14643855.

CONFERENCE PRESENTATIONS

Maria R. Replogle, Andrea Rau, Paul L. Auer, Ava J. Udvadia. 2019. Gene regulatory interactions governing cranial neural crest cell differentiation along neurogenic and chondrogenic lineages. Society for Neuroscience, Chicago, IL

Maria R. Replogle, Paul L. Auer, Ava J. Udvadia. 2019. Chronological transcriptomic analysis of chondrogenic differentiation in the cranial neural crest. Society for Developmental Biology, Boston, MA

Maria R. Replogle, Kurt R. Svoboda, Ava J. Udvadia. 2016. *In vitro* model for characterizing migration and differentiation of primary cranial and trunk neural crest cells isolated from *Sox9-cre/EYFP* mouse embryos. Society for Neuroscience, San Diego, CA

Maria R. Replogle, Dena R. Hammond-Weinberger, Ava J. Udvadia. 2014. Characterization of murine cranial neural crest cell culture models for investigating pathways of chondrogenic and glial differentiation. Society for Developmental Biology, Seattle, WA

Maria R. Replogle, Dena R. Hammond-Weinberger, Ava J. Udvadia. 2013. Cabin1 in cranial neural crest cell development as it relates to craniofacial development and 22q11.2 deletion syndrome. Sixth Aquatic Animal Models for Human Disease and 2013 Midwest Zebrafish Conference, Milwaukee, WI

Dena R. Hammond-Weinberger, **Maria R. Replogle**, Ava J. Udvadia. 2012. Cabin1 knockdown leads to morphological and functional deficits in the developing auditory-vestibular system. Genetic Society of America Conference on Zebrafish Development and Genetics, Madison, WI